

**Assessment of the fate and behavior of naturally
occurring thorium and uranium in the environment
of central Sri Lanka**

Zur Erlangung des akademischen Grades einer
DOKTORIN DER NATURWISSENSCHAFTEN

(Dr. rer. nat.)

von der KIT-Fakultät für Chemie und Biowissenschaften

des Karlsruher Instituts für Technologie (KIT)

genehmigte

DISSERTATION

Von

Sanduni Yasanka Ratnayake

Aus

Ratnapura, Sri Lanka

Dekan: Prof. Dr. Manfred Wilhelm
Referent: Prof. Dr. Horst Geckeis
Korreferent: Prof. Dr. Thorsten Schäfer

Tag der mündlichen Prüfung: 15.04.2021

Erklärung

Hiermit versichere ich, dass ich die vorliegende Arbeit selbständig verfasst und keine anderen als die angegebenen Quellen und Hilfsmittel verwendet habe. Darüber hinaus versichere ich, dass alle Stellen der Arbeit, die wörtlich oder sinngemäß aus anderen Quellen übernommen wurden, als solche kenntlich gemacht sind und die elektronische Version der Arbeit mit der schriftlichen übereinstimmt und dass die Arbeit in gleicher oder ähnlicher Form noch keiner Prüfungsbehörde vorgelegt wurde. Die Satzung des Karlsruher Instituts für Technologie (KIT) zur Sicherung guter wissenschaftlicher Praxis wurde in der jeweils gültigen Fassung beachtet.

Datum, Ort

Unterschrift

ACKNOWLEDGEMENTS

First and foremost, I offer my sincere gratitude to my supervisor Prof. Horst Geckeis, for granting me the opportunity to carry out my research project with him at the Institute for Nuclear Waste Disposal (INE) of the Karlsruhe Institute of Technology (KIT). I am very honored and pleased to have his supervision throughout my project, which was always supported by his immense knowledge and guidance.

I am especially indebted to my direct supervisor, Dr. Johannes Lützenkirchen, for his enormous support, endless patience, time and guidance helped keep this project in the right direction and I was honored and privileged to have the opportunity to work with such a great scientist.

This project would not exist if it were not for the financial support of German Academic Exchange Service (DAAD) under the research grant – Doctoral Programs in Germany, 2017/18 (57299294). Their kind assistance not only with financially but relating to the life in Germany, and as well as understanding my family status throughout my stay in Germany are very much appreciated.

My sincere thanks to all my colleagues who kindly assisted with laboratory analysis of the samples, including Dr. Dieter Schild for SEM-EDX and XPS measurements, Mr. Frank Geyer, Ms. Annika Fried and Ms. Corneila Walschburger for ICP-MS measurements, Ms. Tanja Kisely for BET and NPOC measurements, Ms. Sylvia Moisei-Rabung for ICP-OES measurements, Ms. Stefanie Kraft for IC measurements, and Mr. Marcus Fuss for Gamma spectroscopic measurements. I thanked Dr. Frank Heberling for the assistance in the radon/thoron measurements and fruitful scientific discussions. Ms. Elke Bohnert is acknowledge for her kind support during my work and I would like to thank the Radiation Protection group of INE for their assistance inside the controlled area. Also, Dr. Elisabeth Eiche and Ms. Beate Oetzel for their kind help in XRF analysis at Institute of Applied Geosciences (AGW)-KIT. Dr. Teba Gil-Diaz is exceptionally acknowledged for her kind support, constant motivation and for being a good understandable friend to me throughout this journey and for never doubting I could take this adventure to the end and always ready to help resolving issues with not only in science but also in life.

I especially thanked Dr. Nicolas Finck for his kind support in XRD measurements and mostly in the XAS measurements and subsequent data analysis. In addition, Dr. Jörg Rothe and Dr. Kathy Dardenne are acknowledged for their assistance in μ -XAS and μ -XRF measurements at the INE-Beamline for radionuclide science of the KIT synchrotron light source while the Institute for Beam Physics and Technology (IBPT) is acknowledged for the operation of the storage ring, the Karlsruhe Research Accelerator (KARA). I thanked Dr. Szenknect (Institute of Separation Chemistry, Marcoule, France) for providing the thorite reference material for XAS analysis.

I wish to express my sincere appreciation to Sri Lanka Atomic Energy Board (SLAEB) for granting me the permission to carry out my doctoral project in Germany. Especially, late Dr. R.L. Wijayawardana (former Chairman of SLAEB), Prof. S.R.D Rosa (current Chairman), Mr. Tennakoon (Director General), Dr. Edirisinghe (Director-Industrial Applications Division) and all my friends and staff members of SLAEB are acknowledged for their support. Particularly, the staff of Life Sciences Division, especially, my friends Thiwanka and Dulanjalee, for assisting me in Gamma spectroscopic and XRF measurements and General Scientific Division for providing me radiation survey meters.

My exceptional thank goes to Prof. Weerasooriya at National Institute of Fundamental Studies (IFS), Sri Lanka, for his continuous encouragement and providing me the lifetime opportunity to carry out my research in Germany, as well as for his kind support and guidance during sampling campaigns. Also, Mr. Dilshan Bandara and Ms. Pathmanathan are thanked for their support during sampling campaigns and analytical help at IFS, Sri Lanka.

I would like to thank Mr. De Silva and Mr. Wickramasinghe from the Geological and Mines Bureau (GSMB) and Industrial Technology Institute (ITI) in Sri Lanka for their support in the export clearances regarding the soil and plant materials. Also, I thanked Prof. Chandrajith for facilitating me the ICP-MS analysis of my water samples at the Department of Geology, University of Peradeniya, Sri Lanka.

Many thanks to my friends at INE and for making me feel home in Karlsruhe. My friends, Dr. Yasmine Kouhail and Dr. Nikoleta Morelova, were acknowledged for their support for the final formatting of the thesis.

My special sincere thank goes to Dr. Ruth Haas Nüesch and my landlords, Mr and Mrs. Jung, for being my family in Germany and supporting me all the time not to miss my family.

Nobody has been more important to me in the pursuit of this project than the members of my family. My heartiest gratitude goes to my late mother, Sunila Ratnayake, my father, Chandradasa Ratnayake, and my sisters, Viveka and Inupa, for believe in me. Especially, my beloved husband, Nirmala Wickramasinghe, and my son, Ronal, whose unconditional love, trust, endless inspiration, enormous support and bless are with me in whatever I pursue, and I greatly admit their sacrifices and patience throughout this period.

ABSTRACT

Although Sri Lankan coastal areas are well-known for their high background radiation levels, mostly due to Th-bearing minerals, higher natural background radiation levels inland were discovered in 2015. The radioactivity data collected at this location raised concern regarding the risk of public radiation exposure since the screened area comprised a school playground.

The present study reports on-site radioactivity measurements and geochemical analyses of environmental samples, such as four soil samples, two grass samples and six water samples from around the area of study. Subsequent series of batch and column experiments with the soil samples were carried out to better understand the environmental risk and potential mobility of dose-dominating NRs in the area. Since the mobility and bioavailability of NRs in the environment strongly depend on their aqueous speciation, adsorption behavior and the solubility of relevant solid phases, classical sequential and single extraction methods were applied and modern spectroscopic techniques were used to gain insight.

Gamma spectrometry from the soil samples clearly showed the dominant contribution of Th-232 and progenies to total activity ranging between 4440.0 ± 364.7 and 7037.9 ± 647.0 Bq kg⁻¹ followed by K-40 in the range from 339.6 ± 16.9 to 538.9 ± 55.8 Bq kg⁻¹ and U-238 including progenies in $318.7 \pm 88.7 - 510.9 \pm 106.3$ Bq kg⁻¹. In-situ measurements yielded background radiation levels at one-meter height above the ground of 2.5 ± 1.2 μGv h⁻¹ (maximum of 21.6 ± 10.9 mSv yr⁻¹). The calculated absorbed dose rates in air, $3 - 4.6$ μGy h⁻¹, while the calculated radiation hazard indices yielded mean values of 9300 ± 1800 Bq kg⁻¹, 33 ± 6 , 25 ± 5 , and $20 \times 10^{-3} \pm 4 \times 10^{-3}$ for Radium Equivalent Activity (R_{eq}), Gamma Index (I_γ), External Hazard Index (H_{ex}) and Excess Life Time Cancer Risk (ELCR), respectively. All these indices exceed their corresponding world averages. Activity concentrations of Th-232, U-238 and K-40 in grass sample dry masses are in the range of 770 – 975, 21 – 30, and 540 – 574 Bq kg⁻¹, and the estimated soil-grass transfer factors (TFs) are 0.12 – 0.16, 0.05 – 0.08, and 0.94 – 1.40, respectively. Thoron gas releases from soil samples in exhalation experiments using a closed system result in activities $35 - 76$ kBq m⁻³. Conversion to annual effective doses via the inhalation pathway yields values of 2.49 to 5.46 mSv. Note that

those values do not reflect the real situation, where extensive dilution by air will reduce thoron concentrations by orders of magnitude even in closed rooms.

All soil samples were characterized by several spectroscopic and microscopic techniques. The basic physicochemical characterization evidenced acidic properties and moderate total organic carbon content in the soils. X-ray Diffraction (XRD) data reveal that the major mineralogy of the site is dominated by kaolinite and quartz with minor fractions of Fe crystalline phases like hematite and goethite. Target trace elements were found to be present in different mineral phases, i.e., as oxides, silicates and phosphates, and in mixed phases as identified by Scanning Electron Microscopy (SEM) with Energy Dispersive X-ray (EDX) spectroscopy. Linear Combination Fitting (LCF) of X-ray Absorption Spectroscopy (XAS) data involving Th-monazite (phosphate), thorite (silicate), and thorianite (oxide) provided evidence that Th in the samples is present as Th-monazite ($61 \pm 7\%$), thorite (ThSiO_4 , $24 \pm 7\%$), and thorianite (ThO_2 , $16 \pm 7\%$). Further study of single particles selected from the sediment samples using micro-focus X-ray Fluorescence (μ -XRF) and micro-X-ray Absorption Spectroscopy (μ -XAS) confirmed the nature of the mineral phases and the chemical forms of Th.

Element mobility was tentatively addressed by applying several batch and column experiments. Selective chemical extractions showed that ~ 8 and 16 wt.% of total Th and U could be dissolved/extracted from the operationally defined soil non-residual fractions and >85 wt.% of Th and U are associated with the major residual fraction of NR-containing mineral phases (oxide, phosphate and silicate phases). Mass balance calculations confirmed full recovery of $100 \pm 15\%$ Th while for U it was $100 \pm 40\%$ as compared to the amount quantified by X-ray Florescence (XRF) spectroscopy.

Batch extractions and column leaching experiments with simulated rainwater (SRW), silica nanoparticles (Si NPs) and humic acid (HA), show clearly lower leachability of Th and U when compared to the chemical extractions. Overall potential mobilization of the trace elements with the above solutions in both batch and column experiments are $<1\%$ under the experimental conditions. Column experiments with SRW show relatively higher release of particulate species at the beginning likely due to erosion and eventually reach the measured on-site groundwater concentration levels. Added Si NPs and HA did not cause any significant effect on metal leaching and seemed strongly

retained by the soil. Scoping calculations involving geochemical models qualitatively retrieved the trend of the target elemental mobilities in the experiments.

The obtained results suggest important public, on-site exposure to radioactive NR-containing particles. Complementary results on associated light rare earth elements (REEs) are also presented given current socio-economic interest and in view of potential future environmental impact.

The present study provides for the first time relevant information about NR minerals in Sri Lankan soil, marking the onset for future studies concerning radioactive risk assessment in Sri Lanka.

ABSTRAKT

Obwohl die Küstengebiete Sri Lankas für ihre erhöhten Konzentrationen an natürlichen radioaktiven Stoffen bekannt sind, wurden im Jahr 2015 noch höhere Strahlungswerte im Landesinneren entdeckt. Die an diesem Ort gemessenen Aktivitäten gaben Anlass zur Besorgnis hinsichtlich des Risikos einer Strahlenbelastung der Bevölkerung, da der untersuchte Bereich einen Schulhof umfasst. In der vorliegenden Studie wurden Radioaktivitätsmessungen vor Ort durchgeführt, Umweltproben im Labor charakterisiert und anschließend Serien von Batch- und Säulenexperimenten mit Bodenproben durchgeführt, um mögliche Umweltrisiken und die potenzielle Mobilität natürlicher Radionuklide (NR) in dem Gebiet besser zu verstehen. Gammaskopmetrische Analysen von Bodenproben zeigen einen dominanten Beitrag von NRs der Th-232- und U-238-Zerfallsreihen, gefolgt von K-40, was zu mittleren Dosiswerten in einem Meter Höhe über dem Boden von $2,5 \pm 1,2 \mu\text{Gv h}^{-1}$ führt ($21,6 \pm 10,9 \text{ mSv yr}^{-1}$). Signifikante Exhalationen von Thoron (Rn-220) aus den Bodenproben konnten nachgewiesen werden. Alle Bodenproben wurden mit spektroskopischen und mikroskopischen Methoden charakterisiert. Kaolinit und Quarz mit geringen Anteilen von Hämatit und Goethit dominieren die mineralogische Zusammensetzung des Bodens. Zudem liegen in geringen Massenanteilen Th-, U- und Seltenerdhaltige Oxide, Silikate, Phosphate und Mischphasen vor. Aus der Anwendung selektiver chemischer Extraktionsverfahren ergibt sich, dass ~8 und 16 Gew.-% des gesamten Th und U aus den operational definierten nicht-residualen Fraktionen des Bodens gelöst/extrahiert werden können. >85 Gew.-% des Th / U liegen in der residualen Fraktion der NR-haltigen Mineralphasen vor. Experimente mit simuliertem Regenwasser (SRW), Silica-Nanopartikeln (Si NPs) und Huminsäure (HA) zeigen eine deutlich geringere Auslaugbarkeit von Th und U im Vergleich zu den chemischen Extraktionen. Insgesamt liegt die potentielle Mobilisierung der Spurenelemente (Th, U, La) mit den oben genannten Lösungen unter den Versuchsbedingungen bei <1%. Säulenexperimente mit SRW zeigen anfänglich eine erhöhte Freisetzung von partikulären Th und U Spezies, und erreichen schließlich Konzentrationen, die vergleichbar mit den Konzentrationen in den vor Ort beprobten Grundwässern sind. Zugesezte Si NPs und HA verursachen keinen signifikanten Effekt auf die Metallauswaschung und werden offenbar vom Boden zurückgehalten. Orientierende geochemische Rechnungen konnten den Trend der experimentell beobachteten Mobilisierung von Th, U und La durch Kolloide wiedergeben. Zusammenfassend deuten die erhaltenen Ergebnisse auf die signifikante Rolle partikulärer NR für die lokale radiologische Exposition hin. Die vorliegende Studie liefert zum ersten Mal detaillierte Informationen zu NR-haltigen Mineralien in srilankischen Böden und zur möglichen Mobilisierung von NR und stellt damit den Auftakt für zukünftige Studien zur Risikobewertung durch erhöhte Vorkommen an Ablagerungen natürlicher radioaktiver Minerale in Sri Lanka dar.

TABLE OF CONTENT

ACKNOWLEDGEMENTS	I
ABSTRACT	V
ABSTRAKT	IX
TABLE OF CONTENT	XI
1. INTRODUCTION	1
1.1. Background of the work	1
1.1.1. Motivation	1
1.1.2. Aim, objectives and thesis structure	2
1.2. Review and summary of relevant literature	4
1.2.1. Sources of radiation exposure	4
1.2.2. Naturally occurring radionuclides	6
1.2.2.1. General overview	6
1.2.2.2. Fundamental properties and chemistry of Th and U	11
1.2.3. Mobility of the natural radionuclides in terrestrial systems	17
1.2.3.1. Known potential solid scavengers and carrier phases	17
1.2.3.2. Experimental approaches to identify potential scavenger and mineral-bearing carrier phases	19
1.2.4. Areas with high natural background radiation levels on earth	23
2. EXPERIMENTAL	31
2.1. On site measurements and sampling procedures	31
2.1.1. Gamma measurements	31
2.1.2. Sampling and pre-treatment of soil	31
2.1.3. Sampling of potable water	32
2.1.4. Sampling of grass	34
2.2. Chemicals and solution preparation procedures	34
2.3. Solid phase characterization in the laboratory	35
2.3.1. Radioactivity measurements, sample preparation and radiation dose/radiation risk assessment calculations	35
2.3.1.1. Soil sample preparation for gamma analysis	36
2.3.1.2. Grass sample preparation for gamma and X-ray fluorescence spectroscopic analysis	36
2.3.1.3. Gas sample preparation for radon/thoron analysis	37
2.3.1.4. Evaluation of radiological doses	37
2.3.2. Soil acidity	40
2.3.3. Total organic carbon content in solid phase	41
2.3.4. Total elemental compositions of bulk samples and sieved fractions	42
2.3.4.1. Wavelength dispersive X-ray fluorescence spectroscopy	43
2.3.4.2. Energy dispersive X-ray fluorescence spectroscopy	43
2.3.5. Major mineral compositions in soil: X-ray diffraction of bulk and sieved soil samples	44
2.3.6. Surface morphology and soil composition: Scanning electron microscopy and energy dispersive X-ray spectroscopy	44

2.3.7. Identification and quantification of Th containing mineral phases: X-ray absorption spectroscopy at the Th L ₃ -edge	44
2.3.7.1. Sample preparation and bulk sample analysis: X-ray absorption near edge structure and extended X-ray absorption fine structure	45
2.3.7.2. Sample preparation and analysis of selected individual Th-containing particles	45
2.3.7.3. Data treatment	46
2.4. Analysis for elemental mobility and potential carrier phases	48
2.4.1. Quantification methods and analytical instrumentation	48
2.4.1.1. Trace element analyses	48
2.4.1.2. Major element analyses	48
2.4.1.3. Non-purgeable organic carbon	49
2.4.1.4. Analysis of anionic components: IC	49
2.4.2. Batch extraction procedures	49
2.4.2.1. Sequential chemical extractions of bulk and sieved samples	49
2.4.2.2. Single chemical extractions of bulk samples	51
2.4.3. Batch leaching experiments	51
2.4.3.1. Simulated rainwaters	51
2.4.3.2. Silica nanoparticles	52
2.4.3.3. Humic acid	53
2.4.4. Column leaching experiments	53
2.4.4.1. Simulated rainwater	54
2.4.4.2. Silica nanoparticles	55
2.4.4.3. Humic acid	55
2.5. Geochemical data modelling	55
3. CHARACTERIZATION OF THE ENVIRONMENTAL SAMPLES	57
3.1. Activity measurements and radioactivity dose calculations in the area of study	57
3.2. Basic soil characterization	67
3.3. Speciation of Th in soil minerals	81
3.3.1. Bulk XAS analysis of Th containing minerals	81
3.3.2. Small area analysis of specific Th-containing particles	87
3.4. On-site groundwater characterization	97
3.5. Conclusions	103
4. POTENTIAL MOBILITY AND CARRIER PHASES OF TARGET ELEMENTS	105
4.1. Evaluation of potential mobilization based on chemical batch extractions	105
4.1.1. Overall mass balances and performance of the chemical extraction procedures	106
4.1.2. Identification of potential carrier phases of target elements	111
4.2. Evaluation of potential mobilization in environmentally representative conditions: batch experiments with rainwater and exogenic carrier phases including silica nanoparticles and humic acids	116
4.2.1. Simulated rainwaters	117
4.2.2. Silica nanoparticles	119
4.2.3. Humic acids	120

4.3. Mobilization in column experiments for selected soils	121
4.3.1. Simulated rainwater	122
4.3.2. Silica nanoparticles	124
4.3.3. Humic acid	126
4.4. Discussion of the potential environmental mobility of target elements with relevant carrier phases and environmental implications of the applied methods	129
4.5. Scoping geochemical model calculations	131
4.6. Conclusions	134
5. SUMMARY AND FUTURE PERSPECTIVES	137
REFERENCES	143
APPENDICES	165

List of Figures

Figure 1.1: Decay series of (a) Th-232, (b) U-238, and (c) U-235. Full names of elements showed in the right side illustrate the elements appeared in all three decay series are in green, in two U series are in blue, in Th-232 and U-235 are in brown, and unique in in U-238 and U-235 are in red	8
Figure 1.2: Aqueous speciation of 10^{-11} mol L ⁻¹ Th(IV) in the absence of complexing ligands at I = 0.001 mol L ⁻¹ NaCl and 25 °C (calculations were performed in Visual MINTEQ 3.1). Solid phase formation is not considered	14
Figure 1.3: (a) One meter height dose distribution map of Sri Lanka (black dot with the cross shows the exact location, the school playground) and corresponding radionuclide distributions; (b) Th-232, (c) Ra-226 and (c) K-40 in soil	28
Figure 1.4: (a) Forest cover of one side of the playground, (b) playground with a school building, and (c) graphical side view of the location; A-forest cover in the upper part of the playground (as shown in (a)), B-playground with one school building (as shown in (b)), C-school buildings, D-students assembling area with some school buildings, and E-public road.....	29
Figure 2.1: Aerial view of the study area; numbers denote the sampling locations and labels are in accordance with the Figure 1.3c	32
Figure 2.2: Digital elevation map (DEM) of the surface water runoff around the location and water sampling locations are denoted by WL	33
Figure 2.3: Images of the water sampling locations; (a) WL-01, (b) WL-02 (Spring well), (c) WL-03 (Tap water), (d) WL-04, (e) WL-05, and (f) WL-06.....	34
Figure 2.4: Samples prepared for (a) bulk XAS (b) μ -XAS and μ -XRF, and (c) experimental set up used at the INE-beamline	46
Figure 2.5: (a) Experimental setup of the column experiments and (b) user interface with the process picture reflecting the system configuration.....	54
Figure 3.1: Correlation between (a) Th-232 and U-238 and (b) Th-232 and K-40 in the soil samples by gamma spectrometry	66
Figure 3.2: Comparison of the correlation between Th-232 and U-238 in reported soil/beach samples and this study	67
Figure 3.3: X-ray diffractograms of (a) bulk soil and (b) clay fractions of soil samples	69
Figure 3.4: X-ray diffractograms of the sieved fractions of (a) L-04 and (b) L-05 soil samples.....	70
Figure 3.5: Concentration of (a) Th, (b) U, (c) La, and (d) Fe ₂ O ₃ in each size fraction of L-04 and L-05 soil samples measured by XRF	73

Figure 3.6: Contribution of each size fraction (a) to the bulk and elemental distribution of (b) Th, (c) U, (d) La in each size fraction of L-04 (note that the smallest size fraction < 40 μm is almost invisible in the pie chart. It is indicated by the percentage fraction of 0.1-0.5 %).	74
Figure 3.7: SEM and corresponding EDX spectra of (a) large area analysis, (b) and (c) spot analyses of clay minerals with hexagonal stacking layers in different orientations	76
Figure 3.8: SEM images and corresponding EDX spectra of Ce-rich phases	78
Figure 3.9: SEM images and corresponding EDX spectra of monazite phases	78
Figure 3.10: SEM images and corresponding EDX spectra of (a) Th-phosphate and (b) BSE-SEM image and corresponding EDX spectra of Th-oxide phases	79
Figure 3.11: SEM images and corresponding EDX spectra of Th-silicate phases	79
Figure 3.12: Mixture of mineral phases in soil; C denotes - (Ce,Th)-oxide and P denotes - (Ce, La, Nd, Th)-phosphate phases	80
Figure 3.13: Thorium L ₃ -edge (a) XANES and (b) EXAFS spectra with (c) corresponding FT of all samples and RCs (distance is not corrected for phase shift)	85
Figure 3.14: Thorium L ₃ -edge (a) XANES and (b) EXAFS spectra with (c) corresponding FT of L-05 and sequential extraction residues from F4 (Ex4) and F5 (Ex5)	85
Figure 3.15: Experimental (solid line) and LCF modeled (dashed line) EXAFS spectra of the soil samples with residual (blue line). R-factor and reduced χ^2 are represented for individual fits	86
Figure 3.16: Experimental (solid line) and LCF modeled (dashed line) EXAFS spectra of L-05, L-05-Ex4 and L-05-Ex5 samples with residual (blue line)	86
Figure 3.17: (a) The SEM images, (b) corresponding EDX, and (c) μ-XRF spectra (solid line) with fits (dotted line) of the selected Th-silicate rich particle	89
Figure 3.18: μ-XRF maps of the Th-silicate particle (a) showing total fluorescence and fluorescence lines of (b) Th and (c) Y (maps: 82.5 μm in width, 67.5 μm in height). The scale represents normalized count integral	89
Figure 3.19: (a) SEM image of the Th-silicate particle and corresponding SEM-EDX elemental maps for O, Al, Si, P, Ca, Fe, and Th (b – h) in counts	89
Figure 3.20: (a) The SEM images, (b) corresponding EDX, and (c) μ-XRF spectra with fits of the selected Th-oxide rich particle	91
Figure 3.21: μ-XRF maps of the Th-oxide particle showing (a) total fluorescence and fluorescence lines of (b) Th, (c) Ce, (d) Fe, (e) Ti and (f) Pb (maps: 107.5 μm in width, 55 μm in height). The scale represents normalized count integral	91

Figure 3.22: (a) SEM image of Th-oxide particle and SEM-EDX elemental maps for O, Al, Si, P, Ti, Fe, Mo, Ce, and Th (b – j) of the particle in counts.....	92
Figure 3.23: (a) The SEM images, (b) corresponding EDX, and (c) μ -XRF spectra with fits of the selected Th-phosphate rich particle	93
Figure 3.24: μ -XRF maps of the Th-phosphate particle showing (a) total fluorescence and fluorescence lines of (b) Th, (c) La, (d) Ce, (e) Nd, (f) U, (g) Ca, (h) Y, (i) Fe, and (j) Pb (maps: 230 μ m in width, 183 μ m in height). The scale represents normalized count integral	94
Figure 3.25: (a) SEM image of Th-phosphate particle and SEM-EDX elemental maps for O, Al, Si, P, Ca, Fe, La, Ce, Pr, Nd, and Th (b – l) of the particle in counts	94
Figure 3.26: Micro-X-ray Absorption spectra of (a) Th-silicate, (b) Th-oxide, and (c) Th-phosphate rich particles, respectively	96
Figure 4.1: Percentage distribution of (a) Th, (b) U and (c) La in each chemically extracted fractions of soil sample L-05 in sequential (Seq) and single (Sin) extractions	106
Figure 4.2: Relative percentage values of Th (a,b), U (c,d) and La (e,f) extracted sequentially from each size fraction of sieved L-04, showing both overall F1-F6 (a,c,e) and expanded F1-F4 (b,d,f). A comparison with unsieved L-04 soil sample is included	109
Figure 4.3: Mass balance for (a) Th, (b) U and (c) La obtained in extractions per sieved soil fraction to the total of unsieved L-04 considering F1-F6	110
Figure 4.4: Concentrations of Th, U and La in the supernatant after rotating with different SRW compositions (a) SRW-A1, (b) SRW-A2, (c) SRW-B1, and (d) SRW-B2 for several time periods (7, 14, 21, 50, and 118 days) for L-05.....	118
Figure 4.5: Concentrations of (a) U and (b) La with different SRW compositions SRW-A1, A2, B1, and B2 from samples standing still (not rotated) after several time periods (7, 14, 21, 50, and 118 days) for L-05. Thorium is not shown here because the released concentrations were below the detection limit.....	118
Figure 4.6: Comparison of the (a) leached concentrations of Th, U and La in the supernatant after rotating soil samples with silica AEROSIL 200 suspension and (b) initial concentration of Si (Si_0) with Si in leachates (Si_s) after 7 days.....	120
Figure 4.7: Comparison of the concentrations of Th, U and La in the supernatant after rotating the soil sample L-05 with humic acids, HA1 and HA2.....	121
Figure 4.8: Comparison of the leached amounts of (a) Th, (b) U, (c) La, and (d) NPOC with simulated rain water (SRW-A1). Corresponding pH of the elutes and respective elemental concentration ranges (highlighted in grey color) including averaged pH of the groundwater are also presented. The arrows shown in (c) are the points where the column stopped during the experiment and the durations of stops are specified in hours. CE – column elute and GW – Groundwater	124

Figure 4.9: Comparison of the leached amounts of (a) Si and Fe while arrows showing the places where the column stops and the period, (b) Si and Th, (c) Si and U, (d) Fe and La with simulated rain water(SRW-A1) for the soil sample mixed with silica AEROSIL 200 and (e) comparison of the leached amounts of Si with the simulated rain water(SRW-A1) only with the soil sample (light blue points) and with the soil sample mixed with silica AEROSIL 200 nanoparticles (blue points) 125

Figure 4.10: Comparison of the leached amounts of NPOC with the leached amounts of (a) Th, (b) U, (c) La and (d) only leached with simulated rainwater (SRW-A1) and injected with 100 mg L⁻¹ Humic acid (HA1). The red circle in (c) is the point where the injected humics should come out and arrows showing the places where the column stops and the period..... 127

Figure 4.11: Comparison of column data from simulated rainwater (SRW-A1), mixed with silica nanoparticles, and injected with humic acid (HA1) for (a)Th, (b) U and (c) La 128

Figure 4.12: Comparison of the total dissolved percentages of Th(IV), U(IV), Yb(III) and Y(III) in the presence of (a) Si and humics, (b) humics, and (c) Si 133

Figure 4.13: Percentages distribution of Th in a system with an initial concentrations of 10⁻⁶ mol L⁻¹ Th, 8.5×10⁻⁷ PO₄³⁻ mol L⁻¹ and 2.4×10⁻⁷ mol L⁻¹ H₄SiO₄ with 0.1 mol L⁻¹ NaCl electrolyte concentration 133

List of Tables

Table 1.1: Average annual effective doses to human caused by natural radiation [1]..4	4
Table 1.2: Description of Th and U isotopes with the known natural abundance 13	13
Table 1.3: The most common oxidation states of U and Th 16	16
Table 1.4: Selected extraction protocols for the extraction of Th and U in soil and sediment samples 21	21
Table 1.5: Description of the chemicals used in the chemical extraction protocol in this study..... 22	22
Table 1.6: Comparison of activity concentrations of U-238 (Ra-226), Th-232, and K-40 and corresponding absorbed dose rates (D_R) in surface sand and soil samples from different areas in the world, some areas of Sri Lanka, and the study area. The values inside brackets represent the average..... 26	26
Table 2.1: Summary of the chemical extraction protocol used sequential and single extractions 50	50
Table 2.2: Chemical composition of simulated rainwater at two different pH values 52	52
Table 3.1: Activity concentrations, calculated absorbed dose rates and effective dose rates for soil samples..... 59	59
Table 3.2: Radiation hazardous indices calculated in the study area, some places in India and the world acceptable limits 61	61
Table 3.3: Activity concentrations of NRs accumulated in soil (averaged value) and grass samples ($Bq\ kg^{-1}$ dry weight) with corresponding transfer factors..... 63	63
Table 3.4: Measured thoron concentrations and calculated annual inhalation doses of the soil samples* 65	65
Table 3.5: Physicochemical properties of soil samples*..... 68	68
Table 3.6: Amounts of main components and trace elements present in the samples measured by XRF* and average reported values for the Upper Continental Crust (UCC, [241])..... 72	72
Table 3.7: Atomic concentrations of elements (%) in area and spot analyses for Figures 3.7 - 3.11 80	80
Table 3.8: Thorium L_3 -edge EXAFS spectra linear combination fitting results for soil samples and sequential extraction residues from F4 (Ex4) and F5 (Ex5) 84	84
Table 3.9: Weight and atom contribution of each element (%) obtained by SEM-EDX for the selected isolated particles (i.e., Figure 3.18 – Th-silicate, Figure 3.21 – Th-oxide, Figure 3.24 – Th-monazite) and the monazite RC..... 96	96

Table 3.10: Concentrations of targeted elements, anions, and on-site measurements of groundwater samples with the drinking water limit standards of WHO (W), EPA (E) and SLS (S).....	101
Table 4.1: Amounts of Th, U and La extracted in sequential (Seq) and single (Sin) extractions; mass of element released from the soil sample L-05	111
Table 4.2: Extracted percentages of Th, U and La in both sequential (Seq) and single (Sin) approaches for the soil sample L-05	111
Table 4.3: The amounts of Th, U and La extracted and leached from the batch and column experiments per g of soil.....	129

List of Abbreviations

NRs – naturally occurring radionuclides

HBRAs – High background radiation areas

XRD – X-ray Diffraction

XRF – X-ray Fluorescence Spectroscopy

WD-XRF – Wavelength Dispersive XRF

ED-XRF – Energy Dispersive XRF

SEM – Scanning Electron Microscopy

EDX – Energy Dispersive X-ray Spectroscopy

XAS – X-ray Absorption Spectroscopy

XANES – X-ray Absorption Near Edge Spectroscopy

EXAFS – Extended X-ray Absorption Fine Structure

LCF – Linear Combination Fitting

ICP-MS – Inductively coupled plasma mass spectroscopy

ICP-OES – Inductively coupled plasma optical emission spectroscopy

TOC – Total Organic Carbon

NPOC – Non-purgeable organic carbon

OM – organic matter

TDS – Total dispersed solids

ELCR – Excess lifetime cancer risk

TF – Transfer factor

RCs – Reference compounds

SRW – Simulated rainwater

Si NPs – Silica nanoparticles

HA – Humic acid

1. INTRODUCTION

1.1. Background of the work

1.1.1. Motivation

Human exposure to background radiation levels due to the presence of naturally occurring radionuclides (NRs) has become an important general research focus and a significant issue considering the radiological protection during last decades throughout the world. Characterization of the origin, speciation, potential mobility, transport pathways and subsequent bioavailability of corresponding NRs are key factors in environmental risk and impact assessment or for modelling the future impacts essential for appropriate radiation protection decision making.

Even though many studies referring to the geochemical behavior of NRs like Th and U can be found in the literature, most of them are based on either experimental data under laboratory conditions or studies at contaminated areas like mining sites. Therefore, there is a substantial need to investigate NRs under realistic conditions in areas where people live and to examine their potential mobility in the environment and subsequent transfer to biota, especially considering the fact that the data for many NRs on the above aspects are still missing.

In the current study, one of the high background radiation areas in central Sri Lanka was carefully selected as study area given its precise location and potential implications within the playground of a school. Therefore, proximity of public school and private buildings to the location of interest under increased radiation levels may obviously raise concerns related to potential health issues via direct exposure through external and/or internal pathways (radiotoxicity). Maximum exposure is expected to be related to in-situ external radiation and inhalation of radiological gases or dust particles containing NRs, especially during dry seasons, becoming particularly relevant when pupils are active on the playground.

Nevertheless, systematic studies of measured activity levels, chemical compositions and environmental behavior of NRs in this area are less documented. Subsequently, an estimation of bioavailable NRs concentration and their corresponding impact on the ecosystem is important for the assessment of environmental and human safety. The activity concentration of the NRs in soil, exhalation of Radon isotopes and bioavailability to native plants are vital factors to be evaluated under this perspective.

The potential implications of these results should be interpreted in the context of radioactive risk assessment concerning human exposure and environmental bioavailability.

Overall, it is obvious that proper assessment of the playground soil is vital and urgent due to the current lack of detailed studies concerning inland locations in Sri Lanka. Moreover, such a study is not only crucial to estimate the radiation exposure to the public, it could even become of interest with respect to the possible occurrence of previously unidentified radionuclide-bearing minerals or in the sense of natural analogous studies. Therefore, focusing on the above issues, this PhD thesis mainly addresses a comprehensive environmental analysis and radiological dose estimation in this area.

1.1.2. Aim, objectives and thesis structure

Since the radioactivity from natural sources is the main contribution to global human exposure, more attention has recently been given to the speciation and mobility of NRs. Consequently, this PhD thesis aims at solid state speciation of NRs in the soil samples from the playground of the school presenting higher than average background radiation levels, and at determining potential mobility/bioavailability of mainly Th-232 and U-238 along with some associated REEs, i.e., Lanthanum (La), Neodymium (Nd), and Cerium (Ce). To achieve these perspectives, extensive characterization techniques are applied to investigate the overall solid speciation while the environmental accessibility and mobility studies are carried out through batch extractions and column experiments. Complementary information on some light REEs is included given their natural association to NRs-bearing minerals, their relatively high concentrations in the area and their economic relevance for new technologies. This thesis includes:

- An extensive description of the sampling techniques as well as in- and ex-situ methodologies used for fundamental and advanced solid phase characterization and applied experimental approaches for mobility studies (Chapter 2).
- An evaluation of the solid phase speciation concerning Th and U, the main elements of interest, and subsequent radiation risk assessment caused by the elevated background radiation levels due to presence of high concentration of Th in the area of study (Chapter 3). This approach was carried out based on the obtained data from

both (i) on-site gamma radiation and laboratory radionuclide activity measurements and (ii) analyses of fundamental surface mineralogy and chemical compositions by basic surface (i.e., XRD, ATR-FTIR, XPS, SEM-EDX, and XRF) and advanced solid phase characterization techniques (i.e., XAS – both bulk and microanalysis). The geochemical characterization of natural water samples collected in the targeted area is also discussed to get an idea about the targeted elemental distribution in natural waters.

- Identification of the potential environmental mobility of Th, U, and La (selected as the representative element out of all studied light REE, showing the analogous behavior of Ce and Nd in Appendices) via several batch approaches (Chapter 4), including both extraction and column experiments (for which only one soil sample will be discussed in detail while the results for the rest of the soil samples are included in Appendices). Suitable extraction protocols are applied in batch and/or column experiments to (i) identify soil leachability and element mobility in environmentally representative conditions (i.e., simulated rainwater and soil interactions with silica nanoparticles and humic acids as potential carrier phases), as well as (ii) characterize intrinsic mineral carrier phases of the elements of interest through selective extractions. These results are also contrasted to the knowledge of solid phase speciation gained in Chapter 3, providing a better understanding of the potential environmental behavior, transfer and fate of Th, U, and light REEs in the area of study.

Scoping geochemical calculations taken from the available literature and development of a geochemical model for Th and U based on some results from soil characterization (Chapter 3) and mobility studies will be presented at the end of this chapter. These data will also help evaluating potential interactions and effects of the hypothetical transport of Th and U with simulated rainwater and in presence of silica nanoparticles and humic acids, providing a comparison to assess the real system with laboratory data.

- A final compilation (Chapter 5) of general conclusions, future perspectives regarding radiological safety measures and further potential research lines concerning the study area.

1.2. Review and summary of relevant literature

1.2.1. Sources of radiation exposure

Continuous exposure of all living organisms on earth to ionizing radiation is a natural phenomenon. The main types of radiation exposures that can cause adverse health effects to humans are natural, man-made, medical radiation and occupational radiation. According to United Nations Scientific Committee on the Effects of Atomic Radiation (UNSCEAR) report in 2000, about 87% of the radiation dose received by mankind is due to natural radiation sources and the remaining is due to anthropogenic sources [1]. The sources of natural radiation exposures could be categorized according to their origin such as radiations coming from (1) outer space and from the surface of the sun (cosmic rays) and (2) terrestrial radionuclides that occur in the Earth crust (in soil, air, water, building materials, food, human body, etc.). Some details about terrestrial NRs in soil will be addressed later in this Chapter.

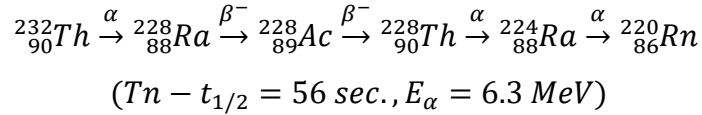
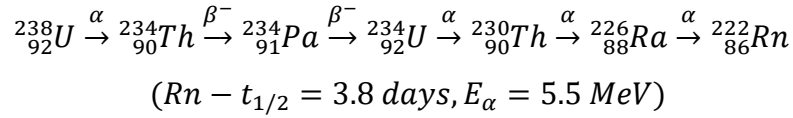
The extent of exposure to any kind of radiation depends on location and human activities. Humans can be exposed to radiation both externally via cosmic rays or terrestrial gamma rays and internally by inhalation of contaminated air (mainly radon) and ingestion of contaminated foodstuff. These exposures lead to the global average effective dose to humans of 2.40 mSv yr^{-1} with a typical range of $1 - 10 \text{ mSv yr}^{-1}$. A summary of various contributions is presented in Table 1.1 [1].

Table 1.1: Average annual effective doses to human caused by natural radiation [1]

Components of exposure	Annual effective dose (mSv)	%
Cosmic rays	0.38	16.1
Cosmogenic radionuclides	0.01	0.4
Terrestrial radiation: external exposure	0.46	19.5
Terrestrial radiation: internal exposure without radon	0.23	9.8
Terrestrial radiation: internal exposure from radon		
Inhalation of Rn-222	1.2	51.0
Inhalation of Rn-220	0.07	3.0
Ingestion of Rn-222	0.005	0.2
Total	2.40	100

According to Table 1.1, half of the global average annual effective dose (1.2 mSv) is due to the radon, thoron and their short-lived decay products. Radon, Rn-222 (Rn), and

thoron, Rn-220 (Tn), originate from the decay chains of U-238 and Th-232, respectively. The corresponding decay chains are shown below.



Alpha decay of Ra-226 in the U-238 decay series generates Rn while Ra-224 in the Th-232 decay series generates Tn with significantly different half-lives. Radon has a half-life of only a few days (3.8 days) with two longer-lived decay products, Pb-210 and Po-210, which are important in dose evaluations. Thoron has a very short half-life of 55 seconds and therefore cannot travel as far from its source as Rn before it decays and it has no long-lived decay products. Both Rn and Tn decay into their progenies, polonium, lead and bismuth, before finally reaching stable isotopes of lead.

The main source of Rn and Tn in the atmosphere is release from soil, rock and building materials and once they exhale, their decay products are generated in the air [1]. The primary defining factors for emanation of these gases involve the content of Radium (Ra) in soil and the soil properties while the moisture content and climatic conditions are also factors [2]. Further, the concentration of atmospheric Rn/Tn depends on the rate of diffusion from the ground and diffusion in the air [3]. The inhalation of these gases may cause some health problems in lungs due to densely ionizing alpha particles emitted by deposited short-lived decay products of Rn, Po-218 and Po-214. Rn is a carcinogen designated by the World Health Organization (WHO) and is the second-leading cause of lung cancer next to smoking [1, 4-9]. Therefore, areas with high concentration of primordial radionuclides might cause some elevated external exposure of these Rn and Tn. Even though the dose from Tn is generally negligible compared to that from Rn in most areas of the world [1], significant contributions of Tn to the inhalation dose were reported in some areas, particularly those with Th-rich monazite sands [10-12].

Additionally, humans can be exposed to radiation by manmade sources or enhanced levels of natural radiation from anthropogenic activities [1]. The latter part includes air travel, mining operations, mineral processing, mine tailing, use of phosphate fertilizers and agricultural practices, building materials, treatment of wastewater and drinking water, geothermal energy, production of industrial minerals, and burning fossil fuels like coal, nuclear weapon tests, etc. All these enhance the levels of environmental radioactivity [1, 13, 14]. Significant amounts of man-made radionuclides (Cs-137 and Sr-90) can be released to the environment via the nuclear related activities and applications. Such as small quantities of radioactive materials released to the environment during nuclear power production and large quantities in nuclear accidents like Chernobyl and Fukushima or nuclear fallouts from nuclear weapon tests for military purposes. Among them, waste generated by the nuclear power plants has a high level of radiotoxicity and should therefore be carefully treated and disposed. Even though used nuclear fuel can be reprocessed to separate U and Pu, the direct disposal of irradiated nuclear fuel has become international consensus in many countries. Such disposal can be done in geological formations like crystalline rock, clay rock and rock salt [15].

1.2.2. Naturally occurring radionuclides

1.2.2.1. General overview

Terrestrially originated NRs are components of the biosphere and thus are found naturally in the environment in all soils and plants at different levels and even inside the human body itself and may irradiate various organs with α and β particles, as well as gamma rays. External irradiation from these NRs is an important component regarding the exposure of human populations. The decay of NRs in soil produces gamma-beta radiation that may cross the soil-air interfaces and results in human exposure to radiation. The exposure rate to a person is determined mainly by the concentrations of NRs in the soil and the time of exposure. The dose rates can be measured by the direct measurements in air from terrestrial NRs or estimated from the concentrations of NRs in soil.

There are three types of NRs are in nature, (i) primordial, (ii) radiogenic, and (iii) cosmogenic radionuclides. Some terrestrial NRs have half-lives comparable to the age of the earth which are called primordial radionuclides implying that they did not

significantly decay after formation of the earth. The principal primordial NRs existing in nature are U-238, Th-232 and K-40, and they constitute the major terrestrial components of natural background radiation. Together with their progenies, they significantly contribute to the total dose from natural sources. Some other terrestrial radionuclides, such as the U-235 series, Rb-87, La-138, Sm-147, and Lu-176, exist in nature but due to low levels, their contributions to the dose to humans are rather small. In general, Th and U are considered as major energy sources, which drive the evolution of the earth and planets. However, such radioactive elements in uppermost soil layers are mostly immobile which may cause problems for the environment and human health as they can be easily integrated in the food chain and thereby induce risk for ecosystems, agro-systems and health [16].

Radiogenic nuclides (most commonly referred to as radiogenic isotopes) are nuclides that are produced by a process of radioactive decay. The most common radioactive decay chains observed in nature, commonly called the thorium ($4n$) series or thorium cascade, the radium or uranium ($4n+2$) series or uranium cascade, and the actinium ($4n+3$) series or plutonium cascade are started with long-lived nuclides, Th-232, U-238 and U-235, respectively, have existed since the formation of the earth. All these chains are ending in three different, stable isotopes of lead, i.e. Pb-208, Pb-206, and Pb-207, respectively, as shown in Figure 1.1 (the images are modified from the decay chains at [17]) while the total energy released from the initial parent nuclide to the final stable isotope of each series including the energy lost to neutrons are 42.6, 51.7, and 46.4 MeV, respectively. The radiogenic nuclides might be radioactive or stable and used in radiometric dating. These radionuclides can be divided into long-lived and short-lived isotopes while their different half-lives have implications for their usage in different fields of science [18].

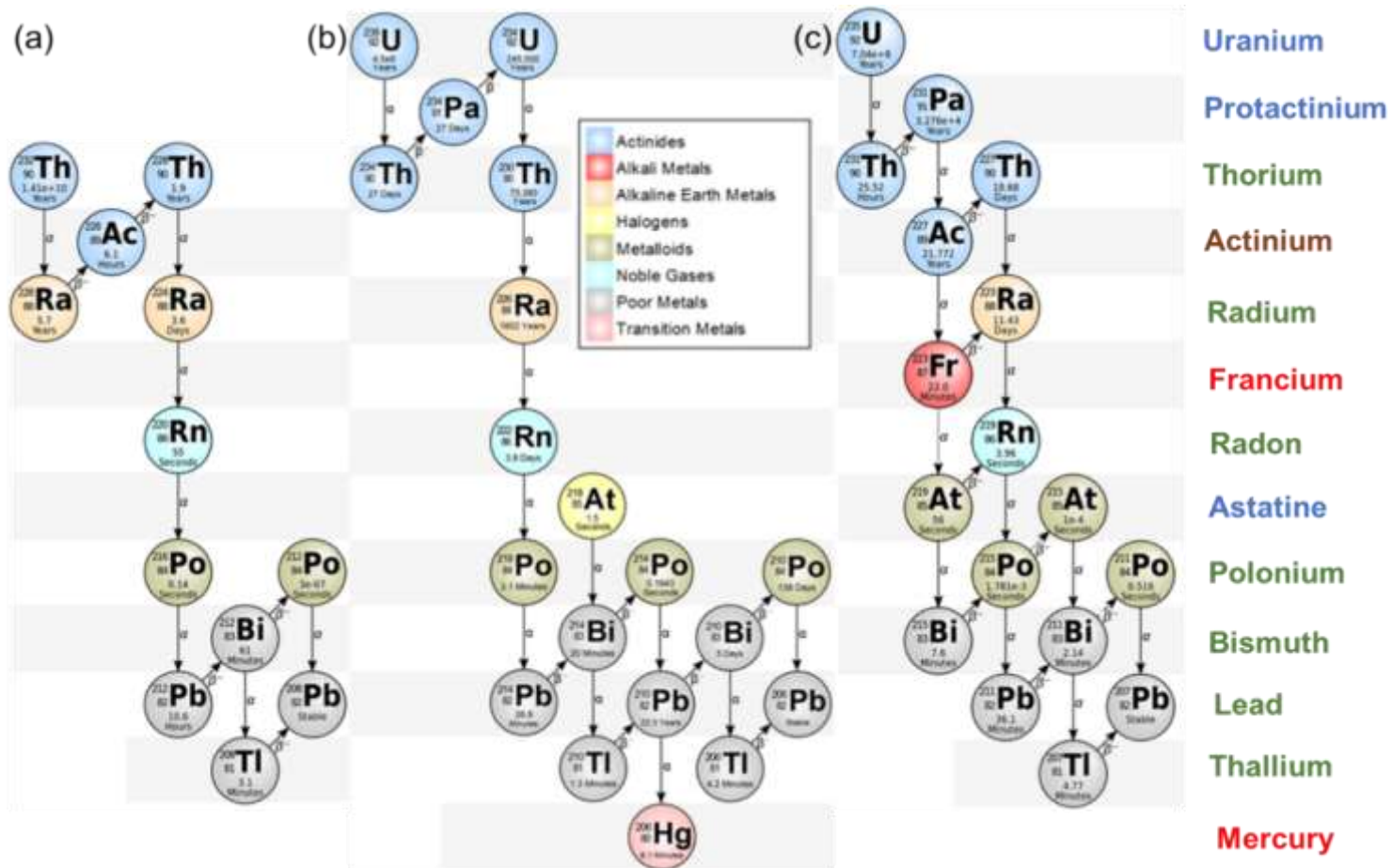


Figure 1.1: Decay series of (a) Th-232, (b) U-238, and (c) U-235. Full names of elements showed in the right side illustrate the elements appeared in all three decay series are in green, in two U series are in blue, in Th-232 and U-235 are in brown, and unique in in U-238 and U-235 are in red

Some unstable isotopes occur naturally by cosmic radiation called cosmogenic radionuclides such as C-14 (half-life ~5730 years) and H-3 (half-life ~12.3 years), and they are constantly regenerated. Most of these radionuclides are formed in Earth's atmosphere but some are formed within the Earth materials such as rocks and soil exposed to cosmic rays. The measurements on these radionuclides give insight into a range of geological and astronomical processes while the two main fields of application of them are dating and tracing [19].

Main sources of the terrestrial NRs in the environment are the minerals containing NRs. These minerals in soil are mainly inherited from the underlying geology and further influenced by the geographical setting [20, 21]. The respective minerals are not uniformly distributed, occur at different levels in various regions on earth, and their concentration depends on the local geology of each region in the world while the specific levels of radiation are related to the types of rock from which the soils originate. Higher radiation levels are normally associated with igneous rocks, such as granite, and lower levels with sedimentary rocks. As an exception, some phosphate rocks also show relatively high content of NRs. Mineral composition may have been potentially modified over long periods of time by weathering of original rock material and minerals, erosion, and volcanic eruptions with consequences for NR mobility in the environment. Mobility and chemical behavior of these NRs in geological settings play a major role in their distribution in the environment [22].

Understanding the bioavailability and bioaccumulation of NRs under natural environmental conditions is a complex and challenging subject of study. The knowledge of the concentration levels of NRs and their distribution and subsequent mobility in the environment is very important in several fields of science. These radionuclides can be used as natural tracers in geological and radioecological processes and hence allow understanding many important phenomena in atmosphere, biosphere, and geosphere and the respective interfaces [23, 24]. The isotopes of U, Th and Ra are particularly interesting to study due to their different chemical properties and long half-lives. Besides, these elements are recognized as toxic if accumulated inside the human body, which motivates studies of these elements. NRs can enter human body mainly via (1) ingestion of food, which can be simulated by assessing the bioaccumulation of NRs and (2) inhalation of contaminated air or dust particles containing NRs. Therefore,

it is crucial in this study to investigate the transfer of NRs in the various compartments of the biosphere.

The availability of NRs to plants, i.e. the amounts taken up, and subsequent bioaccumulation originates from and depends on several factors. The interaction of plants with NRs at a site can occur in two ways: (1) by foliar absorption of NRs deposited upon leaves or (2) uptake from the plant root zone in the soil. These two modes cannot be clearly distinguished in the natural systems, since for the target site of the present work radionuclides can easily be deposited on the leaves by the means of fugitive dust while pupils play in the playground or by wind. Uptake of radionuclides by plants from the soil is influenced by several factors. The major governing factor for the availability of these elements to the plants via root uptake from the adjacent soil is the solubility and thermodynamic activity of uncomplexed ions [25]. The soluble ionic forms of the radionuclides must exist in the soil solution adjacent to the root membrane for some finite period in order to be up taken by the plants [26]. The solubilization of NRs is mainly determined by the form and the NRs concentration in the rhizosphere as well as by the physicochemical characteristics of the soil, such as pH, clay and organic matter content, etc. However, in the geographical perspective, these chemical and physical properties of the soil are continuously varying and are the result of the combined effects of soil parent material, local topography, local climate, biological processes, time, and human activities [27]. Furthermore, some plant factors also affect this process, such as plant species, plant age, stage of growth, rate of physiological activity, plant root characteristics, plant nutritional status, moisture availability, the kinetics of ion transport across the membranes, the metabolic fate of absorbed ions, and ion interactions within the plant [26, 28]. Therefore, it is clear that NR uptake by plants depends on the interrelations between the soil factors and plant factors, which make their subsequent uptake by plants highly complex.

The risk assessment of NR contamination with respect to the biosphere usually includes bioaccumulation factors or transfer factors (TF), for estimating the plant uptake from the soil. Since this factor mainly depends on the corresponding location, it is encouraged/recommended to use such factors preferably as site-specific data [29]. Transfer factors also help understanding the biogeochemical cycling of NRs in the environment and their accumulation in the food chain [30-32]. Even though almost all

foods contain some amount of NRs like K-40, Th-232, U-238 and their progenies [1], their amounts depends on the geographical region, agricultural practices, and type of food. Normally, the food crops growing in the areas with high background radiation levels can be contaminated with higher amounts of NR than the crops growing in regions of normal background levels. Grazing and the consumption of the contaminated water by animals potentially also increases the accumulation of NRs in animal products resulting in access to the human body [33].

1.2.2.2. Fundamental properties and chemistry of Th and U

The major terrestrial NRs, Th and U show some unique fundamental properties. The two elements belong to the actinide series in the periodic table, which in general exhibit different oxidation states following different chemical behavior, which complicates the prediction of their geochemical behavior. Their solubility depends on pH, Eh, reaction with complexants such as carbonate, phosphate, humic acid, etc., and sorption to surfaces of minerals and/or colloids in the water. However, in general, data on the environmental behavior of Th are scarce in literature compared to U.

➤ *Thorium*

Thorium is, probably surprisingly for many, the most abundant radioactive element, three to four times higher in abundance than U and about as abundant as Pb or Mo, in the Earth's crust (crustal abundance 9.6 – 12 mg kg⁻¹ [34]) and can be found in trace amounts in rocks, soils, surface water, groundwater, plants, and animals. Thorium was discovered by the Norwegian amateur mineralogist Morten Thrane Esmark in 1828 and identified by Jöns Jacob Berzelius, a Swedish chemist, from a mineral sample, which is now known as thorite (ThSiO₄). Thorium has a unique chemistry, and yet has remained relatively unexplored. The atomic number is 90 with an atomic mass of 232 and the corresponding electronic configuration is [Rn] 6d² 7s². It has 26 known isotopes but only 12 of them have half-lives above one second while only 3 have half-lives sufficiently long to be of environmental concern. These three notable isotopes are described in Table 1.2.

Essentially, Th-232 is the most abundant isotope in nature with a half-life of about 1.4 × 10¹⁰ years. Both Th-232 and Th-230 are present in soil and ores in secular equilibrium with Ra-228 and Ra-226, respectively, in the absence of any geochemical interactions

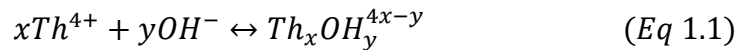
(e.g. no access of water). Th-230 is a radioactive decay product of U-238 and is found in low concentrations in U deposits and mill tailings. Th-229 is produced as a daughter product of artificial U-233 and generally not considered as a radionuclide of concern in environmental contamination [35]. Thorium naturally occurs as oxide (ThO_2), phosphate (ThPO_4), and silicate (ThSiO_4). It is concentrated in natural soil largely either in detrital minerals such as monazite and silicate minerals or adsorbed onto natural colloidal-sized materials. However, it is widely accepted that most of the Th-containing minerals are highly refractory to weathering and considered as very insoluble and Th is considered a more or less immobile element in natural environments.

Thorium has some remarkable chemical and physical properties. Among them, Th metal is liquid over the widest temperature range of any element and ThO_2 has the highest melting point of any known oxide [36]. It has an empty $5f$ orbital and +4 is the stable and exclusive oxidation state in the natural environment and is largely redox inactive, which means that it has a very high standard reduction potential [37, 38]. This Th(IV) has a large cationic radius of 1.14 Å with small electronegativity of 1.0 and an ionization potential of 6.95 eV. Therefore, it shows greatest affinity to other M(IV) elements such as U, Ce and Zr. Because of its large atomic size, high valence and electronegativity, Th cannot form isomorphic series that involve major rock forming minerals and occurs mostly in accessory minerals like zircon, sphene, epidote, uraninite, allanite and apatite in igneous rocks. Further, the large Th(IV) ion is hydrolyzed and significantly adsorbed on organics, clays and oxides in soil under environmental conditions resulting in its immobility [39]. Furthermore, due to its large size, the Th(IV) ion possesses the ability to reach multiple coordination numbers from 4 to 15 allowing a wide-range of ligands to be coordinated with potential in various applications. The most common coordination number is 8 with respect to oxygen [36, 37]. Owing to these high coordination numbers, Th exhibits fascinating properties with diverse topological configuration and rich coordination chemistry [40]. The typical Th compounds are colorless due to the lack of electrons in the $6d$ and $5f$ orbitals of Th(IV). Also, due to the high stability of Th(IV), it is frequently used as a structural analogue for other actinides which are difficult to handle under normal conditions, such as Np(IV) or Pu(IV) [41]. With respect to redox states, Th(III) is a potential oxidation state and has been reported in terms of free Th^{3+} in an aqueous solution of ThCl_4 and HN_3 [42], which is obviously not available under natural conditions.

Table 1.2: Description of Th and U isotopes with the known natural abundance

Isotopes of Th		Decay		Radiation Energy (MeV)			
Abundance %	Half-life (years)	Mode	Product	Alpha (α)	Beta (β)	Gamma (γ)	
Th-229	Trace	7.9×10^3	α	Ra-225	4.9	0.12	0.096
Th-230	0.02	7.5×10^4	α	Ra-226	4.7	0.015	0.0016
Th-232	99.98	1.4×10^{10}	α	Ra-228	4.0	0.012	0.0013
U-234	0.0054	2.4×10^5	α	Th-230	4.8	0.013	0.0017
U-235	0.7204	7.0×10^8	α	Th-231	4.4	0.049	0.16
U-238	99.2742	4.5×10^9	α	Th-234	4.2	0.010	0.0014

The mobility of Th in soil is governed by the formation of hydrated Th^{4+} which is responsible for its solubility over a wide range of soil pH. In aqueous solutions, Th(IV) is capable to form both mono- and poly nuclear hydrolysis products. A wide range of $\text{Th}(\text{OH})_n^{4-n}$ hydroxide complexes and subsequent olation or oxolation result in the formation of polynuclear compounds [43]. A number of polynuclear Th hydroxide species have already been identified, such as dimers: $\text{Th}_2(\text{OH})_2^{6+}$, $\text{Th}_2(\text{OH})_3^{5+}$, $\text{Th}_2(\text{OH})_4^{4+}$, tetramers: $\text{Th}_4(\text{OH})_8^{8+}$, $\text{Th}_4(\text{OH})_{12}^{4+}$, pentamers: $\text{Th}_5(\text{OH})_{12}^{8+}$, and hexamers: $\text{Th}_6(\text{OH})_{14}^{10+}$, $\text{Th}_6(\text{OH})_{15}^{9+}$ [44]. The most important ligands for Th aqueous speciation are hydroxide and carbonate. The formation of hydroxide complexes $\text{Th}_x(\text{OH})_y^{4x-y}$ in the absence of complexing ligands other than water is governed by the following reaction [45],



The distribution of aqueous Th species with pH in water ($\sim 10^{-11}$ mol L⁻¹) is shown in Figure 1.2. The corresponding speciation can be described as follows: free Th^{4+} ion dominates at pH < 3, molecular 1:1, 1:2 and 1:3 hydroxy complexes, $\text{Th}(\text{OH})_3^{3+}$, $\text{Th}(\text{OH})_2^{2+}$ and $\text{Th}(\text{OH})_3^+$ are predominant between about pH 3-7, colloidal $\text{Th}(\text{OH})_4^0$ is the major species above pH 7 where other pseudocolloidal occurrences may also occur [46, 47]. The solubility of Th in aqueous solution in the absence of other complexing ligands is controlled by the solubility of thorium oxide/thorium hydroxide [48].

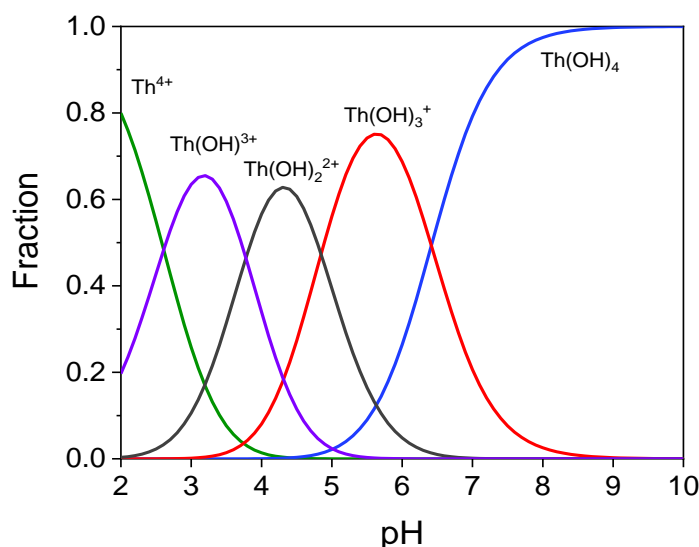


Figure 1.2: Aqueous speciation of 10^{-11} mol L⁻¹ Th(IV) in the absence of complexing ligands at $I = 0.001$ mol L⁻¹ NaCl and 25 °C (calculations were performed in Visual MINTEQ 3.1). Solid phase formation is not considered

Thorium in natural waters is usually complexed with sulfate, fluoride, chloride, nitrate, carbonates, phosphate or organic anions, which can increase the solubility of Th minerals and the mobility of Th in soil and ground waters [46, 49]. However, Th might be virtually absent in soil solutions at high pH due to the strongly decreasing solubility of ThO₂ with increasing pH. Factors like particle size, presence of colloids and ionic strength can affect the solubility of Th [45, 50-52].

There are some known health effects associated with Th in the areas with relatively high concentrations of Th. However, humans are always exposed to small amounts of Th via inhalation through air and ingestion with food and water, due to its availability nearly everywhere on earth. Inhalation of high levels of Th containing dust particles over a long time may be lethal and potentially increases the possibility of developing lung diseases, cancers in lungs, pancreas, hepatic, or kidney, and leukaemia [53-55]. Thorium has the ability to change genetic material and after injection of Th as contrast agent for special X-ray examinations into humans the appearance of liver diseases were reported. Further, Th can be stored in bones and long-term exposure can lead to bone cancer [56].

Even though natural Th is radioactive and ubiquitous, its chemical properties are mainly utilized rather than its nuclear properties. The most revolutionary potential use of Th might be the application in nuclear industry. The theoretical feasibility of using Th as a

nuclear fuel for Th-based nuclear reactor has been recognized for a long time. The Th fuel cycle offers higher burn-up, longer reactor life cycles and most importantly less nuclear waste with no plutonium generation. While Th-232 itself is not fissile, it transforms into the fissile isotope of U-233 upon absorption of a neutron. Even though the performance of Th-232/U-233 fuel cycle has been demonstrated in pilot-scale studies, the use of Th-based nuclear reactors is still in debate [57].

➤ Uranium

Uranium along with Th are the only actinides which naturally occur in considerable quantities. Yet, U is important in nuclear energy as the main source of fuel for commercial nuclear power plants. The crustal abundance of U is 2.7 mg kg^{-1} [58]. Uranium is also commonly found in trace amounts in soil, rock, surface and groundwater, plants, and animals. It was discovered by the German scientist Martin Klaproth in 1789. Uranium is a very important element in the actinide series with atomic number of 92, the highest atomic weight of 238 among the NRs and the electronic configuration of $[\text{Rn}] 5f^3 6d^1 7s^2$. Higher concentrations of U can be observed in phosphate-rich soil and minerals like uraninite, brannerite and carnotite, but these concentrations are often below the ranges for uncontaminated soil. In its natural state, U occurs as an oxide ore, U_3O_8 along with additional oxides, UO_2 and UO_3 . The most common oxidation states of U are shown in Table 1.3.

Uranium has valences ranging from II to VI in the solid state where IV and VI are the most stable which show differences with respect to solubility, mobility and speciation. The hexavalent state, U(VI), is usually found in both solid-state and solution under oxidizing conditions, dominated by the uranyl cation, UO_2^{2+} at $\text{pH} < 2.5$. It is relatively soluble and undergoes complex formation with organic and inorganic ligands. The cation has a linear geometry that can coordinate with four to six ligands forming tetragonal, pentagonal and hexagonal bipyramidal polyhedral structures [59]. The mobility of U in soil is governed by this hydrated UO_2^{2+} cation which is responsible for its relatively high solubility over a wide range of soil pH. In the case of U(IV) which dominates under reducing conditions, relatively insoluble solid phases like uraninite are expected [60]. A similar coordination environment like Th(IV) occurs with a variable number of coordination states from 6-12 with 8 and 9 as the most common.

The study of the hydrolysis of U(VI) is quite complicated as it forms some oligomeric species. At low concentration such as $<10^{-6}$ M in natural waters, the dominant species is $\text{UO}_2(\text{OH})^+$ while at high concentrations, the oligomeric UO_2^{2+} species, such as $(\text{UO}_2)_2\text{OH}^{3+}$, $(\text{UO}_2)_2(\text{OH})_2^{2+}$, $(\text{UO}_2)_3(\text{OH})_4^{2+}$, etc. are formed [61]. About 90-100% of the dissolved U in the oceans mainly consist of uranyl carbonate complexes such as $\text{Ca}_2\text{UO}_2(\text{CO}_3)_3$ and $\text{CaUO}_2(\text{CO}_3)_3^{2-}$ [62, 63]. In natural environment, the uranyl aquo cation prevails under acidic conditions while hydroxide and phosphate complexes are mostly found under neutral and carbonate complexes are predominant under alkaline conditions [64]. The total solubility of U increases with increasing complex formation and at low pH. The bioavailability and uptake by plants correlates with solubility. The radioactivity of U is weak and contributes little to the natural background radiation levels in the environment. Three natural isotopes, U-238, U-235, and U-234 (Table 1.2), and several isotopes ranging from U-217 to U-242 are exist.

Table 1.3: The most common oxidation states of U and Th

	Oxidation states	Basic oxide compounds
U	IV, VI	UO_2, UO_3
Th	IV	ThO_2

Like Th, being naturally available in the environment, humans are always exposed to certain amounts of U from food, air, and water. Even though scientists have detected no harmful effects due to natural levels of U, chemical effects may occur after uptake of larger amounts of U with concomitant health effects. Further, long-term exposure of U through inhalation causes chronic lung diseases, acute leucopenia, anemia, necrosis of the mouth, and bone, cranial, and nasal tumors [65, 66]. Uranium is not likely to accumulate inside the body and even though gastrointestinal absorption from food or water can deposit U internally, those absorbed amounts of U quickly leave the body through urine and faeces. The major health concerns are kidney damage caused by the chemical toxicity of soluble U compounds and bone cancers by U deposition on bones. Radiologically much more relevant than U itself are some of its decay products, especially radon, which can build up in confined spaces, such as inside buildings, and then can contribute to an enhanced risk for lung cancer.

Nowadays, the primary use of U is as fuel in nuclear power reactors to generate electricity via production of thermal energy by nuclear fission of U-235. U-238 acts as a target material for producing plutonium (Pu-239 is produced when U-238 absorbs a neutron).

1.2.3. Mobility of the natural radionuclides in terrestrial systems

In general, NRs in the soil are classified into two groups, immobile and mobile radioactive elements [67]. Even though Th has been clearly identified to belong to the former category, radionuclides in the Th and U decay series (e.g. Rn and Ra) and U under certain (aerobic) conditions can be definitely mobile in the environment. The distribution and potential mobility of NRs in soil and the subsequent environmental toxicity depends on the occurring phases and the characteristic, on-site chemical-physical conditions. It is well-established that bioavailability, toxicity and mobility of these NRs in soils mainly depend on soil texture, pH, element concentrations, and organic matter content, and are thus controlled by a combination of complex processes. These processes may include (i) releases of trace elements through mineral solubilization or surface ion exchange with the subsequent transport as free ions or as aqueous complexes and/or (ii) environmental, site-specific colloidal transport from mineral erosion and/or sorption to scavenger phases and organic matter. The following sections will focus firstly on known scavenger phases and organic complexes responsible of NR mobility in terrestrial environments, and then on published experimental approaches used to identify potential mineral solubilization and solid carrier phases [13, 14, 20, 68-74].

1.2.3.1. Known potential solid scavengers and carrier phases

Th, U and REEs are mainly abundant as bound in refractory host minerals like monazite, cheralite, zircon and thorite. The mobility of U and Th in soils when released from a source is generally limited by their incorporation into sparingly soluble solid phases like phosphates and oxides, and/or adsorption to the soil matrix. Direct evidence for the adsorption of a substantial fraction of these elements onto clay minerals and hydrous oxides of Fe³⁺ and Al³⁺ is also available in the literature [75, 76]. In fact, sorption studies of Th and U onto a variety of minerals and phases has been reported in the literature, including: oxides and silicates [77-81], clays [82, 83], Fe oxides [84-88], alumina [89, 90], organic matter [91, 92], and silica [77-81].

Furthermore, minerals and compounds of Fe and their complexes with organic matter are very important in soil forming processes and they certainly influence element environmental dispersion and fate. The stability of these phases also varies among sites and chemical conditions, e.g., mineral solubility and trace element desorption from mineral surfaces increases with decreasing pH and decreases at high pH values [88, 93], explaining why higher availability and mobility of trace heavy metals, REEs and actinides are found in acidic soils [94]. Many researchers reported sorption of trace concentrations of U(VI) to Fe oxyhydroxides and found adsorption to be maximum at a pH of ~5 [95, 96]. *Quigley et al* reported that the sorption of Th onto hematite is rapid and equilibrium is attained within a few minutes [97]. *Hongxia et al* stated the strong sorption of Th to gibbsite over a wide pH range [98]. Some researches claimed that iron oxides/hydroxides and Fe-Al (hydr)oxides represent major binding phases for NRs in subsurface environments [70, 87, 93, 95, 97, 99, 100]. In addition, it was shown that colloidal Fe-Mn oxyhydroxides are capable of sorbing large amounts of trace metal ions [101]. Also, Th adsorption onto Fe-hydroxides is stronger than that of U and even significant at pH values as low as 2 [102]. Natural samples present a mixture of Fe containing species which may include not only the classical amorphous and crystalline phases but also Fe as potential free ions or associated to carbonates and /or organic matter.

The amount of natural organic matter may also play a relevant role causing potential mobilization and transport of NRs [46, 87, 103], and REEs [104, 105] in the environment. As humic acids are abundant in the environment, complexation by organic ligands can affect the physical and chemical properties of dissolved elements including actinides like Th and U as well as REEs [60, 70, 93, 103, 106-111]. In general, actinides interact with humics either involving redox reaction, Coulombic attractions due to net anionic charge of the humic or direct site-specific binding to surface functional groups on the humics [41]. In soil, the organic content involving humic substances under oxidizing conditions, tend to be degraded by microbes aerobically and anaerobically leading to the release of bound metals. The presence of humic acids as a competing ligand has a strong effect on the retention of heavy metals onto mineral phases [87, 112-114]. Evidence for the importance of soil organic matter concerning the complexation of NRs indicates that complexation by high-molecular-mass organic carbon (humic matter) predominates over low molecular mass organic and/or inorganic

complexation, at least for similar systems as the elements and the environment investigated in this work [115].

Noteworthy, kaolinite and Fe/Al oxides, together with smaller amounts of other components, dominate the clay fraction of lateritic soil. Clays as naturally occurring minerals typically contain admixtures. Clay particles which may dominate the colloidal phase are scavengers for actinides (Ac) like Th, U and lanthanides (Ln) [47, 116]. Clay minerals sorb primarily by surface complexation [117, 118] although additional contribution by cation exchange has been identified in some studies [119, 120]. From such particles, as well as from quartz [121, 122], Ln and Th can in principle be desorbed under favorable physicochemical conditions (i.e. low pH, high salt concentrations, presence of strongly complexing ligands). Especially, in the case of silica, sorption behavior of Th to silica reported in several ways in literature. *Östhols et al.* stated that Th sorption to silica takes place only in the pH range 3 to 6 while in the neutral to alkaline pH range, the hydrolysis of Th cause desorption from silica surface. He also added that it is also unlikely that silica will act as an efficient scavenger when the pH above 7 and the formation of Th-silica colloids at higher pH values decreases the sorption of Th onto silica [80]. Other studies reported Th shows strong sorption to silica over a wide range of pH [81, 123, 124].

1.2.3.2. Experimental approaches to identify potential scavenger and mineral-bearing carrier phases

Several methods exist in the literature to determine the potential mobility and transport of NR under natural conditions. These include extraction methods, quantifying the leachability of NRs through column-leaching experiments with non-vigorous conditions [125, 126] and/or by applying specific leaching steps for of target minerals using different reagents in batch extractions. In this study, batch extraction/leaching and column leaching approaches were used to estimate potential carrier phases and mimic the potential mobility of NRs in the localized natural system.

In general, chemical extraction protocols exist as tools for assessing mobility and bioavailability of NRs in the environment. The extractants are selected such that they are expected to lead to mobilization of ions or dissolution/degradation of targeted mineral lattices with gradual increase in extraction power. The results provide some

information about the different availabilities of NRs among different mineral phases [69]. Even though sequential schemes are frequently used for assessing availability and mobility of trace elements in soil matrices [127-130], there are some major shortcomings associated with sequential extractions. These include (1) potential re-adsorption and redistribution of the trace elements which are released during an extraction step and re-adsorbed onto an undissolved phase, (2) loss of sample during intermediate washing steps to remove excess extractant solutions, (3) non-selectivity of certain reagents to specific solid samples, and (4) incomplete dissolution of the targeted mineral fractions and change in pH from the previous step [131, 132]. As an example of the lack of complete selectivity of reagents, the metal fraction recovered in the second step of the Tessier protocol, i.e. the carbonate fraction, NaOAc/HOAc, might be present as co-precipitate with carbonate minerals but also specifically sorbed to some sites of the surfaces, particularly on clays, organic matter and Fe/Mn oxyhydroxides [132]. Despite the need for larger amounts of sample, single extraction methods have been widely employed for faster analysis and they may help circumvent some of the aforementioned shortcomings of sequential extractions [133-135]. In any case, selective extractions are used to characterize operationally defined carrier phases of given trace metals in soil [136]. That is, the outcome of these extraction protocols should be considered and interpreted with care since the individual schemes are defined “operationally” and are not specifically assigned to selectively extract a particular metal ion or soil component [137].

Furthermore, since the optimum selection of a certain scheme for NRs is still unclear, many protocols are available in the literature which are, moreover, modified from the one originally developed by Tessier et al. [127, 129, 131] and the BCR (Bureau Communautaire de Référence) method [138]. In fact, many studies revealed and confirmed that the results obtained for the same samples using different protocols yielded different results [139, 140]. For now, most common protocols applied for Th extractions, along with the common Tessier and BCR protocols, are shown in the Table 1.4. A summarized description about the specific use of each chemical and the applied chemical extraction protocol in this study is shown in Table 1.5 [132, 136, 141-144].

Table 1.4: Selected extraction protocols for the extraction of Th and U in soil and sediment samples

	Extraction Steps				
	F1	F2	F3	F4	F5
Tessier et al. (1979) [127]	Exchangeable 1 M MgCl ₂ at pH 7	Carbonates 1 M NaOAc/HAc at pH 5	Fe-Mn oxides 0.04 M NH ₂ OH.HCl in 25% (v/v) HAc	Organic matter 30% H ₂ O ₂ / 3.2 M NH ₄ OAc	Residual HF/HClO ₄
Revised BCR [138]	Water and acid soluble, exchangeable, carbonates 0.11 M CH ₃ COOH	Fe-Mn oxyhydroxides 0.5 M NH ₂ OH.HCl at pH 1.5	Organic matter and sulphides 8.8 M H ₂ SO ₄ /1 M CH ₃ COONH ₄	Residual Aqua regia 1 part HNO ₃ +3 parts HCl	
Martinez-Aguirre and Perianez [145]	Carbonates 1 M NaOAc/HAc at pH 5	Organic matter and/or amorphous oxides 0.1 M Na ₄ P ₂ O ₇ / NaOH at pH 9.8	Amorphous Fe-Mn oxyhydroxides 0.2 M NH ₄ C ₂ O ₄ /0.2 M H ₂ C ₂ O ₄	Crystalline Fe-Mn oxides 0.175 M sodium citrate/0.025 M citric acid	
Guo et al. [133]	Exchangeable 1 M MgCl ₂ at pH 7	Carbonates 1 M NaOAc/HAc at pH 5	Organic matter and/or amorphous oxides 0.1 M Na ₄ P ₂ O ₇ / NaOH at pH 9.8	Amorphous Fe-Mn oxyhydroxides 0.2 M NH ₄ C ₂ O ₄ /0.2 M H ₂ C ₂ O ₄	Crystalline Fe-Mn oxides Sodium dithionite in 0.175 M sodium citrate/0.025 M citric acid
Kaplan and Serkiz [130]	Exchangeable 0.44 M CH ₃ COOH/0.1 M Ca(NO ₃) ₂	Organic matter 0.1 M Na ₄ P ₂ O ₇ / NaOH at pH 9.8	Amorphous Fe-Mn oxyhydroxides Tamm's acid oxalate 0.175 M NH ₄ C ₂ O ₄ /0.1 M H ₂ C ₂ O ₄	Crystalline Fe-Mn oxides Coffin's reagent Sodium dithionite in 0.15 M sodium citrate/0.05 M citric acid	Residual Aqua regia 1 part HNO ₃ +3 parts HCl

Table 1.5: Description of the chemicals used in the chemical extraction protocol in this study

Exchangeable fraction	<ul style="list-style-type: none"> Does not attack organic matter, silicates or metal sulfides in soil.
➤ MgCl ₂	<ul style="list-style-type: none"> Decrease of pH also been observed that may lead to partial dissolution of carbonate and Mn-oxide fractions
Acid soluble fraction/carbonate	<ul style="list-style-type: none"> Suitable for soils with low carbonate content. Sensitive to pH changes.
➤ NaOAc/HOAc	<ul style="list-style-type: none"> Recover metals co-precipitated with carbonate minerals. But metal ions specifically sorbed to some sites of the surface of clays, organic matter and Fe/Mn oxyhydroxides can be also extracted. Lowering pH from 7 (F1) to 5 would release the remaining specifically adsorbed trace-metal ions that escaped extraction in F1.
Organic	<ul style="list-style-type: none"> Promotes the dispersion of organic colloids in basic medium.
➤ Na ₄ P ₂ O ₇	<ul style="list-style-type: none"> Targets OM bound to mineral surfaces via ligand exchange and cation bridging as well as MO in metal-OM complexes Useful chelating agent to solubilize organic compounds precipitated by metallic cations (Ca, M, Al, Fe) Does not affect amorphous or crystalline Fe and Al oxyhydroxides Solubilizes some amounts of strongly adsorbed organic compounds due to relatively high pH
Amorphous Fe-Mn oxyhydroxides	<ul style="list-style-type: none"> High Fe complexing capacity (Fe(III)-C₂O₄²⁻) and low reducing properties. Appears to be specific for amorphous iron phases with low degree of crystallinity.
Tamm's acid oxalate (in dark)	<ul style="list-style-type: none"> Solubility of iron oxides depends on nature and concentration of surface hydroxyl groups and so decreases with the degree of crystallinity. Can also enhance solubility of other mineral phases beside Fe-oxi/hydroxides
➤ 0.2 M NH ₄ C ₂ O ₄ /0.2 M H ₂ C ₂ O ₄	<ul style="list-style-type: none"> Oxalate action is light sensitive; UV light could have an enhancing effect which could destroy crystalline iron oxides. Presence of an oxalate-Fe(II) complex in solution would act as a catalyst and promote Fe(III) reduction. Extract Fe from organic complexes, not considered as a specific reagent of amorphous iron oxides.
Crystalline Fe-Mn oxyhydroxides	<ul style="list-style-type: none"> Strongly reducing agent. Dissolves well-crystalline Fe oxides and other redox sensitive oxides such as Mn(IV) oxides. Add a strong ligand like sodium citrate to avoid precipitation of FeS.
➤ Na ₂ S ₂ O ₄	<ul style="list-style-type: none"> This fraction approximates the combined content of amorphous and crystalline Fe oxides.

Due to all the complications involved in using extraction protocols, above and beyond the general knowledge concerning the soil properties, this study complements selective extractions with direct mineral characterization of given samples. This approach will provide better understanding of the different chemical forms or ways of binding of trace elements of interest in natural soils. This information will help identifying potential solid phases and carriers of trace elements, and thus, could help to predict the behavior of NRs and their potential bioavailability once mobilized in terrestrial systems. It is, however, also clear that the interpretation of results obtained from individual extraction protocol steps will need to be critically discussed.

1.2.4. Areas with high natural background radiation levels on earth

In general, one third of the total annual effective dose is from external exposure and two thirds from the internal exposures for areas with normal background radiation levels (Table 1.1). In contrary, these values obviously deviate for high background radiation areas (HBRAs). HBRAs, which occur in several regions on the planet based on both natural and anthropogenic sources, exhibit unusually high radiation levels ranging up to 100 times or more the average values of the world.

Proper global investigations of HBRAs from natural sources are of interest from several aspects; (1) exploration of natural radio-mineral sources regarding geological and geochemical interests, (2) implementation of remedial actions to prevent unwanted human exposure, (3) assessment of human exposure risk by direct observations of the effects cause by the higher doses of natural radiation, (4) application of the data obtained from radiobiological and epidemiological studies to educate the public against irrational fears of radiation (radiophobia), and (5) determination of natural radioactivity levels in detail concerning man-made sources, i.e. identifying anthropogenic contaminations [146].

There are numerous localized areas with high levels of natural radiation in the world and such areas are well known in countries like Brazil, China, India, Egypt, Iran, Sweden, Austria, France, etc. Small areas in these countries show markedly elevated absorbed dose rates in air due to various natural phenomena. Some areas are characterized by monazite sand deposits, which have high levels of Th, for examples Guarapari and Meaipe in Brazil, Yangiang in China, the states of Kerala and Madras in

India, and the Nile delta in Egypt. Some sites involve volcanic soils such as Mineas Gerais in Brazil, Niue Island in the Pacific and parts of Italy while others exhibit high natural radioactivity content in water from some hot springs such as Ramsar and Mahallat in Iran. Since this study is mainly focused on soil samples, some of the HBRA related to monazite beach sand and soil were selected for further discussion.

➤ Selected worldwide known cases

a) Brazil: Guarapari and Meaipe are two coastal cities in Brazil in the monazite sand region along the Atlantic coast in Brazil, one of the most widely known HBRA in the world. The absorbed dose rates in air are found to range from 1 – 10 $\mu\text{Gy h}^{-1}$ in outdoor and up to 87 $\mu\text{Gy h}^{-1}$ at selected spots on the beach, and the average effective dose rate from terrestrial irradiation (outdoor and indoor) is 1.5 mSv yr^{-1} [147, 148]. In some other studies, up to 38 $\mu\text{Gy h}^{-1}$ were detected, particularly on beaches, due to the high Th content with traces of U in the beach sand minerals. Dose rates from 1 – 32 mSv yr^{-1} in Guarapari, up to 40 $\mu\text{Gy h}^{-1}$ in a particular storage room of a monazite separation plant, 1.3 $\mu\text{Gy h}^{-1}$ in the streets of Meaipe, and an average level of 0.5 $\mu\text{Gy h}^{-1}$ in Cumuruxatiba streets were also reported in those studies [146, 149, 150].

b) China: The city Yangiang, located in southern China, is also famous for elevated radiation levels. Based on the geological history, it is believed that monazite in mountains with granitic surface rocks, was washed out by rain and radionuclides containing fine particles of monazite accumulated in the basin in this region resulting in a HBRA. In an early study, the average total annual effective dose rate in this area was 5.4 mSv yr^{-1} [151]. The reported ambient gamma dose rates for indoor and outdoor are 0.1 – 0.4 $\mu\text{Gy h}^{-1}$ and 0.1 – 0.2 $\mu\text{Gy h}^{-1}$, respectively, while the estimated dose rate range received from terrestrial radiation is 0.6 – 1.8 mSv yr^{-1} [152].

c) India: Among the localized HBRA in India, especially Kerala coast, Tamil Nadu coast, Orissa, and Chavara-Neendakara, Kerala and Tamil Nadu coasts have similar levels of absorbed dose rate ranges in air from 0.2 – 4.0 $\mu\text{Gy h}^{-1}$ [146, 153, 154]. In Kerala, the average radiation level was estimated to be 15.7 mSv yr^{-1} while in Tamil Nadu it was 20 – 40 mSv yr^{-1} [146]. Soil samples collected from some locations of the Tamil Nadu area showed gamma dose rates in air in less than 0.2 $\mu\text{Gy h}^{-1}$ with a mean value of 0.1 $\mu\text{Gy h}^{-1}$ [155, 156]. In Orissa beach sands, it is in the range of 0.7 – 3.2 $\mu\text{Gy h}^{-1}$ with a mean value of 1.9 $\mu\text{Gy h}^{-1}$. The annual external effective dose rates in

this area varied from 0.8 to 3.9 mSv yr⁻¹ with an average of 2.4 mSv yr⁻¹ [157], and Chavara-Neendakara shows 1.5 – 28.4 µGy h⁻¹ with an average of 9.8 µGy h⁻¹ [153]. The annual effective dose rates values in this region varied from 1.2 to 9.3 mSv yr⁻¹ with an average value of 1.2 mSv yr⁻¹ [153]. At Kalpakkam coast elevated background radiation levels in the range of 0.3 – 2.7 µGy h⁻¹ with a mean of 1.1 µGy h⁻¹ in the coastal sands were reported and that of the soil samples in this area is less than 0.6 µGy h⁻¹ with a mean of 0.1 µGy h⁻¹ [154].

d) Egypt: Soil samples in some areas close to the Nile delta exhibit higher concentrations of natural radioactivity due to the presence of black sand rich in heavy minerals containing Th. One of the published studies, some soil and sediment samples collected over the entire River Nile basin and its delta reported absorbed dose rates are less than 0.06 µGy h⁻¹ with an outdoor annual effective dose rate in air is < 0.07 mSv yr⁻¹ for both soil and sediment samples [158]. In an another study, for soil samples collected from the northwestern area of the Nile delta an average absorbed dose rate 0.04 ± 0.02 µGy h⁻¹ and annual effective dose rate of 0.05 ± 0.02 mSv yr⁻¹ was obtained [159] while the values for the sediment samples from the Upper Nile river for absorbed dose rates are < 0.04 µGy h⁻¹ [160]. Further, soil samples from Southeastern Nile Delta showed a range between 0.03 and 0.07 µGy h⁻¹ absorbed dose rate and less than 0.2 mSv yr⁻¹ average external outdoor exposure [161].

The comparison of activity concentrations of main NRs and their corresponding absorbed dose rates in the above selected cases in the world with known cases in Sri Lanka and the current location are summarized in Table 1.6.

Table 1.6: Comparison of activity concentrations of U-238 (Ra-226), Th-232, and K-40 and corresponding absorbed dose rates (D_R) in surface sand and soil samples from different areas in the world, some areas of Sri Lanka, and the study area. The values inside brackets represent the average

Location	Type of sample	U-238	Th-232	K-40	D_R ($\mu\text{Gy h}^{-1}$)	Ref.
		Bq kg^{-1}				
<u>Selected worldwide known cases</u>						
Brazil (Guarapari and Meaipe)	Beach sand	10 – 4100	20 – 57000	70 – 3000	<90	[146-150]
China (Yangiang)	Monazite particles	2 – 690	1 – 360	9 – 1800	0.4 average	[1, 152]
India (Kerala, Chavara-Neendakara, Orissa, Kalpakkam)	Beach sand	40 – 41280	230 – 6020	100 – 2530	0.2-4.0	[153, 154, 157, 162]
India (Kalpakkam, Orissa, Tamil Naadu)	Soil	5 – 70	5 – 780	15 – 850	<0.6	[154-156]
Egypt (Nile Delta)	Soil and sediment	2 – 120	2 – 96	29 – 650	<0.4	[1, 158, 159, 163]
World average	Soil	35	30	400	0.06	[1]
<u>Specific known cases for Sri Lanka</u>						
East coast deposits (Pulmudei)	Beach sand	300-650 (540)	630-1670 (1160)	130-175 (170)	0.5-1.3	[164]
Southwestern coastal strip (Beruwala to Crow Island)	Beach sand	7-3150 (450)	11-19600 (2100)	14-1210 (220)	<13.7	[165]
Western coastal strip (Uswetakeyyawa to Chillaw)	Beach sand	7 – 1240 (299)	14 – 6260 (1032)	170 – 650 (335)	<4.6	[166] [167]
Southern coastal strip (Hambanthota to Dondra)	Beach sand	4-1730 (280)	1-10750 (1290)	50-850 (200)		
Sri Lanka (Average)	Soil	5 – 760 (50)	10 – 1170 (140)	20 – 1380 (310)	-	[168]
<u>Target area of the current study</u>						
Kawudupalella, Matale	Soil	320 – 510 (370)	4440 – 7040 (6225)	340 – 540 (470)	2.9-4.6	Present study

➤ *Specific known cases for Sri Lanka*

Some highlighted HBRAs in Sri Lanka are included in Table 1.6. When comparing the results of in-situ natural radiation measurements by the Sri Lanka Atomic Energy Board (SLAEB) with other regions in Asia, Sri Lanka has the highest average Th-232 concentration in soil. The mean value of Th radioactivity in Sri Lankan soil is 138 Bq kg⁻¹ and the range is 9 – 1166 Bq kg⁻¹ according to a study in 2013 [168] while the global average of natural Th-232 content in sediments is 30 Bq kg⁻¹ (range from 11 to 64 Bq kg⁻¹) according to the UNSCEAR 2000 [1]. It is known that Sri Lankan beaches are rich in various industrially valuable minerals, involving ilmenite, rutile, quartz, and zircon. Areas with high background radiation levels due to Th-rich monazite were identified along with the aforementioned beach sand minerals in the coastal areas of the country [169]. Usually monazite is associated with ilmenite and other heavy minerals in beach sands. In addition, other elements of economic interest (i.e., the technology critical elements) such as rare earth elements (REEs) like Lanthanum (La), Cerium (Ce), Neodymium (Nd) also associate with the monazite crystal structure [170-173]. The East Coast deposits in Pulmudei and Kokilai are the largest Th-bearing beach sand deposits in Sri Lanka. Recent research on the soil samples from a placer deposit of monazite in Pulmudei reported an average gamma ray absorbed dose rate of 1.0 (0.5 – 1.3) μGy h⁻¹, mean background radiation level detected by survey meter of 23.4 (14.4 – 28.8) mSv yr⁻¹ and mean effective dose rate of 1.2 (0.6 – 1.6) mSv yr⁻¹ [164]. In another study, sand samples collected along the southwestern coastal strip of Sri Lanka from Beruwala to Crow Island showed that the estimated dose rate at 1 m above ground was < 13.7 μGy h⁻¹, the effective annual gamma dose rate in the area ranged from 0.004 – 16.8 mSv yr⁻¹ [165]. Additionally, sand samples collected from the coastal strip between Uswetakeyyawa and Chillaw on the West Coast of Sri Lanka showed that the calculated external annual effective dose rate was < 4.6 μGy h⁻¹ [166]. Similar mineral sand deposits were found in several coastal areas around the country including the southern coastal strip between Hambanthota and Dondra [167].

In 2015, a base line environmental monitoring program was conducted by the Sri Lanka Atomic Energy Board (SLAEB) in collaboration with the Geological Survey and Mining Bureau (GSMB) of Sri Lanka. The objective was to collect data for the concentrations of natural and artificial radionuclides in near surface soil and plants.

During this project, the Sri Lanka land area was divided into 400 squares and the corresponding soil and grass sampling was carried out. The subsequently published one meter height dose distribution map of Sri Lanka for the overall radioactivity concentrations of soil, and corresponding radionuclide distributions are shown in Figure 1.3 [174].

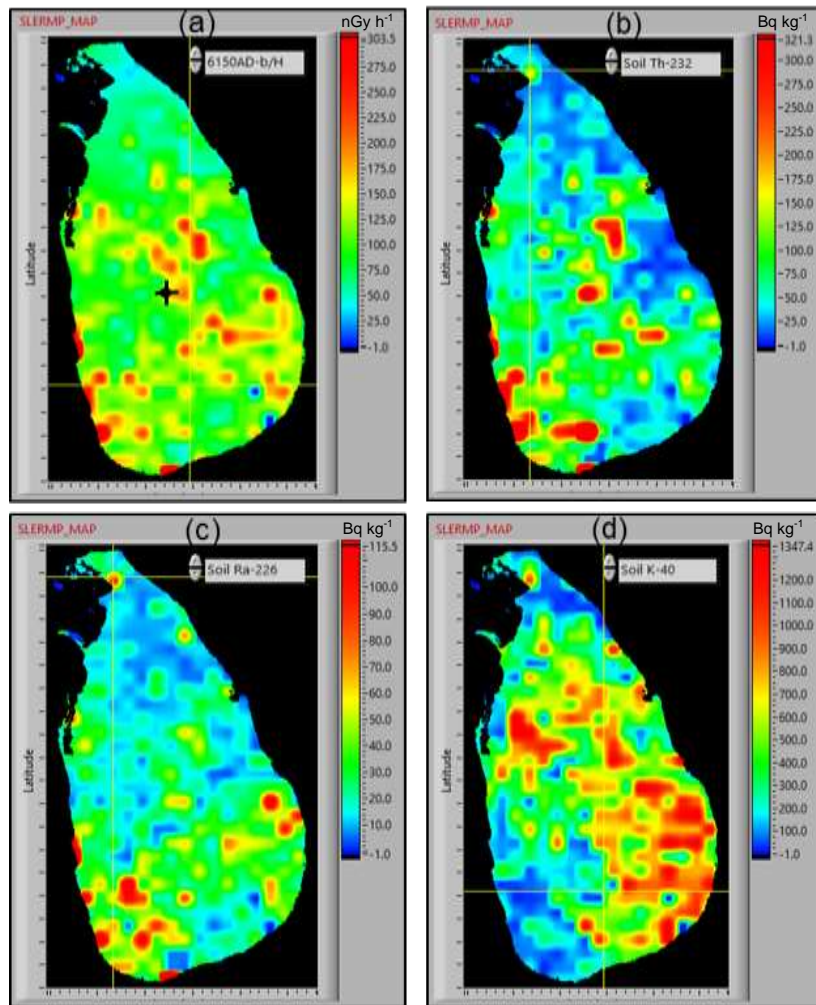


Figure 1.3: (a) One meter height dose distribution map of Sri Lanka (black dot with the cross shows the exact location, the school playground) and corresponding radionuclide distributions; (b) Th-232, (c) Ra-226 and (d) K-40 in soil

➤ Target area of the current study

Some elevated radiation levels in the inland of Sri Lanka were discovered during this project and a specific location was selected for the present study as this location is the playground of a school. The above exploration yielded measured background radiation levels at one-meter height above the ground of $2.5 \pm 1.2 \mu\text{Gy h}^{-1}$ with a maximum contribution of $21.6 \pm 10.9 \text{ mSv yr}^{-1}$ [174].

The study area of interest is located in Kawudupelella village, Matale District, Central Province, Sri Lanka and the exact sampling location is the playground of a school named “Kawudupelella Sinhala Vidyalaya” (Figure 1.3a). The school was inaugurated in 1953 and there have been 346 pupils in this school up to date, and the playground was created in 2011. The population around this area was ~1400 according to the census of population and housing of Sri Lanka in 2012 and about 200 people live close to the location.

The school is situated at the eastern side of a small valley with 7.58 °N 80.63 °E GPS coordinates, ~362 m above the sea level. The maximum average temperature in this area during the day is 26° - 30 °C and the average annual rainfall is between 1500 mm and 2000 mm. The second inter-monsoon period in October and November yields the maximum rainfall [175].

One part of the playground is covered by a forest (Figure 1.4a) and the other bare part has a slight slope next to a school building (Figure 1.4b). A more systematic graphical side view of this location is shown in Figure 1.4c.

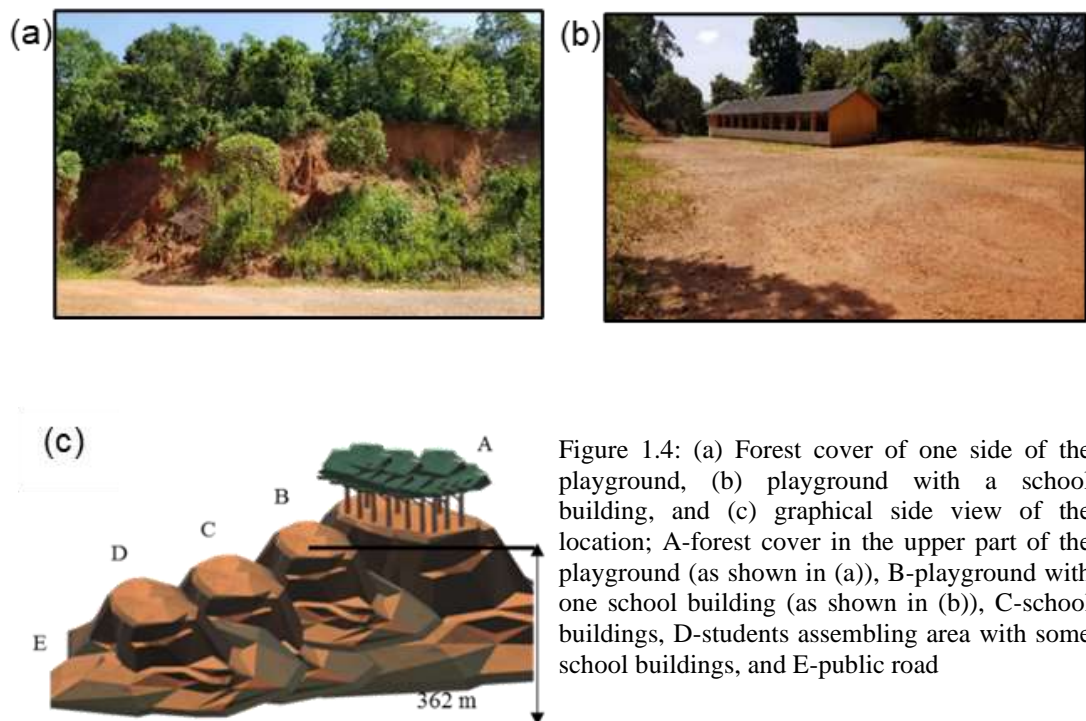


Figure 1.4: (a) Forest cover of one side of the playground, (b) playground with a school building, and (c) graphical side view of the location; A-forest cover in the upper part of the playground (as shown in (a)), B-playground with one school building (as shown in (b)), C-school buildings, D-students assembling area with some school buildings, and E-public road

The location is characterized by a host rock of quartzofeldspathic gneisses with pegmatitic intrusions in the upper area of the playground. Marble, quartzite, khondalite,

garnet-sillimanite-biotite gneisses are the major mineral types in Matale District. The soil type is predominantly laterite, where kaolinite and Fe/Al oxides with smaller amounts of other components typically dominate the clay fraction. According to *Ranasinghe et al.*, laterite soil is formed under high temperature and heavy rainfall conditions with alternating wet and dry periods [176]. It is a reddish clayey rock material. Such soils exhibit high specific surface area, porosity and permeability, but no specific values according to the classification were given by the aforementioned authors. Lateritic soils are acidic in nature [176], acidic soils being defined as having pH less than 5.5 for most of the year [177].

2. EXPERIMENTAL

Both on site and laboratory approaches were used to obtain complementary information on the geochemical environment, the speciation of target elements in solid phases and the leaching behavior of these elements under different conditions. This includes several sampling campaigns, conventional and advanced characterization techniques, batch and column experiments, and finally some simplifying geochemical modelling.

2.1. On site measurements and sampling procedures

The soil sampling campaign took place on July 15th, 2017 after obtaining a proper approval from the school authority. A weekend was selected to avoid any disturbance concerning the activities of the school. The meteorology on that day involved sunny weather around 32 °C with no rain and the humidity was about 60%.

2.1.1. Gamma measurements

Four sampling points were selected according to preliminary screening and after having detected high background radiation levels at one-meter height above the ground using a radiation survey meter equipped with a NaI scintillation detector (model: Automess 6150 AD5/H). The device has in addition a built-in GM counter which makes it very sensitive in environmental radiation monitoring. This detector was issued by the General Scientific Division of SLAEB, Sri Lanka.

2.1.2. Sampling and pre-treatment of soil

The GPS coordinates of the selected points in the playground, where the four soil samples were collected, are: L-03 (07° 34.687', 80° 37.695'), L-04 (07° 34.691', 80° 37.695'), L-05 (07° 34.699', 80° 37.689'), and L-06 (07° 34.707', 80° 37.683') (Figure 2.1). Since this area may have been contaminated with building materials during the construction of the school buildings, the top layer of the soil was removed to minimize the presence of any anthropogenic construction materials. Then a mass of about 1 kg of soil per location was collected by scooping up from a depth of 10 – 20 cm below the surface with a shovel. All samples were packed in polyethylene bags separately, labelled, and transported to the SLAEB laboratory in Sri Lanka. Non-target materials, such as plant debris and large stones, were manually removed in the laboratory. After

air-drying for 24 hours, the soil samples were sieved through 2 mm mesh-sized sieves. All samples were packed in plastic securitainer containers separately for each location, labelled, and sealed. These samples were then shipped to Germany in November 2017 after having obtained approval from GSMB, Sri Lanka and the relevant German authorities.



Figure 2.1: Aerial view of the study area; numbers denote the sampling locations and labels are in accordance with the Figure 1.3c

2.1.3. Sampling of potable water

Potable water samples were sampled for analysis in order to verify ground water contamination by Th, U or REEs and to obtain the drinking water composition in that area since the majority of the households nearby rely on private groundwater wells. The underground water table in this area is at about 3 – 4 m depth with flow in SE direction. The digital elevation map (DEM) of the surface water runoff basin is shown in Figure 2.2 along with the water sampling locations and the actual images of the sampling location are shown in Figure 2.3.

Two in-situ water sampling campaigns were carried out close to the above location. The first took place on January 9th, 2020 and the other on February 21st, 2020. The meteorology of the first day was sunny with an average temperature of 33 °C and no rain. On the second day, the average temperature was around 30 °C with rain.

Sampling tubes of 15 mL, HDPE bottles of 50 mL and the Teflon bucket used to collect water samples from wells had been previously soaked in HNO₃ acid and washed thoroughly with de-ionized water in a laboratory at the National Institute of Fundamental Studies (NIFS), Sri Lanka, before taking the material to the site. The locations were selected such that water samples from locations WL-01, 04, 05, and 06 were from private wells, location WL-02 was a spring well, and location WL-03 involved tap water from a water purification plant.

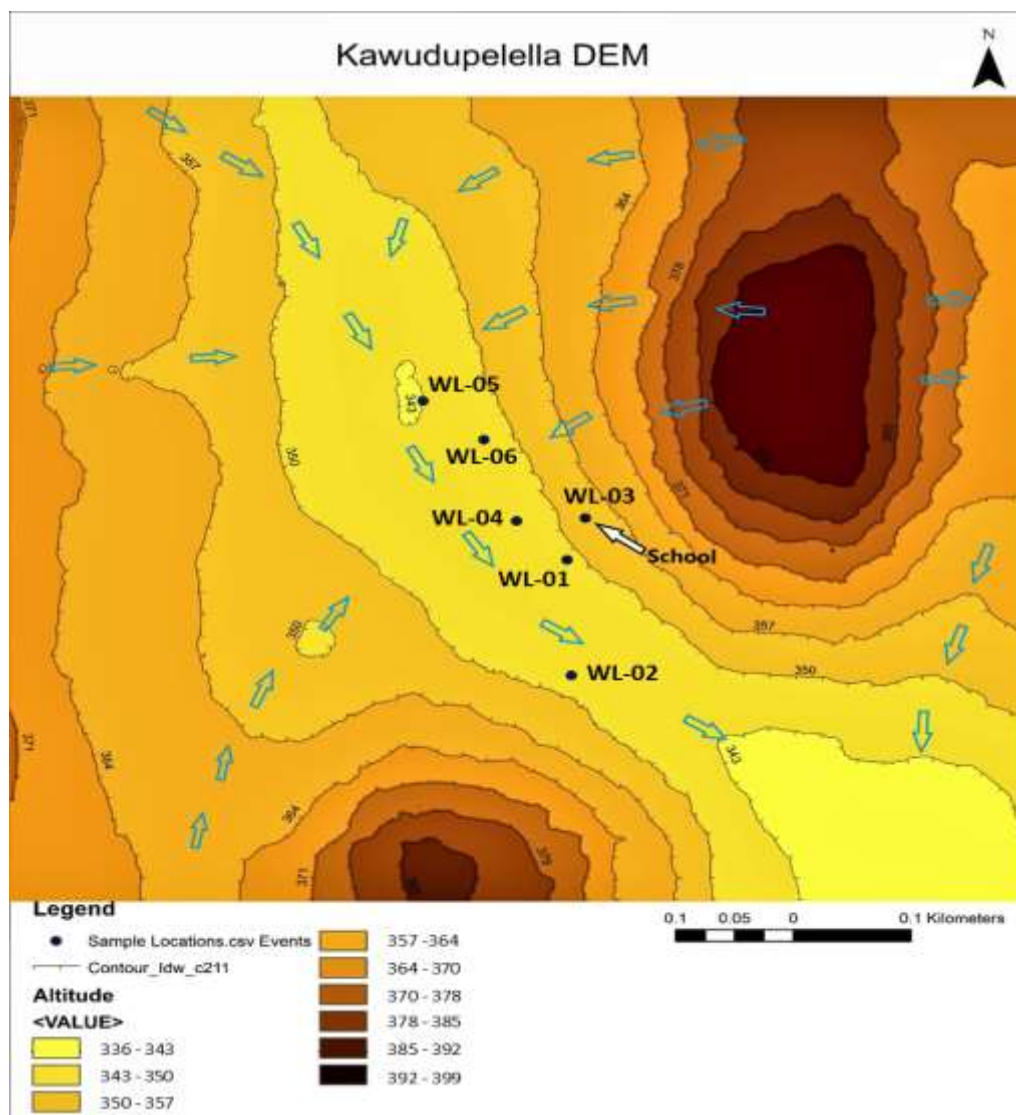


Figure 2.2: Digital elevation map (DEM) of the surface water runoff around the location and water sampling locations are denoted by WL

The bucket was thoroughly rinsed initially with water of each location before taking the final samples. Water samples from the wells and the spring well were collected ~ 1 m depth below the water surface. The in-situ measurements of pH, total dispersed solid

(TDS in mg L^{-1}), and conductivity of the water samples were obtained for each location using field equipment. Each sampling tube was thoroughly rinsed with the corresponding water sample at each location. One sample set was collected at each location without filtering and without acidifying for anion analysis. For the rest of the samples, two filter sizes, $0.20 \mu\text{m}$ and $0.45 \mu\text{m}$, were used and triplicates were collected from each location for each filter size. One drop of ultrapure HNO_3 was added to each 10 mL sample volume. Samples from the first day were transferred to the Geological Department, University of Peradeniya for ICP-MS analysis while the samples from the second day were directly sent to Germany.

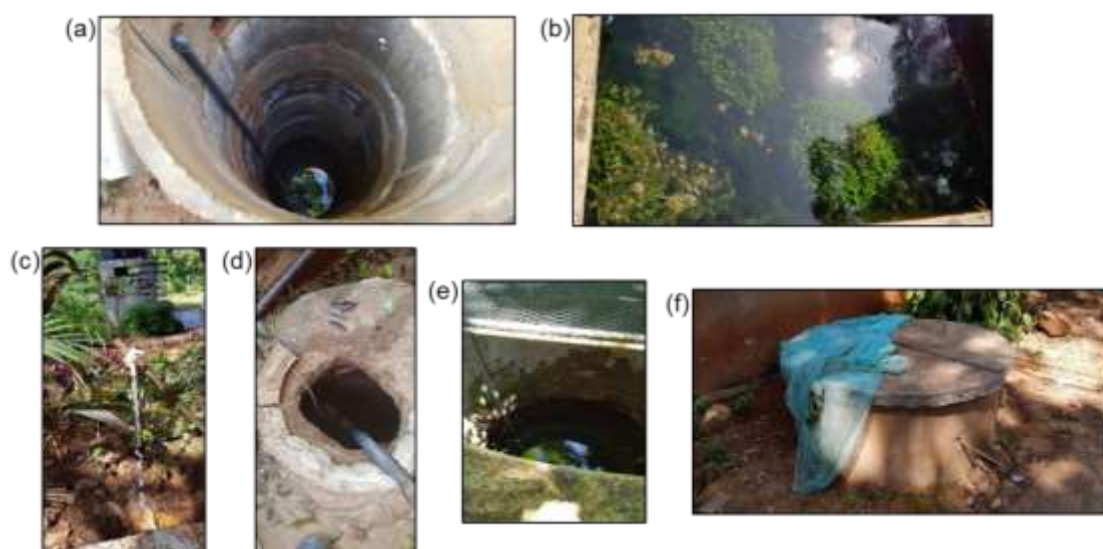


Figure 2.3: Images of the water sampling locations; (a) WL-01, (b) WL-02 (Spring well), (c) WL-03 (Tap water), (d) WL-04, (e) WL-05, and (f) WL-06

2.1.4. Sampling of grass

Grass samples were collected to investigate the potential bioaccessibility of NRs to plant material in the vicinity of the playground. The sampling was done in parallel to the first in-situ water sampling. From some grassy areas next to the forest side of the playground two grass samples were transferred into polyethylene bags and labelled. These samples were then transferred to SLAEB for gamma spectroscopic and XRF measurements.

2.2. Chemicals and solution preparation procedures

All dilutions and solution preparations were carried out using ultrapure water obtained from a Milli-Q system (Millipore Milli-Q Advantage A10 with Milliporepak® 400.22

μm , 18.2 M Ω .cm at 25 °C and maximum 4 ppb TOC). All chemicals were purchased from Merck (Germany), Alfa Aesar (Germany), VWR chemicals (USA and Belgium), Carl Roth (Germany), and Honeywell (USA) and were of analytical reagent grade. Details of all the chemicals used in this study are given in Appendices (Table A2.1).

2.3. Solid phase characterization in the laboratory

2.3.1. Radioactivity measurements, sample preparation and radiation dose/radiation risk assessment calculations

The specific activities of radionuclides in the air-dried soil samples were determined by gamma spectrometry both at SLAEB and INE while the grass samples were analyzed only at SLAEB to overcome the quarantine issue for the plant materials which would have been obligatory for transportation to Germany.

At SLAEB, the gamma spectrometer was equipped with a high purity germanium detector, P-type Coaxial HPGe (model: Gx3020), with a relative efficiency of 32.6% in horizontal cryostat and an energy resolution of 1.84 keV at 1.3 MeV gamma line of Co-60. The detector calibration was done using IAEA certified reference material, a standard soil of known radioactivity - Soil 6, a point source, containing Cs-137 and Co-60 for gamma energies of 661.5 keV for Cs, and 1173.2 and 1332.5 keV for Co. Spectra were analyzed using GENIE 2000 data acquisition Canberra software. The counting time was 72,000 seconds. The specific activities of K-40, Ra-226, Th-232, and Pb-210 were obtained. For the estimation of radium, energy peaks of 186.1 keV from Ra-226, 609.4 and 1764.5 keV from Bi-214 were used while for Th-232 estimation, 911 keV from Ac-228, 238.6 keV from Pb-212, 583.1 and 2614.5 keV from Tl-208 were used. Note that this requires Th-232 being in secular equilibrium. Notably for the first daughter nuclides of Th-232, Ra-228 with a half-life of 5.7 a, this is not necessarily the case. The derivation of Th-232 activity from Ac-228 activity and following progenies will be correct for refractory minerals but needs to be considered with care for sample having experienced significant chemical alteration. For K-40 estimation, the photo peak energy of 1.46 MeV emitted by potassium itself was used [178]. Details about the energy peaks of the progenies used to analyze the gamma data are shown in Appendices (Table A2.2).

At INE, the gamma spectrometer was equipped with an N-type pure Germanium Semi-Coaxial detector (model: GR3019-7500SL). The relative efficiency at 1.3 MeV is $\leq 30\%$ and the energy range is 5 keV – 10 MeV. Detector calibration involved IAEA certified reference material (RGTh-1 IAEA), a point source, made by the dilution of a Th ore OKA-2 (2.89% Th, 219 $\mu\text{g U/g}$) with floated silica powder of similar grain size distribution. Only Th-232 activity was measured. However, data related to this analysis will be given in Appendix 3.1.

2.3.1.1. Soil sample preparation for gamma analysis

Samples were vigorously shaken in the bags and emptied onto clean dry surfaces separately. Then the samples were smoothed out to a thickness of approximately 2 cm and divided into ~5 cm grid squares. A small amount of sample was taken from each grid and placed into a sub-sample container (49×85 securitainer) such that the sub sample corresponded to approximately 10% of the total mass. Containers were sealed to prevent the escape of radiogenic gases (Rn-222 and Rn-220 generated from U-238 and Th-232 decay series, respectively). Samples were kept for one month to attain Rn-222 and its short-lived decay products in secular equilibrium with Ra-226 and then subject to gamma spectrometric analysis. In addition, Rn-220 has a very short half-life (55 s) and if it escapes from the sample container, it disrupts the decay repopulation of the remaining isotopes in the Th-232 decay series thereby lessening the intensity in gamma emissions.

2.3.1.2. Grass sample preparation for gamma and X-ray fluorescence spectroscopic analysis

The collected grass samples were washed several times under running tap water to remove any possible external contamination due to soil particles/dust and were air-dried for some days in a tray to remove moisture from the sample. After air-drying, the samples were packed in plastic containers (49×85 securitainer) and the exact dry weight of each was determined. Then the containers were properly sealed and left about one month to bring Rn-222 and its short-lived decay products into secular equilibrium with Ra-226. Under those conditions, the nuclide pair Ra-224 and Rn-220 in the Th-232 decay series is also equilibrated.

The XRF analysis of the grass samples were carried out at SLAEB, laboratory for Life Sciences. The grass samples were ground and sieved through 62 μm mesh sieve and pellets were produced from this material. Those pellets were then subjected to ED-XRF (model: Canberra M SL30165 XRF detector). The XRF technique will be described in section 2.3.4.

2.3.1.3. Gas sample preparation for radon/thoron analysis

Masses of about 100 g of each soil sample were transferred into 500 mL glass bottles separately, properly closed to avoid any gas leakage, and kept for nearly one month before the measurements. The measurements were carried out via a professional portable measuring system designed to continuously determine airborne radon and thoron concentrations (AlphaGUARD DF2000, Bertin-Instruments) using a flow-through method. Continuous radon/thoron operation mode was used for the analysis by setting the flow rate to 2 L min^{-1} and running the measurement for 10 minutes, where the air is sucked in during the first 3 minutes of each 10-minute measuring cycle.

2.3.1.4. Evaluation of radiological doses

Gamma-ray radiation hazards caused by specific radionuclides of Ra-226, Th-232 and K-40 can be evaluated in different ways and therefore it is very important to assess the radiation hazard to humans from different radiological hazard indices. The following are the most widely used radiation hazard indices to identify radiological effects in worldwide [1, 179-183].

a) Soil

➤ Absorbed dose rates in air (D_R)

The absorbed dose rates in outdoor air, D_R (nGy h^{-1}), at 1 m height above the ground were estimated from the radionuclide activity concentrations of K-40, Ra-226, and Th-232 in the studied soil samples using Eq.2.1 [184] to ensure uniform distribution of radionuclides. The parameter D_R can be used to assess any radiological hazard and radiation exposure from radionuclides in the soil.

$$D_R (\text{nGy h}^{-1}) = 0.0414 A_K + 0.4611 A_{Ra} + 0.623 A_{Th} \quad (\text{Eq. 2.1})$$

This involves the dose coefficients in nGy h⁻¹ per Bq kg⁻¹, while A_K, A_{Ra}, and A_{Th} are the measured activity concentrations of K-40, Ra-226, and Th-232 in Bq kg⁻¹, respectively.

➤ Annual outdoor effective dose equivalent (E_D)

These values from external exposure to gamma rays, E_D (mSv yr⁻¹), received by the population from the soil samples were estimated by substituting the calculated absorbed dose rates (D_R) in equation Eq.2.2 [1].

$$E_D (\text{mSv yr}^{-1}) = D_R (\text{nGy h}^{-1}) \times 8760 (\text{h yr}^{-1}) \times 0.2 \times 0.7 (\text{Sv Gy}^{-1}) \times 10^{-6} \quad (\text{Eq. 2.2})$$

Here, 0.2 is the outdoor occupancy factor, which is equivalent to an outdoor occupancy of 20% and 0.7 Sv Gy⁻¹ is the conversion factor from absorbed dose rate in air to effective dose for external gamma irradiation.

➤ Radium equivalent activity (Ra_{eq})

This index considers the radiation hazard associated to the specific activities of Ra-226, Th-232, and K-40 by a single quantity. Ra_{eq} in Bq kg⁻¹ can be calculated by equation Eq.2.3 [185].

$$Ra_{eq} (\text{Bq kg}^{-1}) = A_{Ra} + 1.43A_{Th} + 0.077A_K \quad (\text{Eq. 2.3})$$

This index represents the weighted sum of activities of the three NRs based on the estimate that 1 Bq kg⁻¹ of Ra-226, 0.7 Bq kg⁻¹ of Th-232 and 13 Bq kg⁻¹ of K-40 generate the same gamma-ray dose rate [179, 186]. According to the recommendation of the Organization for Economic Cooperation and Development (OECD), the maximum value of Ra_{eq} must be less than 370 Bq kg⁻¹ to keep the annual radiation dose below 1.5 mGy yr⁻¹ [187, 188].

➤ Gamma index (I_γ)

This index is proposed by the European Commission to assess excess external gamma radiation from materials, and the safety value for this index should be less than 1 [189].

$$I_\gamma = \frac{A_{Ra}}{300} + \frac{A_{Th}}{200} + \frac{A_K}{3000} \leq 1 \quad (\text{Eq. 2.4})$$

➤ External hazard index (H_{ext})

The extent of external hazard from Ra-226, Th-232 and K-40 can be calculated from Eq. 2.5 [185].

$$H_{ext} = \frac{A_{Ra}}{370} + \frac{A_{Th}}{259} + \frac{A_K}{4810} \leq 1 \quad (Eq. 2.5)$$

The maximum value of H_{ext} equal to unity corresponds to the upper limit of Ra_{eq} (370 Bq kg⁻¹).

➤ Excess lifetime cancer risk (ELCR)

The chance of developing cancer over a lifetime due to human exposure to ionizing radiation can be estimated using the *ELCR* index. This excess lifetime cancer risk can be evaluated from the following equation for long term exposure to the radiation in a given area.

$$ELCR = E_D \times L \times R_F \quad (Eq. 2.7)$$

where L is the duration of life (70 years), E_D is the annual effective dose (Eq.2.2), and R_F is a risk factor (Sv⁻¹) which gives the fatal cancer risk per Sievert and suggested to be 0.057 by ICRP 103 for public exposure regarding the stochastic effects from low-dose background radiation [190].

b) Grass

➤ Transfer factor (TF)

The transfer factor is a commonly used to determine the ability of plant species to take up radionuclides from soil. In the case of soils, it can be calculated from the measured radionuclide content in the soil and grass samples.

$$TF = \frac{R_p(Bq\ kg^{-1},\ dry\ weight)}{R_s(Bq\ kg^{-1},\ dry\ weight)} \quad (Eq. 2.8)$$

where, R_p and R_s are the radionuclide activities of interest in plant and soil, respectively.

c) Gases: Radon/thoron measurements

➤ Annual effective doses (AED)

The annual effective doses (AEDs) due to inhalation outdoors can be estimated using the dose conversion factors reported by UNSCEAR [1] for Rn and Tn gases. The AED (mSv y⁻¹) for Rn, AED_{Rn} , and for Tn, AED_{Tn} , can be calculated using the following equations

$$AED_{Rn} = RC \times F_{Rn} \times D_{Rn} \times t \quad (Eq. 2.9)$$

$$AED_{Tn} = TC \times F_{Tn} \times D_{Tn} \times t \quad (Eq. 2.10)$$

where RC and TC are the measured Rn and Tn concentrations (Bq m⁻³), respectively while D_{Rn} (9×10^{-6} mSv (Bq h m⁻³)⁻¹) and D_{Tn} (40×10^{-6} mSv (Bq h m⁻³)⁻¹) are the Rn and Tn dose conversion coefficients, respectively. Then in the present case, t is the time that might be spent by the pupils in the playground per year (600 h). F_{Rn} and F_{Tn} are the equilibrium factors of Rn and Tn, respectively. The corresponding values for these factors are 0.7 and 0.003 for outdoor according to UNSCEAR Report 2000 and 1993 [1, 191]. This equilibrium factor allows the exposure to be estimated in terms of the potential alpha energy concentration (PAEC) from the measurements of radon gas concentration while it defines as the ratio of the PAEC to the PAEC that would prevail if all the decay products in each series were in equilibrium with the parent radon. These factors depend extensively on environmental factors [10, 192, 193]. Noteworthy, Tn equilibrium factors may significantly vary even for the same environment making it more difficult to estimate because the concentrations of the gas and the decay products at any particular location might not be closely related. This is mainly due to the half-lives of the decay products, which yield very different distributions in the atmosphere of the gas and the decay products [1]. Hence, only an estimation of AED_{Tn} will be given.

2.3.2. Soil acidity

Soil pH is an important parameter to be measured preliminary since it is a measure of acidity and alkalinity in the soil. A pH 7 is considered as neutral, above 7 is alkaline and below 7 is acidic. Soil pH depends on the method that we used and the pH can be measured either in water or in CaCl₂ [194-196]. Therefore, it is important to specify the

method that used to measure the pH. In the present work soil acidity was determined as follows.

A mass of about 10 g of soil sample was mixed with 50 mL of Milli-Q water (solid-to-liquid ratio 1:5). The samples were occasionally stirred for 30 minutes and allowed to stand for 1 hour and then the pH was measured in the supernatant after particle settling [197]. A pH meter (Orion 720A+, Thermo Electron Corporation) and a pH electrode (ORION 8102 BN, ThermoFisher Scientific) were used for these measurements and also for pH adjustments of extractant and leached solutions in sections 2.4.2 - 2.4.4. All the pHs were measured at room temperature and the pH measurement setup was calibrated using at least four buffers with known pH values.

2.3.3. Total organic carbon content in solid phase

Various approaches exist to determine the organic matter content in the soil. Loss after ignition method: weight change after destruction of organic compounds by H₂O₂ treatment or by ignition at high temperature, or by wet combustion analysis of soil by chromic acid digestion. Further, volumetric and colorimetric methods can be used to estimate organic carbon in soil. Potassium dichromate (K₂Cr₂O₇) is most commonly used to oxidize the organic matter and subsequently the amount of unreduced dichromate is determined by oxidation-reduction titration with ammonium ferrous sulfate, which is also referred to as the Walkey-Black method [198]. This method typically yields about 90% recovery of carbon as compared to the dry combustion method [199] and was used in this study.

A mass of about 1 g of air-dried and mildly ground soil samples was weighed into beakers separately. Then volumes of 10 mL of 1 N K₂Cr₂O₇ and 20 mL of concentrated H₂SO₄ solutions were added to a given soil sample in the beaker and swirled to mix the suspension. The suspension was then allowed to stand for 30 min, followed by addition of about 200 mL of Milli-Q water and then 10 mL of concentrated H₃PO₄. After allowing the mixture to cool, 10 – 15 drops of diphenylamine indicator were added and subsequently the sample was titrated with 0.5 mol L⁻¹ ferrous ammonium sulfate [(NH₄)₂SO₄.FeSO₄.6H₂O] solution until the color changed from violet-blue to green. Two blanks were prepared in parallel with the same conditions but without soil and

treated in the same way as the soil suspensions. The equations utilized to calculate the TOC are provided in the Appendix 2.2.

2.3.4. Total elemental compositions of bulk samples and sieved fractions

The elemental compositions of both bulk and sieved fractions were investigated mainly by X-ray fluorescence (XRF) spectroscopy. This relatively nondestructive chemical analysis of rocks, minerals, soils and fluids, is typically used for bulk analyses of large fractions of geological samples. In addition, it is a robust technique with high precision and fast sample preparation, plus XRF provides both qualitative and quantitative information of the analyzed sample, making it one of the most widely used methods for analysis of major and trace elements in environmental samples. Therefore, this technique was used in this study to identify the geochemical compositions of the soil samples. Also, this technique is generally divided into two main groups, wavelength dispersive (WD-XRF) and energy dispersive (ED-XRF). The difference between the two lies in the sample preparation, detection system and achievable spectral resolution. A wavelength dispersive detection system physically separates the X-rays via a grating according to their corresponding wavelengths while an energy dispersive detection system mainly focuses on the trace elemental analysis and directly measures the different energies of the emitted X-rays from the sample with a semiconductor detector. For bulk sample analysis, a mass of about 5 g of each sample was crushed using a vibratory disc mill (model: Scheibenschwingmühle-TS, SIEBTECHNIK) before the analysis. Duplicate samples were prepared for each soil sample.

For the fractionation of the bulk samples, aliquots of soil samples L-04 and L-05 were used in the laboratory at INE/KIT using a standard dry sieving technique to determine whether Th, U, and REEs are specifically bound to any particular size fraction in the soils. Masses of about 900 g of L-04 and 100 g of L-05 samples were oven dried separately at 40 °C overnight, followed by fractionation via dry sieving with different mesh sized sieves. Dry sieving was used to minimize the redistribution of Th and other elements of interest by particle size that might occur during wet sieving. Seven 20 cm × 50 cm test sieves (ISO 3301-1: Retsch GmbH, Germany), with mesh sizes of 40, 75, 125, 180, 250, 425, and 850 μm, were used to obtain eight different soil fractions for further analysis, but also to obtain the soil grain size distribution. The fractionation involved the use of a vibrator machine and subsequently the mass of each fraction was

measured and transferred into plastic zip bags separately with proper labelling. The resulting eight soil fractions were then analyzed via XRF and ICP-OES (corresponding data for ICP-OES will be given in Appendix 3.5) to determine total elemental composition and via XRD (section 2.3.5) to identify major mineral phases in each fraction. A sequential extraction protocol was also applied to these soil fractions as described in detail in section 2.4.2.1 to gain an idea about the mobility of elements of interest in each fraction.

2.3.4.1. Wavelength dispersive X-ray fluorescence spectroscopy

Major components in the samples (i.e., SiO₂, Al₂O₃, Fe₂O₃, etc) were quantified by Wavelength Dispersive XRF (WD-XRF, model: S4 Explorer, Bruker AXS). About 5 g aliquots of the crushed samples were weighed in ceramic crucibles separately and heated up to 950 °C for 8 hours in a muffle furnace to remove moisture and burn carbon/sulphur containing compounds. Loss on ignition (LOI) was determined and the values were later used to correct the WD-XRF data. Then the soil samples were mixed with Li-tetraborate/Li-metaborate (Spectroflux 110) in a 1:10 ratio by weight. These samples were then transferred into platinum crucibles and fused beads were made using a fusion instrument at ~1000 °C. During the fusion, the crucible was shaken slightly on a regular basis to ensure thorough mixing of the melt while keeping an oxidizing atmosphere during fusion. The molten mixture was then rapidly poured onto a metal plate and cooled by a stream of air.

2.3.4.2. Energy dispersive X-ray fluorescence spectroscopy

Energy Dispersive XRF (ED-XRF, model: Epsilon 5, PANalytical) was used to measure concentrations of trace elements (i.e., Th, U, and REEs) directly from the crushed samples. This method was used for both bulk and sieved samples. Small containers (30 cm×20 cm) were approximately half filled with soils separately, properly closed and labelled. Three certified standards, SY-2, SY-3 and BE-N were used for quality assurance. Detailed information about these certified standard materials is given in Appendices (Table A2.3).

2.3.5. Major mineral compositions in soil: X-ray diffraction of bulk and sieved soil samples

Major mineral components in the soil samples can be obtained from X-ray diffraction pattern of the corresponding samples. A few micrograms of each soil sample (bulk or sieved samples) were suspended in iso-propanol separately and aliquots of the resulting suspensions were applied onto a silicon wafer disc using a pipette. Additionally, the clay phases of all four bulk samples were separated by preparing a suspension in iso-propanol, sonicating and decanting. The obtained clay samples were also placed onto silicon wafer discs separately. All these samples were allowed to dry in a fume hood. XRD measurements were performed on a D8 Advance X-ray diffractometer (Bruker AXS) equipped with Cu-K α radiation tube (voltage: 40 kV, current: 40 mA, λ = 0.15418 nm) and energy dispersive detector (Sol-X). The XRD patterns were recorded over the range of $2 \leq 2\theta \leq 80^\circ$ with a step size of 0.015° and a count time of at least 6 seconds per step. The data processing of the spectra was done by Bruker AXS Diffrac^{Plus} EVA software (Bruker AXS, Germany, version 3.1) while phase identification was achieved by comparison with the PDF-2 database.

2.3.6. Surface morphology and soil composition: Scanning electron microscopy and energy dispersive X-ray spectroscopy

More detailed elemental data and surface morphological information on the soil samples were obtained by performing SEM-EDX analysis. Secondary Electron (SE-SEM) and Backscattered Electron (BSE-SEM) images were recorded for the carbon coated sample surfaces using a FEI Quanta 650 FEG environmental scanning electron microscope. Quantitative and semi-quantitative chemical analyses in the energy dispersive mode for selected areas were performed to support the mineral characterization using a Thermo Scientific UltraDry, i.e. Peltier cooled, silicon drift X-ray detector. The NORAN System7 microanalysis system, software version 3.3 was utilized for data analysis while the primary electron beam energy was set at 30 keV.

2.3.7. Identification and quantification of Th containing mineral phases: X-ray absorption spectroscopy at the Th L₃-edge

X-ray absorption spectroscopy (XAS) is an advanced spectroscopic technique that could effectively been used to investigate the local chemical environment of Th in its host minerals. X-ray absorption spectra at the Th L₃-edge (16.3 keV) were recorded at

the INE-Beamline for radionuclide science [200] of the KIT synchrotron light source (Karlsruhe, Germany). The energy of the storage ring is 2.5 GeV and the maximum current is 150 mA. The incoming X-ray beam was monochromatized using a pair of Ge<422> crystals and the energy was calibrated by assigning the first inflection point of the Th L₃-edge XANES recorded from ThO₂ to 16.3 keV. Measurements and data evaluations were done with close supervision and guidance of the beamline scientists.

2.3.7.1. Sample preparation and bulk sample analysis: X-ray absorption near edge structure and extended X-ray absorption fine structure

Aliquots of the four soil samples (L-03, 04, 05, 06) and residues from sequential extraction steps (F4 and F5 of L-05 soil sample, the extractions and the resulting fractions are explained in detail in section 2.4.2) were mildly ground and placed between two Kapton tapes as shown in the Figure 2.4a. Reference compounds (RCs) were selected to represent the major mineral phases that had been previously identified. The RCs include monazite ((Ce, La, Nd, Th)PO₄) from Brazil, synthetic ThSiO₄ (courtesy Dr. Stéphanie Szenknect, Institute for Separation Chemistry, Marcoule, France) and ThO₂ [51]. For the measurements, the monazite and ThSiO₄, RCs were prepared in the same way as the soil samples (between Kapton tapes) while the ThO₂ RC was prepared as a pellet. Samples and RCs were put in a sample container and transferred to the beamline following the radioprotection requirements. XAS spectra for RCs were collected in transmission mode, while fluorescence detection mode was applied for bulk and extracted soil samples. A Vortex-ME4, Hitachi USA silicon drift detector was used for these measurements. Several scans were collected at room temperature and averaged to obtain adequate counting statistics.

2.3.7.2. Sample preparation and analysis of selected individual Th-containing particles

a) SEM-EDX

Soil samples were dispersed in isopropanol in separate vials. Aliquots of those suspensions were dried on polished glassy carbon substrates mounted on sample holders (Figure 2.4b). Then the locations of the particles of interest, i.e., Th-containing particles, within the dried particles on these carbon surfaces were triangulated primarily during SEM-EDX analysis. The applied primary electron beam energy was 20 keV. Secondary Electron and Backscattered Electron images were recorded and analyzed using the instrument and software described in section 2.3.6.

b) μ -XRF and μ -XAS

These analyses were performed using the existing experimental setup at the INE-Beamline (Figure 2.4c) to obtain more detailed insight concerning the elemental composition and Th-elemental distribution. The beam footprint is about 28 μm in size, i.e., FWHM of the beam intensity profile. Initial μ -XRF scans at the beamline provided first information on elemental distribution in the regions (which had been previously identified in SEM-EDX) in order to relocate the particles of interest for subsequent detailed μ -XRF analyses. For the detection of the possible presence of U in the sample, the excitation energy was set at 17.5 keV. A Vortex-60EX, SII Nano Technology USA silicon drift detector was used for spatially resolved XRF/XAS measurements with this μ -focused beam. Subsequently, μ -XAS analyses by recording Th L_3 -edge μ -XANES spectra in fluorescence mode were carried out for the points of interest, where Th-containing phases were identified.

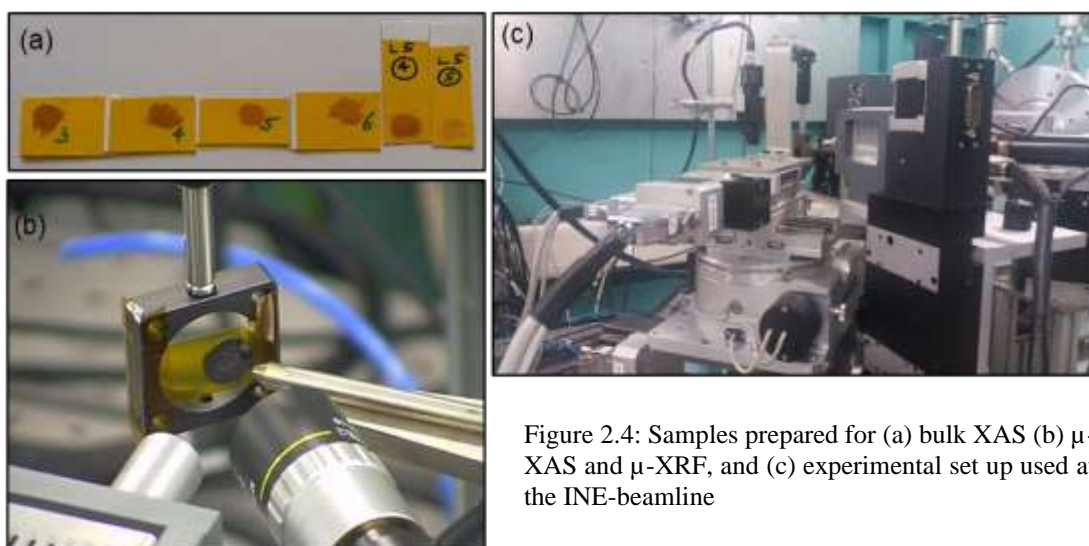


Figure 2.4: Samples prepared for (a) bulk XAS (b) μ -XAS and μ -XRF, and (c) experimental set up used at the INE-beamline

2.3.7.3. Data treatment

a) Bulk XAS

Standard procedures using the *Athena* interface to the Ifeffit software were followed to process the collected XAS data [201] and the information on the composition of the soil samples was inferred from linear combination fitting (LCF) of experimental EXAFS spectra involving the spectra of the RCs. The LCF analysis provides direct information on the contribution of each mineral phase to the experimental data. LCF requires proper identification of the minerals present and inclusion of their respective spectra in fits of spectra of the unknown multi-mineral assemblages. The accuracy of

this method depends on the extent to which the spectra of the chosen RCs actually do represent these components in the unknown samples. The RCs used in the bulk XAS were selected for LCF analysis. LCF analysis also provides goodness of fit parameters via R-factor and reduced χ^2 along with the weight percentage contribution of each RC to a given soil sample. The k-range from $2.9 \text{ \AA}^{-1} - 7.5 \text{ \AA}^{-1}$ was selected for this EXAFS-LCF analysis.

b) μ -XAS and μ -XRF

The μ -XAS and μ -XRF data were reduced and analyzed using the PyMca Fluorescence Toolkit [202] and the *Athena* software [201]. Insight into Th containing particle mineralogy and coordination environment can be obtained by comparing the spectra with the selected RCs. Separate information obtained from μ -XRF, elemental mapping, and μ -XAS can be combined to describe geochemical matrices and to identify differences in the individual Th-containing mineral particles. This combination was used to determine the coordination environment of Th within isolated particles from the soil samples.

The statistical significance of the elemental distributions inside each particle based on the μ -XRF elemental maps was quantitatively estimated by Spearman correlation coefficients (ρ). The detector counts of fluorescence lines from μ -XRF maps corresponding to different elements were used for this purpose. The Spearman correlation assesses monotonic relationships whether linear or not. A perfect Spearman correlation of +1 or -1 occurs when each variable is a perfect monotone function of the other whereas $\rho=0$ indicates the absence of correlation between the variables. When interpreting these correlations, the beam effect on the measurements needs to be carefully considered. In the present work, only the Spearman correlation coefficient values are included in the discussion whilst both scatter plots and corresponding frequency histograms are given as Appendices in Chapter 3. The statistical program R version 3.6.0 [203] was used to perform the data treatment and all calculated correlation factors showed significant values, i.e. p-values < 0.01 (see results in Appendix 3.6).

2.4. Analysis for elemental mobility and potential carrier phases

2.4.1. Quantification methods and analytical instrumentation

2.4.1.1. Trace element analyses

The determination of trace element concentrations (such as Th, U, and REEs) in the liquid phase of all the investigated extractants (sections 2.4.2 and 2.4.3), eluants from column experiments (section 2.4.4) and groundwater samples was performed using Inductively Coupled Plasma Mass Spectrometry (ICP-MS). This analytical technique is a type of mass spectrometry that uses an inductively coupled plasma to ionize the sample. It is a well-established, highly sensitive fast analysis and used to detect metals and several non-metals in liquid samples down to very low concentrations. The samples were introduced to the device using an analytical nebulizer, which converts liquids into aerosols that are subsequently swept into the plasma to create the ions. Dilutions were necessary to keep the salt content in the samples below 50 mg L^{-1} because the detection capability is highly influenced by a concentrated matrix solution of the samples. Importantly, the liquid samples were acidified to 2% HNO_3 to ensure that the elemental composition persists in the samples. A volume of 5 mL of 2% HNO_3 was used as blank samples. Both X-Series II, Thermo Scientific and iCAP TQs, Thermo Scientific were utilized during this study. The reference material SPS-SW1 specified for measurement of elements in surface waters was used for the quality assurance and the details of the analytical quality with the detection limits of each trace element analyzed are given in Appendices (Table A2.4).

2.4.1.2. Major element analyses

The determination of major elements (such as Si, Fe, Al) was performed by Inductively Coupled Plasma Optical Emission Spectroscopy (ICP-OES). An Optima 4300 DV (PerkinElmer Inc.) analytical device was used in this study. The technique was used for major elements since it involves a wide linear dynamic range and better matrix tolerance than the ICP-MS. The liquid samples were introduced into the device using a peristaltic pump to ensure a constant flow. A high-speed argon gas was used to generate from the liquid droplets aerosols that subsequently enter the plasma. The samples to be analyzed were acidified to 2% HNO_3 to maintain the elemental components in the samples. While the liquid samples (extractions and column leachates) can be introduced directly into the plasma, the solid samples, the soil samples used in this study, had to

be digested using KOH and HCl and were transferred into solutions before the injection (corresponding data for soil samples will be given in Appendix 3.2).

2.4.1.3. Non-purgeable organic carbon

The Non-Purgeable Organic Carbon (NPOC) technique was used to determine OC in liquid samples, such as extracted aliquots, column leachates and groundwater. This method measures the OC remaining in an acidified sample after purging the sample with gas. The volatility of inorganic carbon (carbonates, bicarbonates and carbon dioxide) allows for distinction from organic carbon when applying the method at low pH. This technique assumes that the non-purgeable inorganic carbon is insignificant. In the direct method used in this study, a volume of ~7 mL of sample was acidified to pH 2-3 with HCl acid and the inorganic carbon was blown out by bubbling with pure oxygen gas for a certain duration and then subjected to the analysis. This analysis was carried out using a TOC-L (Shimadzu, measuring range: $4 \mu\text{g L}^{-1} - 30,000 \text{ mg L}^{-1}$).

2.4.1.4. Analysis of anionic components: IC

Ion Chromatography (IC) Dionex ICS-3000 (Thermo Scientific, measuring range: $0.1 - 10.0 \text{ mg L}^{-1}$) was used to determine major anions in the leachates from the column experiments and in water samples. The water samples (which had not been acidified in the field) were filtered using $0.2 \mu\text{m}$ filters before analyzing via IC.

2.4.2. Batch extraction procedures

2.4.2.1. Sequential chemical extractions of bulk and sieved samples

All glass and plastic ware used in the extractions was soaked in $2.7 \text{ mol L}^{-1} \text{ HNO}_3$ overnight, and then thoroughly rinsed with Milli-Q water prior to use.

The selected chemical extraction was applied to triplicate samples of each batch soil adopting the protocol previously used by *Guo* focusing on Th [133], which is based on a sequential extraction procedure applied by Martinez-Aguirre [129].

A mass of approximately 2 g of air-dried original soil samples was used during the extractions for both bulk and sieved samples. For the sieved fractions, only the sequential extraction protocol was followed due to insufficient sample material for single extractions. The adopted sequential extraction protocol including the duration for each extraction step is summarized in Table 2.1.

Table 2.1: Summary of the chemical extraction protocol used sequential and single extractions

Fraction	Target phase	Extractive reagent at room temperature	pH	Shaking time (hrs)
F1	Exchangeable	20 mL of 1 mol L ⁻¹ MgCl ₂	7	2
F2	Carbonates	30 mL of 1 mol L ⁻¹ Sodium acetate in Acetic acid	5	7
F3	Organic matter and/ or amorphous oxides	20 mL of 0.1 mol L ⁻¹ Na ₄ P ₂ O ₇ (pH adjusts with 0.1 mol L ⁻¹ Na ₂ H ₂ PO ₄)	9.8	2
F4	Amorphous Fe-Mn- oxyhydroxides	20 mL of 0.2 mol L ⁻¹ (NH ₄) ₂ C ₂ O ₄ in H ₂ C ₂ O ₄ , in dark (Tamm's reagent)	3	5
F5	Crystalline Fe-Mn- oxyhydroxides	20 mL of 0.175 mol L ⁻¹ Sodium citrate in 0.025 mol L ⁻¹ Citric acid, dithionite (Coffin's reagent)	5	6
F6	Residual	N/A		

The sixth fraction (F6), i.e. the residual solid phase after all extraction steps, included in this work was investigated using two methods after freeze-drying of the samples: (i) F6_{M1}, direct XRF measurements on solid residuals after washing and freeze-drying the remainder of F5 solids as described in section 2.3.4, and (ii) F6_{M2}, calculating the differences between total element content (XRF of bulk soils) and the sum of the extracted contents from F1 to F5. Fractions F1-F4 target the adsorbed amounts and secondary phases, considered to represent the non-residual part of Th in soil, whereas fractions F5 and F6 define the residual phase, which is not expected to react on short time scales [129]. The extracted samples were centrifuged for 10 min at 3000 rpm after each extraction step and the decanted supernatant from each step was analyzed by ICP-MS. The extracted samples had to be diluted accordingly to keep the salt concentration of each matrix below 50 mg L⁻¹ for the ICP-MS analysis. Each residue was washed with 15 mL of MilliQ-water between each extraction step, centrifuged and subsequently the decanted supernatant after each washing was also analyzed by ICP-MS to check for any loss of elements during washing. The chemical compositions of the residual phases were further studied by SEM-EDX as described in section 2.3.6.

The accuracy of the utilized extraction protocol for the extraction of the target elements can be verified by evaluating the total percentage recovery, OR [133] as shown in Eq.2.11,

$$OR = \left[\sum_{F1}^{F6} \frac{m_{Seq,Fi}}{m_T} \right] \times 100 \quad (Eq. 2.11)$$

where $m_{Seq,Fi}$ is the amount of the element of interest in individual fractions (F1 to F6) while m_T is the total amount of the given element obtained by XRF.

2.4.2.2. *Single chemical extractions of bulk samples*

The same reagents and conditions used for the sequential extractions were also applied in a single extraction procedure, as described in [133] with ~2 g of soil sample for each individual extraction step. The solid residue after each extraction was not further required with this procedure. The supernatant from each extraction was analyzed by ICP-MS and the residue after each single extraction was studied by SEM-EDX. The final pH values of the extracted solutions were also measured.

2.4.3. *Batch leaching experiments*

2.4.3.1. *Simulated rainwaters*

Batch leaching studies on soil samples targeting Th, U, and REEs with simulated rainwater (SRW) were carried out using different compositions of SRWs at different periods and two different pH values. This approach is probably the most convenient way to simulate the mobilization of Th, U, and REEs in natural systems.

Overall, four different compositions of SRW were used by adopting the recorded rainwater chemistry values in the literature [175] which are shown in the Table 2.2. Maximum and minimum pH values were selected from the same literature source based on the categorized rainfall zones in the respective area [175]. The charge balances of the reported SRWs were not exact. Therefore, the final compositions were selected as shown in Table 2.2.

A mass of approximately 0.2 g of soil sample was added into 50 mL centrifuge tubes and 50 mL of SRW was added separately to each tube. One sample set was rotated for different time periods while the other stood still. Rotating samples assure contact with

the full sample but may cause erosion of the particles with the rainwater. Keeping samples unstirred/still in turn may simulate how the elements of interest concentrate in an area where rainwater can be collected such as in a small pond but this procedure has the disadvantage that not the whole sample is in contact with SRW.

Table 2.2: Chemical composition of simulated rainwater at two different pH values

	pH	Ca²⁺ ×10⁻⁷ mol L⁻¹	Mg²⁺ ×10⁻⁷ mol L⁻¹	Na⁺ ×10⁻⁷ mol L⁻¹	K⁺ ×10⁻⁷ mol L⁻¹	SO₄²⁻ ×10⁻⁷ mol L⁻¹	Cl⁻ ×10⁻⁷ mol L⁻¹	NO₃⁻ - N ×10⁻⁷ mol L⁻¹
A1	5.1	6.5	8.6	5.7	0.3	--	Counter ion	--
A2	6.8	40.4	43.2	21.3	6.9	--	Counter ion	--
B1	5.1	--	--	Counter ion	--	--	174.9	1.8
B2	6.8	--	--	Counter ion	--	92.7	315.9	26.3

The sampling periods were selected as 7, 14, 21, 50, and 118 days. The samples were centrifuged at 4000 rpm for 10 minutes and three replicates were prepared for ICP-MS analysis by taking out 500 µL aliquots from each sample and diluted to 50 mL using 2% HNO₃.

2.4.3.2. Silica nanoparticles

Silica nanoparticles were used to mimic anthropogenic nanoparticle contamination, which could potentially enhance colloidal migration of Th, U and REEs in the soil. AEROSIL 200 silica nanoparticles were used because absorption data of Th and a model with Th are already available for this material and, therefore, development of a new model is not required.

Different Silica AEROSIL200 suspensions with 0.5, 1, 2, 4, and 8 g L⁻¹ at pH 5 were prepared and mixed with 0.2 g of L-04 and L-05 soil samples separately (data for L-04 will be given in the Appendix 4.5). The pH value was adjusted using HCl and NaOH. The samples were rotated for 7 days and then centrifuged at 4000 rpm for 20 minutes. Three replicates were prepared by pipetting out 500 µL aliquots from 0.5 – 4 g L⁻¹ and 250 µL aliquots from 8 g L⁻¹ of each decanted sample. All the samples were then diluted up to 5 mL using 2% HNO₃ for ICP-MS analysis. Samples with a volume of 5 mL of 2% HNO₃ were used as blanks for the ICP-MS analysis.

2.4.3.3. Humic acid

Humic acid (HA) was selected as a potential carrier phase since the target area has a forest cover, which potentially supplies the soil with organic substances which may facilitate the mobilization of Th, U and REEs in the corresponding environment.

There were two types of HAs were used, humic acid crystalline powder from Alfa Aeser and humic acid sodium salt from Sigma-Aldrich. A 10 mg L⁻¹ HA solutions were prepared by dissolving solid HA initially in a very small volume of 0.1 mol L⁻¹ NaOH due to its low solubility in Milli-Q water. The pHs were adjusted to 7 using HCl. Then a volume of 50 mL of this solution was added to 0.2 g of soil sample and shaken for 25 hours. Three replicates were prepared by pipetting 500 µL aliquots from each sample supernatant for ICP-MS analysis after centrifugation at 4000 rpm for 20 minutes. All samples were then diluted to 5 mL using Milli-Q water. No HNO₃ was added since HA might precipitate in acidified solutions.

2.4.4. Column leaching experiments

The column experiments were carried out to investigate the extent of potential vertical migration of Th, U, and REEs in the soil. The column setup and user interface in the software used in this study are shown in Figure 2.5. The ÄKTATM pure 25-chromatography system with a XK 50 borosilicate glass column (GE Healthcare, Sweden) and UNICORNTM software was used as the hardware and software support for these experiments, respectively. Based on the previous batch experiments and the availability of material, L-05 and L-04 were selected for these experiments (data for L-04 will be given in Appendix 4.6). For each leaching experiment a mass of about 150 g of the corresponding soil was filled into the glass column without compressing. A gap of ~0.5 cm was kept between the soil surface and the plunger at the column outlet to reduce the pressure development inside the column. Initial tests had shown that probably due to the clay fraction of the soils, a tight column caused clogging of the column and/or blocking of filters causing the above-mentioned pressure build-up. However, intermittent discontinuation of the column due to software failure or computer shutdown could not be avoided during all column experiments.

2.4.4.1. Simulated rainwater

The SRW – A1 [Cations (Ca^{2+} , Mg^{2+} , Na^+ , K^+), Cl^- as counter ion at pH 5.1] rainwater composition was selected for soil column experiment with L-05. The flow was from bottom to top and the flow rate was adjusted in two stages during the experiments. Initially, a fast flow rate of 0.5 mL min^{-1} was applied manually until the soil was saturated, i.e. the first water layer appeared on the top of the soil surface. After that, the flow rate was changed to 0.05 mL min^{-1} . From this point a macro was applied for the rest of the experiment. The macro was designed to collect 5 mL fractions in tubes that already contained $50 \mu\text{L}$ of 69% HNO_3 . Some tubes were put into the fraction collector without adding HNO_3 for pH measurements, NPOC, and IC analysis. All pH measurements were made in the sample collecting tube. Approximately 1 L of the SRW A1 was passed through the column.

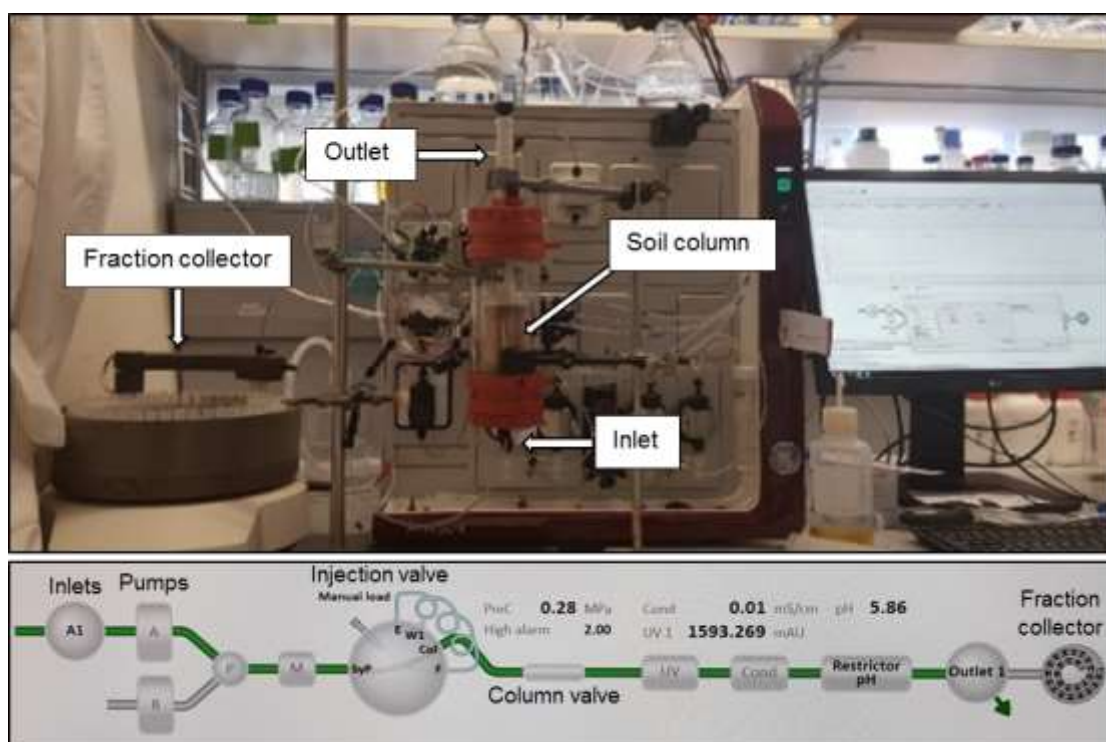


Figure 2.5: (a) Experimental setup of the column experiments and (b) user interface with the process picture reflecting the system configuration

The potential for colloidal transport was assessed by comparing filtered and unfiltered column samples. A filter pore size was used such that any suspended or colloidal materials above about $0.2 \mu\text{m}$ size are removed. The difference will therefore represent potential colloidal migration since a wide range of colloidal or suspended particles

would be removed by filtration. Finally, after all the samples were collected at the fraction collector, the acidified samples were analyzed by ICP-MS and all other measurements were carried out.

2.4.4.2. Silica nanoparticles

About 150 g of fresh L-05 soil sample was mechanically mixed with ~750 mg of dry AEROSIL200 silica inside the column. The SRW – A1 rainwater composition was used as the infiltration leachant in the subsequent leaching experiment. The initial flow rate was adjusted to 0.7 mL min^{-1} until saturation of the silica/soil column and the first water layer was visible at the surface. Then the column was equilibrated overnight. After that, the flowrate was set to 0.05 mL min^{-1} and the sample volume adjusted to 10 mL for each fraction. About 290 μL of 69% HNO_3 was added to each tube. Each tenth tube was inserted into the column fractionator without adding acid for separate pH measurements. After about 1 L of the SRW A1 passed through the column, the program macro was stopped, and all the fractions collected were analyzed by both ICP-MS and ICP-OES.

2.4.4.3. Humic acid

About 150 g of fresh L-05 soil was filled inside the cleaned column. For this experiment, a 100 mg L^{-1} HA solution at pH 5 was prepared using SRW A1 as the infiltration leachant. The required volume of HA solution was injected into the system using a separate syringe. The initial flowrate was adjusted into 0.7 mL min^{-1} for the saturation of the soil and until the first water layer appeared at the interface. Then a macro was designed fixing a flowrate of 0.05 mL min^{-1} , automatic injection of 15 mL of HA into the system, and subsequent continuous flow of SRW A1 through the system until nearly 1 L of total volume had passed through the column. The sample volume for each fraction was set to 10 mL and no acid was added. Then 5 mL samples were prepared from these fractions and analyzed in ICP-MS after the digestion with HF and 7 mL fractions were taken out from different sample fractions for NPOC.

2.5. Geochemical data modelling

Scoping calculations concerning the speciation of Th(IV), U(VI) and REEs(III) were carried out using Visual MINTEQ 3.1 [204]. The thermodynamic data base included in this computer program can be used to calculate metal speciation, solubility equilibria,

sorption etc. for natural waters. Even though the default inorganic speciation database was used for computations which includes the NICA-Donnan model [205] for simulating the complexation of protons and metals to humic substances, some modifications in the database were required concerning the solubility of thorite and monazite, or adsorption on silica. Despite the modifications, self-inconsistent parameters that include solid phase formation, adsorption on silica and interaction with humic acid do not seem to be available.

3. CHARACTERIZATION OF THE ENVIRONMENTAL SAMPLES

This chapter will discuss the results of on-site radiological measurements followed by the solid phase geochemical characterization based on both conventional and advanced techniques. The geochemical analysis on the groundwater samples collected around this area will also be discussed. Data for all four soil and water samples will be given in this chapter to provide a general geo-chemical overview of the location. All these results will be discussed to provide a proper insight into the speciation of Th, U, and REEs in these samples along with comprehensive radiation risk assessment based on the radioactivity measurements considering the applicability of proper radiological investigation in this area.

3.1. Activity measurements and radioactivity dose calculations in the area of study

The radiation doses received by a population includes contributions from (a) the exposure to terrestrial primordial radionuclides (U-238 decay series, Th-232 decay series, and K-40), (b) ingestion of radionuclides by consumption of food, milk, etc via radionuclide uptake by plant materials, and (c) inhalation of radon (Ra-222), thoron (Rn-220), and their progenies. In the present study, all these possible modes of exposures in the target area were investigated and will be discussed.

➤ *Activities in soil*

The collected soil samples were subjected to gamma spectrometric analysis in the laboratory to investigate the latent NRs present at the location which are responsible for the elevated levels and to evaluate their corresponding activity concentrations. The results indicated that members of the Th-232 decay series have the highest contribution to the elevated background radiation levels in this area which agrees with the Th dose distribution map of Sri Lanka (Figure 1.1b). The activity concentrations of primordial radionuclides such as U-238 (assuming secular equilibrium between U-238, Ra-226 and their progenies), Th-232 and K-40 in soil samples (all values reported as Bq kg⁻¹, dry weight) collected from the terrestrial environment of the study area are given in Table 3.1. Even though the radionuclide concentration of U-238 is assumed to equal that of Ra-226, Ra-226 in the U-238 decay chain may have concentrations slightly

deferent from U-238, because this radionuclide has greater mobility in the environment. The comparison of activity concentrations of the same radionuclides in surface soil samples of the study area, some specific sites in Sri Lanka and different areas in the world are shown in Table 1.4.

Thorium and uranium primarily undergo alpha and beta decay, and unable to detect easily. However, many of their daughter products are strong gamma emitters. The activity of U was estimated rely on the establishment of secular equilibrium in the samples and determined from the average concentrations of Ra-226, Pb-214 and Bi-214 while for Th with Ac-228, Pb-212 and Tl-208 in their respective decay series due to the much smaller lifetime of daughter radionuclides in their decay series, but the activity concentration of K-40 was assessed directly from its gamma ray peak as explained in section 2.3.1. thus, an accurate measurement of Th-232 and U-238 radiological concentrations was made, whereas the true measurement of K-40 concentration was achieved. According to Tables 3.1 and 1.4, the mean activity of U-238 ($\sim 372 \text{ Bq kg}^{-1}$) in these soils is about ten times higher than the world average (35 Bq kg^{-1}), whereas the average Th-232 activity ($\sim 6227 \text{ Bq kg}^{-1}$) in the present study is two orders of magnitudes higher than the world average (30 Bq kg^{-1}) as reported by UNSCEAR (2000). The average K-40 activity of the soil ($\sim 468 \text{ Bq kg}^{-1}$) is found to be almost at similar level as the world average value of 400 Bq kg^{-1} [1]. In addition, both the mean activities of U-238 (372 Bq kg^{-1}) and Th-232 (6227 Bq kg^{-1}) in the soils observed in the present study are three times and one order of magnitude higher than the all-Sri Lanka average values of U-238 (49 Bq kg^{-1}) and Th-232 (138 Bq kg^{-1}), respectively [168]. The calculated absorbed dose rates in air using the radionuclide activity data, exceeds the world average of 57 nGy h^{-1} and the range of $18 - 93 \text{ nGy h}^{-1}$ [1], c.f. values in Table 3.1. For monazite bearing sands in the coastal areas of Kerala and Madras, absorbed dose rates in air ranges from 200 to 4000 nGy h^{-1} according to the UNSCEAR report whereas Sri Lankan soil samples from this study show rather higher values in comparison. Noteworthy, significant variations in the activity concentrations were observed within a distance of a few meters. Even though somewhat unexpected, it implies the existence of local heterogeneities on a small scale. Similar phenomena were reported elsewhere [94].

Table 3.1: Activity concentrations, calculated absorbed dose rates and effective dose rates for soil samples

Sample	K-40 (Bq kg ⁻¹)	U-238 (Bq kg ⁻¹)	Th-232 (Bq kg ⁻¹)	Th-232 (×10 ⁻³ mol kg ⁻¹)	Calculated Absorbed Dose Rate (μGy h ⁻¹)	Calculated Effective Dose Rate (mSv yr ⁻¹)	Measured Effective Dose Rate (mSv yr ⁻¹)
L-03	339.6±16.9	319.8±79.9	4440.0±364.7	4.7±0.4	2.9	3.6	36.3±0.1
L-04	530.3±24.5	510.9±106.3	7037.9±647.0	7.5±0.7	4.6	5.7	28.9±0.4
L-05	538.9±55.8	338.2±109.0	6835.1±639.1	7.3±0.7	4.4	5.4	12.2±0.1
L-06	461.9±43.6	318.7±88.7	6595.5±879.6	7.0±0.9	4.3	5.2	9.2±0.2
World average	400	35	30		0.06		2.4
World range (UNSCE AR 2000)	140-850	17-60	11-64		0.02-0.09		1-10

➤ External radiation exposures

The present study was initiated by measuring on-site radiation levels using an environmental radiation monitoring survey meter and the measured effective dose rates on the location are in the range of 9 – 36 mSv yr⁻¹ (Table 3.1). However, the effective dose rates calculated using activity concentrations of NRs (Eq. 2.2) showed significant differences compared to the values measured on-site (Table 3.1). Though the calculated annual effective dose rates are much lower and in the range of 3.6 – 5.7 mSv yr⁻¹, they are still above world average annual exposure to natural radiation sources (2.4 mSv yr⁻¹) but within the acceptable range of 1 – 10 mSv yr⁻¹, while at the same time similar to some other HBRAs in the world (Table 1.4, Section 1.2.3). The reasons for the differences between the measured and the calculated values might be due to the assumed limited residence time in the area (outdoor occupancy factor of 0.2, section 2.3.1.4) and/or might be that the calculated dose rate is based on the specific contents of the isolated representative sample collected at a specific location whereas the on-site measured dose rates at the sampling locations include radiation from greater depths as well as radiation from the surroundings.

➤ Hazardous indices

Knowing the activity concentrations of available NRs, it is worthwhile to assess ensuing possible radiation hazards related to the area. There are several radiation hazard indices in the literature to estimate the radiological hazards to the general public. Even though

the main two indices, absorbed and effective dose rates, were already discussed, several other indices are utilized in different perspectives all over the world. Some of the well-known and accepted indices were used in this study via measured radionuclide activity concentrations of K-40, U-238 and Th-232. They are given in Table 3.2 together with some comparable values from India.

The radium equivalent activity (R_{eq}) is a widely used radiation hazard index, which considers as a measure of the radiation dose likely to be delivered externally to the general public. The maximum value of R_{eq} must be below 370 Bq kg^{-1} to keep the annual radiation dose below 1.5 mSv yr^{-1} . This value is in the range of $6700 - 10600 \text{ Bq kg}^{-1}$ for the target site, i.e. obviously much higher than the threshold value recommended by the Organization for Economic Cooperation and Development (OECD) [187]. Yet, it is only half of the value reported in Chavara-Neendakara, India [153] and close to values reported in some other places in India and some locations around Sri Lankan beaches (Table 3.2) [162, 166, 206]. In addition, the values of the two indices estimated in this study, i.e. the gamma index (I_γ) and the external hazard index (H_{ex}), must be below unity as established by the European Commission on Radiation Protection (1999) to keep the radiation hazard insignificant, which means it is safe for humans to carry out their activities in the area [207]. The estimated I_γ values are in the range of 23.4 to 37.1 while calculated H_{ex} values range from 18.1 to 28.7, exceeding the recommended limit but close to the values reported in some HBRAs in India (Table 3.2). Lifetime cancer risks (ELCR) were calculated to assess the radiological risk using effective dose rate values. The calculated values are in the range of 14.3×10^{-3} to 22.7×10^{-3} and the maximum is two orders of magnitude above the world average of 0.29×10^{-3} [1]. Although the excess seems obvious due to the higher concentration of NRs in this study site, these are only estimated values, which require proper supplementary studies for confirmation. Nevertheless, several epidemiological studies have been conducted to analyze the risk of cancer in world-known HBRAs, most of these studies concluded that there is no link between an increased rate of cancer or mortality and exposure to high background natural radiation, but still a debatable topic [208-210]. It should also be noteworthy that the “permissible limits” for dose values exist in legislations for nuclear facilities and nuclear accidents, but explicitly not for natural radioactivity in the environment.

Table 3.2: Radiation hazardous indices calculated in the study area, some places in India and the world acceptable limits

Sample	Ra_{eq} Bq kg ⁻¹	I_{γ}	H_{ext}	$ELCR \times 10^{-3}$	Ref.
L-03	6700	23.4	18.1	14.3	Current study
L-04	10600	37.1	28.7	22.7	
L-05	10200	35.5	27.4	21.7	
L-06	9790	34.2	26.4	20.9	
Sri Lanka	1000 – 10000	-	-	-	[166]
Chavara-Neendakara	23200	-	-	14.8	[153,
Gopalpur	100 - 8770	0.3 – 30	-	-	162, 206,
Rushikulya	70 - 8490	0.5 – 29.5	-	-	211]
Kerala	15 - 8800	0.05 – 30.6	0.04 – 23.7	0.03 – 16.2	
World acceptable limits	370	1	1	0.29	[1]

➤ Bioavailability and insights to internal exposure via ingestion

The subsequent possible way of human exposure to radiation next to external is internal exposure. Internal radiation exposure caused by ingestion of radionuclides via consumption of foodstuff can be evaluated by considering the potential bioaccumulation/bioaccessibility of NRs in the ecosystem. It was attempted to evaluate this exposure pathway in this work by measuring the concentrations of NRs of grass samples collected in the vicinity of the study site. The data listed in Table 3.3 show the measured activity of each radionuclide in the leaves of grass samples of *Cynodon dactylon* by gamma spectrometry and the corresponding transfer factors (TF) calculated using these measured activities of the grass and corresponding activities of the soil. This table also includes elemental concentration of Th in mg kg⁻¹, estimated using the measured gamma activity data and directly analyzed by XRF.

The data from the present study clearly shows that the gamma activity levels and elemental concentrations of NRs in grass samples collected in the target area are higher than for plant material collected in normal background areas. It was observed that the values for both activity/elemental concentrations and TF vary with the corresponding radionuclide. The accumulated activities reflect the relative abundance observed in the underlying soil (Table 3.1). However, surprisingly huge differences were observed for the elemental concentrations of Th (in mg kg⁻¹) estimated from radionuclide activities and XRF. This might be due to the difficulties associated with the applied analytical

methods because it is less likely that gamma spectroscopy and XRF provide comparable data.

Regardless of relatively lower activities in the soil, K-40 showed the highest calculated TF, in accordance with its bio essential character to plants. Noteworthy, the TF values estimated in this study are similar for Ra-226 and approximately two to five times higher than the TF values of Th-232 and K-40 reported for similar grass samples (leaves + roots) from the city of Chittagong, Bangladesh [212]. Another study on grass samples (species not specified) collected in the North-west of West Bank (Palestine) reported TF values for Th-232 and Ra-226 which are about eight to twenty times higher than our results while showing similar TF values for K-40 [213]. Furthermore, only the average values of TF for Th-232 and K-40 in the currently studied samples (Table 3.3) were found to be higher than the IAEA values specified for the grass samples from tropical environments [29]. These results could imply that other local vascular plants with developed root systems may also accumulate important amounts of Th-232 and K-40. Additionally, such high plant uptake seen in this current study site is supported by the batch extraction results in Chapter 4, section 4.2 that show the presence of potentially bioaccessible fractions in the soil. Concentrations of U and Th in a plant species can significantly vary with the sampling site and even for different parts of a given plant sample, i.e. between roots and aboveground parts in accordance with findings of similar radionuclide studies available in literature [94, 214, 215]. Therefore, these values can be highly influenced by several plant and local environmental factors as discussed in the Chapter 1 (Section 1.2.2.1).

The unexpectedly enhanced radionuclide, particularly Th- 232, uptake by grass could be explained in the perspective of soil pH as well. The corresponding high TF values, at least an order of magnitude higher than the recommended IAEA value, might be due to the low soil pH, i.e. in this location in the range of 4 – 5 (Table 3.5). In such acidic soil, hydrogen ions can displace other cations, so that radionuclides like Th-species in soil pore water could possibly be enhanced. In highly alkaline soils, insoluble precipitates may be formed instead with carbonates, phosphates or sulphide ions which will significantly reduce the availability of cations to plants. Moreover, adsorption of cations to minerals is favored at this pH.

In general, it is expected that Th is normally bound in the soil in a very immobile form. Therefore, the increased activity of the grass samples is unexpected around the present study area and potentially due to the high enrichment of Th in the soil. Another possible reason for the excessive TFs might be the washing step during sample preparation prior to analysis. Washing the leaves of grass samples probably does not completely remove small particles from the surface since aerosols can be tightly attached to trichomes at leaf surfaces [216] and in this case, Th transfer to the plant is not only being accounted via root uptake but also via interception of strong deposition of NRs at the plant surface. Therefore, the TF itself cannot distinguish between root uptake and interception. When discussing the potential bioavailability of Th, the nature (speciation) of the “dissolved” Th is of relevance and will be investigated later.

Table 3.3: Activity concentrations of NRs accumulated in soil (averaged value) and grass samples (Bq kg⁻¹ dry weight) with corresponding transfer factors

Sample	K-40	Ra-226*	Th-232 Gamma	Th-232 Gamma	Th-232 XRF
Soil	467.7 ± 92.1 Bq kg ⁻¹	371.9 ± 93.1 Bq kg ⁻¹	6227.1 ± 1205.1 Bq kg ⁻¹	1534.0 ± 296.9 mg kg ⁻¹	1276.2 ± 341.7 mg kg ⁻¹
Grass 1	573.6 ± 261.8 Bq kg ⁻¹	30.1 ± 17.4 Bq kg ⁻¹	771.1 ± 284.2 Bq kg ⁻¹	190.0 ± 70.0 mg kg ⁻¹	564.7 ± 9.4 mg kg ⁻¹
Grass 2	539.5 ± 236.2 Bq kg ⁻¹	21.1 ± 8.8 Bq kg ⁻¹	975.4 ± 340.5 Bq kg ⁻¹	240.3 ± 83.9 mg kg ⁻¹	573.5 ± 8.4 mg kg ⁻¹
Transfer factor	0.94 – 1.40	0.05 – 0.08	0.12 – 0.16		
IAEA TF (IAEA, 2010)	0.87	1.7	0.058		

*Analogous to U-238

➤ Insights to internal exposure via inhalation

The other pathway of internal exposure to radiation is inhalation, which was investigated by measuring the released concentrations of radiogenic gases from the soil samples assuming that this mode of exposure also contributes to the inhalation dose in the area other than the inhalation of the re-suspended dust particle. Here, only the measured Tn values and corresponding annual outdoor effective doses are indicated in Table 3.4. Reliable measurements of Rn-222 concentrations could not be obtained due to the high concentrations of Tn in these soil samples, which also suggests the Tn exposure cannot be ignored. Such high Tn concentrations in the samples are uncommon

in most areas of the world. Even though many studies reported dose calculations for Rn/Tn indoor measurements, their corresponding outdoor data and particularly Tn data are still scarce or absent in most areas. Yet, Tn has recently been recognized as a potential health hazard in areas rich in Th-232, calling for its determination and risk estimation [1, 217, 218]. The main reason for the lack of Tn data is the difficulty in measuring an equilibrium factor for both indoor and outdoor Tn due to its short half-life (55 s). As a consequence, this factor has a wide range due to the specific spatial distribution of Tn. Numerous researchers attempted to estimate equilibrium factors for Tn, which range between 0.003 and 0.1 [1, 217, 219-222]. The lowest value reported (i.e. 0.003) was considered during the estimation of effective doses in the present study.

According to the UNSCEAR 2000 report, estimated total outdoor annual effective doses from Rn and Tn are 1.2 mSv and 0.07 mSv, respectively (Table 1.1), while the typical outdoor concentration of Tn is of the order 10 Bq m^{-3} with a range from 1 to 100 Bq m^{-3} [1]. The measured activity and estimated dose values for Tn in this study are considerably higher than reported outdoor values in UNSCEAR reports and also higher than some values reported for annual effective doses from Tn by Popic and co-workers with similar Th-232 radionuclide activities in their soil samples [192]. Yet, the total annual outdoor effective doses (sum of annual effective doses from gamma, from Rn, and from Tn) reported by those authors are in the range of the estimated effective doses from Tn in our study [192]. However, it should be noted that the corresponding values in the current work are obtained from gas samples released from soils inside closed containers which were equilibrated for a short time, while the other researchers performed continuous measurements of Rn and Tn outdoors for a long time using commercially sold passive Rn-Tn discriminative detectors [192, 223]. Therefore, the comparison of our data with the available literature should be considered with caution at this stage. Moreover, there is a high possibility that the actual dose values in the authentic environment are significantly lower due to dilution effects by wind and open air spaces without even causing any radiotoxicity exposure for the public.

Table 3.4: Measured thoron concentrations and calculated annual inhalation doses of the soil samples*

Sample	Thoron (kBq m ⁻³)	Estimated annual effective dose from Tn (mSv)
L-03	34.62 ± 4.78	2.49
L-04	45.77 ± 5.23	3.30
L-05	75.82 ± 4.00	5.46
L-06	66.79 ± 4.97	4.81

*The results listed are average values of two replicates

➤ Insights from NRs ratios

The analysis of the NRs relative abundance (Th/U, K/U, and K/Th ratios) can give information on the enrichment/depletion processes occurred in a complex metamorphic history and alteration and/or weathering processes, which affected the investigated area. The calculated ²³²Th/²³⁸U ratio in the target area was in the range of 14 – 21, i.e. there is more Th-232 in these soil samples compared to U-238. The ratio is much higher than the Upper Continental Crustal (UCC) average of 4.2 and the world average of 0.86 [1, 224] but closer to the beach sand samples from Areia Petra, Brazil (13.9) and Kalpakkam, India (1.5 – 13.7) [154, 225]. Uranium is typically more soluble than Th and hence it is often deficient with respect to Th in surface soil environments. Additionally, such lower concentrations of U-238 suggest the correspondence of the lower abundance of U-238 in the bedrock of the study area. High activity ratios suggest that there is no contribution from U series members from external factors like contamination with phosphate fertilizers in the study area (i.e., way before using this location as a playground). The calculated ⁴⁰K/²³⁸U ratios ranged from 1.0 – 1.6 and are much lower than that of the UCC, 1.0 – 1.3 × 10⁴, as given by *Tufail et al.* [226] and world average of 11.43 [1]. Moreover, ⁴⁰K/²³²Th ratios are in the range of 0.07 – 0.08, much lower than world average of 13.33 [1]. Noteworthy, ⁴⁰K/²³⁸U and ⁴⁰K/²³²Th ratios are reported to be highly variable in soils worldwide [21, 227]. However, these results can be compared with future similar measurements to support the fact that the area of study may be subjected to effective erosive regime or anthropogenic activities, as expected from the monsoon seasons or population development.

Furthermore, in literature, researchers discussed correlation between Th-232 and U-238 in soil samples and with that perspective, inferred whether soil samples contain

monazites or not [154, 223, 225]. In those studies, they used data from more than 10 sampling points, whereas in the current study, only four data points are available and therefore the outcome should be carefully assessed. The correlation between Th-232 and U-238 in the soil samples is found to be weak, $R=0.49$ (Figure 3.1a), whereas Th-232 and K-40 exhibit a strong correlation of $R=0.96$ (Figure 3.1b). The weak correlation of Th-232 and U-238 indicates that the presence of large amounts of monazite mineral phases in these soil samples is less possible. However, we used only four data points, precise correlations among the data points are difficult (see e.g. the point at the highest concentration in Figure 3.1a). *Kannan et al.* reported the same weak correlation ($R=0.47$) for soil samples from Kalpakkam, India, which were collected close to the beach, indicating that the presence of monazite minerals in those soil samples was also less likely [154]. In contrast, *Kannan et al.* for beach sand from India, *Vasconcelos et al.* for beach sand from Brazil, and *Prajith et al.* for soil samples from Antarctica showed much stronger positive correlations ($R=0.99$, $R=0.91$, and $R=0.95$, respectively) indicating that monazite could be the major source of the elevated background radiation levels in those areas [154, 223, 225]. However, though this study shows a weak correlation itself among the samples, these data are in line with the trends observed in the aforementioned literature, rendering an overall correlation of $R=0.99$ (Figure 3.2). This means that in areas dominated by monazite mineral composition, there is a characteristic U/Th ratio, found worldwide as a general indicator of solid composition. Nevertheless, direct analyses on soil samples should verify these observations (as will follow in sections 3.3 and 3.4).

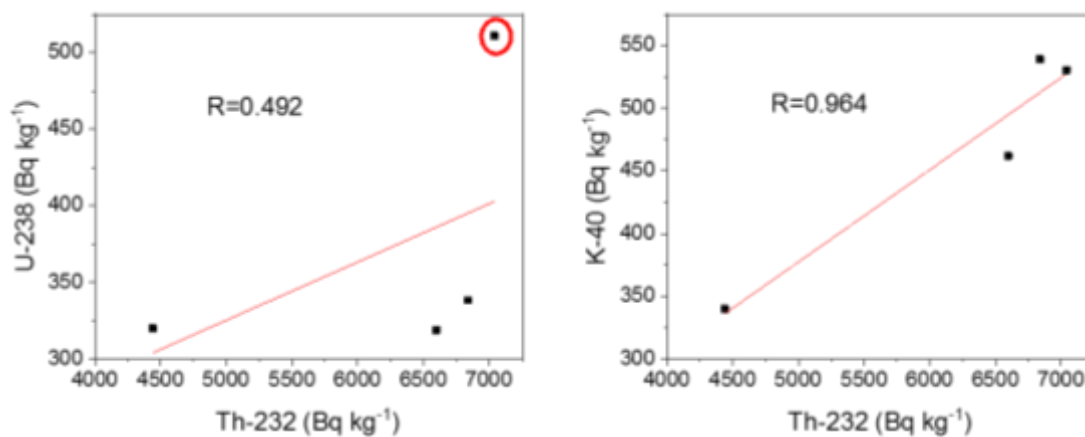


Figure 3.1: Correlation between (a) Th-232 and U-238 and (b) Th-232 and K-40 in the soil samples by gamma spectrometry

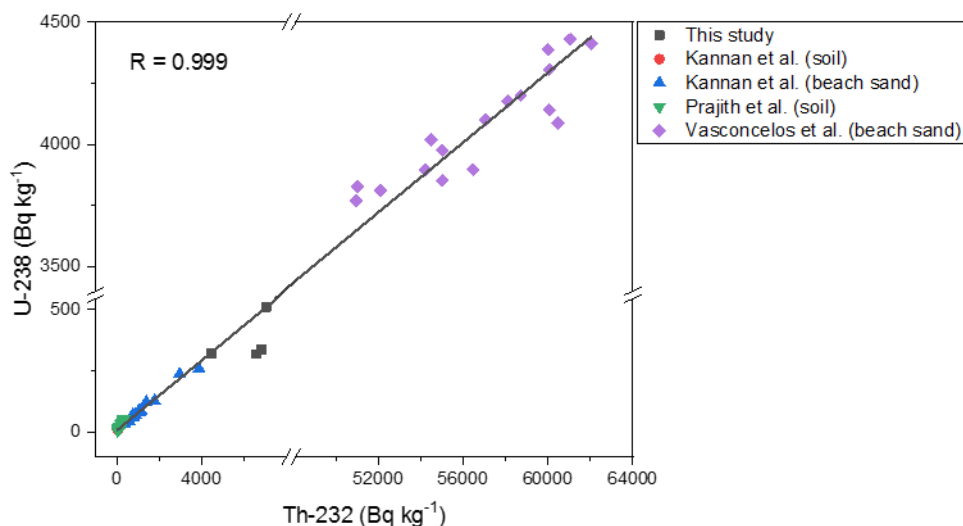


Figure 3.2: Comparison of the correlation between Th-232 and U-238 in reported soil/beach samples and this study

3.2. Basic soil characterization

This section will cover different characterization techniques starting with the measurements on physico-chemical properties followed by some conventional and advanced characterization approaches to evaluate the solid-state speciation of elements of interest.

➤ *General soil properties*

Bioavailability of metals mainly depends on the physiochemical properties of the environmental media such as pH, organic matter, presence of Fe, Mn-hydroxides and clays, etc. Therefore, two basic properties of the soil samples relevant to this study are presented in Table 3.5. In average, the pH of the soil samples is 4.4 ± 0.2 (Table 3.5) which is extremely acidic according to the classification of soil pH by the United States Department of Agriculture Natural Resources Conservation Service (NRCS) [228]. The pH of natural soils mainly depends on the soil mineral composition. The study area has lateritic type soil with inherent acidic pH under natural conditions. Three major effects cause acidity in soils: 1) organic matter and minerals that break down in soil over time are acidic in nature and acidify the soil, which is a quite reasonable cause for this site as the playground has a forest cover, 2) leaching of the soil due to excessive rainfall or irrigation, a natural phenomenon that could occur in this study area, and 3) use of

ammonia-based synthetic fertilizers, which also increases soil acidity, is a more unlikely effect for the location of study [229, 230].

Soils contain large amounts of organic materials which may play important roles in natural systems [231]. Therefore, it is important to determine the TOC in site characterization studies since its presence or absence can remarkably influence the chemical behavior of the soil. TOC is a non-specific test, which does not resolve particular compounds. Natural samples are complex mixtures of thousands of different organic carbon compounds. Instead, TOC provides the sum of all organic carbon contained in those compounds. The TOC contents of the soil samples in this study are moderately high based on the classification of *Kaplan et al.* [130], consistent with the forest cover on one side of the location (Figure 1.3a). These results suggest that on-site leaching of the studied soils under natural conditions (e.g., rainwater from the Monsoon) would result in acidified water containing organic matter as potential carrier phases for trace elements.

Table 3.5: Physicochemical properties of soil samples*

Sample	L-03	L-04	L-05	L-06
pH	4.4 ± 0.1	4.2 ± 0.2	4.6 ± 0.4	4.2 ± 0.3
TOC (g kg ⁻¹)	1.68 ± 0.01	0.69 ± 0.01	1.77 ± 0.00	1.28 ± 0.01

*The results listed are average values of triplicate samples

➤ Major soil mineralogy

(a) Bulk composition:

The main mineralogy of the soil was characterized by XRD. The obtained diffractograms in Figure 3.3a with the main peaks indicating the minerals identified, suggest the presence of two major mineral phases, i.e. silicate (clay) type minerals and silica (quartz). The clay phase was identified as kaolinite and it was the dominant phase in all the samples. Kaolinite is a typical dioctahedral species with an ideal structural formula of $\text{Al}_2\text{Si}_2\text{O}_5(\text{OH})_4$. Such silicate minerals are relevant in many settings because of their relative natural abundance and importance in nature. The silica phase was identified as quartz (SiO_2) and it is consistently present in all the samples and most clearly detected in L-03 and L-06. The other minerals present in the soil could not be detected by XRD due to their low concentrations (i.e., typically, 1-5 wt.% of a mineral are required to be detectable) and/or amorphous nature. Despite the above fact, the color

variation of the soil samples varies from dark reddish to light reddish suggests the possible presence of Fe phases in the samples with variable contents. This hypothesis was tested for the separated clay fractions as described in the section 2.3.5, and the resulting diffractograms are shown on Figure 3.3b. However, the XRD patterns still show correspondence mainly to kaolinite. Regardless of the fact that kaolinite associated iron oxy-hydroxides, hematite and goethite are considered as the main iron containing mineral components of lateritic soil [232], no distinct peaks were observed for Fe containing crystalline phases in any of the spectra. This rather suggest the presence of poorly crystalline Fe minerals such as ferrihydrite or any other trace constituents in the soil which are insensitive to bulk XRD [233] or the crystalline grains might be covered by clay.

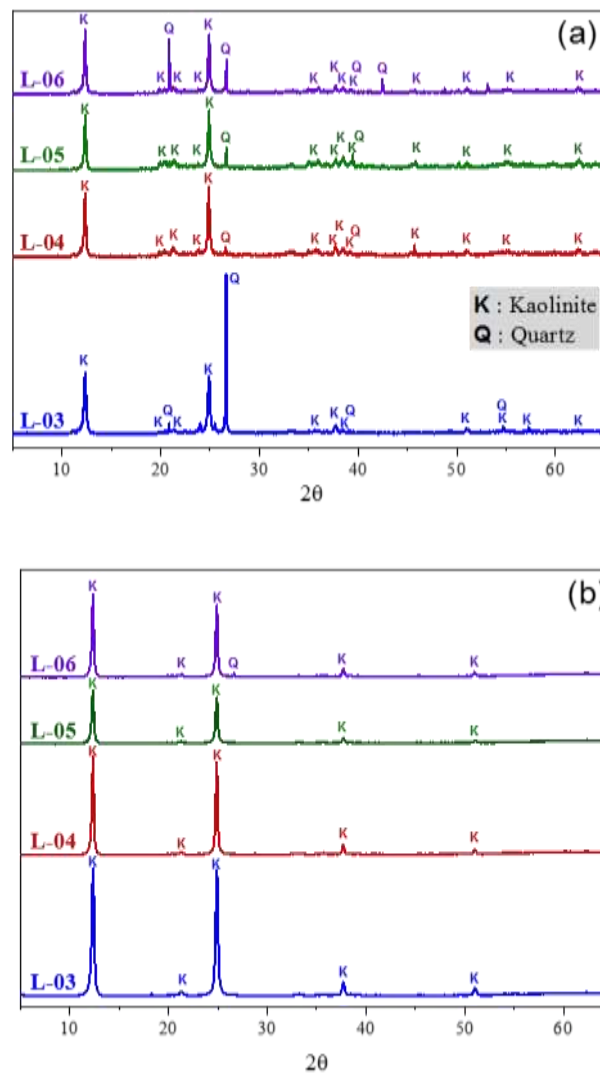


Figure 3.3: X-ray diffractograms of (a) bulk soil and (b) clay fractions of soil samples

(b) Sieved fractions:

In contrast, XRD analysis of the sieved soil fractions revealed some more details about the mineralogy of the soil. Diffractograms were collected for the size fractions of L-04 and L-05 samples and are shown in Figures 3.4a and b, respectively. The color of the sieved fraction less than 40 μm is dark brown compared to the rest and only few milligrams could be collected in both cases, and some differences can be observed between the two soil samples and among their corresponding size fractions.

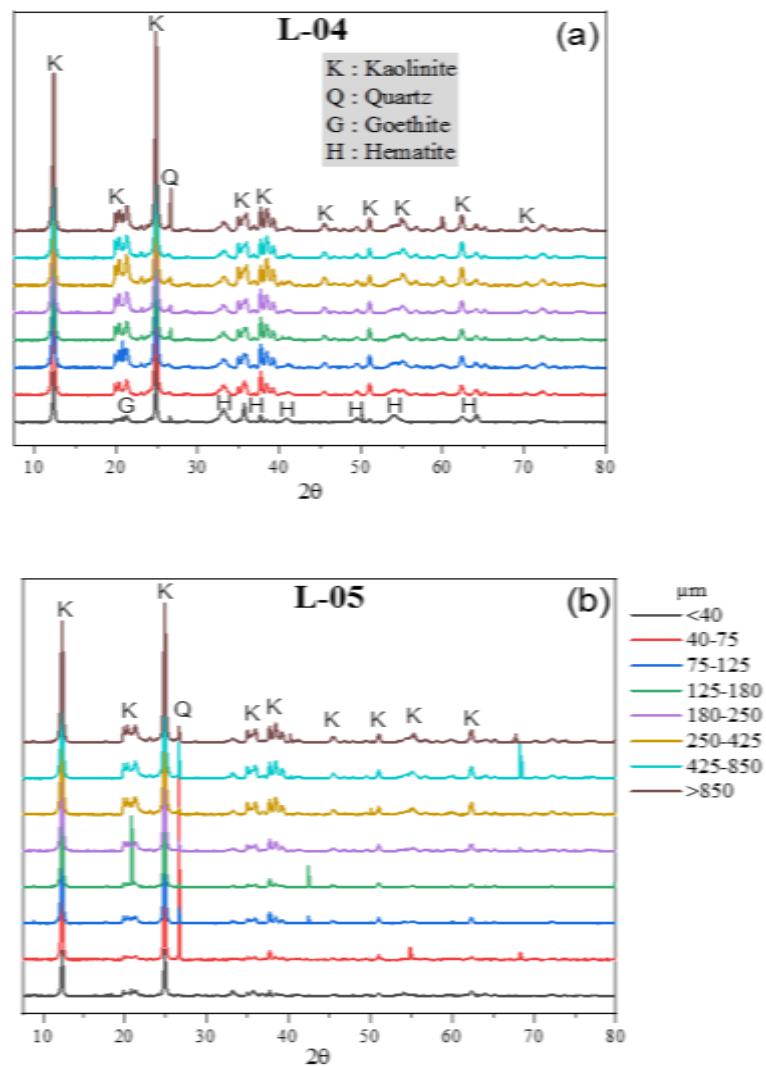


Figure 3.4: X-ray diffractograms of the sieved fractions of (a) L-04 and (b) L-05 soil samples

Especially, the fraction below 40 μm in L-04 clearly indicates the presence of some crystalline iron phases, mainly goethite and hematite while those phases could not be resolved in L-05. It was expected that iron and most other elements are rather

concentrated in small size fractions [234-237]. In contrast to L-04, quartz appears clearly in almost all fractions of L-05 and especially in the 40 – 75 μm fraction. Yet, all other fractions in both soil samples have the same mineralogy dominated by kaolinite (Figure 3.4), may be due to covering of other mineral phases by dominating clay phases which occurs when the dry sieving method is used instead of wet sieving. The latter might concentrate other mineral phases. According to the literature, minerals like clay, quartz and iron phases are likely to adsorb trace elements and move them to the fine particulate matter, in particular the clay minerals [238-240].

➤ Total contents of major and trace elements

(a) Bulk composition

The amounts of major and trace elements in each sample were analyzed by XRF. The results and their corresponding upper continental crust (UCC) abundances [241] are shown in Table 3.6. The results specify that Si, Al, and Fe oxide phases dominate the soil matrix, in agreement with the expected dominant oxide phases in Sri Lankan lateritic soil, i.e. Fe_2O_3 , Al_2O_3 and SiO_2 [242]. The recalculated relative abundances in our samples to weight percent for Fe_2O_3 , Al_2O_3 and SiO_2 are 9-16, 25-32, and 42-53 wt.%, respectively, in accordance with those reported, i.e. about 13, 26, and 60 wt.%, respectively, by Dahanayake (1982) for samples collected close to the study area. Furthermore, the amount of P_2O_5 identified in all samples is in the range of 0.17-0.24 wt.%, in the range of REEs and Th content (Table 3.6). The abundances of the REEs Cerium (Ce), Lanthanum (La) and Neodymium (Nd) are 0.16-0.49, 0.09-0.13 and 0.04-0.06 wt.%, respectively, while Th and U show percentages of 0.08-0.16 and 0.001-0.004 wt.%, respectively.

Even though several studies estimated the abundance of REEs, Th and U in beach mineral sands in Sri Lanka, such data are scarce for inland locations. In one of the studies such data on inland locations showed similar abundance of Ce and La for sediment samples collected from a river basin [243] while two other studies on whole-rock chemical analysis on carbonated rocks and gem-bearing sediments showed much lower values compared to our study [244, 245]. In addition, the abundances of all elements shown in Table 3.6 are higher than the values reported for the UCC, except for SiO_2 , notably in Th, U and REEs. This also provides evidence of some mineral

anomaly in the study area and Table 3.6 also show significant special heterogeneity even within short distances for the four samples.

Table 3.6: Amounts of main components and trace elements present in the samples measured by XRF* and average reported values for the Upper Continental Crust (UCC, [241])

		Amounts of main components and trace elements				
		L-03	L-04	L-05	L-06	UCC
SiO₂	(g kg⁻¹)	501.8±0.6	413.8±48.8	507.1±1.2	527.8±1.0	666
Al₂O₃	(g kg⁻¹)	248.0±6.0	317.1±22.5	248.8±1.5	260.2±3.2	154
Fe₂O₃	(g kg⁻¹)	129.0±1.2	161.4±8.7	101.1±0.8	85.3±0.2	50
P₂O₅	(g kg⁻¹)	2.4±0.4	2.1±0.2	2.4±0.3	1.7±0.1	1.5
Ce	(×10³ mg kg⁻¹)	1.6±0.2	4.9±0.4	3.1±0.1	2.3±0.3	0.06
La	(×10³ mg kg⁻¹)	1.3±0.4	0.9±0.0	1.2±0.1	0.9±0.1	0.03
Nd	(×10³ mg kg⁻¹)	0.6±0.2	0.5±0.0	0.6±0.1	0.4±0.0	0.03
Th	(×10³ mg kg⁻¹)	0.8±0.2	1.5±0.0	1.6±0.1	1.3±0.1	0.01
U	(mg kg⁻¹)	13.4±7.4	35.7±3.5	19.8±0.7	22.3±4.1	3

*The results listed are average value of duplicate samples

(b) Size effects

The variations of Th, U, La and Fe₂O₃ content with the size fractionation measured by XRF are shown in Figure 3.5. Data for the below 40 µm fraction of L-05 were not obtained due to lack of sample material. All elements showed higher amounts in <40 µm fraction of L-04 except for La which exhibit an increase in above 850 µm fraction (same behavior can be seen in the ICP-OES data in Appendix 3.6, Figure A3.5). Overall, the contents seem to continuously decrease with the increase of size fraction for L-05 in accordance with the surface area increasing with decreasing particle size. These small sized particles may either bind trace metals by their higher surface areas or the presence of iron oxides and clay minerals in the fine particle fraction may, however, also host those metal ions in their crystal structure. Several studies reported the same behavior for Th and U [246-248]. Further, L-04 has a high amount of Fe oxides compared to L-05 in each fraction with ~1.6 ratio between them and these data agree with the bulk XRF amounts, with high amounts of Fe oxides in L-04 showing the same concentration ratio between bulk L-04 and L-05 (Table 3.6) and with the XRD peaks

which confirmed the concomitant Fe-mineral phases in L-04 compared to L-05 (Figure 3.4).

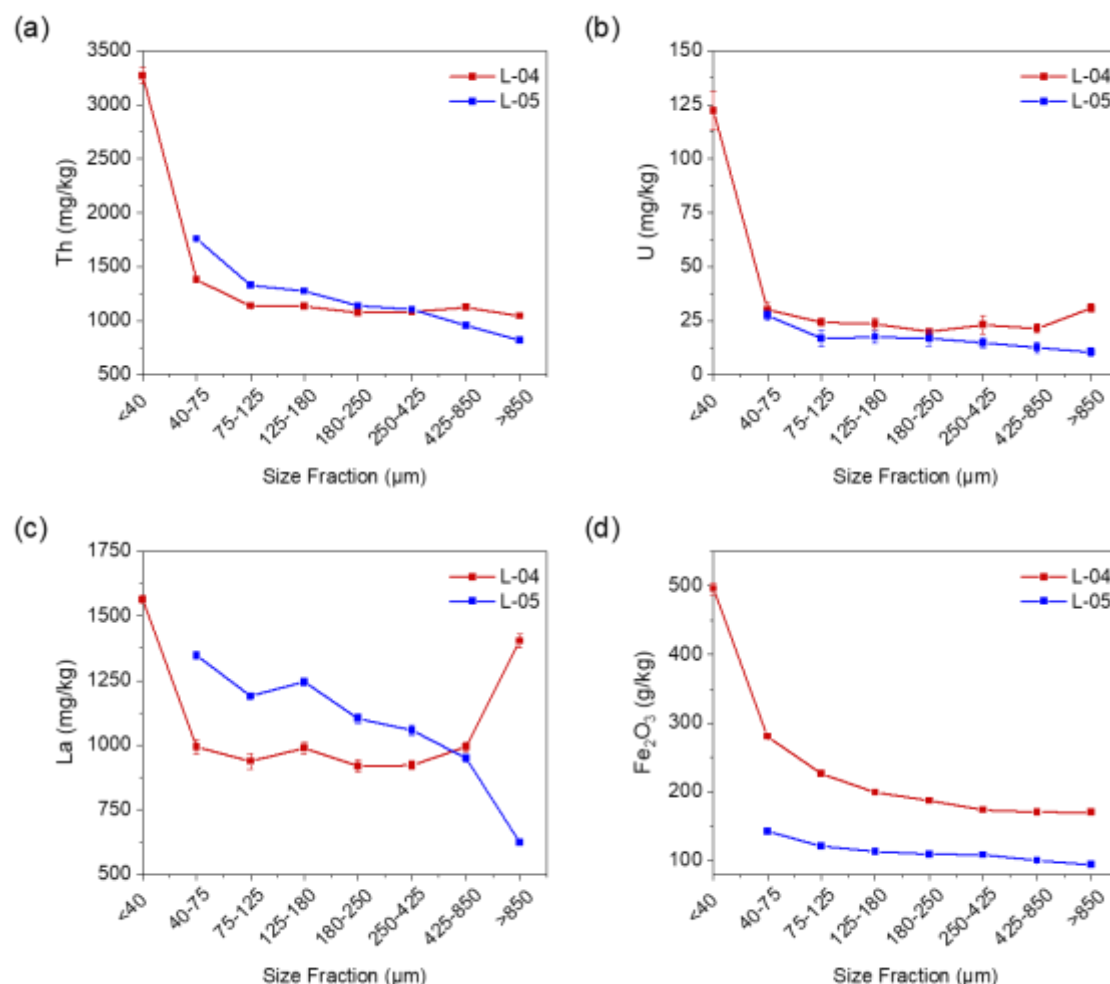


Figure 3.5: Concentration of (a) Th, (b) U, (c) La, and (d) Fe₂O₃ in each size fraction of L-04 and L-05 soil samples measured by XRF

The percentages of the contribution from each size fraction to the bulk increase with increasing particle size and the trace elemental distribution follow the same trend (Figure 3.6). Nevertheless, the elemental distribution of Th has a slight difference percentagewise, with higher percentage in smaller sizes compared to U and La, suggesting the slight particle affinity of Th towards smaller size fractions of soil. Contrary to this in the literature for some samples from a beach deposit it was noted that the concentration of heavy minerals is confined to 43-62, 62-125 and 125-250 μm fractions while particularly monazite grains tend to accumulate in 100-200 μm and 200-400 μm fractions [249]. Another study reported higher accumulation of Th, U, and

REEs in fractions 63-125 μm and 125-177 μm (as compared to fractions $<63 \mu\text{m}$ and 177-250 μm) for a sediment sample collected from a river basin in Sri Lanka [243]. These element distributions among grain sizes depend on several factors such as on-site mineralogy, mineral erosion rate and location of the sampling site along the erosion-transport-deposition path of minerals from elevated grounds (e.g., mountains) to the coast (e.g., beach areas and deep sea basins).

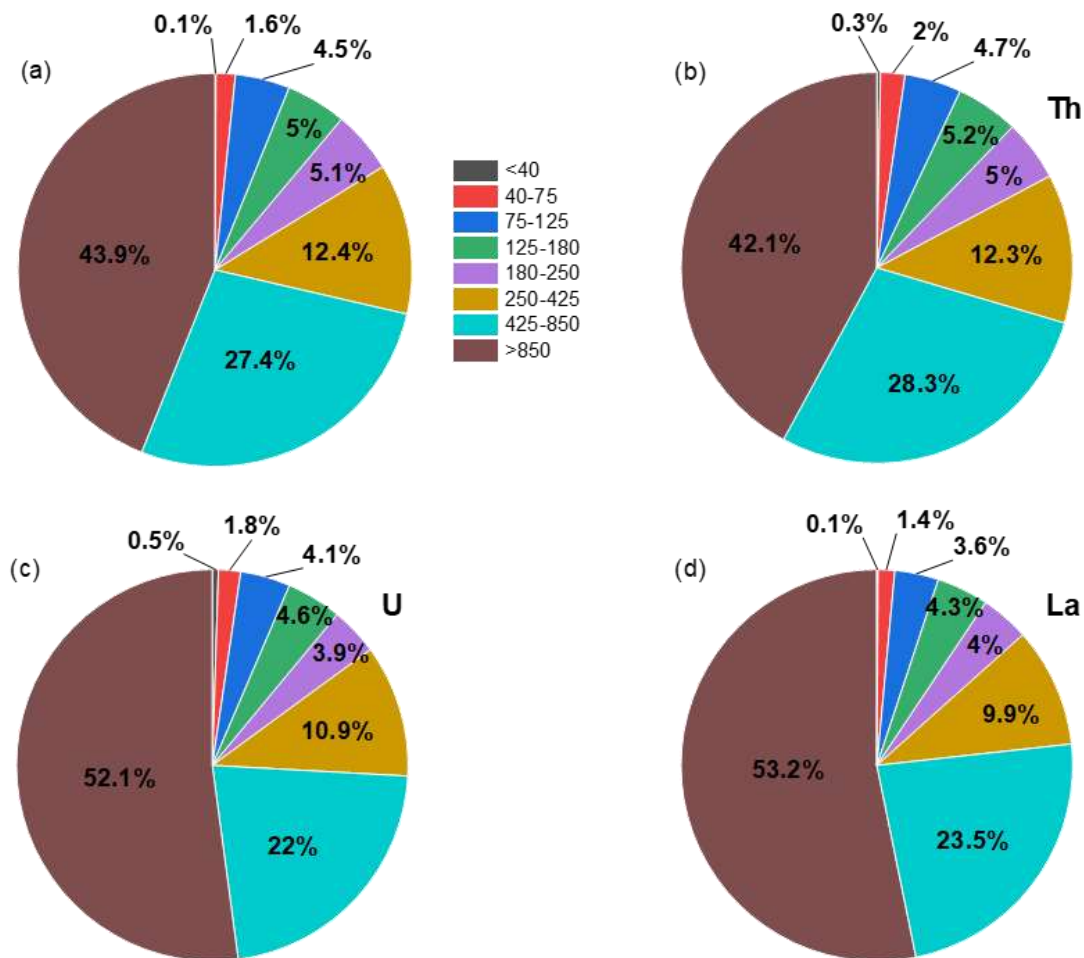


Figure 3.6: Contribution of each size fraction (a) to the bulk and elemental distribution of (b) Th, (c) U, (d) La in each size fraction of L-04 (note that the smallest size fraction $<40 \mu\text{m}$ is almost invisible in the pie chart. It is indicated by the percentage fraction of 0.1-0.5 %)

➤ *Element content of trace minerals*

Detailed microscopic scale information on the mineralogy was obtained by SEM and corresponding EDX spectroscopy. Both large area and spot analyses were carried out

to obtain a clearer picture of the mineralogy. The obtained atomic concentrations of elements (%) for Figures 3.7 – 3.12 are given in Table 3.7.

The SEM images and EDX spectra in Figure 3.7 suggest the presence of aluminosilicates and iron as major phases along with titanium (Ti) as traces in the large area analysis (the area given by the red frame in the inset), typically observed in all samples. Different orientations of hexagonal stacking layers of kaolinite clay minerals are visible in Figure 3.7b and c. A ratio close to 1:1 of Al:Si atomic concentration in both cases corroborates the presence of kaolinite inferred from XRD (Figure 3.3b).

The spot-chemical analysis mode in SEM-EDX yields more conclusive results concerning local abundance of Ln and Th in soil grains. Concerning Th-bearing minerals, several morphologies were identified. Typical spherical morphology of Ce-rich minerals containing Th is shown in Figure 3.8 (25 at.-% Ce, 5 at.-% Th). The low contents of P and Si in this example suggest that Ce and Th could be present as some oxide ((Ce,Th)O₂) phase. In fact, literature data provide evidence for (Th,Ce)O₂ solid solutions owing to the comparable ionic radii of Th(IV) and Ce(IV) [250].

La-rich monazite crystals were also identified together with kaolinite (Figure 3.9), with about 18 at.-% P and a total of ~13 at.-% for La, Ce, Nd and Th, suggesting that even in close vicinity to clays, these elements are present as phosphates. The kaolinite associated monazite mineral phases here always display needle like crystal morphology, while in a study from Sri Lanka monazite from the bottom sediments of the southwestern coast is well-rounded and has ellipsoidal and flattened-spherical shapes, and is predominantly angular prismatic crystal fragments in beach placers [249].

An elongated and rectangular Th-rich phosphate mineral (Figure 3.10a) was observed also presenting a total of ~14 at.-% for Th and P, while Si and Al are below 2 at.-%. The high amount of P suggests a phosphate phase in which Th occurs without any REEs, atypical for monazite-like phases.

Thorium associated with the oxide phase (Figure 3.10b) shows a Th-rich area with 18 at.-% Th and 77 at.-% O along with traces of Ce and clay minerals. Unambiguous crystal structures cannot be reported for this phase. Interestingly, the SEM-EDX spectrum of such a particle acquired using a 30 kV electron beam shows 3 at.-% U, which cannot be

seen with low voltages. Possible explanations are that (i) low energies intended for surface analysis, cannot detect U (which does not necessarily imply an absence of U at the surface), (ii) presence of mixed phases within the particle, do not show surface U exposure or (iii) differences in redox activity of U and Th preferentially solubilized U species. Solubility and speciation of metals in soils strongly depend on redox potential and pH [251]. The redox activity of U and U-oxides makes this element readily soluble in oxygenated water. Uranium has two main redox states in typical environments, U(IV) and U(VI). Under aerobic conditions, uranium oxidizes to the more mobile aqueous uranyl ion, UO_2^{2+} (section 1.2.2.2) [252].

Enrichment of Th-silicate phases potentially with a trace amount of Th-phosphate is alleged to be present in the studied soils with 19 at-% Th with high Si and low P. No definite crystal structure can be resolved for this phase either (Figure 3.11). The size of the largest Th-silicate mineral identified in one of the samples via SEM is $\sim 200 \mu\text{m}$ while Th/REE containing phosphate minerals are normally in the range of 50 – 250 μm . All these results provide evidence that most of the minerals found in these soil samples are not pure but rather present mixed solid phases. Other examples of mixed phases involve CeO_2 (crystalline spheres) and $(\text{Ce}, \text{La}, \text{Nd}, \text{Th})\text{PO}_4$ (needle-like crystals), within a single particle (Figure 3.12).

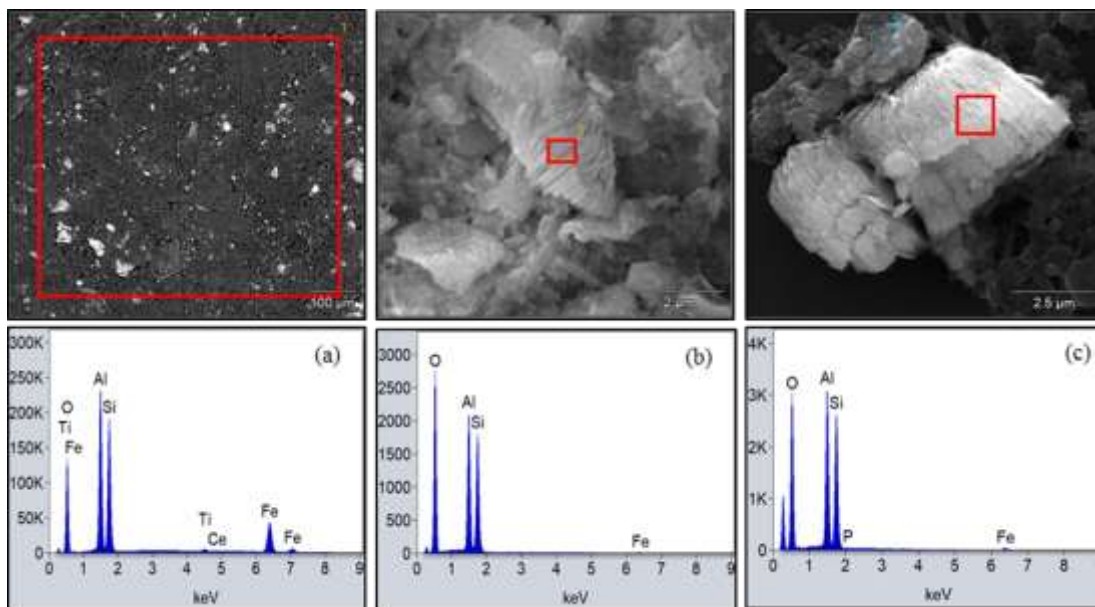


Figure 3.7: SEM and corresponding EDX spectra of (a) large area analysis, (b) and (c) spot analyses of clay minerals with hexagonal stacking layers in different orientations

Overall, three distinct Th containing mineral phases were identified: Th-oxide, Th-silicate and Th-phosphate. The identification of the exact mineral phases present in this work not possible from the SEM-EDX results and needs more sophisticated approaches. Examples of the specific Th mineral phases present in nature and in Sri Lankan sediments include monazite, thorite, thorianite, uranothorianite, ekanite, allanite, zirkelite, baddeleyite, samarskite, fergusonite, thorium pyochlore, oraganite, bastnaesite, thorogummite, cheralite, zircon, among others [253-255]. Many of these mineral phases are rare and not found in pure forms in nature. For instance, thorianite (ThO_2) and thorite (ThSiO_4) crystals are commonly associated with zircon, monazite, uranite, among others (as also observed in this study), and even incorporated in the zircon structure [46, 253, 256].

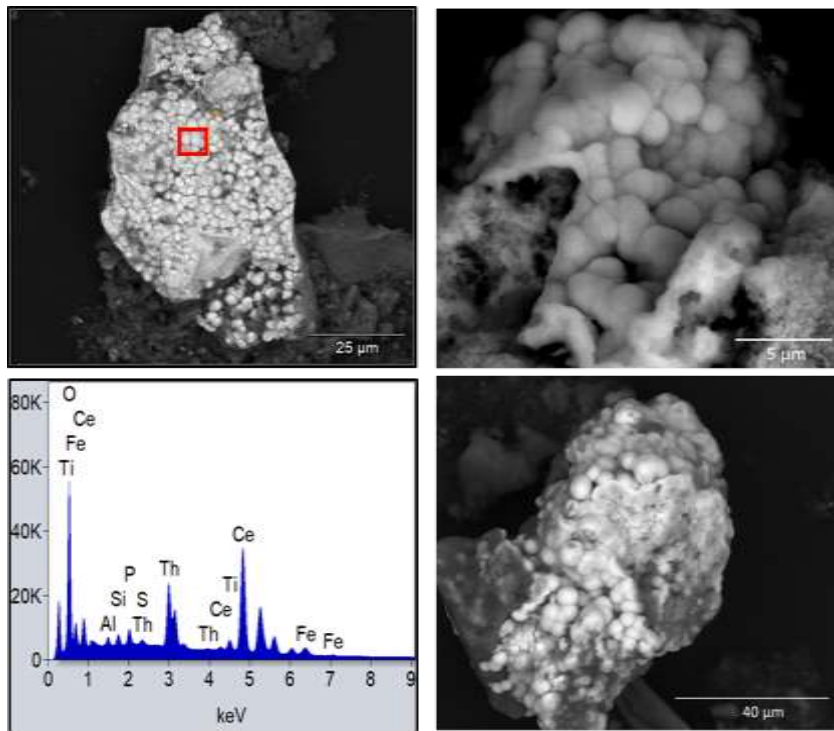


Figure 3.9: SEM images and corresponding EDX spectra of Ce-rich phases

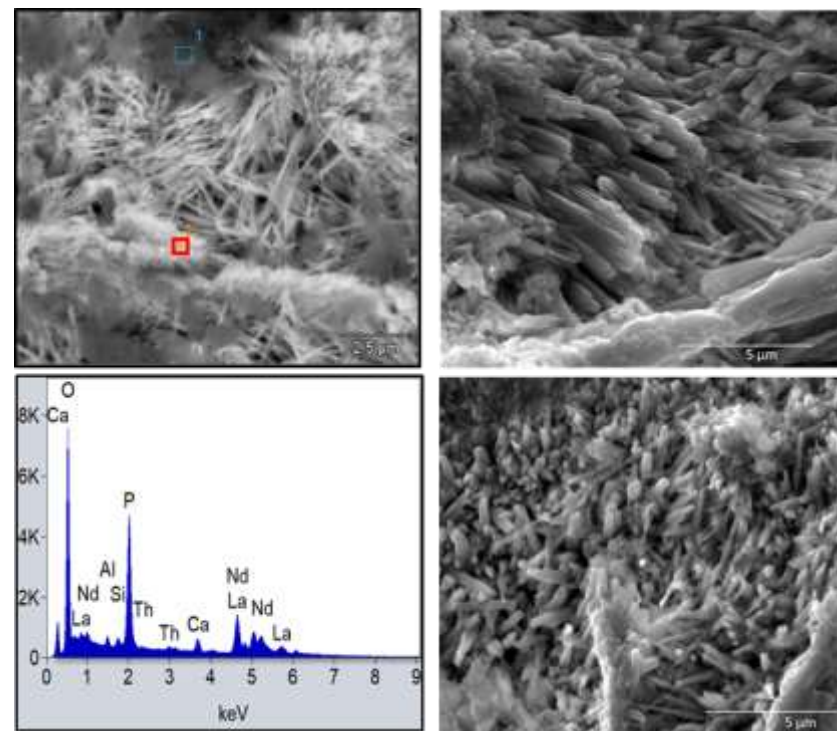


Figure 3.8: SEM images and corresponding EDX spectra of monazite phases

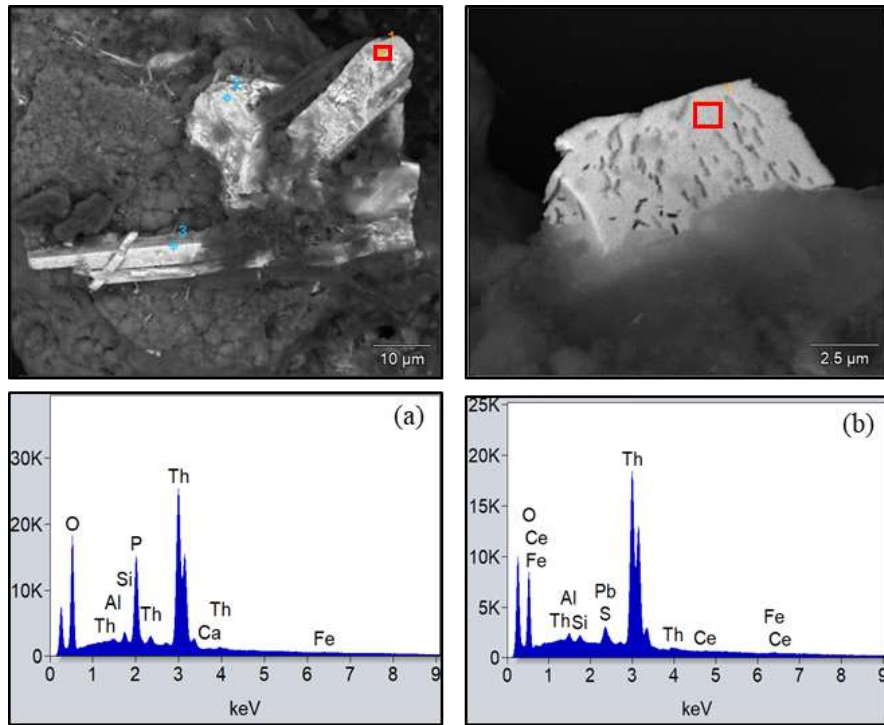


Figure 3.10: SEM images and corresponding EDX spectra of (a) Th-phosphate and (b) BSE-SEM image and corresponding EDX spectra of Th-oxide phases

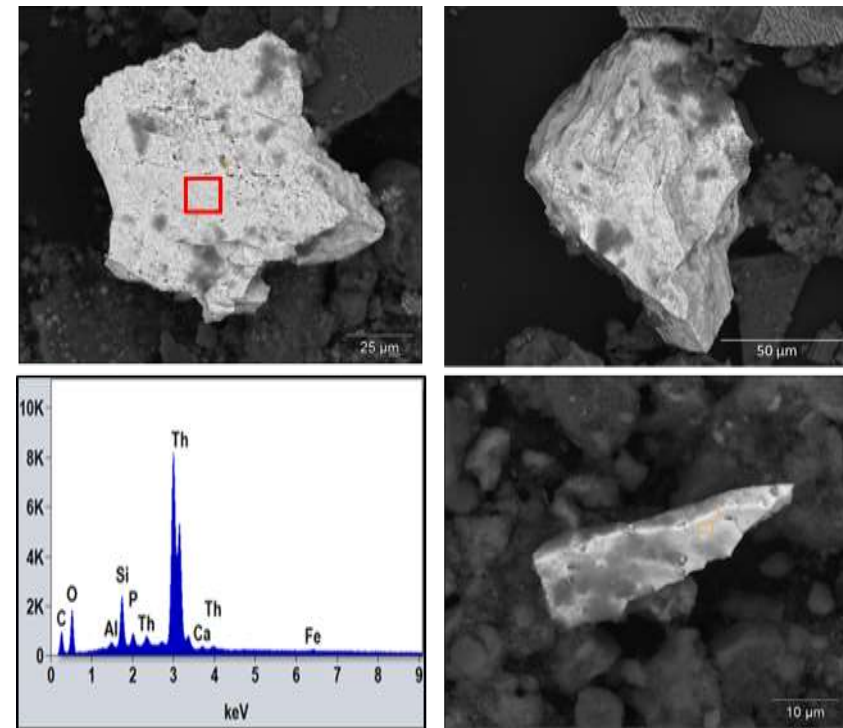


Figure 3.11: SEM images and corresponding EDX spectra of Th-silicate phases

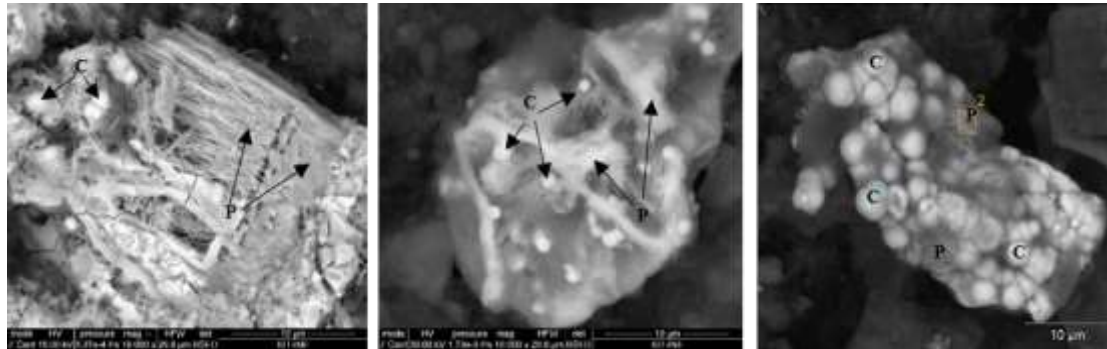


Figure 3.12: Mixture of mineral phases in soil; C denotes - (Ce,Th)-oxide and P denotes - (Ce, La, Nd, Th)-phosphate phases

Table 3.7: Atomic concentrations of elements (%) in area and spot analyses for Figures 3.7 - 3.11

Figure	Element – Atom %									
	O-K	Al-K	Si-K	Fe-K	Ti-K	P-K	Ce-L	La-L	Nd-L	Th-M
3.7										
(a)	62.8±0.5	16.6±0.1	17.2±0.1	3.2±0.0	0.2±0.0	-	-	-	-	-
(b)	67.4±1.5	15.7±0.5	16.5±0.6	0.4±0.2	-	-	-	-	-	-
(c)	68.0±1.7	15.1±0.3	16.4±0.5	0.5±0.1	-	-	-	-	-	-
3.8	59.2±0.6	1.6±0.1	1.9±0.1	2.2±0.2	2.7±0.2	2.7±0.1	25.2±0.3	-	-	4.6±0.1
3.9	64.3±1.3	1.3±0.3	1.0±0.2	-	-	18.0±0.3	2.4±0.4	8.6±0.6	2.1±0.5	0.3±0.1
3.10										
(a)	70.9±1.1	0.5±0.1	1.7±0.1	0.3±0.1	-	13.8±0.2	-	-	-	13.7±0.2
(b)	77.0±2.1	1.6±0.3	1.5±0.2	0.5±0.3	-	-	0.1±0.2	-	-	18.1±0.3
3.11	62.9±2.5	1.5±0.4	12.5±0.3	0.5±0.3	-	3.3±0.2	-	-	-	18.6±0.4

3.3. Speciation of Th in soil minerals

Detailed information on solid phase speciation of Th can be revealed via X-ray absorption spectroscopy (XAS), which is element specific and provides molecular-scale information. Several studies on Th speciation using XAS are available in the literature focusing on: (i) Th(IV) containing materials synthesized in the laboratory [51, 257], (ii) Th(IV) interaction with organic matter [258, 259], (iii) Th(IV) in natural minerals from ores [260], and (iv) adsorption studies of Th(IV) by mineral surfaces [261-263]. However, XAS studies of Th(IV) in natural soil samples from topsoils are to our knowledge not available in the literature.

3.3.1. Bulk XAS analysis of Th containing minerals

For bulk analyses, the two main regions in X-ray absorption spectra, i.e. X-ray Absorption Near-Edge Structure (XANES) and Extended X-ray Absorption Fine Structure (EXAFS), were used to study the chemical environment of Th (Figure 3.13a). The XANES region of the sample spectra is compared to that of reference compounds (RCs) to gain information on coordination geometry, whereas EXAFS spectra are employed to gain quantitative information on the phase assemblage. XANES and EXAFS are highly sensitive to the local chemical environment and can be considered to some extent as a “fingerprint” of certain chemical species. In this sense, chemical speciation of Th was investigated using XAS in different aliquots from the same soil samples and from some soil residues after sequential extractions (Chapter 4). Since the previous solid phase characterizations showed that the target samples are quite heterogeneous, it is obvious that recorded bulk XAS data would correspond to the sum/average of the various Th species.

The normalized XANES spectra, k^2 -weighted EXAFS ($k^2 \cdot \chi(k)$) spectra and corresponding Fourier transformations (FT) of all soil samples and selected residues from sequential extraction steps (F4 (Ex4) and F5 (Ex5) of L-05) along with the RCs are shown in Figures 3.13a,b,c, and 3.14a,b,c, respectively. The Ex4 fraction is obtained after the treatment with Tamm’s reagent and Ex5 after treatment with Coffin’s reagent (Table 2.1), which according to the definition should extract the metals attached to amorphous and crystalline Fe-Mn oxyhydroxides, respectively (Section 2.4.2). The RCs were chosen to represent the main mineralogical species of Th identified in section 3.3, i.e. Th-silicate, Th-oxide, and Th-phosphate containing mineral phases.

A main feature at 16304 eV can be seen in all absorption edges of the recorded Th L₃-edge XANES spectra (Figures 3.13a and 3.14a), which is consistent with Th in tetravalent oxidation state in all analyzed soil samples and residual samples from chemical extraction steps, as expected for natural samples [46]. The second feature at 16320 eV is more pronounced only in ThO₂ RC and virtually absent in the rest. For ThO₂ this second feature can be assigned to a solid phase of relatively high degree of crystallinity arising from different transition probabilities due to backscattered electrons. In amorphous ThO₂ and Th(OH)₄, this feature is less pronounced or even absent [264]. Therefore, the XANES spectra could probably hold as an indication that the Th-minerals in the soil have a higher degree of disorder, even after some chemical extractions.

Analyses were performed in the k-range and R-range from 2.9 – 7.5 Å⁻¹ and 1 – 5 Å, respectively, for all samples and RCs. The data in Figures 3.13b and 3.14b (i.e. k²-weighted $\chi(k)$ functions) and in Figures 3.13c and 3.14c (the corresponding FT magnitudes) suggest minor variability in the mineralogy of Th among the studied soil samples, but significant differences with respect to the RCs. It can be inferred that Th in the bulk soils (< 0.17% wt.) is not present as pure single phase ThO₂, ThSiO₄ or monazite. This agrees with the SEM-EDX results, which highlighted the heterogeneity of the studied soil samples in terms of Th speciation.

Interestingly, for the bulk soil samples, despite the limited k-range ($\Delta k = 4.6 \text{ \AA}^{-1}$) all FTs (Figure 3.13c) contain two main peaks, located at $R + \Delta R \sim 1.8 \text{ \AA}$ and $\sim 3.4 \text{ \AA}$. The intense peak around 1.8 Å, which corresponds to a phase-corrected value of about 2.4 – 2.5 Å, represents backscattering from oxygen atoms (Th – O) in the first coordination shell of the central absorbing Th atom and is in accordance with XAS measurements on pure Th(IV) oxide/hydroxide phases [51]. The second peak at around $R + \Delta R \sim 3.4 \text{ \AA}$ is located at a phase corrected distance of 3.8 – 3.9 Å and can be assumed to originate from nearest Si/Th/P neighbours, in agreement with the thorite [265], monazite [266], or thorianite (pure ThO₂ [51]) crystal structures. This suggests similarities between the soil samples and thorite, while the observed differences among the spectra suggest the presence of more than one mineral phase of Th in the natural samples.

Another captivating observation in Figure 3.14c, the FTs of the residues after F4 and F5 chemical extractions of L-05 compared to the same bulk sample, show that none of

the FTs of extracted residues are similar to that of the originating bulk soil sample suggesting that the chemical extraction steps alter the mineralogy of the soil sample. However, some similarities can be seen with respect to the RCs. Thus, Ex4 seems to follow the shape of the thorite while Ex5 rather resembles thorianite. The second peak of Ex4 located at the phase corrected distance of about 3.5 Å is closer to that of thorite while the peaks of Ex5 at 2.6 – 3.2 Å and 3.2 – 4.2 Å follow the peak pattern of thorianite. However, these observations are somewhat unexpected since the extraction with Tamm's reagent used for Ex4 leaves the very stable silicate while the stronger extractant, Coffin's reagent, used in Ex5 leaves the less stable ThO₂. Yet, since none of the spectra shows the exact pattern of any of the RCs, mineral heterogeneity of the samples still prevails.

Linear combination fitting (LCF) was carried out to estimate the weight percentage contribution of each major mineral phase to the bulk. LCF treatment of the XAFS data was preferred over typical shell-by-shell EXAFS fitting for the soil samples here as it was expected that soil samples contain mixtures of various Th(IV) phases. In fact, modelling the data using single scattering paths (i.e., Th-O, Th-Si, Th-P, Th-Th, etc.) is complicated by possible overlaps from shells located at comparable distances in the host structures, especially with limited k-ranges as for these low concentration samples. The LCF analysis of the EXAFS spectra of the four soil samples (Figure 3.15) and the extracted mineral contributions (Figure 3.16) yielded the RCs with comparable proportions (Table 3.8).

Fitting the bulk soil sample data revealed that monazite has the highest contribution to the experimental spectra with $61 \pm 7\%$, followed by thorite with $24 \pm 7\%$, while thorianite has the smallest proportion with $16 \pm 7\%$ (percentages are averaged over all four samples). Besides, some fine details can be highlighted with LCF data of the extracted soil samples, which agree well with the features of the corresponding FTs (Figure 3.14c). Notably, Ex4 sample showed higher weight percentage of thorite (35%) whereas Ex5 illustrated more percentage of thorianite (32%) in their matrices with lower percentages of monazite compared to the average bulk soil samples. Even though these data seem promisingly fitting with the remarks of their FTs, the differences in the spectra might still be either due to the extractions or the consequences of the heterogeneities of the sample aliquots.

In addition to the mixed mineral phases and inherent heterogeneity, samples may also contain minor amounts of other species such as Th sorbed to various minerals or bound to organic matter. Phases for which Th has a high sorption affinity are present in the sample such as clay minerals dominated by kaolinite, iron phases and organic matter. One may assume that in the soil samples Th might occur as Th-bearing mineral phases (i.e., Th-phosphate, Th-silicate, Th-oxide) along with traces of Th retained within mineral lattices or adsorbed at surfaces (i.e., iron oxides, organic matter and clay minerals). This heterogeneity widens the perspectives for chemical batch extractions (discussed in detail in Section 4.2.1) meaning that Th could be extracted via single extraction procedures aiming at identifying ion exchange, carbonate or organic matter bound metal ions.

Table 3.8: Thorium L₃-edge EXAFS spectra linear combination fitting results for soil samples and sequential extraction residues from F4 (Ex4) and F5 (Ex5)

Sample	Weight contribution (%)			Fit parameters*
	Monazite	Thorite	Thorianite	
L-03	67	14	19	R = 0.052106 $\chi^2 = 0.012900$
L-04	54	26	20	R = 0.042861 $\chi^2 = 0.011761$
L-05	63	24	13	R = 0.043632 $\chi^2 = 0.011060$
L-06	59	31	10	R = 0.042318 $\chi^2 = 0.011144$
Average	61 ± 7	24 ± 7	16 ± 7	
L-05-Ex4	50	35	15	R = 0.057586 $\chi^2 = 0.016553$
L-05-Ex5	46	22	32	R = 0.080901 $\chi^2 = 0.026112$

*R: R-factor; χ^2 : goodness of fit for the k-range 2.9 – 7.5.

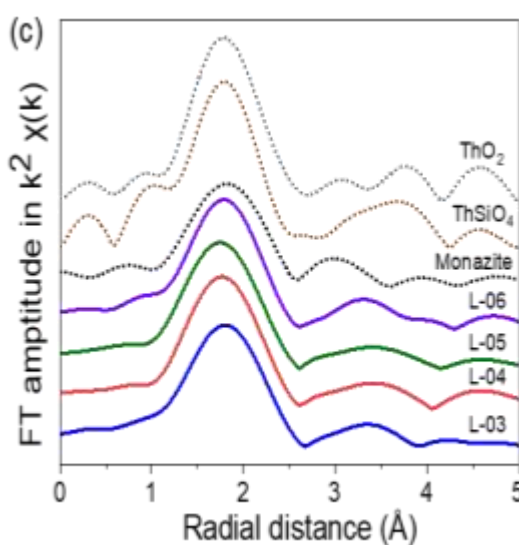
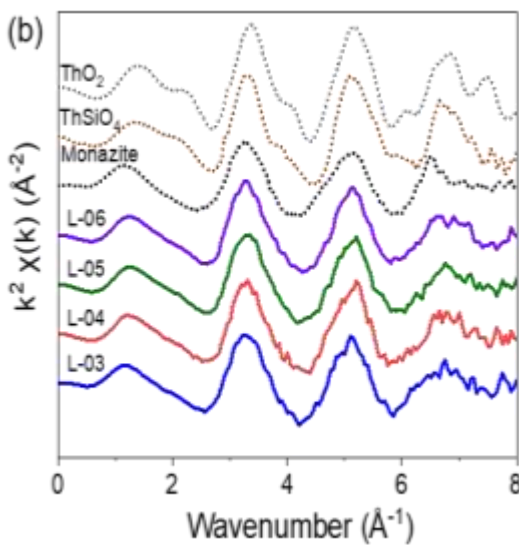
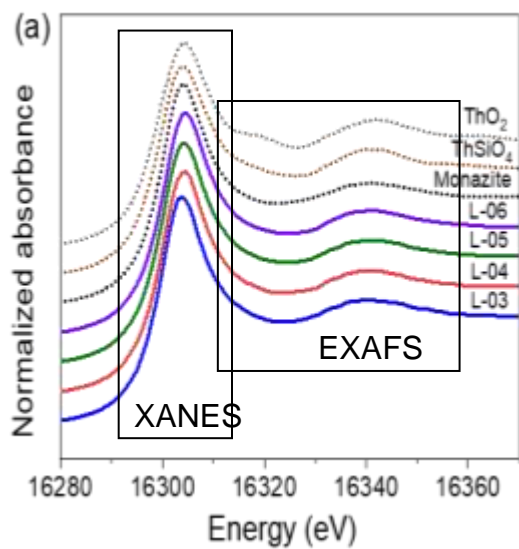


Figure 3.13: Thorium L₃-edge (a) XANES and (b) EXAFS spectra with (c) corresponding FT of all samples and RCs (distance is not corrected for phase shift)

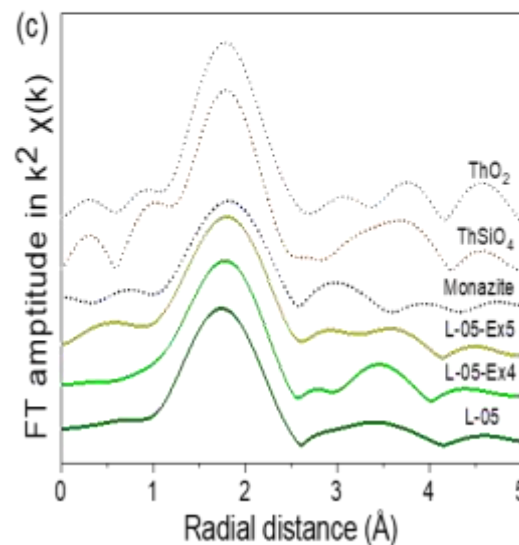
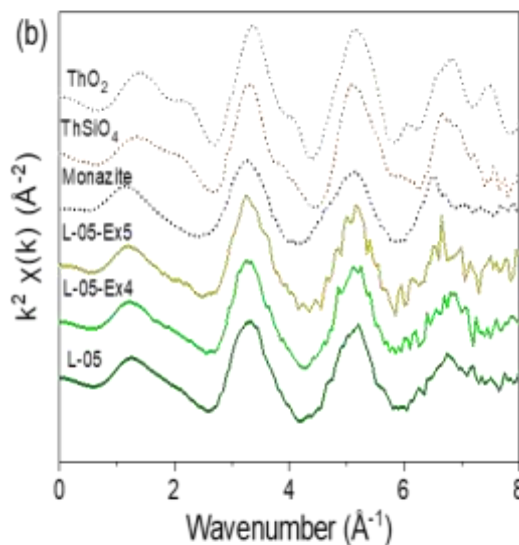
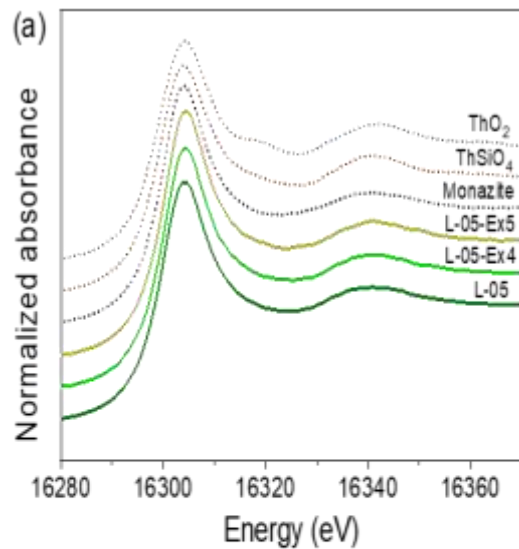


Figure 3.14: Thorium L₃-edge (a) XANES and (b) EXAFS spectra with (c) corresponding FT of L-05 and sequential extraction residues from F4 (Ex4) and F5 (Ex5)

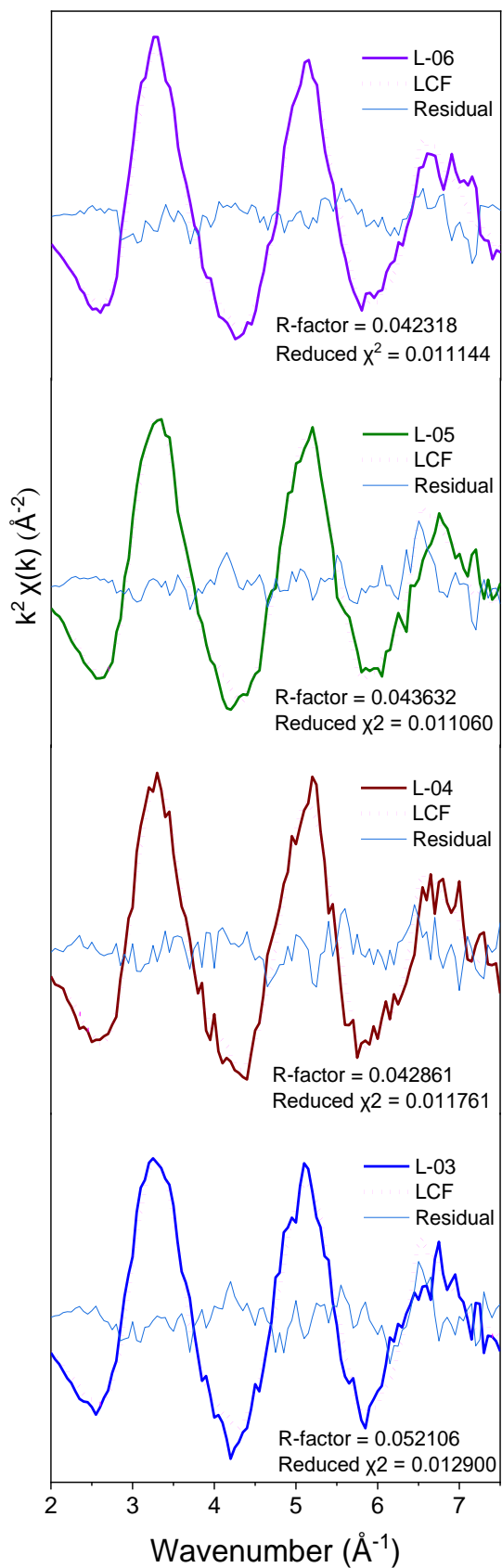


Figure 3.15: Experimental (solid line) and LCF modeled (dashed line) EXAFS spectra of the soil samples with residual (blue line). R-factor and reduced χ^2 are represented for individual fits

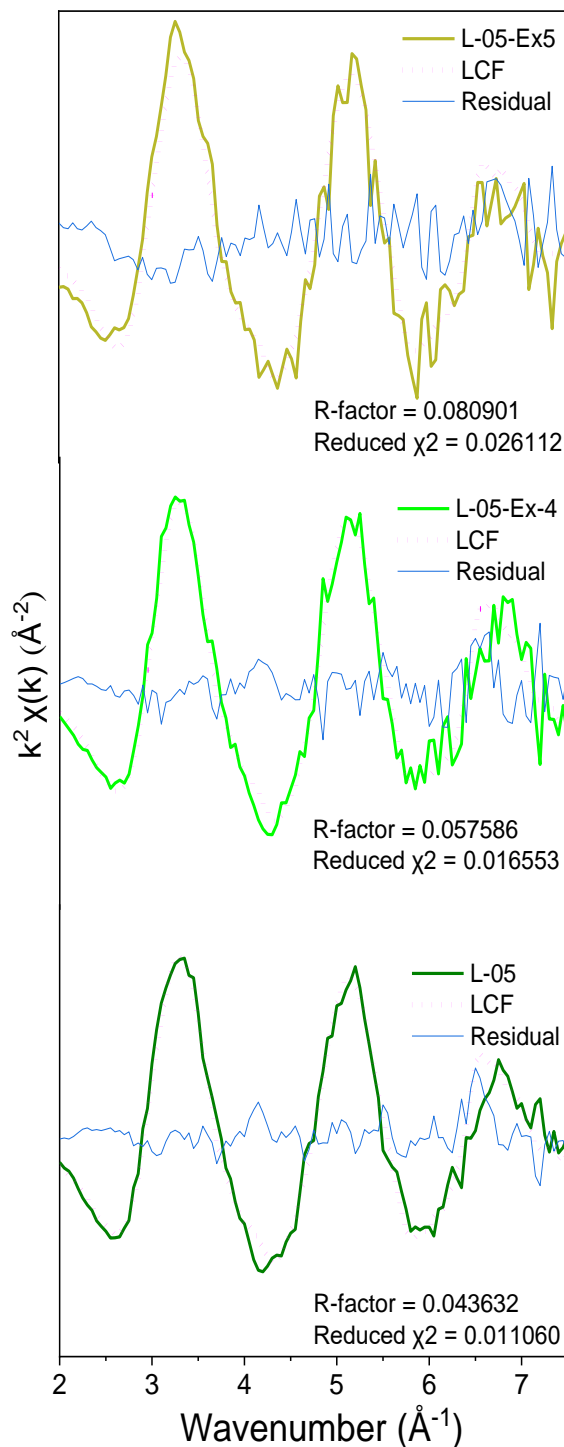


Figure 3.16: Experimental (solid line) and LCF modeled (dashed line) EXAFS spectra of L-05, L-05-Ex4 and L-05-Ex5 samples with residual (blue line)

3.3.2. Small area analysis of specific Th-containing particles

Since these soil samples are mineralogically heterogeneous, additional investigations on selected particles of these samples by both SEM-EDX and XAS with a micron size beam footprint (μ -XAS) were performed. The objective was to analyze small isolated grains in the soil samples at higher spatial resolution utilizing a micro-focused beam in order to collect X-ray fluorescence data (μ -XRF) and further select points of interest for application of X-ray absorption spectroscopy (μ -XAS). The μ -XRF technique can be used to determine elemental composition and distribution (elemental mapping) for a given particle due to its relative simplicity and non-destructive character. Although, SEM-EDX has higher spatial resolution than μ -XRF, the latter has certain advantages over SEM-EDX particularly in this study due to the effect of beam size vs particle sizes. μ -XRF has certain advantages over SEM-EDX regarding the elemental analysis. Additionally, high penetration depth of X-rays, absence of sample pre-treatments [267], and improved resolution for the analysis of heavy elements are helpful. The composition resulting from μ -XRF characterizes the entire particle while the near surface composition is obtained by SEM-EDX since it probes only a few μm below the surface, depending on the material composition and the electron acceleration voltage. However, if the size of the particle is a few μm only, SEM-EDX may also provide information on the entire particle.

Elemental analysis using SEM-EDX was performed under high vacuum mode allowing the detection of fluorescence at low energies, whereas analyses by μ -XRF were performed with X-rays of high energies under ambient conditions allowing the detection of fluorescence energies above ~ 3 keV. The two techniques provide complementary information since SEM-EDX is better suited to detect light elements (e.g., O, Na, Mg, Al, Si) which cannot be detected using μ -XRF at ambient conditions. From the elemental point of view and the information depth of the analysis, SEM-EDX provides higher resolution for surface composition while μ -XRF prone to explain the entire mineral composition. Both approaches consistently depict that the soil samples are assemblages of particles with variable compositions, and the nature of the particles agrees with XAS analyses of the bulk samples.

Three particles with different size and mineralogy, which had been identified as Th-silicate-, Th-oxide-, and Th-phosphate dominated phases by SEM-EDX were selected

for further investigations. The corresponding weight (wt.%) and atomic (at.-%) contributions of the detected elements of each particle are shown in Table 3.9. The electron images of the selected particles together with the corresponding SEM-EDX spectra and fitted μ -XRF spectra are displayed on Figures 3.17, 3.20 and 3.23. The μ -XRF spectra were fitted using the PyMca Fluorescence Toolkit to identify the elements present in each particle.

The selected Th-silicate particle is $\sim 10 \mu\text{m}$ in size (Figure 3.17a) according to SEM imaging and contains $\sim 70 \text{ wt.}\%$ of Th based on EDX analysis (Figure 3.17b, Table 3.9). The particle appears to have a size of $\sim 30 \mu\text{m}$ based on μ -XRF mapping (Figure 3.18a) which is due to the much larger beam footprint. The particle contains significant amounts of Si, compared to other major elements (Table 3.9) and the molar Th/Si ratio of 1.1 in the particle and the O/Si ratio of 4.2 indicate predominance of ThSiO_4 . The SEM-EDX spectra of the particle (Figure 3.17b) also illustrate the presence of small amounts of Al, P, Fe and, to a smaller extent, Ca (mapped in Figure 3.19c,e,g,f). These elements could stem from trace amounts of surface attached clays and other mineral phases, such as kaolinite and goethite. These findings are validated by μ -XRF spectra (Figure 3.17c), which further highlight the presence of small amounts of Pb and Y, and possibly minor levels of Ni, Cu and Zn. Further information on the association of various elements within the particle was obtained by recording μ -XRF maps. The total fluorescence yield are depicted in Figure 3.18a, whereas Figure 3.18b,c show the fluorescence of selected elements recorded for the Th-silicate particle. Visual differences in μ -XRF maps (Figure 3.18b,c) are supported by a weak correlation between Th and Y ($\rho = 0.667$), suggesting the presence of a single major phase containing Th with smaller contributions of Y. Information on the element composition of the particle surface layer down to some μm depth, especially for the elemental distribution of the light elements, is obtained from the SEM-EDX elemental maps (Figure 3.19). Both XRF (Figure 3.18b) and EDX (Figure 3.19h) maps show homogeneous Th distribution across the particle. Indications for heterogeneities in the Y distribution could not be evidenced by EDX. This might be due to the low Y-content in the sample which is close to or below the detection limit of EDX. Another possibility is that Y is mainly located below a Th silicate surface layer. The EDX maps illustrate the existence of a uniform Th silicate phase with Si and O being uniformly distributed all over the particle (Figure 3.19b,d).

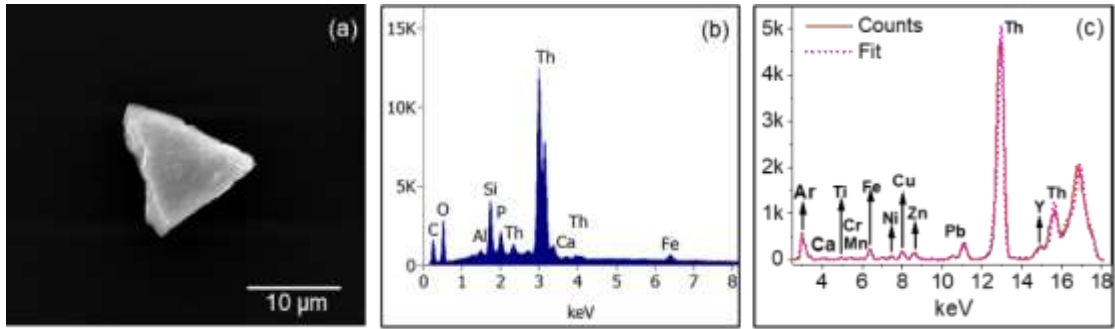


Figure 3.17: (a) The SEM images, (b) corresponding EDX, and (c) μ -XRF spectra (solid line) with fits (dotted line) of the selected Th-silicate rich particle

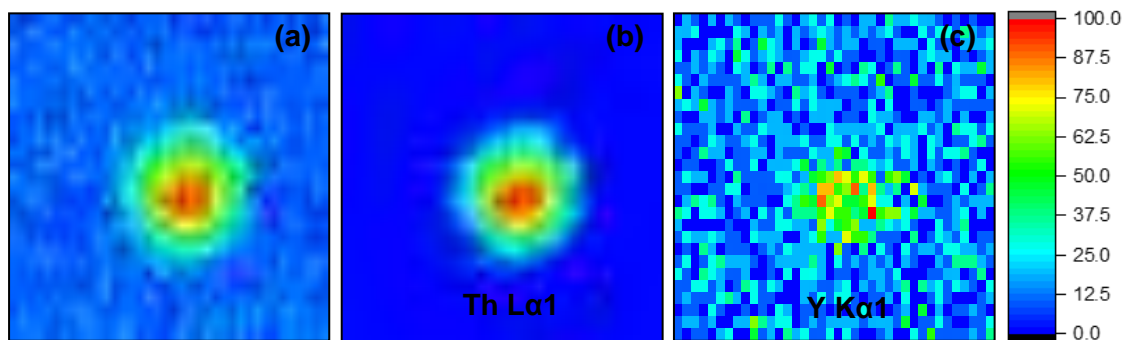


Figure 3.18: μ -XRF maps of the Th-silicate particle (a) showing total fluorescence and fluorescence lines of (b) Th and (c) Y (maps: 82.5 μ m in width, 67.5 μ m in height). The scale represents normalized count integral

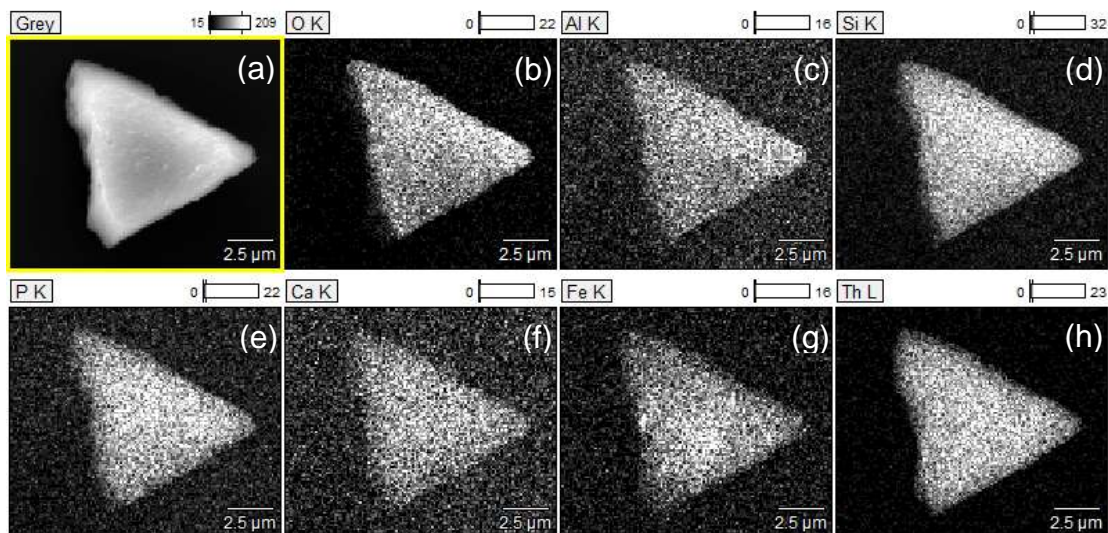


Figure 3.19: (a) SEM image of the Th-silicate particle and corresponding SEM-EDX elemental maps for O, Al, Si, P, Ca, Fe, and Th (b – h) in counts

The Th-oxide particle studied is ~25 μm in size as observed by SEM (Figure 3.20a) and has high Th (~15 wt.%) and Ce (~38 wt.%) contents with relatively small amounts of Fe, Al, and Si identified by EDX spectra (Figure 3.20b, Table 3.9). In addition, when fitting XRF spectra (Figure 3.20c), it was found that this particle contains Pb and possibly low levels of Cu and Ni. The molar ratio of 5.7 from O:(Th+Ce) clearly indicates the presence of distinct oxide phases. Considering the presence of phosphates, Fe-oxides and silicates, the O:(Th+Ce) ratio is too high for the presence of only Th/CeO₂. The EDX analysis would rather point to some kind of Th/Ce(OH)₄ or Th/CeO(OH)₂. This would also agree with the XANES spectra. As a conclusion, the data suggest that the particle is mostly composed of oxides, apparently Th-oxide or hydroxide mixed with Ce-oxide/hydroxide as the major component, which is further confirmed by the distribution of Th and Ce in the fluorescence maps (Figure 3.21a-c), yielding significant correlation (i.e., $\rho = 0.970$; Appendix 3.7, Figure A3.6). In fact, literature data provide evidence for (Th,Ce)O_x(OH)_y solid solutions owing to the comparable ionic radii [250, 268] of Th(IV) and Ce(IV). EDX maps (Figure 3.22g, j) show an inhomogeneous distribution of Fe compared to Th, i.e. higher density areas of accumulation at the lower part of the particle, suggesting iron oxide phases, being slightly depleted in Th, attached to the (Th, Ce)O₂ particle. The seemingly homogeneous Fe-distribution in the fluorescence maps (Figure 3.21b, d) and significant correlation with Th (i.e., $\rho = 0.806$; Appendix 3.7, Figure A3.6) are due to lack of spatial resolution. A small clay mineral flake is observed (Figure 3.22c, d) at the bottom corner of the particle. A relatively consistent surface distribution of Ce can be seen in the EDX map (Figure 3.22i), matching that of O and to a lesser extent to traces of Si and Al in spite of the mapping shadow effect, and adsorbed clay fractions containing REEs (Figure 3.22b-d). The weaker intensities for the Th and Ce signal in the area where the Fe signal is enhanced could be interpreted by overlay of a Th/Ce-oxide particle by iron oxide. Both Ce and Th are related to a small extent ($0.65 < \rho < 0.85$; Appendix 3.7, Figure A3.6) to traces of Ti and Pb (Figure 3.21e, f), indicating that the correlation analysis mostly reflects counting statistics. In summary, these data show that the natural Th-oxide particles are not pure ThO₂ (thorianite), but presumably consist of a (Ce, Th)oxyhydroxide solid-solution covered by accessory clay minerals and Fe-oxide phases, including traces of P, Ti, Mo, and potentially also Ce (Figure 3.22e, f, h, i). However, it is impossible to draw conclusions with regard to the direct binding of Th

to those accessory mineral phases due to the fact that iron oxide and clay minerals are closely associated with Th-minerals and EDX cannot clearly distinguish between them.

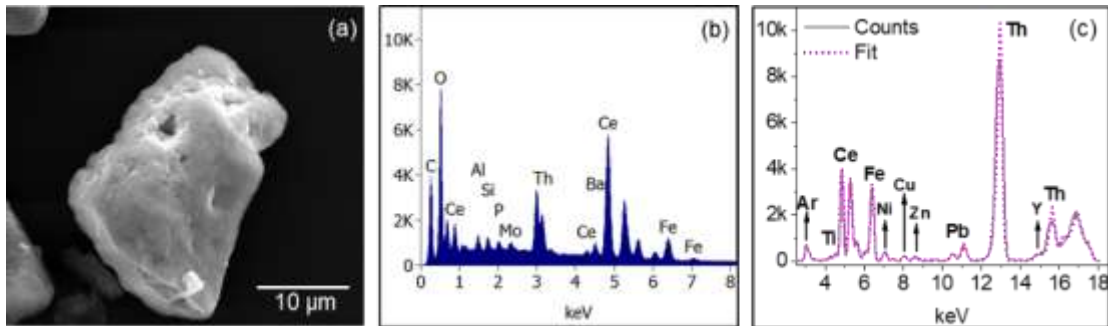


Figure 3.20: (a) The SEM images, (b) corresponding EDX, and (c) μ -XRF spectra with fits of the selected Th-oxide rich particle

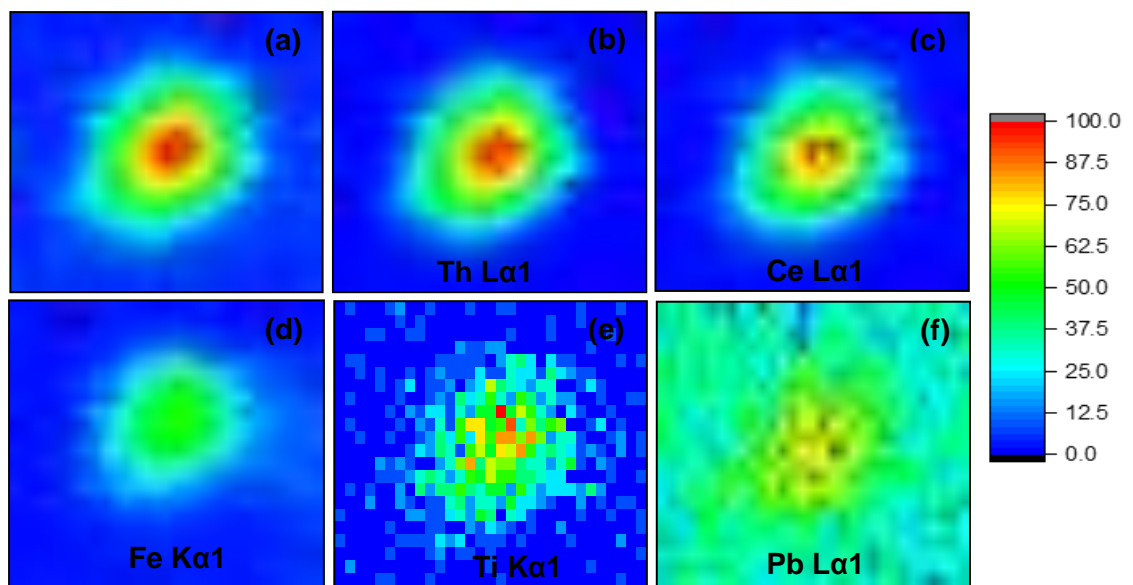


Figure 3.21: μ -XRF maps of the Th-oxide particle showing (a) total fluorescence and fluorescence lines of (b) Th, (c) Ce, (d) Fe, (e) Ti and (f) Pb (maps: 107.5 μm in width, 55 μm in height). The scale represents normalized count integral

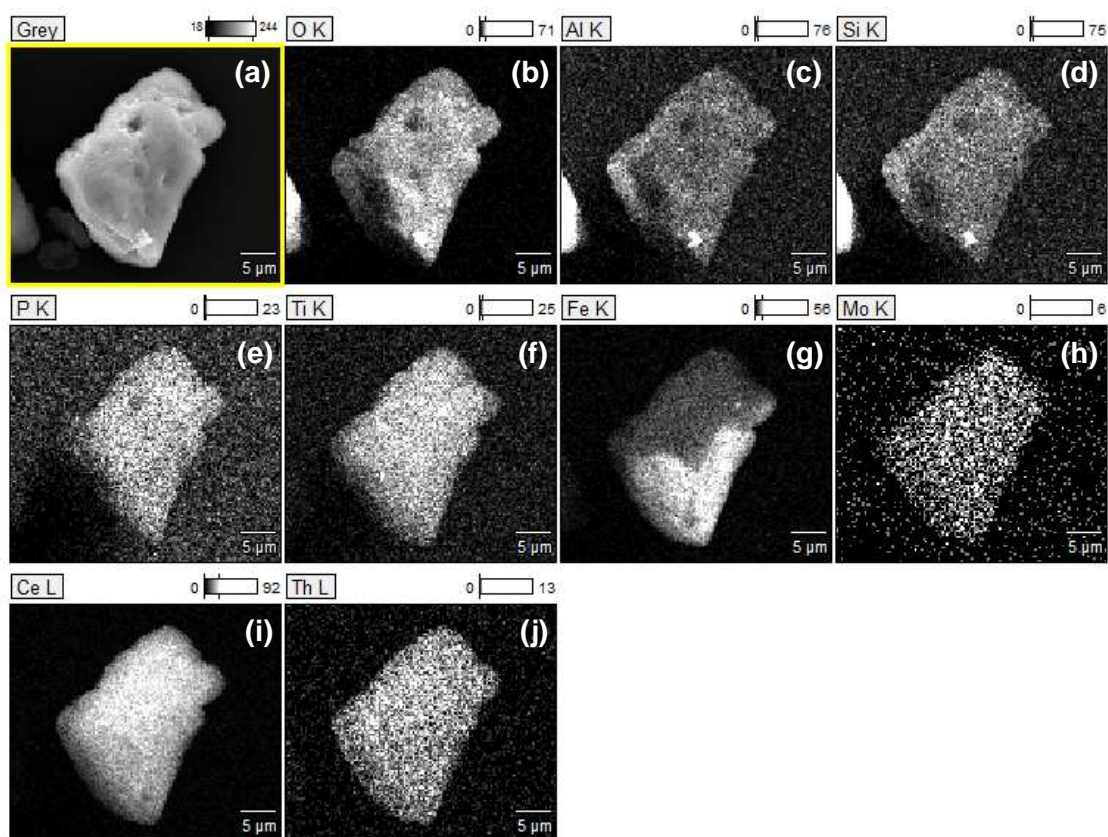


Figure 3.22: (a) SEM image of Th-oxide particle and SEM-EDX elemental maps for O, Al, Si, P, Ti, Fe, Mo, Ce, and Th (b – j) of the particle in counts

The $\sim 50 \mu\text{m}$ sized Th-phosphate containing particle (Figure 3.23a) has lower Th content ($\sim 1 \text{ wt.}\%$, Figure 3.23b), compared to the silicate and oxide particles, but contains significant amounts of P and light REEs (Table 3.9). The total REE (La, Ce, Nd, Pr) content amounts to $\sim 44 \text{ wt.}\%$ (Figure 3.23b), comparable to $\sim 45 \text{ wt.}\%$ in the RC-monazite (Table 3.9). Hence, it can be assumed that this soil particle is depleted in Th, $(\text{Ce}_{0.43}, \text{La}_{0.25}, \text{Nd}_{0.16}, \text{Pr}_{0.04}, \text{Th}_{0.01}, \text{Ca}_{0.10})(\text{P}_{0.98}, \text{Si}_{0.02})\text{O}_4$, compared to the RC monazite from Brazil, $(\text{Ce}_{0.41}, \text{La}_{0.11}, \text{Nd}_{0.27}, \text{Pr}_{0.06}, \text{Th}_{0.14}, \text{Ca}_{0.01})(\text{P}_{0.96}, \text{Si}_{0.04})\text{O}_4$. The high P content and the absence of significant amounts of Al and Si based on the EDX spectra (Figure 3.23b) clearly suggest that the particle mostly consists of a phosphate phase. μ -XRF measurements further indicate that this particle contains more elements than the two other studied particles (c.f. the fluorescence spectra and maps in Figures 3.23c and 3.24b-i). Iron shows a non-negligible contribution and the highest correlations with the analyzed light REEs and Ca (i.e., $\rho > 0.92$; Appendix 3.7, Figure A3.7). Despite the low Th concentrations in this particle, its distribution is clearly correlated to those of the REEs (i.e., $\rho > 0.75$), though the highest correlations of Th are found with Y and Pb

(i.e., $\rho > 0.87$; Appendix 3.7, Figure A3.7). Additionally, Th, Pb, Ca, and U show positive skewness of the data distribution (Appendix 3.7, Figure A3.7). All these observations suggest the presence of different compositions of monazite-type minerals, in accordance with EXAFS observations, which is further confirmed by results from A.-M. Seydoux-Guillaume *et al.* [269] who studied low temperature alteration of a Sri Lankan monazite sample. The REEs seem to be present in mixed phases, since the EDX maps for REEs and P show a uniform distribution of these elements over the particle (Figure 3.25e, h-k). Nevertheless, REEs, and in particular Ce, show higher element abundance compared to P, pointing towards the presence of REEs as both, mixed phosphate phases (i.e., in accordance with the main monazite mineralogy) and oxide phases. A uniform distribution of Th is also provided by the EDX map (Figure 3.25l). To some extent, the data sets again suggest the presence of clay minerals and Ca-/Fe-phases suggesting potential correlation with lanthanides and actinides within the particle and/or at surface (Figure 3.25c,d,f,g).

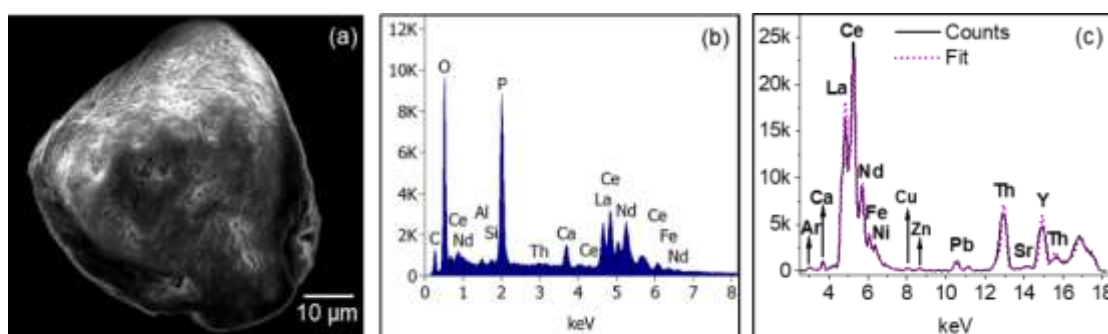


Figure 3.23: (a) The SEM images, (b) corresponding EDX, and (c) μ -XRF spectra with fits of the selected Th-phosphate rich particle

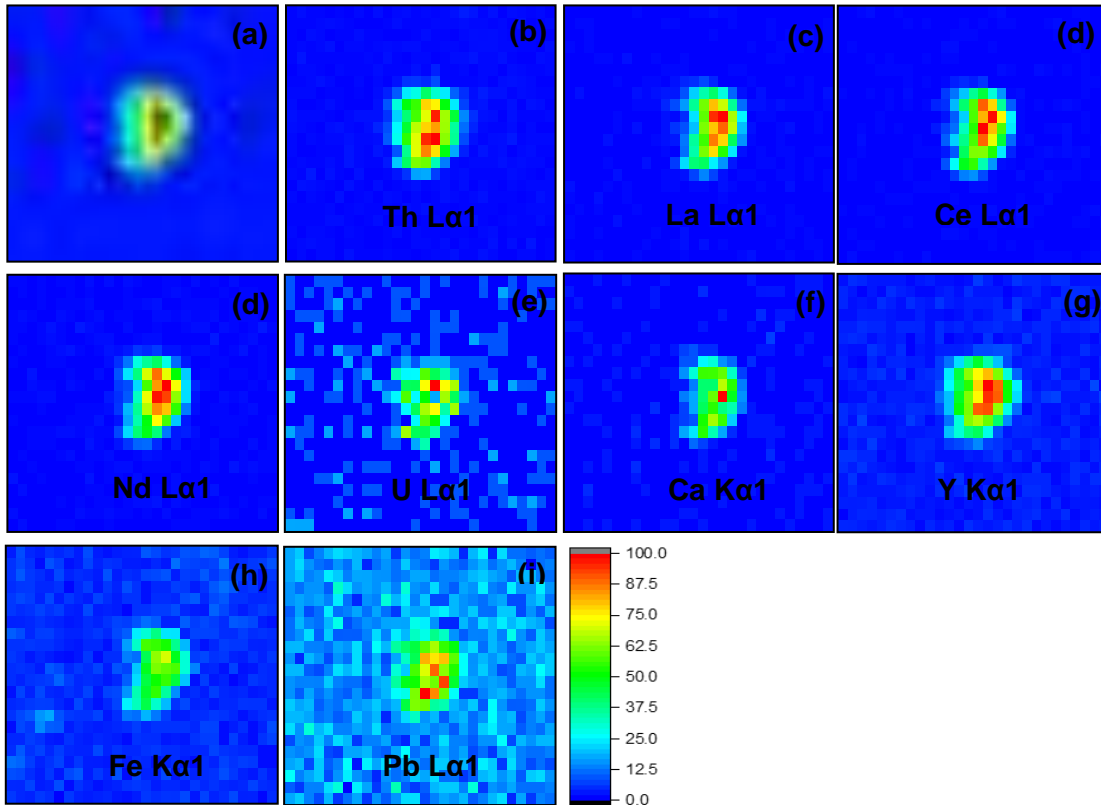


Figure 3.24: μ -XRF maps of the Th-phosphate particle showing (a) total fluorescence and fluorescence lines of (b) Th, (c) La, (d) Ce, (e) Nd, (f) U, (g) Ca, (h) Y, (i) Fe, and (j) Pb (maps: 230 μm in width, 183 μm in height). The scale represents normalized count integral

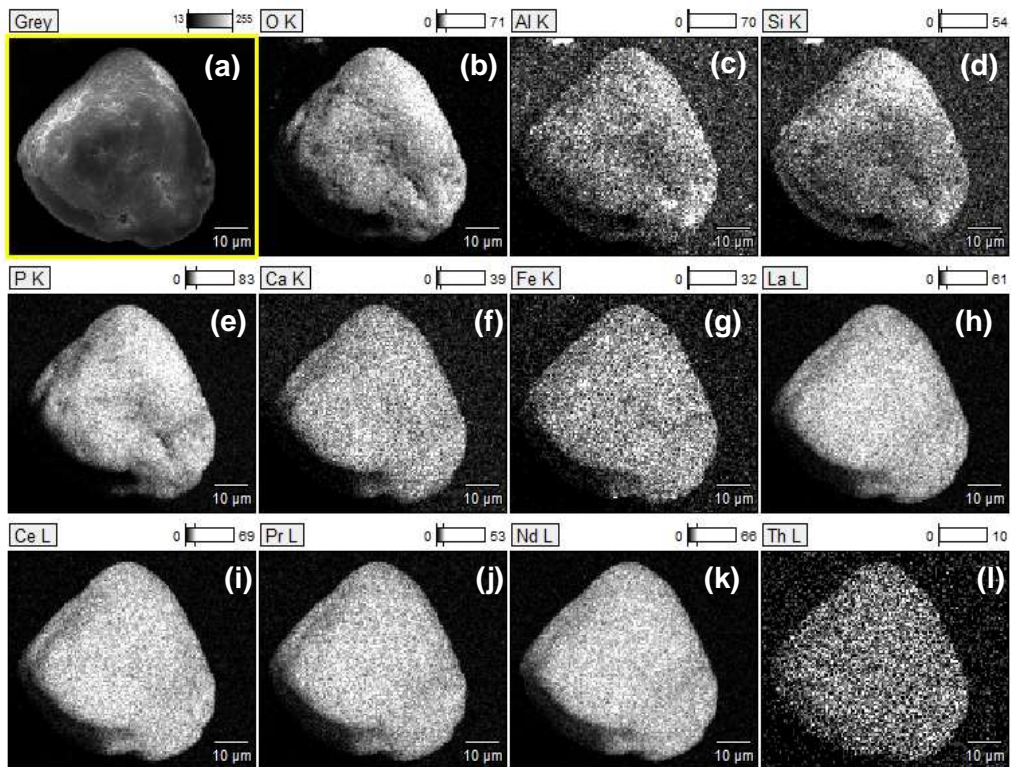


Figure 3.25: (a) SEM image of Th-phosphate particle and SEM-EDX elemental maps for O, Al, Si, P, Ca, Fe, La, Ce, Pr, Nd, and Th (b – l) of the particle in counts

Additional Th L₃-edge μ -XANES spectra were collected for the selected three mineral particles (Figure 3.26a, b, and c). The energy position of the XANES white line in all analyzed particles is identical to that of the bulk soil samples. This is not surprising as the oxidation state of Th in environmental samples is always IV. It is obvious that the X-ray absorption spectra of these particles closely follow those of the corresponding RCs even though their XAS signals are quite noisy. Theoretically, the identified particles could be used as local RC, to fit the bulk soil spectra in both XANES and EXAFS regions, which should lead to more conclusive results compared to the synthetic Th-silicate/oxide RCs and the natural monazite RC from another location. Such an attempt was made for the XANES region, because only μ -XANES spectra had been recorded for the selected particles. It should be noted that the EXAFS region was not measured during μ -XAS because fluorescence intensities were not sufficient. Unfortunately, the backfitting of the μ -XANES spectra was hampered by the relatively high intensity of the white line from the identified Th-phosphate particle. This may be related to differences in composition between the natural Th-monazite particle from Sri Lanka and the monazite RC from Brazil and/or to the difference in particle sizes (i.e. RC particles were ~40 times bigger than the Th-phosphate particle used in this study), which further highlights the challenges in characterizing the speciation of Th in natural samples, composed of multiple mineral phases compared to studies on pure samples.

The aim of all these measurements was not only to identify the heterogeneous nature of the sample (as this was already clear from SEM-EDX analysis), but also to look for possible accessory phases like iron oxides which have coprecipitated or adsorbed Th or lanthanides. As a summary, all the extensive spectroscopic studies described in this chapter suggest the heterogeneity of both the natural samples and particle sizes and they have an impact on spectra, for instance in XANES. However, although it is possible to identify the accessory iron oxide and clay minerals, a clear assignment of direct Th or REE binding to those accessory minerals or coprecipitated and adsorbed Th, Ln forms could not be found in the frame of the present thesis either due to low concentrations or because they do not exist.

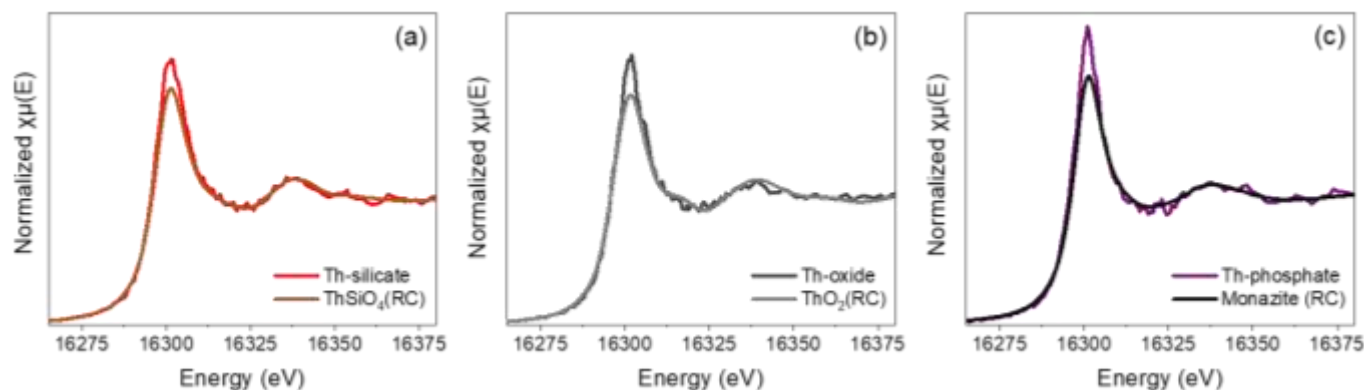


Figure 3.26: Micro-X-ray Absorption spectra of (a) Th-silicate, (b) Th-oxide, and (c) Th-phosphate rich particles, respectively

Table 3.9: Weight and atom contribution of each element (%) obtained by SEM-EDX for the selected isolated particles (i.e., Figure 3.18 – Th-silicate, Figure 3.21 – Th-oxide, Figure 3.24 – Th-monazite) and the monazite RC

Figure	Element – wt. %											
	O-K	Al-K	Si-K	Fe-K	Ca-K	Ti-K	P-K	Ce-L	La-L	Nd-L	Pr-L	Th-M
3.16	17.8±0.3	1.2±0.1	7.5±0.1	1.0±0.1	0.3±0.0	-	2.8±0.1	-	-	-	-	69.4±0.4
3.17	30.1±0.2	4.2±0.1	3.2±0.1	7.2±0.1	-	1.6±0.1	0.6±0.1	37.6±0.2	-	-	-	14.6±0.2
3.18	35.4±0.2	1.2±0.0	1.5±0.0	0.4±0.1	2.2±0.0	-	13.9±0.1	21.4±0.3	12.4±0.2	8.1±0.2	2.4±0.3	1.1±0.1
Monazite - RC	23.0±0.2	0.9±0.0	1.6±0.0	1.2±0.0	0.2±0.0	-	12.4±0.1	21.8±0.4	5.8±0.2	14.6±0.3	3.2±0.5	9.5±0.1
Element – Atom%												
3.16	60.6±3.0	2.4±0.5	14.5±0.5	1.0±0.1	0.4±0.1	-	4.9±0.4	-	-	-	-	16.3±0.3
3.17	70.4±1.2	5.8±0.3	4.2±0.3	4.8±0.2	-	1.3±0.1	0.7±0.2	10.0±0.1	-	-	-	2.3±0.1
3.18	70.5±1.4	1.4±0.1	1.7±0.1	0.2±0.1	1.7±0.1	-	14.3±0.3	4.9±0.2	2.8±0.1	1.8±0.1	0.5±0.2	0.1±0.0
Monazite - RC	61.0±1.2	1.5±0.2	2.5±0.1	0.9±0.1	0.2±0.0	-	17.0±0.3	6.6±0.4	1.8±0.2	4.3±0.3	1.0±0.4	1.7±0.0

3.4. On-site groundwater characterization

Elemental concentrations in groundwater depends on lithology, geomorphology and geological conditions of a given region. Numerous environmental factors influence these concentrations such as pH, redox conditions, soil matrix porosity, particle size, dissolved CO₂ concentration, temperature, presence of inorganic and organic compounds, colloids, etc. [102, 270, 271].

This section summarizes results of on-site measurements of pH, total disperse solid (TDS), and conductivity of groundwater samples and the laboratory measurements on cation, anion and NPOC concentrations. The on-site data, elemental and anion concentrations of filtered samples using two filter pore sizes, i.e. for 0.2 µm and 0.45 µm, are given for all locations in Table 3.10.

The average well water pH is slightly acidic (~5.9) and somewhat lower than the standard range. The tap water shows the lowest concentrations of Th and La, which is probably due to the water purification process and relatively high pH. The pH is quite important, and normally the highest concentrations of trace elements are generally found at the lowest pH values. However, a clear correlation of Th, U and REEs concentrations with measured pH was not found except in few cases, for instance, Th concentration was mostly found to be highest in the water with the lowest pH (Table 3.10). The TDS, conductance and pH of a particular location always seem to follow the same trend for the water samples from S1 and S2 (Table 3.10). TDS usually comprise inorganic salts and small amounts of organic matter dissolved in water and their values largely depend on the geological regions suggesting different mineral solubilities. The WL-02 and 03 locations correspond to spring well and tap water, respectively, with higher pHs, TDS and conductivity (Table 3.10) and in accordance with the literature with respect to the spring water [272]. Normally, the chemical compositions of groundwater and spring water are influenced by the mineral composition of the contacting rocks along their flow paths.

Anion concentrations were measured only in the second sampling campaign (S2). The geochemical analysis of the water samples shows that the type of the groundwater is Na-Cl type with some sulfate and bromide while fluoride and phosphates are below the detection limit of 0.01 mg L⁻¹. The current study location belongs to the intermediate

climatic zone of Sri Lanka and the anion concentrations measured in this study are in the range of previously reported groundwater analysis data in this zone [273].

The Th concentrations in groundwater samples are very low, as expected (in the range of 10^{-10} to 10^{-8} mol L⁻¹, Table 3.10). These very low amounts reflect the low solubility of Th, which seldom exceeded 10^{-8} mol L⁻¹ even at very low pH values and high affinity to surfaces. The minimum value of the Th concentration in groundwater is within the range of the solubility of ThO₂. Thorium oxide is an insoluble phase, which will limit the fraction of potentially mobile Th. In contrast, U concentration varies enormously with the environmental factors and geological regions. For instance, some researchers from India reported that the amount of U in groundwater was in the range of 0.3 to 1443 µg L⁻¹ [274]. The attention towards REEs in groundwater was taken more recently and the resulting studies showed that these elements may be useful as geochemical tracers in groundwater aquifer systems [275-277], even if the geochemistry of REEs in groundwaters is still not completely understood. The solubility of REEs may be controlled by several processes with respect to minerals such as dissolution of Ca-PO₄-minerals. In some studies, experimentally determined REE concentrations are found to be higher than calculated values from speciation and solubility data. REEs mostly are found bound in apatite phases and are known to adsorb strongly to Fe, Al or Mn-(hydr)oxides [278]. The literature data for the groundwater concentration of La is reported to be below 3 µg L⁻¹ [72, 279], consistent with the concentrations reported in this work (Table 3.10).

Differences among target elemental concentrations are observed between the two sampling campaigns. U and REEs show some kind of dilution phenomena in S2 compared to S1 while Th and major elements such as Fe, Mn, Si, Al show otherwise (Table 3.10 and Appendix 3.8, Table A3.3.) potentially related to the meteorological conditions during the sampling campaigns (S1 – sunny day and S2 – rainy day). This suggests that U and REEs may be easily washed out with rain due to their high mobility while the erosion due to rain or some kind of out washing of colloidal species from the soil might cause the increase of Th and major elemental concentrations in S2, further supporting evidences for the mobilization of Th in this study area associated with the particulate phase. However, this effect is not prominent for WL-03 (tap water). Other than to the local meteorology, there are several other potential factors which might

influence the results, such as the effect of: (i) time period (sampling was done on two separate dates), (ii) sensitivity of the measuring instrumentation (S1 – analysis in Sri Lanka and S2 – analysis in Germany, section 2.1.3.), and (iii) sampling reproducibility between individuals. Although the differences in the values exist, the patterns between sampling sites are consistent among sampling campaigns, potentially indicating local characteristics and heterogeneity in water composition for a relatively small sampling area.

In general, there is a consistency between the measured amounts involving 0.2 μm and 0.45 μm pore size filters, suggesting little influence of the colloidal phase in the transport of target elements in groundwater. Some samples show slightly higher values for 0.2 μm than 0.45 μm (Figure 3.29), indicating potential analytical variability ($\pm 20\%$) and/or sample contamination (e.g., aerosols or tube composition) as it is unlikely that there would be more elements passing through a smaller filter than the larger filter. Even though U and La show similar amounts in both filtered samples, concentrations of Th are inconsistent. These observations indicate the presence of Th-containing particulates with different sizes. However, in some samples the opposite finding is stated. This might be due to the relatively high analytical uncertainty of measuring Th concentrations at such low concentration levels (ng L^{-1} range). The variable Th concentrations of samples passed through filters with different sizes may, however, hint to the significant presence of particulate and colloidal Th species. The best conceivable way to detect any type of colloids in the groundwater is direct analysis of such particles in the groundwater at the site [280]. Direct measurements on unfiltered groundwater samples were not carried out in this part of the study. Therefore, colloidal transport cannot be discarded for trace element mobility. This is similar to studies with column experiments (soil leaching), discussed later by analyzing filtered and unfiltered samples from flow-through column experiments in Chapter 4.

The drinking water limits imposed by the world health organization (WHO) [281], United States Environmental Protection Agency (EPA) [282] and the Sri Lanka Standards Institution (SLS) [283] are included in Table 3.10. The pH, concentrations of U and anions of the tap water sample from the purification plant are within the limits of WHO, EPA and SLS standards. Standards are set to ensure drinking water quality based on the latest scientific evidence as well as to secure efficient monitoring and

assessment drinking water quality. No standards are currently available for REEs in any of the above guidelines, but it might become important since natural and human sources may lead to elevated levels of REEs in natural water resources. For instance, weathering processes, enhanced by deposition of acid rains, as well as the use of phosphate fertilizers could release REEs to the environment [284].

Table 3.10: Concentrations of targeted elements, anions, and on-site measurements of groundwater samples with the drinking water limit standards of WHO (W), EPA (E) and SLS (S)

Sampling campaign – S1							W	E	S
	WL-01	WL-02	WL-03	WL-04	WL-05	WL-06			
Th (ng L⁻¹)							--	--	--
0.45 µm	0.63±0.03	0.68±0.02	0.23±0.04	0.74±0.02	0.35±0.02	0.75±0.02			
0.20 µm	0.15±0.01	0.45±0.04	0.06±0.00	0.08±0.00	0.50±0.05	2.42±0.03			
U (µg L⁻¹)							30	--	--
0.45 µm	0.10±0.01	1.41±0.07	1.12±0.00	0.22±0.01	3.06±0.07	0.17±0.03			
0.20 µm	0.12±0.01	1.52±0.05	1.18±0.07	0.20±0.01	3.09±0.02	0.15±0.00			
La (µg L⁻¹)							--	--	--
0.45 µm	2.42±0.24	0.45±0.06	0.12±0.02	1.97±0.07	2.45±0.04	2.83±0.04			
0.20 µm	2.75±0.07	0.54±0.03	0.11±0.01	1.97±0.20	2.60±0.10	2.53±0.32			
On-site measurements									
pH	5.5	6.6	6.7	5.9	6.1	4.8		6.5-8.5	
TDS	120	650	580	240	520	130		500	
(mg L⁻¹)									
Conductivity (µS cm⁻¹)	250	310	280	110	250	50	--	--	--

Table 3.10 Cont. Sampling campaign – S2

	WL-01	WL-02	WL-03	WL-04	WL-05	WL-06			
Targeted elements									
Th (ng L⁻¹)							--	--	--
0.45 µm	4.04±0.14	2.49±0.16	1.24±0.05	3.55±0.41	4.80±0.05	3.79±0.04			
0.20 µm	4.00±0.00	3.31±0.02	1.39±0.05	3.29±0.31	2.31±0.01	5.17±0.00			
U (µg L⁻¹)							30	--	--
0.45 µm	0.03±0.00	0.34±0.01	0.14±0.00	0.05±0.00	0.55±0.00	0.03±0.00			
0.20 µm	0.04±0.00	0.37±0.01	0.15±0.01	0.05±0.00	0.52±0.00	0.03±0.00			
La (µg L⁻¹)							--	--	--
0.45 µm	0.41±0.00	0.03±0.00	0.25±0.00	0.19±0.00	0.15±0.00	0.20±0.01			
0.20 µm	0.51±0.00	0.10±0.00	0.28±0.00	0.20±0.00	0.15±0.00	0.22±0.00			
Anions (mg L⁻¹)									
Cl⁻	14.9±0.2	10.8±0.1	9.7±0.1	14.9±0.	12.0±0.2	14.8±0.1	--		250
NO₃⁻	6.96±0.08	4.81±0.05	9.97±0.26	7.77±0.07	1.28±0.02	10.53±0.21	50	10	50
SO₄²⁻	6.89±0.66	4.80±0.33	1.93±0.29	4.75±0.64	10.3±0.8	2.73±0.81	--		250
Br⁻	0.00±0.00	0.15±0.08	0.15±0.06	0.11±0.00	0.13±0.01	0.11±0.01	--	--	--
NPOC (mg L⁻¹)	5.90±0.80	7.77±0.30	3.61±0.70	7.36±0.51	5.25±0.06	4.43±0.76	--	--	--
On-site measurements									
pH	6.0	6.9	7.1	6.1	6.9	5.3			6.5-8.5
TDS (mg L⁻¹)	130	630	440	250	500	180			500
Conductivity (µS cm⁻¹)	280	310	210	120	240	80	--	--	--

3.5. Conclusions

The direct analysis of environmental samples from the area of study suggests:

- The area of study is a hot-spot of radioactivity relative to Sri-Lankan average levels, showing high absorbed gamma dose rates in air ($> 2000 \text{ nGy h}^{-1}$) and enhanced soil radionuclide activity concentrations (Th-232: $> 4000 \text{ Bq kg}^{-1}$ and Ra-226: $> 300 \text{ Bq kg}^{-1}$), 100- and 10-fold higher than world average concentrations, respectively. Corresponding on-site effective dose rates are slightly above the acceptable range of $1\text{-}10 \text{ mSv y}^{-1}$ and radiological risk assessment shows high hazard indices implying cancer risks. Although, these calculations might not always give accurate output, they are useful in providing upper limits of possible hazards and allow preliminary risk estimation for the location of interest. These results suggest that the current location should be considered as a HBRA, although the specific criteria for a location to be a HBRA still need to be clearly defined.
- Both external and internal exposure pathways seem to play non-negligible roles in the area. The results suggest that further evidence and risk assessment are required for this area of study, as well as for similar anomalous sites over the country, to better address the concern for the local population subjected to chronic exposure of potentially elevated natural radiation levels. The present thesis does not provide direct information on internal exposure pathways. However, there are indications for the relevant transfer of Th from soil to plants, which needs to be investigated further.
- The results from different solid characterization methods agree well with each other. XRD data reveal that the major mineralogy of the site is dominated by kaolinite and quartz while the diffractograms of sieved fractions add evidence for the presence of Fe crystalline phases including hematite and goethite.
- SEM images and corresponding EDX spectra provide finer details of the grains and reveal the variable mineralogy with regard to Th, U and REEs. The combination of the different spatially resolved techniques such as synchrotron-based $\mu\text{-XRF}$ (i.e., providing the bulk particle composition) and SEM-EDX (i.e., giving potentially the composition of both surface and a few μm -depth layer) mapping provides insight into the composition and heterogeneity of

single mineral grains in natural soil samples on the μm scale. The data show that clay and iron mineral phases may be attached to larger mineral grains in natural samples, with potential implications for the environmental behavior and fate of associated trace elements. Overall, the data confirm the presence of distinct dominant Th-containing mineral phases inside the soil samples (Th-silicate, Th-phosphate and Th-oxide phases) and highlight the strong mineral phase heterogeneity within the same sample. Probably due to the low concentrations, no clear indication could be obtained related to the presence of Th, U, REE associated with accessory minerals (clay, iron oxides) via adsorption or incorporation.

- There are some indications but no clear evidence for colloidal or particulate phase importance for Th, U and REEs transport in groundwater. A general spatial variability can be inferred from results of the sampling campaigns though higher frequency sampling over a longer period of time is required to better understand both element dispersion/mobility and local variability. In addition, a focused investigation of colloidal species (particles with sizes > 1 nm) is required.
- Despite the high radiological levels detected on-site, dissolved concentrations for target elements in groundwater samples remain within drinking water limits according to several local and worldwide guidelines.

4. POTENTIAL MOBILITY AND CARRIER PHASES OF TARGET ELEMENTS

This chapter studies the potential release of Th, U and REEs in the area of study by several laboratory experiments under simulated static (batch) and flow-through (column) conditions. As column experiments can be considered as more representative of environmental settings, results will be compared with onsite analytical data discussed in Chapter 3. Although more systems were studied, only the soil sample L-05 will be comprehensively discussed in this chapter while the results of the other samples are reported in the Appendices. In addition, since the focus of this work is mainly on Th and U, only the data for those elements will be discussed in detail with a comparison of La (selected as a representative of REE mobility). All weight percentages of leached elements as obtained from different experimental approaches were calculated based on total element concentrations in the bulk L-05 soil measured by XRF (Chapter 3). Scoping calculations involving geochemical models will be discussed at the end of the chapter.

4.1. Evaluation of potential mobilization based on chemical batch extractions

The mobility of NRs in soil, i.e. their potential toxicity in the environment, depends on the phases they occur in and which chemical and physical processes these phases are subject to. In addition, the concentrations of these metals in soil solutions are most likely controlled by sorption-desorption reactions. In this perspective, sequential and single batch extraction protocols, based on operationally defined fractions, provide more detailed information on the potential retention/mobility of NRs, and potentially yield insight into fractions of soil in which these metals exist besides assessing their bioavailability. The operationally defined fractions were summarized in Table 2.1 (Chapter 2) and the corresponding extracted amounts of Th, U and La are evaluated in this section for unsieved (bulk) and sieved soils. However, care was taken not to over interpret the corresponding data since such operationally defined fractions may not really be selective for target elements and solid host phases. For this reason, the performance of the extractions will be presented first (section 4.2.1.) followed by a more detailed tentative interpretation of the results (section 4.2.2.).

4.1.1. Overall mass balances and performance of the chemical extraction procedures

➤ Unsieved soil

The percentage distribution of the target elements in each sequentially and singly extracted fraction is shown in Figure 4.1 (absolute values are in Appendix 4.1, Tables A4.2-A4.11). The mass balance for the sequential extraction steps validates the procedure by yielding overall recoveries of 91, 107 and 87 wt% for Th, U and La (Figure 4.1), respectively. This means that the sum of the six fractions (i.e., five sequential extractions and direct XRF measurement on F5 residual solids) is in fair agreement with the independent quantification of total Th, U and La (i.e., obtained by direct XRF measurements of overall soil, section 3.3, Table 3.6). These observations are backed-up by direct measurements of element concentrations in Milli-Q from inter-fraction washing steps during sequential extractions, which show negligible leaching of the target elements after F3 (i.e. <1% of total corresponding element content in the soil, Appendix 4.1, Table A4.12).

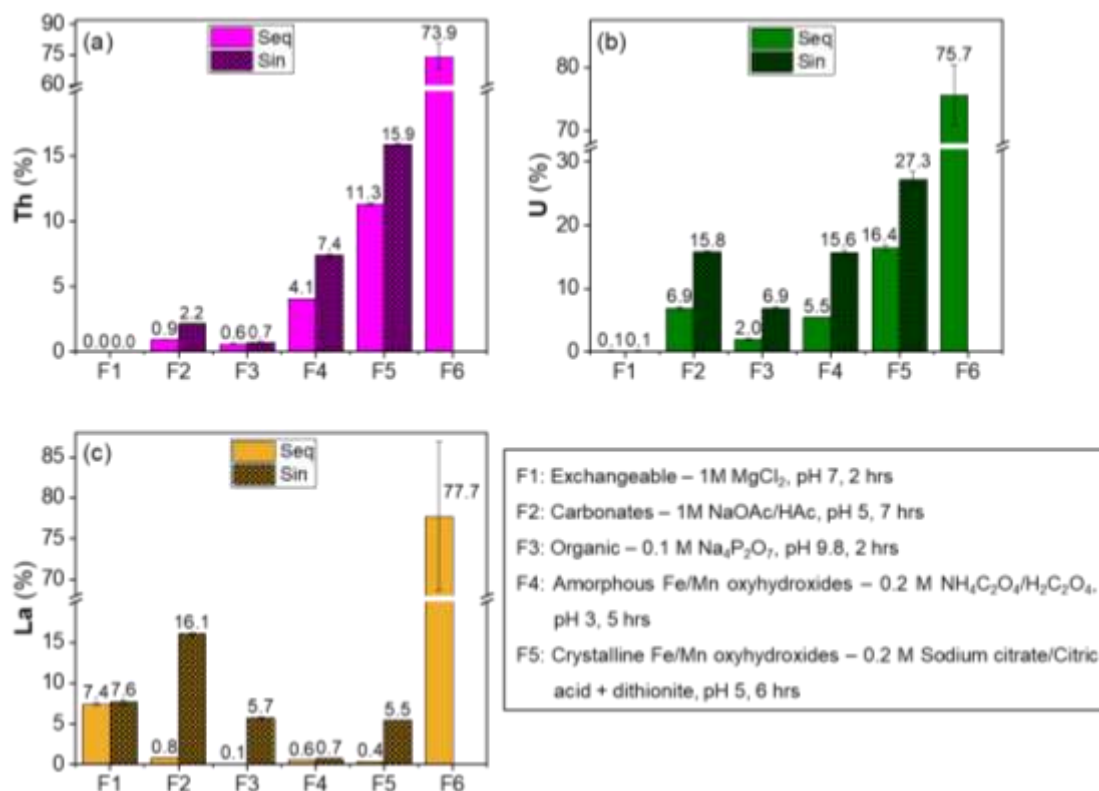


Figure 4.1: Percentage distribution of (a) Th, (b) U and (c) La in each chemically extracted fractions of soil sample L-05 in sequential (Seq) and single (Sin) extractions

The residual analysis after sequential extractions obtained via both methods described in section 2.4.2.1, revealed that Th, U and La in these samples are mainly present in fraction F6 (Figure 4.1), with corresponding percentage >70 wt.%. The difference between the values for F6 from direct XRF measurements of F5 residual solids (i.e., method F6_{M1} described in section 2.4.2.1) as well as the difference between extracted amounts and the total content of each element (i.e., method F6_{M2} described in section 2.4.2.1) is <15% for Th and La while it is 10% for U (Table 4.2).

In general, it is clear that single and sequential extractions will provide diverse results for each individual fractions and elements (Figure 4.1). Only in few cases, extracted concentrations of all target elements in single and sequential extractions provided <25% relative difference between common fractions, i.e., Th in fractions F1/F3, U in F1 and La in F1/F4. These results would suggest little overlap between operationally defined fractions or a certain consistency of the extracting power of the reagents. However, fractions F2 of Th, F2/F3/F4 of U and F2/F3/F5 of La exhibit more than 50% of discrepancies between the two approaches. Single extractions in these cases show enhanced leaching compared to sequential extractions, in accordance with the inherent implications of the procedures (i.e., original soil in each fraction of single extractions vs leached soil in subsequent fractions). Two potential explanations emerge for these observations: (i) sample heterogeneity (i.e., given the fact that each extraction required 2 grams), and/or (ii) a non-selectivity of the reagents for a given target element. For instance, a significant fraction of La was easily released in extraction step 1 (Figure 4.1c) with no further significant extraction in sequential F2 and F3. In the single extraction experiments, the exchangeable La fraction in F1 is desorbed as well in F2 and, to a lower extent, in F3 and F5. Furthermore, differences observed in F5 for Th, U and La can only be possible because if citrate/dithionite is able to dissolve crystalline Fe-oxides, then it must also be able to dissolve amorphous Fe-(hydr)oxides (i.e., <3% relative difference) [132]. In fact, the sum of the elemental amounts leached in sequential extractions from F1 to F5 is in agreement with the single extraction of F5 for U as in the case of Th and not in the case of La as can be seen in Figure 4.1. In the case of U, the relative difference is +13% (i.e., the sum of sequential fractions extracts more than F5 in single). Nevertheless, this variability may fall within the ranges of experimental error due to the washing steps during sequential extractions. For La, non-negligible concentrations of dissolved La were observed in some washing solutions

between extractions (Appendix 4.1, Table A4.12). These observations could imply that (i) sequential extractions may not be specific for potential carrier phases of relatively easily exchangeable elements such as La since the applied reagents in F2 to F5 are clearly non-selective for binding modes of La and there might be re-adsorption of released La onto remaining (non-dissolved/non-attacked) solid phases during F3 and F5 extractions (e.g., as already reported for other elements during selective extractions; [132]), which would explain the high concentrations in the washing steps (i.e., releasing re-adsorbed, loosely bound La), and (ii) elements present in different operationally defined carrier phases (e.g., Th and U) show relatively consistent trends and overall releases between fractions from both single and sequential extractions despite the non-selectivity of different reagents.

In an attempt to further understand the extraction efficiency of the reagents and to identify which soil components associated with Th, U, REEs-minerals are removed by the respective extracting solutions in each step, solid residues from each extraction step were analyzed by SEM-EDX. The results suggest that the main Th, U, REEs mineral phases (i.e., phosphates, silicates and oxides) have not selectively disappeared after a given extraction step. This would be expected for such insoluble phases and supports the hypothesis of reduced mobility of these elements in Sri Lankan soils due to the presence of mixed solid phases of low solubility, combined with other elements, or a dominance of mineral phases presenting crystalline structures.

➤ Soil size fractions

The main targeted elements, Th, U and La, were sequentially extracted to learn about their release behavior from different soil size fractions. The percentage distribution of Th, U and La from the sequential extraction studies on the different size fractions of L-04 are shown in Figure 4.2 and the corresponding absolute values are given in the Appendix 4.1 (Tables A4.13-A.15). The data from F1 to F6 are illustrated together with separate graphs for the fractions F1-F4 for better comparison of the lower percentages.

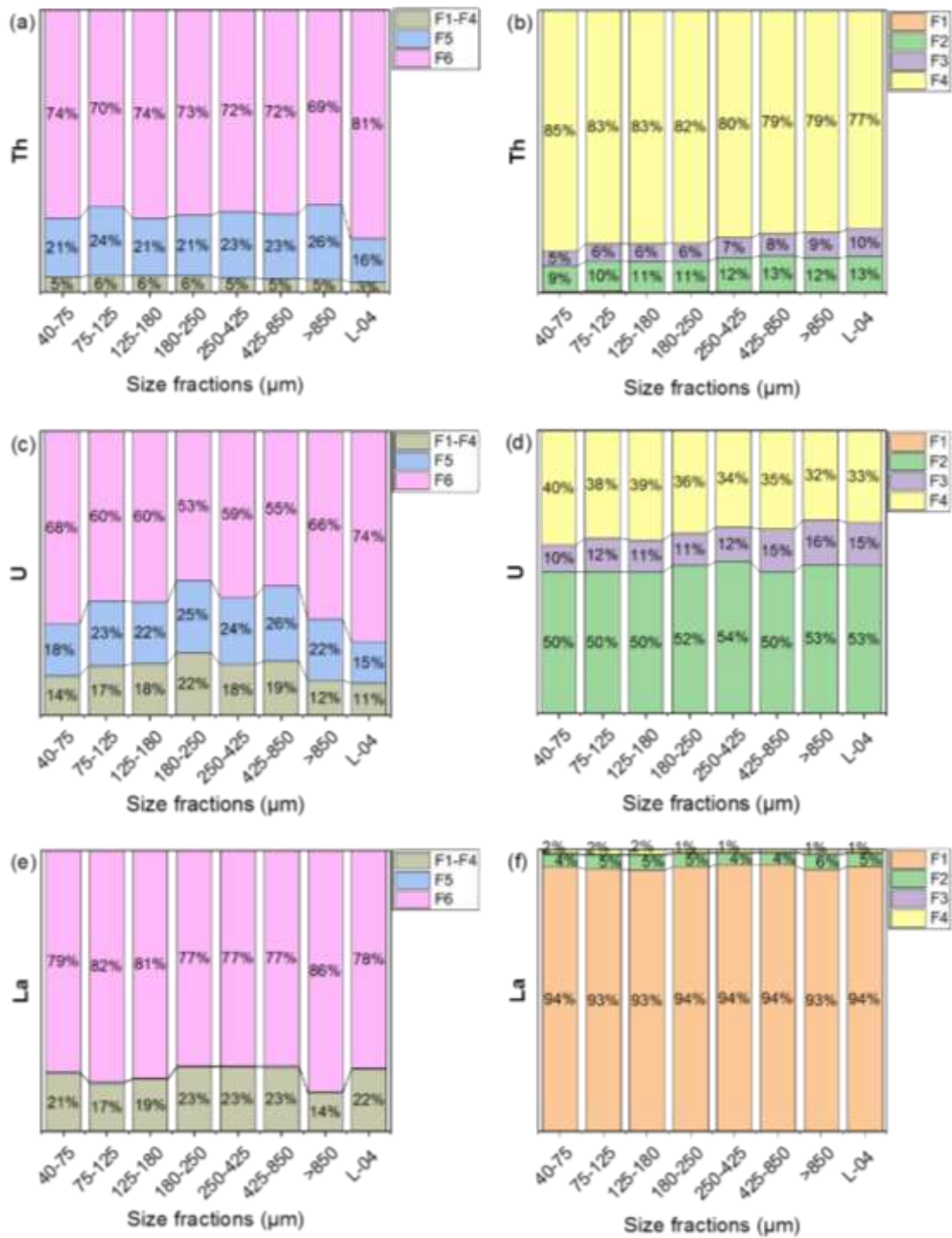


Figure 4.2: Relative percentage values of Th (a,b), U (c,d) and La (e,f) extracted sequentially from each size fraction of sieved L-04, showing both overall F1-F6 (a,c,e) and expanded F1-F4 (b,d,f). A comparison with unsieved L-04 soil sample is included

The extraction patterns of each fraction of Th, U and La are consistent with their respective patterns observed in the unsieved bulk soil sample. Noteworthy, the extractions assigned for carbonates (F2), organic (F3), and iron oxides (F4, F5) are present in all soil size fractions implying that the extraction of Th, U and La in those

fractions is largely independent of the soil particle size based on dry sieving (Figure 4.2). This agrees with the conclusions from XRD data, which also showed that different size fractions do not contain specific phases (Figure 3.3), except for the smallest fraction, <40 μm . Unfortunately, due to the inadequate amounts of material available (i.e. the size fractionation yielded only about 1 g of soil for this fraction), the extraction protocol could not be performed on the size fraction <40 μm . This fraction showed some iron phases in XRD (Figure 3.3), and these observations will be useful for further interpretations and discussions of potential carrier phases (section 4.1.2) based on bulk (unsieved) soil.

Mass balance calculations were carried out to further quantify the consistency of Th, U and La extractions in different size fractions. Mass balances for Th, U and La extractions per size fraction agree with the extractions from the unsieved soil sample (within <20% error) giving further evidence that the overall soil heterogeneity is not caused by grain size (Figure 4.3).

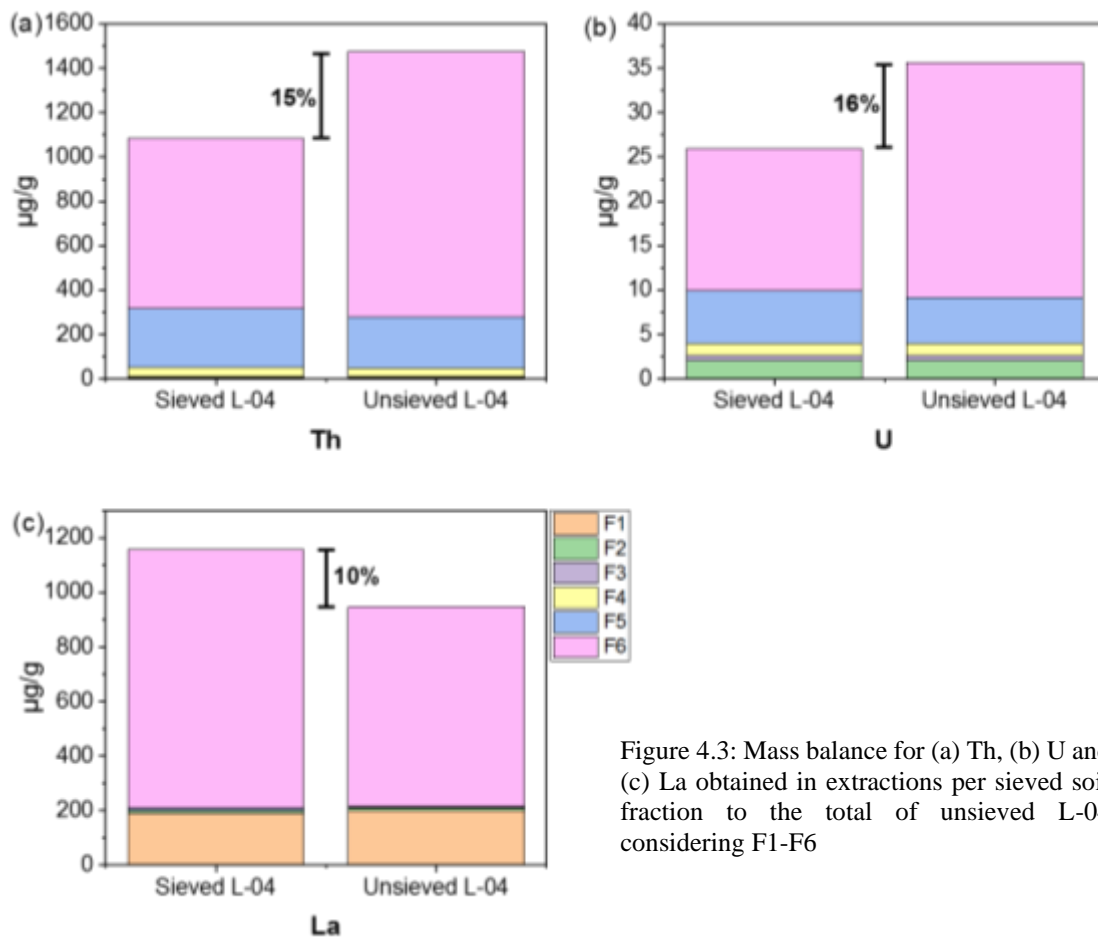


Figure 4.3: Mass balance for (a) Th, (b) U and (c) La obtained in extractions per sieved soil fraction to the total of unsieved L-04 considering F1-F6

4.1.2. Identification of potential carrier phases of target elements

Results from extractions for each target element and operationally defined fractions for unsieved soil are presented in Table 4.1 for L-05. The corresponding percentages of these extractions are given in Figure 4.1. A summary of accumulated percentages with environmental relevance are shown in Table 4.2.

Table 4.1: Amounts of Th, U and La extracted in sequential (Seq) and single (Sin) extractions; mass of element released from the soil sample L-05

L-05	F1 (ng g ⁻¹)	F2 (µg g ⁻¹)	F3 (µg g ⁻¹)	F4 (µg g ⁻¹)	F5 (µg g ⁻¹)	F6 (mg g ⁻¹)	Total (mg g ⁻¹)
Th							
Seq	35.1±5.9	14.6±0.3	9.6±0.3	63.8±0.1	172±5	1150±100	1560±98
Sin	39.3±0.0	33.5±0.3	11.6±0.3	115±1	258±1		
U							
Seq	25.6±11.8	1.4±0.0	0.4±0.0	1.1±0.0	3.3±0.1	15±1	20±1
Sin	27.1±12.2	3.1±0.0	1.4±0.1	3.1±0.1	5.4±0.2		
La							
	F1 (µg g ⁻¹)						
Seq	89.3±1.2	9.9±0.1	1.4±0.0	6.7±0.0	4.9±0.1	934±110	1201±138
Sin	91.8±3.1	193.0±1.6	68.6±1.3	8.7±0.1	65.7±0.1		

Table 4.2: Extracted percentages of Th, U and La in both sequential (Seq) and single (Sin) approaches for the soil sample L-05

%	Th		U		La	
	Seq	Sin	Seq	Sin	Seq	Sin
“Easily” mobile (F1+F2)	0.9 ± 0.0	2.2 ± 0.0	7.0 ± 0.2	15.9 ± 0.2	8.3 ± 0.1	23.7 ± 0.4
Non-residual fraction (F1+F2+F3+F4 for sequential and F4 for single)	5.7 ± 0.0	7.4 ± 0.1	14.5 ± 0.3	15.6 ± 0.4	8.9 ± 0.1	0.7 ± 0.0
Residual fraction F6-XRF (F6 _{M1})	73.9 ± 6.4		75.7 ± 4.7		77.7 ± 9.1	
F6-Calculated (F6 _{M2})	83.0		69.1		90.7	

➤ Thorium

Although Th is well-known to be mostly bound to the immobile fraction, the chemical extractions show that a small fraction of Th can be mobilized in the environment, potentially relevant given the inherent, high content at the study site. It should also be noted that colloidal species play an important role for the aquatic chemistry of Th [285].

The distribution of Th over the fractions in sequential extractions is, as expected, in the order of F6>F5>F4>F2>F3>F1 (Table 4.1, Figure 4.1). *Guo et al.* reported similar behavior and showed that Th was primarily associated up to 81% with the residual fraction, after microwave digestion with HF, in samples collected from a REE-related industrial area in Baotou, Inner Mongolia [133]. *Martinez-Aguirre and Perianez* also observed ~70% of Th in the residual fraction, via the approach F6_{M2} as described in section 2.5.1, for samples from a marsh area in southwestern Spain [145].

The experimental results from the extraction scheme suggest that, despite the predominance of Th-bearing mineral phases (mainly silicate-, oxide- and phosphate-related), the second highest amount of Th extracted was found in the (operationally defined) crystalline ferro-manganese oxyhydroxides (F5) fraction (<16%, Figure 4.1). In fact, the extracted Fe in both F4 and F5 fractions in sequential (i.e., 0.4% in F4 and 26% in F5 relative to the overall Fe content) and single extractions (i.e., 0.2% in F4 and 16% in F5 relative to the overall Fe content, data not shown) suggest that Fe predominantly occurs as a crystalline phase. Corresponding iron containing mineral phases, however, could not directly be identified via bulk soil characterization techniques (section 3.3), but were found to some extent as goethite and hematite in the XRD analysis in the smallest soil size fraction (Figure 3.3). Therefore, they might be present in smaller amounts or as coatings on other mineral surfaces as has been also found within the present investigations. Crystalline Fe oxides are stable but may dissolve under strongly reducing conditions or by microbial activities, which would contribute to the release of trace metals.

Lower but still important amounts of Th may also be present in F4 as co-precipitates with amorphous ferro-manganese oxyhydroxides (F4, <8%, Figure 4.1, Table 4.1) another potential fraction containing Th. The reagent used in this step is the oxalate buffer (Table 2.1), which may occur in natural systems, in many plants, and released upon organic decomposition. Both oxalic and citric acids are two of the main organic

acids in forest soil and litter [46]. Even though not uncommon in nature, their concentrations are much lower than those of humic substances. The extracted amounts of F4 in sequential extraction should approximately equal to the extracted amounts of F4 reduced by F1 + F2 in single extraction, but extraction recoveries of F4 is ~three-fold higher for Th. Thus, the extractant used in F4 may extract F1+F2+F4 because of its low pH (pH~3). Despite the specification that Tamm's oxalate extraction should be conducted in the dark (Table 1.6), occasionally, these extractions show enhanced extractive power when natural soils present Fe(II)-bearing minerals, even for extractions in the dark [286]. In fact, Tamm's reagent is characterized by relatively low pH (pH=3) and a high concentration of the complexing ligand oxalate. A solubility control by equilibration with ThO₂ phase for F4 conditions due to low pH can be excluded for Th given the fact that the concentrations of Th found in the leachate of F4 are 2.8 and 5.0×10⁻⁵ mol L⁻¹ (6.4 and 11.5 mg L⁻¹, Appendix 4.1, Table A4.2) for sequential and single, respectively. However, this is valid for the amorphous phases of ThO₂ since the solubility for crystalline or microcrystalline ThO₂ phases are even much lower [48] while solubility of Th-phosphate is even lower [287, 288]. In addition, it should be noted that the experimental conditions used in these selective extractions are probably not sufficient to attain the solubility equilibria of ThO₂ within short period of time.

Results for F3 (extracted Th content in both methods nearly 1%, Figure 4.1, Table 4.1) suggest a minor fraction of Th is associated with organic matter (OM). A source for the OM content in the soil might be an extensive forest cover in the vicinity, which could continuously supply organic substances to the location. The alkaline (i.e., pH ~9.8, Table 2.1) sodium pyrophosphate solution used in F3 is a well-known agent to solubilize OM and OM-bound metal cations, such as Ca, Mg, Fe, Al [141, 142]. Interestingly, the study of *Kaplan and Serkiz*, with OM content similar to our samples for soils from a wetland site adjacent to a pilot-scale nuclear facility in South Carolina and involving the same F3 reagent, showed ~65% extraction of Th [130] whereas *Guo et al.*, again with the same reagent, observed <17% of Th in F3 from a soil sample with much higher OM content (4-23 g kg⁻¹) [133] compared to our study (<2 g kg⁻¹, Table 3.5). Those studies indicate that Th could indeed be associated with soil OM. The large variety of Th found in this fraction suggests that the differences in the chemical speciation of Th in different geological settings.

Both exchangeable fraction (F1) and carbonates fraction (F2) are extracted together in the F2 single extraction (<2.2% in both extraction approaches). The F2 fraction is generally attributed to carbonate bound ions, though it is not restricted to this operationally defined fraction as many trace elements can be mobilized due to the relatively low pH applied during the extraction (i.e., pH 5). The latter assumption may be valid for Th extraction from Sri Lankan soil as no significant carbonate mineral phases were observed in the solid characterization. Measured Th concentrations in the F2 solutions are 4.2 and 9.6×10^{-6} mol L⁻¹ (1.0 and 2.2 mg L⁻¹, Appendix 4.1, Table A4.2) for sequential and single extractions, respectively, somewhat higher than expected concerning the solubility of freshly prepared hydrated thorium oxide (2×10^{-7} mol L⁻¹ at pH=5 [287]). Solubility of thorium phosphates (e.g. Th₃(PO₄)₄) is expected to be even lower (<10⁻⁹ mol L⁻¹) under these conditions [288]. Therefore, if the measured Th concentration arises from dissolution of a solid phase, it could be suspected that it is due to thorium oxide.

Only trace amounts of Th were observed in the exchangeable fraction F1 (single and sequential extractions are obviously identical for this fraction), $\sim 1.6 \times 10^{-8}$ mol L⁻¹ (3.7 µg L⁻¹, Appendix 4.1, Table A4.2). The F1 fraction is assumed to represent the ion exchangeable portion released due to the presence of a solution of relatively high ionic strength (i.e., 1 mol L⁻¹ MgCl₂, Table 2.1), but it seems unlikely that an ion exchange between Mg²⁺ and Th⁴⁺ would explain the obtained results. In fact, the pH conditions during F1 extraction (pH ~ 7) combined with the expected low solubility of ThO₂ resulting in concentrations at around 10⁻⁸ mol L⁻¹ (~2 µg L⁻¹; [287]) are in accordance with these observations, suggesting that the F1 extraction might be influenced by ThO₂ solubility. Despite the seemingly low extracted percentages, these results suggest that relatively high concentrations of Th e.g., higher than average worldwide concentrations of ~0.01-1 µg L⁻¹ in surface and groundwaters [289] could be released from the soil. The fact that Th concentrations in groundwater from the site are < 0.005 µg L⁻¹ (table 3.10) clearly points to retention or dilution processes, resulting in concentration reduction by more than two orders of magnitude.

➤ Uranium

The percentage distribution of U over the fractions in the sequential extraction scheme is in the order of F6>F5>F2>F4>F3>F1. As shown in Figure 4.1 and Table 4.1, U is

mainly associated with the residual fraction (>70%) as was observed by *Kaplan and Serkiz* for some uncontaminated surface sediment samples from a wetland site in South Carolina. However, in the same study, U followed the sequence F3>F1>F6>F4>F5 for some contaminated sediment samples involving the same extractants as in our study [130]. Other studies also evidenced that U is mainly associated with the non-residual fractions. *Martinez-Aguirre* found U particularly within F4, 45% or more of the total U for some sediment samples collected along a riverside in Spain again involving the same chemicals we used in the extractions [145]. However, *S.M. Peter-Moreno* reported that U in lacustrine sediments was mainly bound in F3 around 25% but these authors used a modified version of BCR procedures [290]. Considerably different percentage distributions can be observed over the non-residual fractions F2 to F4 in this current study and U seems to be equally distributed between fractions F2 and F4, with about 7% of the total from the sequential and 16% from the single approach. In addition, the carbonate fraction (F2) contributes more (~7% in sequential and ~16% in single) to the total U in the soil than the adsorbed fraction F3 (~2% in sequential and ~7% in single). Uranium bound with the oxidizable fraction (<7%) is formed by organic matter (F3) and it is an efficient sorbent for U [291].

Under aerobic conditions, U exist only in VI oxidation state and the solubility of U(VI) solid phases are much higher [292]. However, in the present situation, U in natural systems is quite complex. The U present as an accessory mineral along with stable crystalline Th-phases (monazite, thorite and thorianite) most probably exists as U(IV) as UO₂. At the mineral surface/oxic water interface, some may be oxidized to VI state, releasing into the dissolved phase as i.e. UO₂²⁺ species. Therefore, concentrations of U in solution are then hardly predictable during the extractions.

➤ Lanthanum

The comparison of La percentage distribution in sequential and single extractions is included in Figure 4.1 and Table 4.1. The distribution over the fractions from the sequential extraction scheme is in the order of F6>F1>F2>F4>F5>F3. The extraction pattern of La is significantly different from those of Th and U. The highest percentage of La is associated with the residual fraction, ~78%, in agreement with some literature by *Xinde et al* and *Casartelli and Miekeley* [115, 293]. On the contrary, *Usmanova et al* for some samples collected from gold-bearing ore in Russia using Tessier's protocol [294]

and *Rao et al* utilizing the BCR revised sequential extraction procedure for some natural soil samples collected in Bangalore, India [69], reported relatively low values for the F6 of about only 20% and 32-35%, respectively. Instead <65% of La was bound strongly in F4 and F5, accumulating on Fe-Mn oxyhydroxides due to adsorption reactions [69, 294] whereas F4 and F5 fractions in our study had much lower contribution (<6%). The oxidizable fraction (F3) was two-fold higher in *Rao et al* [69] and similar in *Usmanova et al* [294] and *Casartelli and Miekeley* [115] to the values obtained in this study, i.e. <6% release in single extractions.

The second highest contribution after F6 in the sequential approach is from F1 with a value of 7.4% and the maximum value in the single extraction is from the carbonate fraction, F2, with ~16%. These values disagree with some literature where lower values are reported [69, 115, 294], while *Xinde et al* found <10% and <25% of La in water soluble/exchangeable and carbonate/organic fractions, respectively, in soil samples from China using Tessier protocol [293]. *Aubert* and co-workers reported that REEs are mobile in the upper soil horizon and may also accumulate in deeper layers, adsorbed onto organic matter based on samples collected from Vosges mountains, France [295]. Contrary to this, *Land et al* observed a more important amount of REEs bound to organic matter in the surface soil layers rather than in deep layers, while REEs were found to be mostly associated with Fe-Mn oxyhydroxides in a spodosol from Sweden [296].

The solubility phenomena can indeed not explain the outcome of the extraction studies of lanthanides (Ln) in this context, while the solubility concentrations of Ln-oxides at neutral pH might be in the range of 10^{-5} mol L⁻¹ [297] and the solubility of LaPO₄ is even much lower, i.e. $\sim 10^{-13}$ mol L⁻¹ [298]. Therefore, the average extracted value of La in sequential and single extractions 6.52×10^{-4} mol L⁻¹ (9.06 mg L⁻¹, Appendix 4.1, Table A4.6) are suspected to be from other labile phases.

4.2. Evaluation of potential mobilization in environmentally representative conditions: batch experiments with rainwater and exogenic carrier phases including silica nanoparticles and humic acids

The mobilization of Th, U and La was further investigated via several batch extraction experiments using conditions closer to natural scenarios, namely with simulated rainwater (SRW), and solutions containing silica nanoparticles (Si NPs) or humic acid

(HA). The SRW approach is the most realistic way to mimic the mobility of Th, U, and La in the site. The target area is affected by heavy monsoon and inter-monsoon rains during some periods of the year, which could be a possible mode for mobilization and subsequent transport. The silica nanoparticles can imitate some anthropogenic nanoparticle contamination that subsequently aid trace element mobilization, a relatively recent field of research in environmental chemistry. Silica was chosen since a model for a silica samples was available for Th adsorption. The last option chosen involves the transport by enhanced organic matter content, not unrealistic given the potential continuous supply of organic matter at the study site from the forest cover in the vicinity. All these modes of transport were investigated in laboratory conditions with batch and column approaches.

4.2.1. Simulated rainwaters

The batch leaching studies of Th, U, and La with SRW were carried out using different compositions (SRW-A1, -A2, -B1, -B2, Table 2.2) and involved different time frames. For each composition, one sample set was rotated over selected time periods, while another sample set was kept standing still for the same time period. This should allow to see possible effects of mechanical erosion on NR release. The corresponding concentrations of target elements are shown in Figure 4.4 and Figure 4.5, respectively, for L-05 and their masses eluted per mass of soil are given in the Appendix 4.2 (Tables A4.26-A4.29).

Even though some variations can be observed among the experimental data (Figures 4.4 and 4.5), it is very difficult to explain all in detail due to the inherent complexity of the system and the low overall extractions. A straightforward interpretation considering all the factors into account requires more investigations than performed within this thesis. Different Th, U and La leaching behaviours are unexpected for different rainwater simulates given the fact that the concentrations of anions are in a range such that a significant impact on Th, U and La solubilities are unlikely. The data of La seems to agree with the behavior in the chemical extractions, where higher extraction is obtained for the exchangeable fraction of the chemical extractions (F1 ~8 wt.%, Figure 4.1).

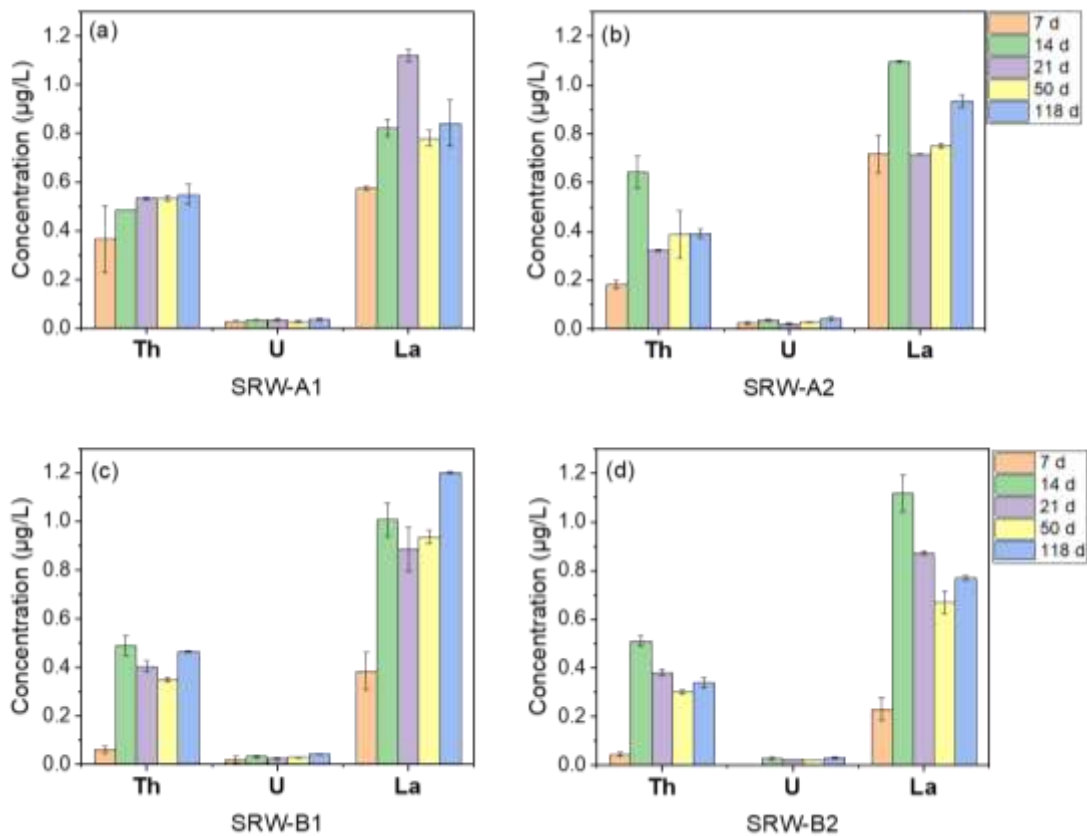


Figure 4.4: Concentrations of Th, U and La in the supernatant after rotating with different SRW compositions (a) SRW-A1, (b) SRW-A2, (c) SRW-B1, and (d) SRW-B2 for several time periods (7, 14, 21, 50, and 118 days) for L-05

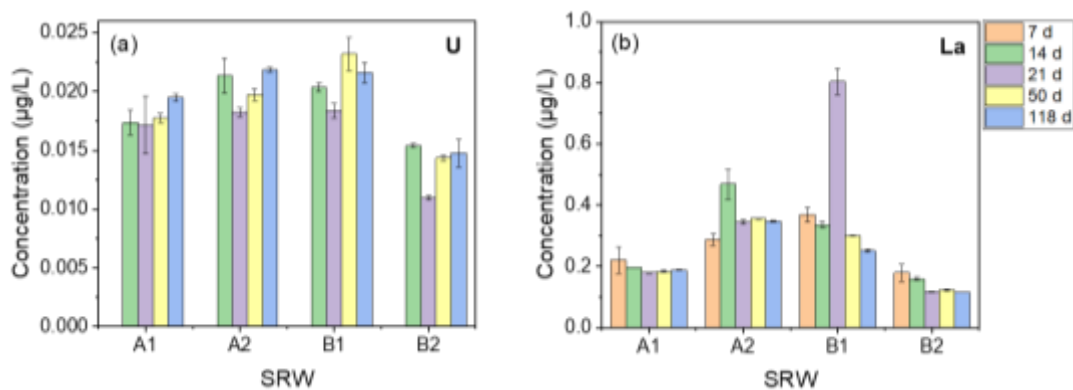


Figure 4.5: Concentrations of (a) U and (b) La with different SRW compositions SRW-A1, A2, B1, and B2 from samples standing still (not rotated) after several time periods (7, 14, 21, 50, and 118 days) for L-05. Thorium is not shown here because the released concentrations were below the detection limit

Further, the ionic strengths of each SRW are very low thereby any kind of colloids or even small sized particulates released from the soil could be kept stable in suspension. In the case of Th, it is well-known that colloidal species play a decisive role in aquatic chemistry of Th. The data from the undisturbed samples illustrated that Th is below the

detection limit (when operated in the semi-quantitative mode of ICP-MS) in the supernatant even after 118 days, clearly pointing to the fact that Th species could be even exclusively colloidal in the rotated samples. The differences in metal concentrations in rotated and non-rotated samples are very likely mainly due to some kind of mechanically enhanced colloidal release. Such colloidal species are often the reason for unexplainable variations in concentrations (as e.g. seen for La in SRW after 21 days).

For both U and La, the released amounts are decreased by nearly 50% for all compositions of SRW for the stagnant samples compared to the rotating samples supporting the idea that mechanical rotation may enhance trace element extractions even for the more soluble elements like U and REEs. Additionally, the experiment with the undisturbed samples could mimic natural conditions present in calm situations like ponds, or lakes where the water could remain for a long time during the dry season. Likewise, rotating conditions could mimic situations of heavy rain, physically moving soil particles. The results also imply that different mobility (though at very low concentrations compared to the total solid content, <0.1%) may be expected for the elements of interest in the area of study along the year given the contrasting conditions during dry and monsoon periods.

As it is not expected that the four SRW compositions resulted in similar leached amounts for Th, U, and La, only the SRW-A1 was selected for subsequent column studies since it extracted relatively higher amounts of Th and U at the shortest time period exposed, i.e. after 7 days, as shown in Figure 4.4.

4.2.2. Silica nanoparticles

Another series of batch experiments was carried out to mimic potential (future) anthropogenic contamination from aerosols or other nanoparticle (NP) applications. Such particles may enhance the mobility of the target elements due to interaction with these particles. Such a scenario was studied using Si NPs. Silica particles are known for their ability to scavenge metal ions while dissolved silica is ubiquitously present in natural waters [80] and can be a (colloidal) complexing agent. Furthermore, the soil contains 42-53% of SiO₂ (XRF data in section 3.3), so that the silica particles can be seen as reasonable compromise, for model substrates, in combination with anthropogenic nanoparticles.

The concentrations of Th, U, and La leached with different Si NP concentrations are shown in Figure 4.6a (their masses eluted per mass of soil are given in the Appendix 4.3, Table A4.34). In the case of U, the amounts released are increasing ~10-fold when increasing the added concentration of Si NPs from 0.5 to 8 g/L. The increase in Th and La is in the same range (~5- fold). Interestingly, in the case of La, where a relatively high fraction is easily mobilized in the exchangeable fraction, is not much leached by the silica colloid suspension. The outcome suggests a clear effect of high Si NP concentration on the mobilization of the target elements. It is remarkable, though, that Si NPs appear to strongly adsorb to the soil (Figure 4.6b). This might be due to different surface charges of Si NPs (Isoelectrical point, IEP = 2.3 – 3.8 [299] and soil). At least for one component of the soil, ThO₂, it is known that the IEP = 6.8-9.8 [299]. This finding suggests Si NPs being of limited mobility in the lateritic soil. This means that Si NPs in principle may induce the desorption of target elements from the soil, but the transport via Si NP in the environment will be affected by their size, surface charge and concentration and the interaction with the soil.

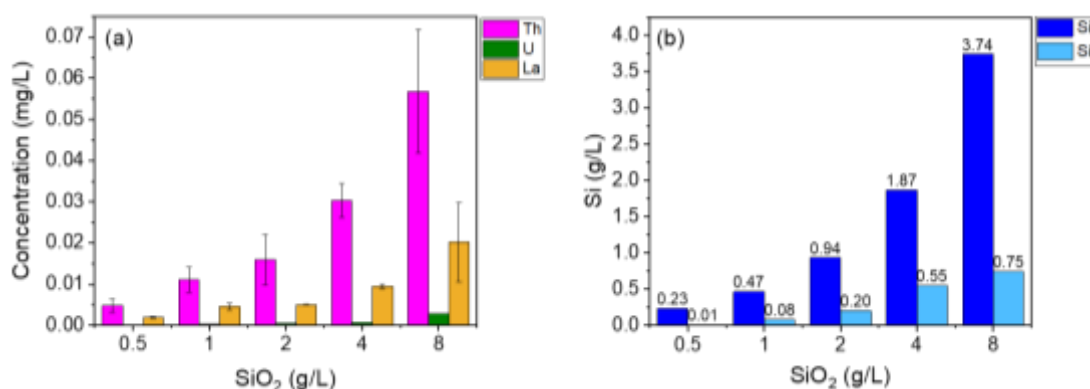


Figure 4.6: Comparison of the (a) leached concentrations of Th, U and La in the supernatant after rotating soil samples with silica AEROSIL 200 suspension and (b) initial concentration of Si (Si₀) with Si in leachates (Si_L) after 7 days

4.2.3. Humic acids

A potential increase of mobility of Th, U, and La with HA is expected because organic matter in natural environments is more prone to bind Th, U, and REEs [1, 2]. However, a detailed evaluation of the effects of humic substances on the sorption of metal ions on to the natural soil particles is considered to be difficult due to the contribution of various other solid phases such as clay minerals and hydrated Fe/Mn oxyhydroxides is unavoidable in natural systems. These minerals may e.g. bind organic matter.

The comparison of the concentrations of Th, U and La with the two humic acid samples (10 mg L⁻¹ each) used is depicted in Figure 4.7 and their masses eluted per mass of soil are given in the Appendix 4.4 (Table A4.36). According to the data, both HA1, i.e. the sodium salt of humic acid, and HA2, i.e. the crystalline powder of humic acid leached the same amounts of Th and La (~0.02 mg L⁻¹) with relatively low amount of U (0.3 µg L⁻¹). HA1 was used in the subsequent column experiments.

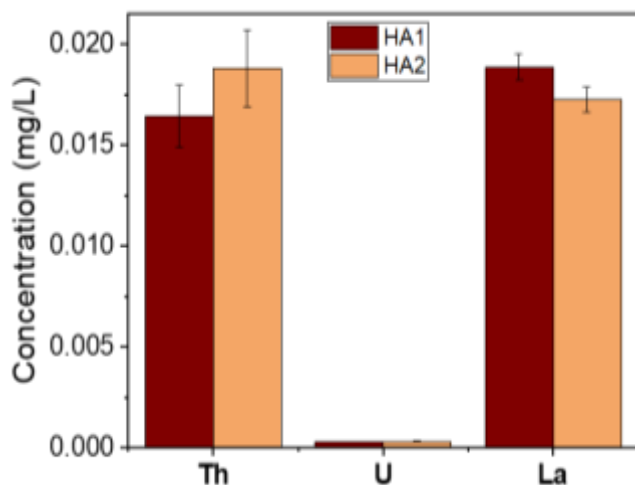


Figure 4.7: Comparison of the concentrations of Th, U and La in the supernatant after rotating the soil sample L-05 with humic acids, HA1 and HA2

The overall comparison of the leached amounts of targeted elements with SRW-A1, Si NPs, and HA1 (leached amounts with SRW-A1 after seven days rotation with results from 0.5 g/L Si NPs in the suspension after rotation for the same time period, both at pH 5) depicts a leaching sequence of SRW-A1 < Si NPs < HA1 in accordance with the literature which provided evidences for enhanced mobility of metal ions in the presence of silica and humics [41, 80].

4.3. Mobilization in column experiments for selected soils

Column experiments allow studying the mobility of trace elements for the large soil-to-liquid ratios that are more realistic in the natural setting. In addition, column experiments assist investigations of the vertical mobilization of Th, U, and La, generally via a continuous constant flow of solution. This approach may also minimize mechanical erosion effects, which may affect the results in batch type experiments. The closest phenomenon to mimic this kind of column experiments is percolation, consisting in elemental leaching from topsoil into the groundwater. On the way to the groundwater concomitant with increasing pH, sorption phenomena may reduce metal ion concentrations in solution. Our results show net transport for a given column size

and solution composition while in the environment subsequent processes may occur. The column experiments can be viewed as “close-to-reality” mobilization tests. Studying the mobility of Th, U and La, here involves column leaching experiments with simulated rainwater along with focusing on the same potential carrier phases used during batch extractions in the previous section 4.2. Columns were infiltrated with SRW-A1 and HA1 solution or modified by homogenizing the soil with Si NPs. Moreover, the column data were compared with results from batch experiments and with analytical data obtained for the on-site groundwater data.

4.3.1. Simulated rainwater

The comparison of the released amounts of Th, U, La and NPOC with SRW-A1 and corresponding pH of the leachates are depicted in Figure 4.8 along with the respective elemental concentration ranges detected in groundwater samples and the averaged pH of the groundwater around the target location (section 3.8). At the beginning of the leaching experiment, the released amounts of Th, U, and La from the column are relatively high, i.e. Th: $\sim 25 \text{ ng L}^{-1}$, U: $< 0.12 \text{ } \mu\text{g L}^{-1}$, and La highest with up to $24 \text{ } \mu\text{g L}^{-1}$, subsequently decreasing with time (Figure 4.8a and c). Given previous results (sections 4.1) La is most likely easily mobilized from the exchangeable fraction (Figure 4.1c) and Th and U, which are less easily leached, may be released from initial erosion of particulates and colloids. Several flowrates were tested for both L-05- and L-04-based columns and observations suggest that the leaching is soil-dependent rather than a flowrate-based behaviour (Appendix 4.8, Figure A4.10). Overall, the most interesting observation is that Th and La eventually reached their corresponding local groundwater ranges with time while U is always found within the groundwater range (Figure 4.8, Table 3.10) and much lower than “mobile” fractions in chemical batch extractions.

The data might suggest a correlation between pH, NPOC, and elemental concentrations in the column elutes at the eluted volume around 700 mL where a first small hump appeared. Here, the pH decreases as the amount of NPOC (Figure 4.8d) and targeted elements (Figure 4.8a, b and c) increases. Although the decrease and subsequent increase of pH (Figure 4.8) is not explainable at present, three possible explanations can be given for this observation. (i) During the experiment, the flow stopped several times for several hours prior to these alterations, i.e. especially around 300 – 500 mL due to software failure or computer shutdown over night or during weekends allowing

the target elements to increase in concentration in stagnant water (towards solid/liquid partitioning equilibrium) and leached out from the column later. (ii) Microbially induced activities within the column over time may be induced, enhancing OM degradation or release of organic acids, causing a change in pH and release of trace elements. For instance, it is known that the presence of phosphate solubilizing bacteria could produce some organic acids which may also partially be responsible for increasing Th, U, and La elution [300]. (iii) A potential release of target metals could occur with NPOC as humate like complexes or NPOC stabilized colloidal/particulates. Although, this correlation cannot explain the enhanced levels at the beginning of the column and at the second hump ~1000 mL making it difficult to put forward some general relationship between pH, NPOC and leached elemental amounts, SEM-EDX measurements of effluent filtered with 1 kDa filter size indicate the presence of Al, Si, Fe particles and some bacteria further support the above explanations.

The integrated total amounts of Th, U and La leached out from our column are 0.04 ng, 0.38 ng and 0.04 µg per g of soil, respectively, and these values are clearly much lower in percentages (~0%, 0.002%, and 0.003%, respectively) relative to the total bulk concentrations of each element from XRF results (Chapter 3).

The possibility that released elements are bound to colloidal carriers or eroded particles was checked by comparing unfiltered and filtered (0.2 µm mesh) samples for leachates during the whole column experiment with L-04 (Appendix 4.8, Figure A4.12). For these samples, both major (e.g., Al, Fe, Si, etc) and trace elements were analyzed, and Th concentrations were below the detection limit (when operated in the semi-quantitative mode of ICP-MS). The obtained data evidenced that about 90% of the total U and >99% of total La were retained by the 0.2 µm filter, indicating the presence of U and La on suspended particles of dimension >0.2 µm. Thus, both U and La are probably leached predominantly in the colloidal phase or as suspended particulate matter rather than as dissolved ions or complexes. The formation of Th and U colloids has been widely reported by many researchers due to their effect on the increased mobility in aqueous environments. Moreover, Th, in particular, tends to absorb onto carrier colloidal phases or forms intrinsic colloids when its solubility limit is exceeded even at low pH [45, 301, 302]. *Miekeley et al* reported that a considerable fraction of La (>90%) is associated with the solution phase in colloidal forms for groundwater samples from

the Osamu Utsumi mine and the Morro do Ferro Th-REE deposit [303]. These authors added that suspended particles ($>0.45 \mu\text{m}$) composed mainly of amorphous hydrous ferric oxides with sorbed organics control the mobility of U and REEs in groundwater confirming the strong affinity of U and REEs to particles. Such sorption processes involve the removal of elements from aqueous phase onto suspended matter via binding to organic matter, coprecipitation, surface complexation and cation exchange. It was further reported that Th was below detection limits. Some other studies done at the Koongarra uranium deposit also revealed that Th was associated with mobile colloids, mainly composed of iron and silicon species [304]. Concerning the results of the current column studies, it can be assumed that transport of these U and La in subsurface soil samples of the area of study occur mainly in colloidal/particulate forms.

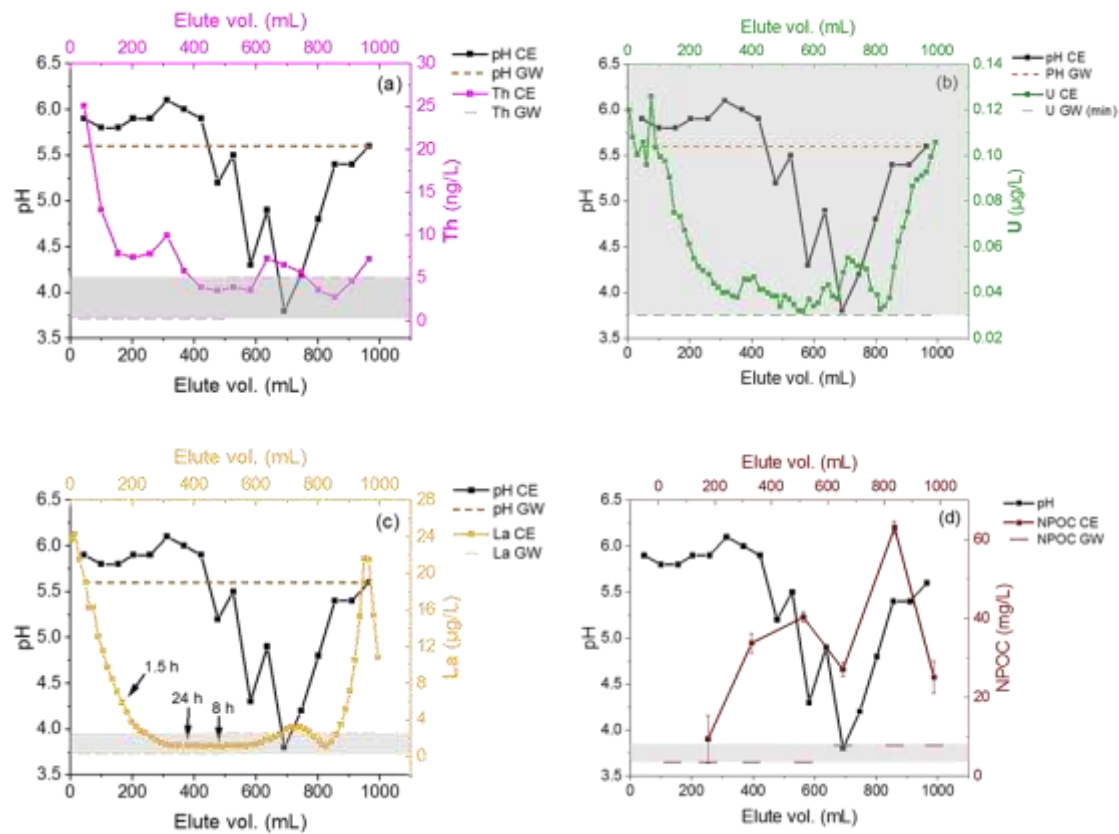


Figure 4.8: Comparison of the leached amounts of (a) Th, (b) U, (c) La, and (d) NPOC with simulated rain water (SRW-A1). Corresponding pH of the elutes and respective elemental concentration ranges (highlighted in grey color) including averaged pH of the groundwater are also presented. The arrows shown in (c) are the points where the column stopped during the experiment and the durations of stops are specified in hours. CE – column elute and GW – Groundwater

4.3.2. Silica nanoparticles

The next column experiments were carried out with Si NPs that were mixed prior to filling the column with the soil and SRW-A1 rainwater simulate was passed through

the column. The leaching patterns are shown in Figure 4.10. The pH of the elute fractions are not shown here as they do not demonstrate any significant changes compared to the initial pH of SRW. Several major elements were measured in the elutes but only Si and Fe are shown due to their contrasting trends, comparable to those of the trace elements of this study.

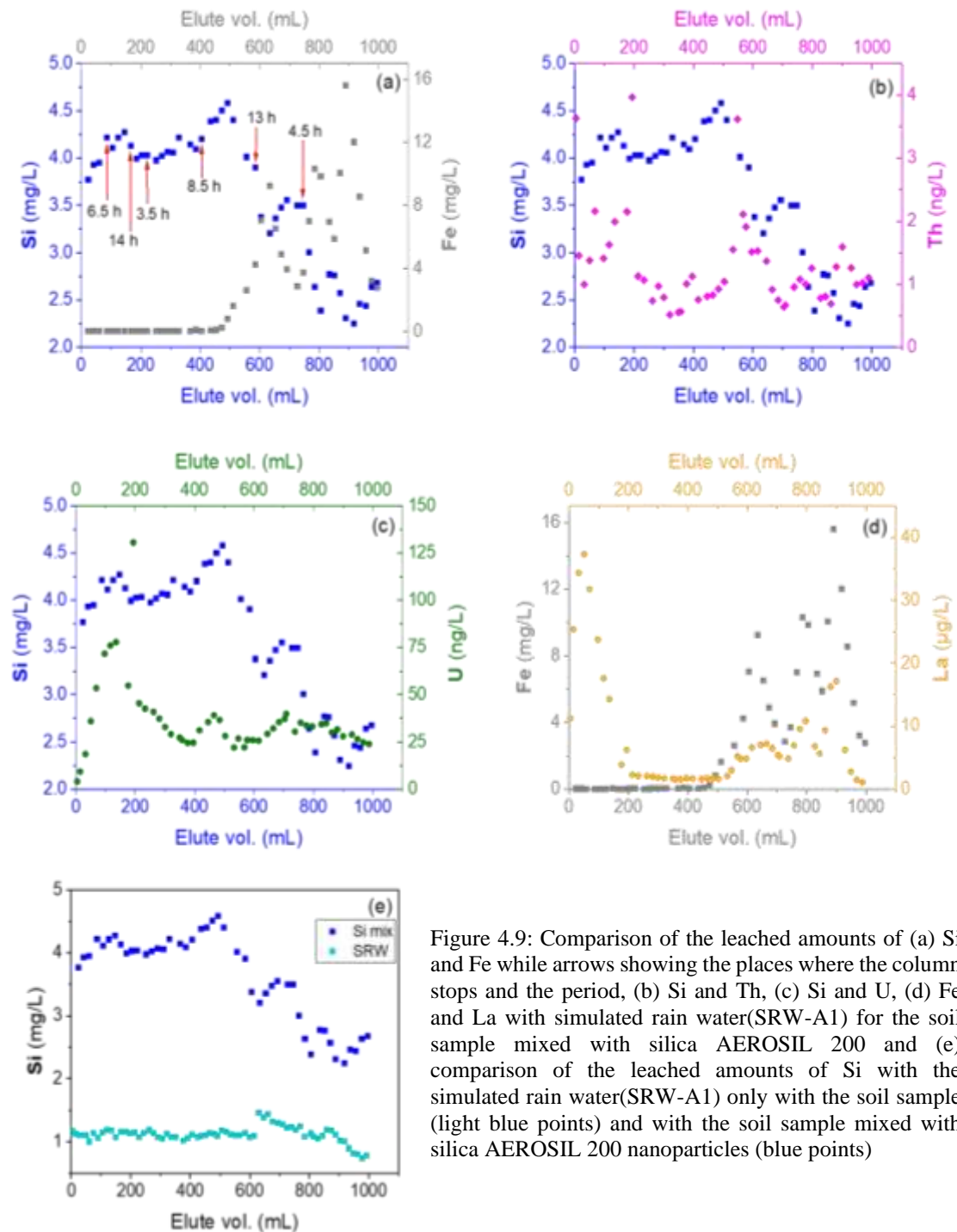


Figure 4.9: Comparison of the leached amounts of (a) Si and Fe while arrows showing the places where the column stops and the period, (b) Si and Th, (c) Si and U, (d) Fe and La with simulated rain water(SRW-A1) for the soil sample mixed with silica AEROSIL 200 and (e) comparison of the leached amounts of Si with the simulated rain water(SRW-A1) only with the soil sample (light blue points) and with the soil sample mixed with silica AEROSIL 200 nanoparticles (blue points)

The leached amounts of Si over time are relatively constant up to about 500 mL, where Si concentrations slightly decrease. Thorium elutes at an even lower concentration level as observed in the column experiments with SRW alone. The initially increased elution level of Th is much less pronounced, and U behaves similarly. Si NPs, when intermixed with the soil, therefore, seems to have a much lower effect as observed in batch experiments. Lanthanum showed a different elution profile which resembles that of Fe indicating a similar erosion or dissolution behavior. The integrated total amounts of Th, U and La leached from this column are 0.008 ng, 0.244 ng and 0.052 μg per g of soil, respectively. Interestingly, the concentration enhancement around 600 – 1000 mL as seen for the SRW-A1 elution experiments is also apparent for all elements in this experiment as well but less pronounced.

Leaching with SRW-A1 and Si NPs is compared in Figure 4.10e and the integrated value of the SRW-A1 experiment gave a total 7.4 μg Si per g of soil while the Si NPs experiment showed 23.6 μg Si per g of soil for 0-1000 mL. Even though the integrated value for SRW-A1 is approximately three times lower than the amounts detected in the Si NPs column, it is not possible to distinguish between Si originating from soil and Si from added NPs. Clearly more Si was leached when Si NPs were added to the column as should be expected.

4.3.3. Humic acid

The leached element amounts were compared with the corresponding NPOC values of the elutes (Figure 4.11). In addition, the leached amount of NPOC in SRW-A1 column is included in Figure 4.11d. The total amount of NPOC leached with SRW-A1 seems lower than that from the column with added HA1. The balance of integrated eluted NPOC with SRW (only) and added HA (with SRW), i.e. ~ 2.8 mg, revealing an enhanced release of OM from the column related to the addition of HA (i.e., 1.5 mg) into the system. Nevertheless, it is not clear the overall fate of the added HA, i.e., complete/partial sorption onto the soil and/or instrument tubing (i.e., deduced from visual observation).

Elution levels for Th and U are much lower than the corresponding amounts with SRW-A1 experiment, while La shows otherwise. In addition, an early elution of La is found

as in the previous column experiments. The integrated total leached amounts of Th, U and La from this column are 0.6 ng, 7.7 ng and 9.7 μg per g of soil, respectively.

Again, the unexpected changes in trends around the elute volume 600-1100 mL appeared even in this column and showing enhanced effects in the presence of added humic acids implying that this feature is a characteristic of the nature of the soil itself. However, there is no obvious explanation for this behavior. Nevertheless, a clear correlation with the NPOC peak is found for Th and La but not for U, pointing to a preferential association of Th and La to humic acid, while the behaviour of U is in contradiction to the finding in batch experiments (unless the added HA enhanced U mobility but effectively retained in the column/tubes).

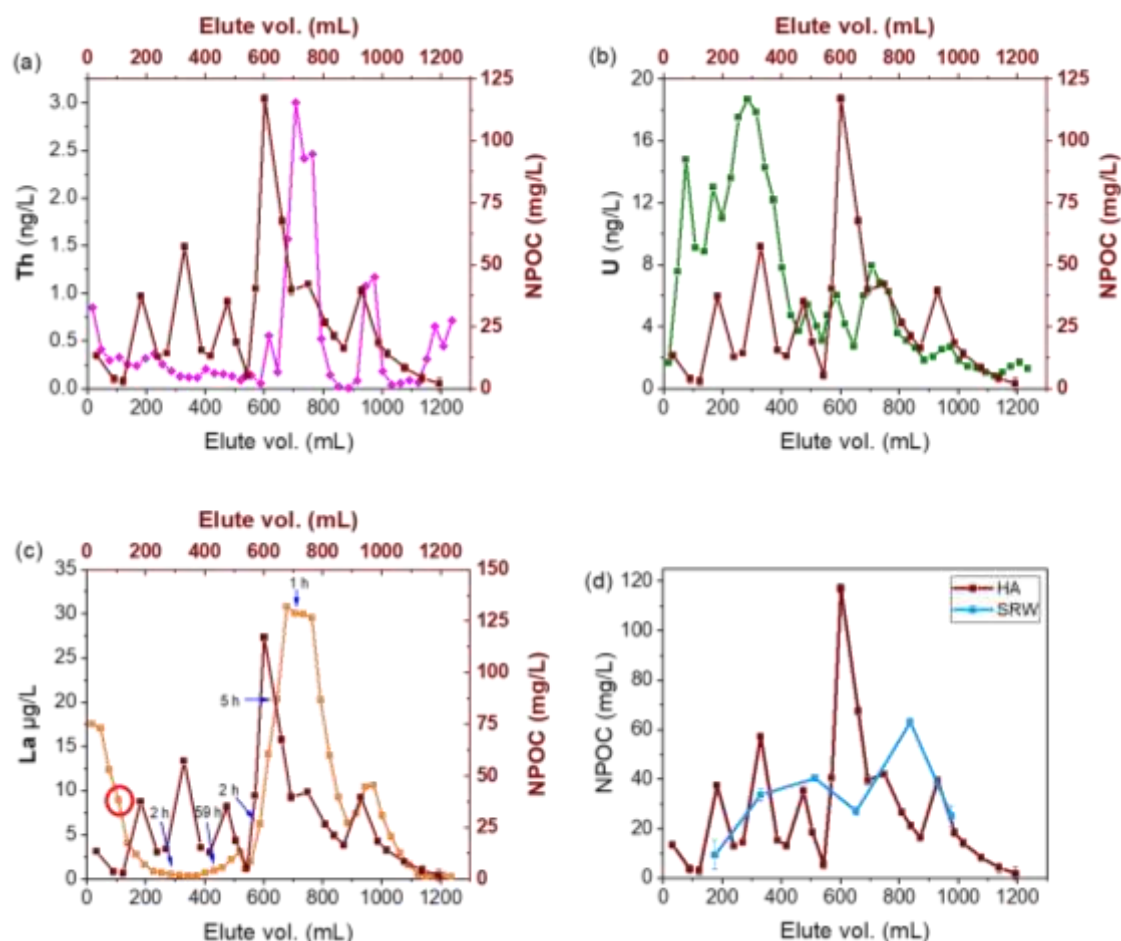


Figure 4.10: Comparison of the leached amounts of NPOC with the leached amounts of (a) Th, (b) U, (c) La and (d) only leached with simulated rainwater (SRW-A1) and injected with 100 mg L⁻¹ Humic acid (HA1). The red circle in (c) is the point where the injected humics should come out and arrows showing the places where the column stops and the period

Results from all three columns are compared in Figure 4.12 and Table 4.4. Some remarks highlighting the leaching behavior of each element has their own characteristics can be made. Slight discrepancy at specific elute volumes were observed for all the elements at different stages. The most interesting region is the range 500-1100 mL revealing some kind of column retardation phenomenon for all three elements in all columns. The most noticeable increase occurs at 600-800 mL with a hump for which no profound explanation is available. One option might be organic matter related transport and/or potential development of microbiological activities due to the column acting as a bioreactor overtime might be another possible explanation as already mentioned in section 4.4.1.

The extent of extraction for all targeted elements in the batch experiments followed the sequence HA1>Si NPs>SRW-A1. This sequence is not found in column experiments (Figure 4.11, Table 4.3). Significantly fewer metal ions are released in column as compared to batch experiments. Possible hypotheses for the lower eluted metal concentrations with humic acid and Si NPs might involve that humics and Si NPs are strongly retained in the soil and by this can adsorb Th, U and La to variable extent, thus, decreasing their mobility significantly.

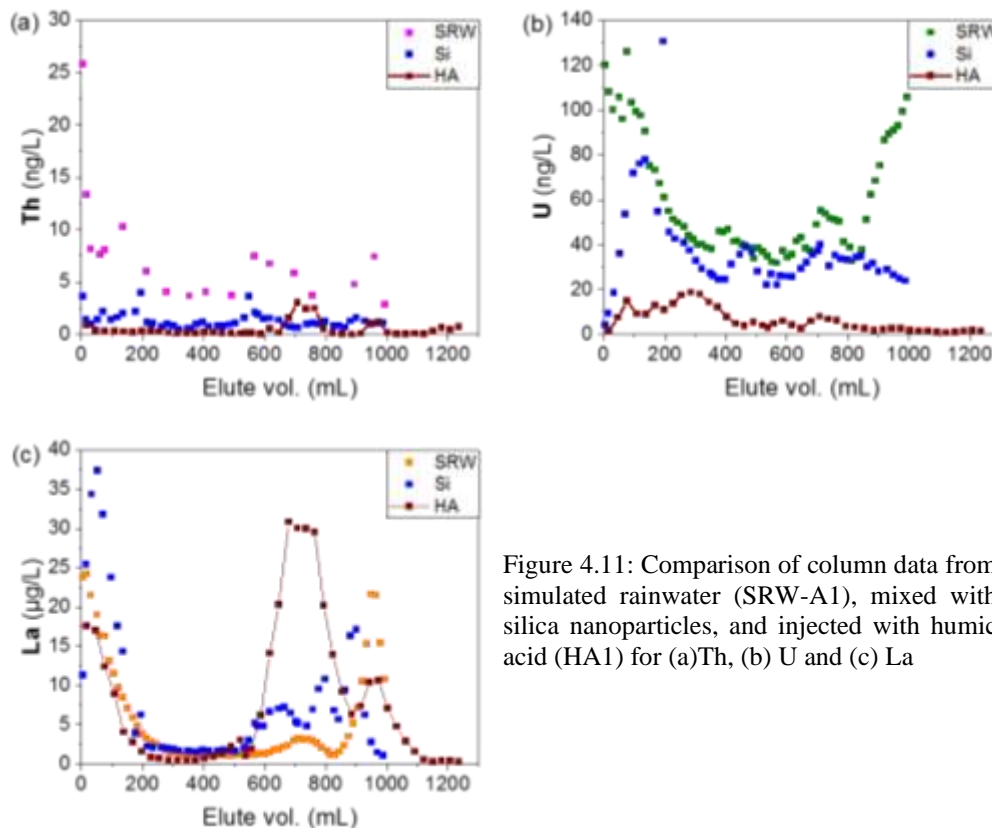


Figure 4.11: Comparison of column data from simulated rainwater (SRW-A1), mixed with silica nanoparticles, and injected with humic acid (HA1) for (a)Th, (b) U and (c) La

Table 4.3: The amounts of Th, U and La extracted and leached from the batch and column experiments per g of soil

	Th (ng g ⁻¹)		U (ng g ⁻¹)		La (µg g ⁻¹)	
	Batch	Column	Batch	Column	Batch	Column
SRW-A1	88.4	0.040	6.73	0.38	0.14	0.04
Si NPs	1190	0.008	66.0	0.24	1.09	0.05
HA1	4500	0.004	76.0	0.05	4.13	0.06

4.4. Discussion of the potential environmental mobility of target elements with relevant carrier phases and environmental implications of the applied methods

Overall, the elements of interest in this study, i.e. Th, U and La, are rather weakly released in chemical extractions and batch and column experiments with simulated rainwater, silica nanoparticles and humic acid. This was expected particularly for Th due to its insoluble nature and very low mobility under most environmental conditions. The following discussion connects particularities of each experiment with the corresponding relevance for this study.

In the case of selective extractions, less than 8 wt.% of Th, 16 wt.% of U and 9 wt.% of La (Figure 4.1, Table 4.2) was associated with non-residual fraction due to solid host phase dissolution (i.e., sum of the sequentially extracted amounts in F1, F2, F3 and F4 or the single F4 extraction), which reflects some possible mobility in the environment under specific conditions. For instance, environmental processes involving degradation/dissolution of OM and amorphous Fe/Mn mineral phases via remineralization or early diagenesis [38-40] may play a role in transferring a small fraction of natural Th (i.e., max. 8 wt.%) to the environment. Other relatively mild environmental perturbations taking place throughout the hydrological cycle (i.e., interaction between rocks and plants during water runoff, percolation, underground water, (acid) rain, etc.) could also lead to Th, U and La mobilization to some extent as suggested by *Bednar et al* [125]. This means that the largest fraction of Th, U and La are associated with F6 probably reflecting the most resistant Th, U and La-containing minerals, such as monazite, thorite, thorianite, uraninite, zircon, which are unaffected by the reagents used.

The batch extractions and column leaching studies with SRW-A1, Si NPs and HA1 took place at the “natural” pH of the soil, i.e. pH ~5. The soil shows an important buffering effect given that final pH measurements of samples covering initially adjusted pH values between 2 and 10 converged to the soil pH at the end (Appendix 4.12, Figure A4.17).

Further, very low Th, U and La concentrations in the column studies might be considered somewhat unexpected considering the much higher solid-to-liquid ratio (~0.15 g mL⁻¹), opposed to the corresponding batch studies (~0.004 g mL⁻¹). The obtained values for both cases are shown in Table 4.3. This independence on solid-to-liquid ratio is an indication that Th, U and La in this site is not highly reactive, as expected, whereas the concentrations of targeted elements in the leachate solutions during column experiments are controlled by adsorption and/or ion exchange processes on the soil minerals. The extractions of batch experiments were physically enhanced by continuous rotation which induce abrasion resulting enhanced amounts of particulates and colloids. Even though, the total concentration of Th in the soil is higher than U, higher concentrations of U were detected both in batch extraction and column leaching experiments. The possible explanation might be the fact that Th species (e.g. the solids clearly identified in the XAS and SEM-EDX) are chemically inert in the system, while some U species are more easily leached from the soil due to the different redox behaviour. Overall, these experiments illustrate the leaching of elements from soil columns and provide evidence that leached species are in particulate forms, which further confirmed by the filtration analysis on the column.

Finally, it can be concluded that, although the selective extractions provide an estimation for elemental fractions which could be potentially mobilized, the assignment of a certain metal ion fraction to a host phase is still difficult. Meanwhile, the batch extractions and corresponding column experiments, where the impact of potential colloidal carrier phases such as inorganic nanoparticles and humic acid were examined in order to estimate potential environmental impact scenarios on the studied site, provided information on the nature of the leaching species. As a result, both approaches converge to reveal to some extent an insight into the mobilization of Th, U and La in this natural system.

4.5. Scoping geochemical model calculations

The scoping calculations involving geochemical models were done by using several data sets from the literature [80, 122, 205, 305-307]. The comparison of the total truly dissolved phases of Th(IV), U(VI), and REE(III), i.e. aquo ions, presented as percentages of total, simulated 10^{-6} mol L⁻¹ initial concentrations was done as a function of pH for constant background electrolyte composition of 0.1 mol L⁻¹ for systems in the presence of (i) Si NPs and HA, (ii) HA (absence of Si NPs), and (iii) Si NPs (absence of HA) and results are shown in Figure 4.13a, b, and c, respectively. Although Yttrium (Y) is a transition metal, it was selected here since it is chemically similar to the light lanthanides while Ytterbium (Yb) was selected as a heavy member in the lanthanide series. With La as the REE discussed in the main text, the two chosen elements should cover the behavior of La. Moreover, the choice of the two elements was triggered by the availability of a self-consistent model for adsorption on amorphous silica. Therefore, for both Yb and Y there is an availability of parameters with SiO₂ and humics even though the parameters as pointed out earlier are probably not self-consistent between the silica and humics models. These two elements would give a range of possible distribution for the REEs. Even though the pH of the batch and column experiments is around 5, the behavior were modelled in the range of 2 to 8 to predict the nature of the species at low and high pHs (i.e. to see differences among elements and cover a wider range of extraction conditions).

System (i) illustrates the percentages of the total dissolved species in the presence of both silica and humics. The models were set up in such a way that the total site concentrations of the respective silicas and the humics were 0.57 mmol L⁻¹ each. Under the experimental pH, i.e. at pH ~5, no dissolved species (aquo ion, hydroxo complexes) are observed as expected (Figure 1.2 for Th, section 1.2.2.2). At pH<4, the Y⁺³ aquo ion has the highest concentration in solution while the respective aquo ions of Yb⁺³ and UO₂²⁺ are following.

In the presence of only humics, i.e. system (ii), the same pattern as for the system (i) for all the elements is obtained, suggesting that the humic substances are the predominant interacting agents in the medium. Above pH 4, all the ions are complexed with humics. In both these systems, according to the models, Th would be complexed by humics even at low pHs. In addition, the results suggest that Th binds more strongly in the presence of humics. If these data are compared with the corresponding batch

experiment with humic acids, the released percentage of about 0.29 wt.% (Figure 4.7a) of Th represents the soluble and/or colloidal fraction of Th complexed with humics. Under the experimental pH in these batch experiments (pH ~5), uranyl and other trivalent ions are also complexed with the humics according to the model and the released percentages in those batch experiments, 0.38 wt.% (Figure 4.7a), denote the soluble and/or colloidal species complexed to humic substances too.

In system (iii), the effect of humics is clearly revealed due to the differences in Figure 4.13 c to that of a and b. In the presence of only silica in the system, all ions of interest are 100% dissolved at pH 2 and the total dissolved amounts of Th^{+4} drastically decrease and becomes zero at pH 3 while for the amount of dissolved UO_2^{2+} starts to increase gradually at pH 6.5 and reached 100% at pH 3. The total dissolved concentration of Y^{3+} and Yb^{3+} ions remaining in the solution until the pH reaches 6 and then decreased dramatically and other species are formed pH >7.5. In the corresponding batch experiment with SiO_2 NPs at pH ~5, 0.08 wt.% of Th (Figure 4.7b) were released and this is much less than one would expect based on these calculations, potentially indicating that other solid species should be included in the model in order to have more representative calculations. This is similar for $\text{UO}_2^{2+}/\text{U}$. Even Yb and Y show 100% total dissolved ions at pH 5 (Figure 4.13c) suggesting that the increased La release in presence of Si NPs as compared to the SRW extraction (Figure 4.7b) do not represent mobilization by silica.

For Th it is interesting to relate calculations to the experimentally observed simultaneous presence of different, environmental element-related mineral phases (e.g. section 3.3). A comparison of the percentage distribution of Th minerals is shown in Figure 4.14. The observed solid species concentrations are weight percentages estimated in the EXAFS LCF data (section 3.4.1, Table 3.8) showing the averaged contribution of about 61 wt.% from monazite, 24 wt.% from thorite and 15 wt.% from ThO_2 to the total amount of Th minerals in the bulk soil. Even though the precise conditions are not properly defined, the modelling data do indicate that all these three solid phases can co-exist in the system below pH 4.5. Modifying relative concentrations like those of phosphate or silicate could change this simulation, indicating that depending on the initial concentrations of mineral phases, all three possible phases of Th can exist in natural system. One also has to consider that solubilities and

concomitantly chemical stabilities of mineral phases depend on their size and crystallinity. Considering such parameters can also change the outcome of calculations.

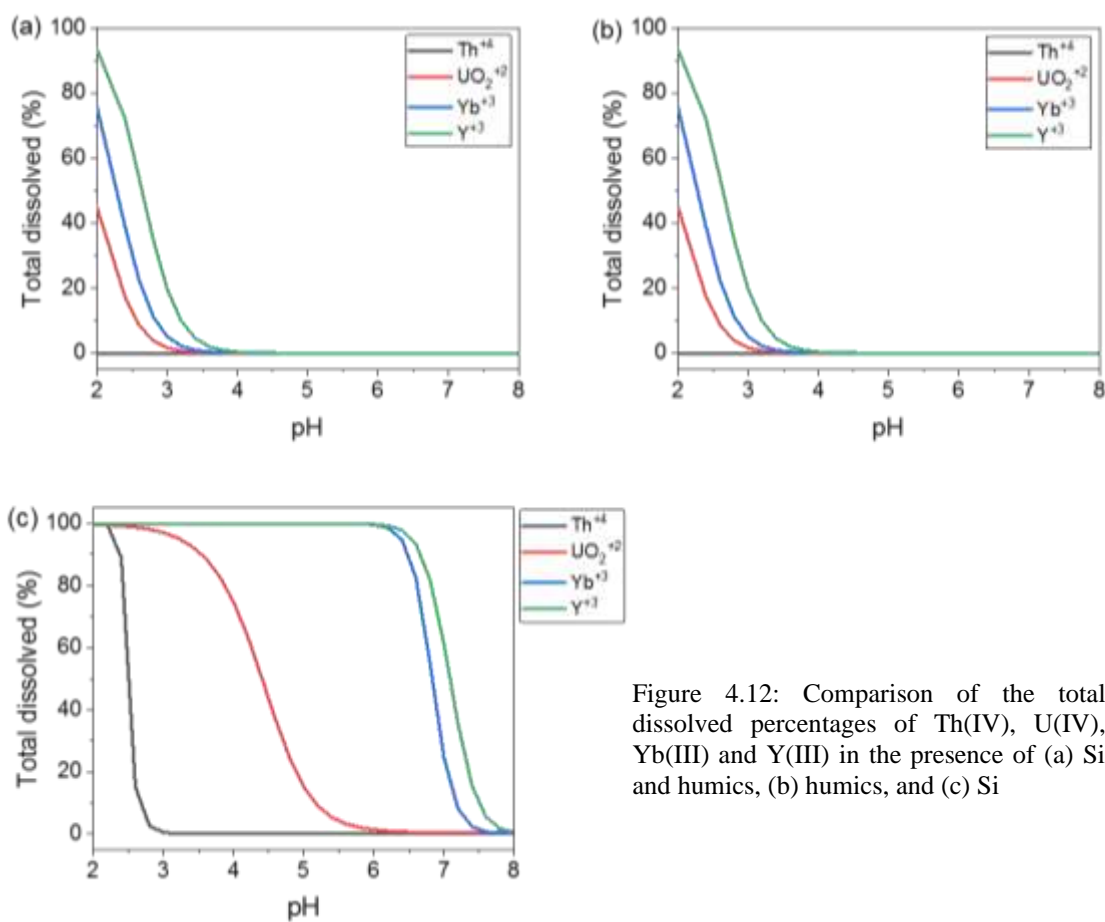


Figure 4.12: Comparison of the total dissolved percentages of Th(IV), U(IV), Yb(III) and Y(III) in the presence of (a) Si and humics, (b) humics, and (c) Si

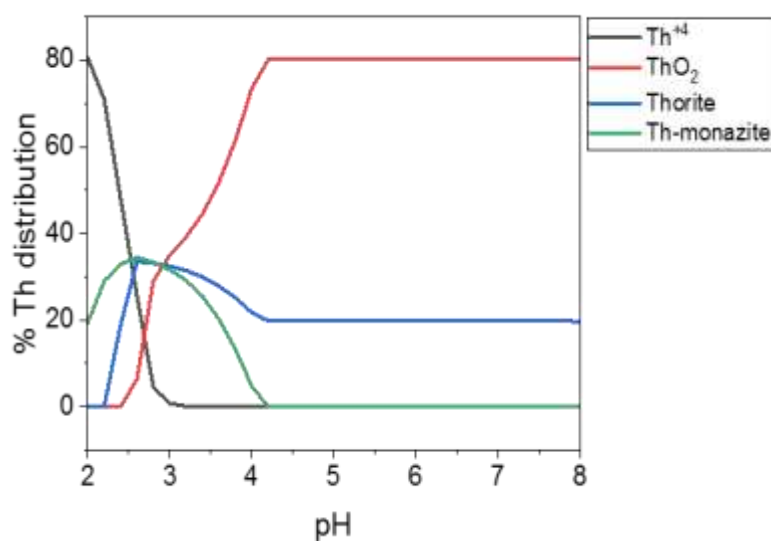


Figure 4.13: Percentages distribution of Th in a system with an initial concentrations of 10^{-6} mol L⁻¹ Th, 8.5×10^{-7} PO₄³⁻ mol L⁻¹ and 2.4×10^{-7} mol L⁻¹ H₄SiO₄ with 0.1 mol L⁻¹ NaCl electrolyte concentration

Overall, the above geochemical data are based on certain assumptions so that the correlation of the geochemical data with the real system is much more complex and a more conclusive outcome would require more advanced approaches. The trend in ion mobility is to some extent well retrieved in the calculation results and help better understand the geochemical processes behind the observations encountered during batch experiments.

4.6. Conclusions

Laboratory experiments involving batch and column approaches with different extraction abilities (from chemical to environmentally relevant solutions) suggest that:

- Chemical extractions are not necessarily as selective for the operationally defined fraction and the target elements as the methods often imply. However, applying both single and sequential extractions allows to (i) account for potential artefacts during the extractions, (ii) potentially identify relative solid carrier phases (especially during sequential extractions), and (iii) estimate element general mobility (particularly from single extractions).
- Extractions in bulk and sieved soils suggest a common distribution of target elements among operationally defined phases independent of the soil grain size. Overall, low amounts of Th were extracted within the exchangeable fraction (0.02 – 0.04 wt.%), with no U, but 13 – 22 wt.% of La. Carbonates and organic matter bound fractions of Th operationally defined by the extraction scheme were about 0.8 wt.% , 8 – 15% for U, and 0.8 – 1.2% for La. Around 33 wt.% of Th and U was bound to iron phases including both amorphous and crystalline phases according to the operational definition of the scheme whereas they were 0.7 wt.% for La in all size fractions. The metal ions released by the extraction agents might also come from other sources, e.g. by dissolution from Th, U, REE containing minerals. La leaches easily probably due to ion exchange reactions. The high concentrations of U in the carbonate fraction (which does not exist), might be due to the inherently low pH conditions at that extraction step. Overall, target elements were mainly associated with the residual fraction F6: >70, >50 and >75 wt.% for Th, U and La, respectively. As stated above, the overall results from the extractions are in accordance with other areas of study for Th and U solid partitioning.

- Extractions in closed systems (batch) with simulated rainwaters and external carrier phases such as silica nanoparticles and humic acids suggest an overall potential mobilization of trace elements below 1% for the given experimental conditions. Despite the relative differences observed for the different conditions (extraction efficiencies being $SRW < Si\ NPs < HA$, with Si NPs mobilizing Th from some carrier phase other than the exchangeable fraction), these results indicate that these target elements show very low mobility and are expected to continue to reside in the area of study. Experiments reveal the strong sorption of Si NPs (and HA) to the acidic soil as well.
- The vertical leachability as observed in column experiments with SRW suggest that trace elements show higher mobility during the first days and eventually reach measured groundwater levels. Much less Th, U, La is mobilized in column experiments as compared to batch studies and adding Si NPs or HA had no significant effect. Stagnant conditions or inherent column properties regarding soil type may affect the fates of trace elements over time. The occurrence of unexpected peaks/higher concentrations in the column experiments might imply the presence of other processes which could potentially enhance metal ion mobility. The origin of such peaks could not be identified. Column experiments seem to provide more relevant data for NR mobilization than those obtained from sequential extraction and batch studies. The amount of target elements released from the column is mostly associated to colloidal forms and the aquatic chemistry of La, Th, U strongly dominated by colloidal or particulate species. Thus, their environmental dispersion and biological implications must be further studied. Even though HA has the potential to mobilize target metal ions as in the case of Si NPs, HA appears to be relatively immobile in the soil. Strong HA retention is observed in the column studies and, thus HA may even enhance retention of metal ions.
- Even though the geochemical data are based on certain assumptions, the trend in ion mobility observed in batch experiments is retrieved in the calculation results to some extent. The correlation of the geochemical data with the real system is much more complex and a more conclusive outcome would require more advanced approaches.

5. SUMMARY AND FUTURE PERSPECTIVES

This thesis is a first, preliminary, but still comprehensive effort for radiological characterization and corresponding environmental mobility studies of selected NRs for a natural area in central Sri Lanka with high background radiation levels. The exact location is the playground of a school and therefore, attention was driven towards this location since it is directly in contact with local population and there is a potential risk for the population living in this area.

The first part of this study mainly focused on the characterization of environmental samples such as soil, grass and groundwater and corresponding radiation risk estimations. The enhanced activity levels in the soil were identified to be due to Th-232 ($> 4000 \text{ Bq kg}^{-1}$) and Ra-226 ($> 300 \text{ Bq kg}^{-1}$) including progenies, showing high absorbed dose rates in air ($> 2 \mu\text{Gy h}^{-1}$) compared to world average values (10- and 100-fold higher, respectively) and other investigated HBRA in the world. The estimated TFs (for Th-232 ~ 0.16), effective inhalation doses (due to Tn in the range of 2.49 – 5.46 mSv) and radiation hazardous indices (Ra_{eq} : 6695 – 10616 Bq kg^{-1} , I_{γ} : 23.4 – 37.1, H_{ext} : 18.1 – 28.7, ELCR: 14.3×10^{-3} – 22.7×10^{-3}) all exceeded world averages and limits. Even though these calculations might not always give accurate values, they provide upper limits of possible hazards and allow preliminary risk estimations at the location. The results suggest that the current location should be considered as a HBRA, although the specific criteria to define a location as a HBRA still need to be clearly defined.

External radiation exposure due to the presence of terrestrial NRs is mainly influenced by the geological settings. The corresponding soil is an indirect indicator of such geological background, used for monitoring and locating potential risk areas for the public. Furthermore, the existing knowledge on the radiation levels in soil and subsequently measured or estimated dose rates in this study can be used in the future as baseline data (or time zero information) and utilized to trace or quantify changes in environmental radioactivity due to unexpected or unforeseen anthropogenic activities such as fallouts from nuclear power plant accidents.

Based on the studied samples, the following relevant radiation exposure pathways in the area can be identified: (i) external exposure due to radioactive soils containing NRs,

(ii) internal exposure via inhalation of radiogenic gases such as Rn-222 and Rn-220, and dust particles containing Th-232 and progenies, and (iii) potential internal exposure via ingestion of local crops, evidenced by uptake in grass samples, to be further investigated on specific edible species. The radiological risk via drinking water should be further observed as overall element concentrations are not of concern regarding chemotoxicity, i.e., they show concentrations for constituents below established limits in water quality guidelines. Among all identified pathways, the maximum exposure will probably be related to in-situ external radiation and inhalation of dust particles emitting radiation from relatively stable and immobile Th-232 and its progenies from small mineral particles, especially during dry seasons, and this is particularly relevant in places such as school playgrounds, where young pupils are.

The results from different solid characterization methods agree well with each other, suggesting the following geochemical composition/characteristics of the local soil. XRD data reveal the major mineralogy of the site to be dominated by kaolinite and quartz while the diffractograms of sieved fractions indicate some Fe crystalline phases like hematite and goethite. The XRF data yielding the elemental distribution on the site showed high concentrations of Th ($\sim 1.6 \text{ g kg}^{-1}$), U (35.7 mg kg^{-1}) and REEs (total of La, Ce, and Nd is $\sim 6.8 \text{ g kg}^{-1}$), which support the radiological data. SEM images and corresponding EDX spectra provided finer details of the grain composition and revealed the variable mineralogy of Th, U and REEs solid phases together with synchrotron based XAS at Th L_3 -edge and μ -XRF. These approaches confirmed the presence of distinct dominant Th-containing mineral phases, namely Th-silicate, Th-oxide, and Th-phosphate, within the soil samples. Results also provided insights into the composition and heterogeneity of both bulk soil and single mineral grains in natural soil samples showing that clay and iron mineral phases may be attached to large mineral grains with potential implications for the environmental behavior and fate of associated trace elements beyond simple dissolution of single mineral phases. This study presents the first thorough characterization of soil from this area.

Studies on elemental mobility through well established selective extractions suggested that: (i) Th, U and REEs, are mainly associated with the residual fraction (>70 , >50 and >75 wt.% for Th, U and La, respectively) most likely as the major minerals identified, silicates, oxides, and phosphates, which are not destroyed by the different steps of the

applied selective extraction schemes, (ii) ~16 and 27 wt.% of Th and U, respectively, could be associated with crystalline iron oxides, and (iii) less than 8 wt.% of Th, 16 wt.% of U and 9 wt.% of La were associated with non-residual fraction due to solid host phase dissolution, which reflects some possible mobility in the environment under specific conditions. It is, however, unclear to what extent the extraction agents exert an increased solubility of Th/U/REE oxides, silicates or phosphates. A relatively high fraction of La, as a representative of the light REEs, is leached out easily pointing to a weak La binding to mineral surfaces, possibly to ion exchange sites.

Batch and column experiments with HA and Si NPs have demonstrated clearly, that colloidal species such as HA and Si NPs are not as mobile as assumed and predominantly retain within the soil. Moreover, the column experiments (in presence and absence of “mobile” colloidal species), representing potential transfer to underground water systems, result in very much lower mobile fractions of Th, U, La than observed in batch and selective chemical extraction studies, yet providing more relevant data for the mobilization of NRs than aforementioned batch experiments. Apparently, the soil acts as an important filter. Experimental data obtained in the present thesis provide strong indications that, at least for Th, particulates and colloids play a cardinal role for the environmental behavior. Th, U, REE concentration levels in column effluents seem to be very consistent with those found in the groundwater samples, collected on-site. Under certain conditions such as heavy rainfall or flooding, it is thus conceivable that Th and also U and REE mobilization by resuspension can play a certain role.

The geochemical scoping calculations supported experimental observations revealing that Th and UO_2^{2+} may strongly bind to humics explaining the higher released amounts ($\sim 0.02 \text{ mg L}^{-1}$), in the respective batch experiments, and may represent both soluble and colloidal fractions of Th complexed with humics. The modelled data in the presence of silica NPs suggest weak binding of U agreeing with its behaviour in the respective batch experiment. Moreover, scoping calculations based on existing thermodynamic data confirm that under given conditions the three main Th solid phases (monazite, thorite and thorianite) identified during the solid phase characterization can co-exist.

Overall, this work highlights the need for comprehensive studies including several environmental compartments in order to better understand the environmental

dispersion, fate and impact of NRs for risk assessment purposes. In fact, the complexity of the field site suggests that multiple mechanisms, are responsible for NRs migration and for the metal ions under investigation colloids and particulates are of special importance. By combining different experimental approaches, it is possible to achieve insight into possible mobilization mechanisms for Th and U in the actual setting. Local, spatial heterogeneity was observed in both soils and groundwater samples, highlighting the importance of a higher sample representativity of the study site for future studies. The variability of groundwater compositions points to different local processes being active, which are presently not understood. Overall, this work constitutes (i) a contribution to research on Th, U and light REEs environmental behavior in a specific terrestrial system, as well as (ii) a conceptual basis and guideline for future development of more precise radionuclide risk assessment and management strategies in Sri Lanka.

Future perspectives

Key outcomes of this work support the following future lines of research concerning both radionuclide dispersion and radiological measures:

Th transfer factors to grass are higher than expected, which highlights a knowledge gap concerning the understanding of the interactions between target elements and plant/microbial activities, especially in the rhizosphere. This effect surely plays a major role in the environmental system, especially concerning element mobility during dry/wet transition periods and soils with more vegetation cover.

Despite the low contribution of Th-minerals to the overall mineralogy of the soil (< 0.17 wt.%), further work is needed to evaluate the potential mobilization of Th during weathering (i.e., during rainfall and under biological influence) to better understand its fate and/or its accumulation in both aquatic and biological systems. For instance, determining particle transport via air and gross fluxes into groundwater for variable and extreme environmental conditions (e.g., monsoon periods, dry seasons, erosion from local activities, etc.) combined with meteorological data acquisition, analyzing erosion rates and land-use would provide the basis for identifying and assessing critical scenarios. Such information will be helpful for decision making.

Future research also needs to include more complex models along with more extensive and self-consistent thermodynamic and kinetic data to better simulate environmental

processes, required for environmental risk assessment. In addition, the geochemical data found in this thesis can be utilized in solute-transport modelling which can be used to interpret and understand the water flow and solute transport in soils.

Identification of the industrially valuable minerals was one of the main aims during the baseline environmental monitoring program, which was conducted by the SLAEB and GSMB of Sri Lanka in 2015 (the same project that this study location was identified). Therefore, high levels of REEs in the area may also be of economic interest for technological applications in future. The present study revealed that REEs are bound in mixed phases (e.g. oxides, phosphates, etc.) with Th. However, selective extraction experiments provide indications that at least a part of the lanthanides might be as well easily extractable without application of acids. Those bonding states of lanthanides should be explored more in detail. Consideration of REE mining should as well consider potential environmental impacts of local ores extracting REEs (together with released elements from gangue minerals containing NRs). Anticipating REEs impact the soil environment because of potential increase of industrial REE utilization in this area is another study of interest

May be most importantly, the estimated excess lifetime cancer risks were found to be higher than the recommended limits. Yet it was impossible to evaluate the radiation health hazard of these values on the population. Further research should focus on the radiological hazardous effects on humans from such long-term exposure to in-situ and develop appropriate management measures when possible also considering the potential health impact of radionuclide containing dust inhalation as well. Since reliable, standardized mortality and morbidity statistics are not yet accessible for this target location, it is advisable to start by carrying out proper bio dosimetry and investigations in this area in future, best in consideration with epidemiological and medical studies.

REFERENCES

1. UNSCEAR, *Sources and Effects of Ionizing Radiation*. 2000, United Nations: New York.
2. Ramola, R., et al., *Dose estimation derived from the exposure to radon, thoron and their progeny in the indoor environment*. Scientific reports, 2016. **6**(1): p. 1-16.
3. Rahman, S., M. Rafique, and J. Anwar, *Radon measurement studies in workplace buildings of the Rawalpindi region and Islamabad Capital area, Pakistan*. Building and environment, 2010. **45**(2): p. 421-426.
4. Akiba, S., et al., *Thoron: its metrology, health effects and implications for radon epidemiology: a summary of roundtable discussions*. Radiation protection dosimetry, 2010. **141**(4): p. 477-481.
5. Shang, B., et al., *Thoron levels in traditional Chinese residential dwellings*. Radiation and environmental biophysics, 2005. **44**(3): p. 193-199.
6. Schery, S., *Thoron in the environment*. Journal of the Air & Waste Management Association, 1990. **40**(4): p. 493-497.
7. Al-Zoughool, M. and D. Krewski, *Health effects of radon: a review of the literature*. International journal of radiation biology, 2009. **85**(1): p. 57-69.
8. NRC, *Health effects of exposure to radon: BEIR VI*. Vol. 6. 1999: National Academies Press.
9. Organization, W.H., *WHO handbook on indoor radon: a public health perspective*. 2009: World Health Organization.
10. Omori, Y., et al., *Radiation dose due to radon and thoron progeny inhalation in high-level natural radiation areas of Kerala, India*. Journal of Radiological Protection, 2016. **37**(1): p. 111.
11. Omori, Y., et al., *Long-term measurements of residential radon, thoron, and thoron progeny concentrations around the Chhatrapur placer deposit, a high background radiation area in Odisha, India*. Journal of Environmental Radioactivity, 2016. **162**: p. 371-378.
12. Ramachandran, T., *Environmental thoron (^{220}Rn): A review*. Iran. J. Radiat. Res., 2010. **8**(3): p. 129-147.
13. Forkapic, S., et al., *Correlations between soil characteristics and radioactivity content of Vojvodina soil*. Journal of environmental radioactivity, 2017. **166**: p. 104-111.
14. Dragović, S., et al., *Edaphic factors affecting the vertical distribution of radionuclides in the different soil types of Belgrade, Serbia*. Journal of Environmental Monitoring, 2012. **14**(1): p. 127-137.
15. Metz, V., et al., *Radionuclide behaviour in the near-field of a geological repository for spent nuclear fuel*. 2012. **100**(8-9): p. 699.

16. Gavrilesco, M., L.V. Pavel, and I. Cretescu, *Characterization and remediation of soils contaminated with uranium*. Journal of hazardous materials, 2009. **163**(2-3): p. 475-510.
17. wikipedia. *Decay chains*. 2021 [cited 2021 17.02]; Available from: https://en.wikipedia.org/wiki/Decay_chain.
18. Bilström, K., *Radiogenic isotopes and their applications within a range of scientific fields*. Instrumental techniques applied to mineralogy and geochemistry. Madrid: Spanish Society of Mineralogy, 2008: p. 111-131.
19. Beer, J., *Cosmogenic Radionuclides*, in *Encyclopedia of Paleoclimatology and Ancient Environments*, V. Gornitz, Editor. 2009, Springer Netherlands: Dordrecht. p. 211-213.
20. Belivermis, M., et al., *The effects of physicochemical properties on gamma emitting natural radionuclide levels in the soil profile of Istanbul*. Environmental monitoring and assessment, 2010. **163**(1-4): p. 15-26.
21. Guidotti, L., et al., *Gamma-spectrometric measurement of radioactivity in agricultural soils of the Lombardia region, northern Italy*. Journal of environmental radioactivity, 2015. **142**: p. 36-44.
22. Von Gunten, H. and P. Beneš, *Speciation of radionuclides in the environment*. Radiochimica Acta, 1995. **69**(1): p. 1-30.
23. Froehlich, K., *Environmental radionuclides: Tracers and timers of terrestrial processes*. 2009: Elsevier.
24. Swarzenski, P., *U/Th series radionuclides as coastal groundwater tracers*. Chemical Reviews, 2007. **107**(2): p. 663-674.
25. Jenne, E.A. and S.N. Luoma. *Forms of trace elements in soils, sediments, and associated waters:-An overview of their determination and biological availability*. in *Biological Implications of Metals in the Environment*. 1975. Washington: Technical Information Center.
26. Cataldo, D. and R. Wildung, *Soil and plant factors influencing the accumulation of heavy metals by plants*. Environmental Health Perspectives, 1978. **27**: p. 149-159.
27. Brady, N.C., R.R. Weil, and R.R. Weil, *The nature and properties of soils*. Vol. 13. 2008: Prentice Hall Upper Saddle River, NJ.
28. Dvorak, A. and B. Lewis, *Impacts of coal-fired power plants on fish, wildlife, and their habitats*. 1978, Ann Arbor, Mich.: Department of the Interior, Fish and Wildlife Service, National Power Plant Team.
29. IAEA, *Handbook of parameter values for the prediction of radionuclide transfer in terrestrial and freshwater environments*. 2010: International Atomic Energy Agency.
30. Shtangeeva, I., *Uptake of uranium and thorium by native and cultivated plants*. Journal of environmental radioactivity, 2010. **101**(6): p. 458-463.

31. Chen, S., Y. Zhu, and Q. Hu, *Soil to plant transfer of ²³⁸U, ²²⁶Ra and ²³²Th on a uranium mining-impacted soil from southeastern China*. Journal of Environmental radioactivity, 2005. **82**(2): p. 223-236.
32. Hegazy, A., et al., *Soil characteristics influence the radionuclide uptake of different plant species*. Chemistry and Ecology, 2013. **29**(3): p. 255-269.
33. Howard, B., et al., *Radionuclide transfer to animal products: revised recommended transfer coefficient values*. Journal of environmental radioactivity, 2009. **100**(3): p. 263-273.
34. Krauskopf, K. and D. Bird, *Surface chemistry: the solution-mineral interface. Introduction to geochemistry (Ed MG-HI Editions) Mc Graw-Hill International Editions edn*. Earth sciences and geology series, 1995: p. 135-163.
35. Peterson, J., et al., *Thorium*. Radiological and Chemical Fact Sheets to Support Health Risk Analyses for Contaminated Areas. Argonne National Laboratory Environmental Science Division, 2007.
36. Greenwood, N.N. and A. Earnshaw, *Chemistry of the Elements*. 2012: Elsevier.
37. Tutson, C.D. and A.E.V. Gorden, *Thorium coordination: A comprehensive review based on coordination number*. Coordination Chemistry Reviews, 2017. **333**: p. 27-43.
38. Natrajan, L.S., et al., *Redox and environmentally relevant aspects of actinide (IV) coordination chemistry*. Coordination Chemistry Reviews, 2014. **266**: p. 171-193.
39. Syed, H., *Extrapolation studies on adsorption of thorium and uranium at different solution compositions on soil sediments*. Journal of radioanalytical and nuclear chemistry, 1998. **237**(1): p. 125-128.
40. Vasiliu, M., et al., *Spectroscopic and energetic properties of thorium (IV) molecular clusters with a hexanuclear core*. The Journal of Physical Chemistry A, 2012. **116**(25): p. 6917-6926.
41. Choppin, G., *Actinide speciation in the environment*. Journal of Radioanalytical and Nuclear Chemistry, 2007. **273**(3): p. 695-703.
42. Klapötke, T.M. and A. Schulz, *The first observation of a Th³⁺ ion in aqueous solution*. Polyhedron, 1997. **16**(6): p. 989-991.
43. Knope, K.E., et al., *Thorium (IV)-selenate clusters containing an octanuclear Th (IV) hydroxide/oxide core*. Inorganic Chemistry, 2012. **51**(7): p. 4239-4249.
44. Knope, K.E., et al., *Thorium (IV) molecular clusters with a hexanuclear Th core*. Inorganic Chemistry, 2011. **50**(19): p. 9696-9704.
45. Neck, V. and J. Kim, *Solubility and hydrolysis of tetravalent actinides*. Radiochimica Acta, 2001. **89**(1): p. 1-16.
46. Langmuir, D. and J.S. Herman, *The mobility of thorium in natural waters at low temperatures*. Geochimica et Cosmochimica Acta, 1980. **44**(11): p. 1753-1766.

47. Rachkova, N., I. Shuktomova, and A. Taskaev, *The state of natural radionuclides of uranium, radium, and thorium in soils*. Eurasian Soil Science, 2010. **43**(6): p. 651-658.
48. Neck, V., et al., *Solubility of crystalline thorium dioxide*. Radiochimica Acta, 2003. **91**(5): p. 253-262.
49. Östhols, E., *Some Processes Affecting the Mobility of Thorium in Natural Ground Waters*. 1994, Department of Chemistry, Royal Institute of Technology: Stockholm, Sweden.
50. Bitea, C., et al., *Study of the generation and stability of thorium (IV) colloids by LIBD combined with ultrafiltration*. Colloids and Surfaces A: Physicochemical and Engineering Aspects, 2003. **217**(1-3): p. 63-70.
51. Rothe, J., et al., *XAFS investigation of the structure of aqueous thorium(IV) species, colloids, and solid thorium(IV) oxide/hydroxide*. Inorganic Chemistry, 2002. **41**(2): p. 249-258.
52. Felmy, A., D. Rai, and M. Mason, *The solubility of hydrous thorium (IV) oxide in chloride media: Development of an aqueous ion-interaction model*. Radiochimica Acta, 1991. **55**(4): p. 177-185.
53. EPA *United States Environmental Protection Agency*. EPA.gov, 2017.
54. ATSDR. *Toxic Substances Portal - Thorium*. Atlanta, GA: Centers for Disease Control and Prevention. 2014 [cited 2020 13.05].
55. Ackerman, H., *Preliminary studies of the toxicity of thorium*. Vol. 2283. 1949: US Atomic Energy Commission, Technical Information Branch.
56. ATSDR, *Toxicological Profile for Thorium*. 1990, U.S. Public Health Service: Georgia.
57. Humphrey, U.E. and M.U. Khandaker, *Viability of thorium-based nuclear fuel cycle for the next generation nuclear reactor: Issues and prospects*. Renewable and Sustainable Energy Reviews, 2018. **97**: p. 259-275.
58. Taylor, S., *Abundance of chemical elements in the continental crust: a new table*. Geochimica et cosmochimica acta, 1964. **28**(8): p. 1273-1285.
59. Loiseau, T., et al., *The crystal chemistry of uranium carboxylates*. Coordination Chemistry Reviews, 2014. **266**: p. 69-109.
60. Langmuir, D., *Aqueous environmental*. Geochemistry Prentice Hall, NJ, 1997.
61. Grenthe, I., et al., *Chemical thermodynamics of uranium*. Vol. 1. 1992, Amsterdam: Elsevier
62. Beccia, M., et al., *New insight into the ternary complexes of uranyl carbonate in seawater*. Journal of environmental radioactivity, 2017. **178**: p. 343-348.
63. Endrizzi, F. and L. Rao, *Chemical speciation of uranium (VI) in marine environments: complexation of calcium and magnesium ions with [(UO₂)(CO₃)₃] 4⁻ and the effect on the extraction of uranium from seawater*. Chemistry—A European Journal, 2014. **20**(44): p. 14499-14506.

64. Langmuir, D., *Uranium solution-mineral equilibria at low temperatures with applications to sedimentary ore deposits*. *Geochimica et Cosmochimica Acta*, 1978. **42**(6): p. 547-569.
65. ATSDR, U., *Toxicological profile for uranium*. 1999, Agency for Toxic Substances and Disease Registry Atlanta, GA.
66. Keith, S., et al., *Toxicological Profile for Radon*. Agency for Toxic Substances and Disease Registry (ATSDR) Toxicological Profiles. 2012: Agency for Toxic Substances and Disease Registry (US), Atlanta (GA).
67. Schulz, R.K., *Soil Chemistry of Radionuclides*. *Health Physics*, 1965. **11**(12): p. 1317-1324.
68. Hogg, D.S., R.G. McLaren, and R.S. Swift, *Desorption of copper from some New Zealand soils*. *Soil Science Society of America Journal*, 1993. **57**(2): p. 361-366.
69. Rao, C.R.M., A. Sahuquillo, and J.F. Lopez-Sanchez, *Comparison of single and sequential extraction procedures for the study of rare earth elements remobilisation in different types of soils*. *Analytica Chimica Acta*, 2010. **662**(2): p. 128-136.
70. Janssen, R.P. and W. Verweij, *Geochemistry of some rare earth elements in groundwater, Vierlingsbeek, The Netherlands*. *Water Research*, 2003. **37**(6): p. 1320-1350.
71. Navas, A., et al., *Spatial distribution of natural and artificial radionuclides at the catchment scale (South Central Pyrenees)*. *Radiation Measurements*, 2011. **46**(2): p. 261-269.
72. Biddau, R., R. Cidu, and F. Frau, *Rare earth elements in waters from the albitite-bearing granodiorites of Central Sardinia, Italy*. *Chemical Geology*, 2002. **182**(1): p. 1-14.
73. Byrne, R.H. and K.-H. Kim, *Rare earth element scavenging in seawater*. *Geochimica et Cosmochimica Acta*, 1990. **54**(10): p. 2645-2656.
74. Erel, Y. and E.M. Stolper, *Modeling of rare-earth element partitioning between particles and solution in aquatic environments*. *Geochimica et Cosmochimica Acta*, 1993. **57**(3): p. 513-518.
75. Wedow, H., *The Morro do Ferro thorium and rare-earth ore deposit, Poços de Caldas District, Brazil*. 1967: US Geological Survey Bulletin.
76. Chapman, N., et al., *The Poços de Caldas project: natural analogues of processes in a radioactive waste repository*. 1993, Amsterdam: Elsevier.
77. James, R.O. and T.W. Healy, *Adsorption of hydrolyzable metal ions at the oxide—water interface. II. Charge reversal of SiO₂ and TiO₂ colloids by adsorbed Co (II), La (III), and Th (IV) as model systems*. *Journal of Colloid and Interface Science*, 1972. **40**(1): p. 53-64.
78. Zaki, M. and K. Kolta, *On the sorption of thorium ions from aqueous nitrate solutions by silica gel*. *Indian Journal of Chemistry*, 1980. **19A**: p. 630-633.

79. Östhols, E., et al., *Adsorption of Thorium on Amorphous Silica: An EXAFS Study*. Journal of Colloid and Interface Science, 1997. **194**(1): p. 10-21.
80. Östhols, E., *Thorium sorption on amorphous silica*. Geochimica et Cosmochimica Acta, 1995. **59**(7): p. 1235-1249.
81. Chen, C. and X. Wang, *Sorption of Th (IV) to silica as a function of pH, humic/fulvic acid, ionic strength, electrolyte type*. Applied Radiation and Isotopes, 2007. **65**(2): p. 155-163.
82. Akcay, H. and S. Kilinc, *Sorption and desorption of thorium from aqueous solutions by montmorillonite*. Journal of Radioanalytical and Nuclear Chemistry, 1996. **212**(3): p. 173-185.
83. Akcay, H., S. Kilinc, and C. Karapire, *A comparative study on the sorption and desorption of Hg, Th and U on clay*. Journal of radioanalytical and nuclear chemistry, 1996. **214**(1): p. 51-66.
84. LaFlamme, B.D. and J.W. Murray, *Solidsolution interaction: The effect of carbonate alkalinity on adsorbed thorium*. Geochimica et Cosmochimica Acta, 1987. **51**(2): p. 243-250.
85. Hunter, K.A., D.J. Hawke, and L.K. Choo, *Equilibrium adsorption of thorium by metal oxides in marine electrolytes*. Geochimica et Cosmochimica Acta, 1988. **52**(3): p. 627-636.
86. Cromières, L., et al., *Sorption of thorium onto hematite colloids*. Radiochimica Acta, 1998. **82**(s1): p. 249-256.
87. Murphy, R.J., J.J. Lenhart, and B.D. Honeyman, *The sorption of thorium (IV) and uranium (VI) to hematite in the presence of natural organic matter*. Colloids and surfaces A: physicochemical and engineering aspects, 1999. **157**(1-3): p. 47-62.
88. Reiller, P., et al., *Retention behaviour of humic substances onto mineral surfaces and consequences upon thorium (IV) mobility: case of iron oxides*. Applied Geochemistry, 2002. **17**(12): p. 1551-1562.
89. Righetto, L., et al., *Surface interactions of actinides with alumina colloids*. Radiochimica Acta, 1988. **44**(1): p. 73-76.
90. Chen, C. and X. Wang, *Influence of pH, soil humic/fulvic acid, ionic strength and foreign ions on sorption of thorium (IV) onto γ -Al₂O₃*. Applied geochemistry, 2007. **22**(2): p. 436-445.
91. Glaus, M.A., W. Hummel, and L.R. Van Loon, *Experimental determination and modelling of trace metal-humate interactions: a pragmatic approach for applications in groundwater*. 1997, Paul Scherrer Institute: Villigen, Switzerland.
92. Saito, T., et al., *Application of the NICA-Donnan model for proton, copper and uranyl binding to humic acid*. Radiochimica Acta, 2004. **92**(9-11): p. 567-574.
93. Lenhart, J.J. and B.D. Honeyman, *Uranium (VI) sorption to hematite in the presence of humic acid*. Geochimica et Cosmochimica Acta, 1999. **63**(19-20): p. 2891-2901.

94. Popic, J.M., et al., *Transfer of naturally occurring radionuclides from soil to wild forest flora in an area with enhanced legacy and natural radioactivity in Norway*. Environmental Science: Processes & Impacts, 2020. **22**(2): p. 350-363.
95. Waite, T., et al., *Uranium (VI) adsorption to ferrihydrite: Application of a surface complexation model*. Geochimica et Cosmochimica Acta, 1994. **58**(24): p. 5465-5478.
96. Ho, C. and D. Doern, *The sorption of uranyl species on a hematite sol*. Canadian journal of chemistry, 1985. **63**(5): p. 1100-1104.
97. Quigley, M.S., B.D. Honeyman, and P.H. Santschi, *Thorium sorption in the marine environment: equilibrium partitioning at the hematite/water interface, sorption/desorption kinetics and particle tracing*. Aquatic Geochemistry, 1995. **1**(3): p. 277-301.
98. Hongxia, Z., D. Zheng, and T. Zuyi, *Sorption of thorium (IV) ions on gibbsite: Effects of contact time, pH, ionic strength, concentration, phosphate and fulvic acid*. Colloids and Surfaces A: Physicochemical and Engineering Aspects, 2006. **278**(1-3): p. 46-52.
99. Payne, T., J. Davis, and T. Waite, *Uranium adsorption on ferrihydrite-Effects of phosphate and humic acid*. Radiochimica Acta, 1996. **74**(s1): p. 239-243.
100. Bau, M., et al., *Geochemistry of low-temperature water-rock interaction: evidence from natural waters, andesite, and iron-oxyhydroxide precipitates at Nishiki-numa iron-spring, Hokkaido, Japan*. Chemical Geology, 1998. **151**(1-4): p. 293-307.
101. Backes, C.A., et al., *Kinetics of cadmium and cobalt desorption from iron and manganese oxides*. Soil Science Society of America Journal, 1995. **59**(3): p. 778-785.
102. Chabaux, F., J. Riotte, and O. Dequincey, *U-Th-Ra fractionation during weathering and river transport*. Reviews in Mineralogy and geochemistry, 2003. **52**(1): p. 533-576.
103. Zhang, Y., et al., *Selectivity in the complexation of actinides by humic substances*. Environmental Pollution, 1997. **96**(3): p. 361-367.
104. Zhang, Q., et al., *Geochemical Characteristics of Rare Earth Elements in Soils from Puding Karst Critical Zone Observatory, Southwest China*. Sustainability, 2019. **11**(18): p. 4963.
105. Zhenghua, W., et al., *Adsorption isotherms of lanthanum to soil constituents and effects of pH, EDTA and fulvic acid on adsorption of lanthanum onto goethite and humic acid*. Chemical Speciation & Bioavailability, 2001. **13**(3): p. 75-81.
106. Li, B. and R.H. Byrne, *Ionic strength dependence of rare earth-NTA stability constants at 25 C*. Aquatic Geochemistry, 1997. **3**(2): p. 99-115.
107. Miekeley, N. and I.L. Kuchler, *Interactions between thorium and humic compounds in surface waters*. Inorganica Chimica Acta, 1987. **140**(1-2): p. 315-319.

108. Millero, F.J., *Stability constants for the formation of rare earth-inorganic complexes as a function of ionic strength*. *Geochimica et Cosmochimica Acta*, 1992. **56**(8): p. 3123-3132.
109. Morton, L., C. Evans, and G. Estes, *Natural uranium and thorium distributions in podzolized soils and native blueberry*. *Journal of environmental quality*, 2002. **31**(1): p. 155-162.
110. Bednar, A., et al., *Effects of organic matter on the distribution of uranium in soil and plant matrices*. *Chemosphere*, 2007. **70**(2): p. 237-247.
111. Gu, Z., et al., *Determination of stability constants for rare earth elements and fulvic acids extracted from different soils*. *Talanta*, 2001. **53**(6): p. 1163-1170.
112. Ragnarsdottir, K. and L. Charlet, *Uranium behaviour in natural environments*. 2000, Mineralogical Society: London, UK. p. 245-289.
113. Grenthe, I., et al., *Chemical thermodynamics of uranium*, NEA. 1992, North-Holland Elsevier Science Publishers BV, Amsterdam.
114. Davis, J.A. and J.O. Leckie, *Effect of adsorbed complexing ligands on trace metal uptake by hydrous oxides*. *Environmental science & technology*, 1978. **12**(12): p. 1309-1315.
115. Casartelli, E.A. and N. Miekeley, *Determination of thorium and light rare-earth elements in soil water and its high molecular mass organic fractions by inductively coupled plasma mass spectrometry and on-line-coupled size-exclusion chromatography*. *Analytical and bioanalytical chemistry*, 2003. **377**(1): p. 58-64.
116. Kretzschmar, R. and T. Schäfer, *Metal retention and transport on colloidal particles in the environment*. *Elements*, 2005. **1**(4): p. 205-210.
117. Wu, W., et al., *Sorption-desorption of Th (IV) on attapulgite: effects of pH, ionic strength and temperature*. *Applied radiation and isotopes*, 2007. **65**(10): p. 1108-1114.
118. Schmidt, M., et al., *Sorption of tetravalent thorium on muscovite*. *Geochimica et Cosmochimica Acta*, 2012. **88**: p. 66-76.
119. Xu, D., et al., *Sorption of Th (IV) on Na-rectorite: effect of HA, ionic strength, foreign ions and temperature*. *Applied Geochemistry*, 2007. **22**(12): p. 2892-2906.
120. Yu, S., et al., *Adsorption of Th (IV) onto Al-pillared rectorite: Effect of pH, ionic strength, temperature, soil humic acid and fulvic acid*. *Applied clay science*, 2008. **38**(3-4): p. 219-226.
121. Olin, M. and J. Lehtikoinen, *Application of surface complexation modelling: Nickel sorption on quartz, manganese oxide, kaolinite and goethite, and thorium on silica*. 1997, Posiva Oy: Finland.
122. Rand, M. and F.J. Mompean, *Chemical thermodynamics of thorium*. 2009, Amsterdam: Elsevier.

123. Weijuan, L. and T. Zuyi, *Comparative study on Th (IV) sorption on alumina and silica from aqueous solutions*. Journal of Radioanalytical and Nuclear Chemistry, 2002. **254**(1): p. 187-192.
124. Reiller, P.E., et al., *On the study of Th (IV)-humic acid interactions by competition sorption studies with silica and determination of global interaction constants*. Radiochimica Acta, 2003. **91**(9): p. 513-524.
125. Bednar, A., et al., *Mechanisms of thorium migration in a semiarid soil*. Journal of environmental quality, 2004. **33**(6): p. 2070-2077.
126. Février, L. and A. Martin-Garin, *Biogeochemical behaviour of anionic radionuclides in soil: Evidence for biotic interactions*. Radioprotection, 2005. **40**(1): p. S79.
127. Tessier, A., P.G. Campbell, and M. Bisson, *Sequential extraction procedure for the speciation of particulate trace metals*. Analytical chemistry, 1979. **51**(7): p. 844-851.
128. Strok, M. and B. Smodis, *Comparison of two sequential extraction protocols for fractionation of natural radionuclides in soil samples*. Radiochimica Acta International journal for chemical aspects of nuclear science and technology, 2010. **98**(4): p. 221-229.
129. Martinez-Aguirre, A., M. Garcia-León, and M. Ivanovich, *U and Th speciation in river sediments*. Science of the total environment, 1995. **173**: p. 203-209.
130. Kaplan, D. and S. Serkiz, *Quantification of thorium and uranium sorption to contaminated sediments*. Journal of Radioanalytical and Nuclear Chemistry, 2001. **248**(3): p. 529-535.
131. Schultz, M.K., W.C. Burnett, and K.G. Inn, *Evaluation of a sequential extraction method for determining actinide fractionation in soils and sediments*. Journal of Environmental Radioactivity, 1998. **40**(2): p. 155-174.
132. Gleyzes, C., S. Tellier, and M. Astruc, *Fractionation studies of trace elements in contaminated soils and sediments: a review of sequential extraction procedures*. TrAC Trends in Analytical Chemistry, 2002. **21**(6-7): p. 451-467.
133. Guo, P., et al., *Evaluation of a sequential extraction for the speciation of thorium in soils from Baotou area, Inner Mongolia*. Talanta, 2007. **71**(2): p. 778-783.
134. Tack, F., H. Vossius, and M. Verloo, *A comparison between sediment fractions, obtained from sequential extraction and estimated from single extractions*. International Journal of Environmental Analytical Chemistry, 1996. **63**(1): p. 61-66.
135. Barreto, S.R.G., et al., *Comparison of metal analysis in sediments using EDXRF and ICP-OES with the HCl and Tessie extraction methods*. Talanta, 2004. **64**(2): p. 345-354.
136. Bacon, J.R. and C.M. Davidson, *Is there a future for sequential chemical extraction?* Analyst, 2008. **133**(1): p. 25-46.

137. Du Bray, E.A., *Preliminary compilation of descriptive geoenvironmental mineral deposit models*. 1995, US Geological Survey: Denver, CO. p. 272.
138. Rauret, G., et al., *Improvement of the BCR three step sequential extraction procedure prior to the certification of new sediment and soil reference materials*. Journal of Environmental Monitoring, 1999. **1**(1): p. 57-61.
139. Strok, M. and B. Smoldis, *Comparison of two sequential extraction protocols for fractionation of natural radionuclides in soil samples*. Radiochimica Acta, 2010. **98**(4): p. 221-229.
140. Vandenhove, H., et al., *Comparison of two sequential extraction procedures for uranium fractionation in contaminated soils*. Journal of environmental radioactivity, 2014. **137**: p. 1-9.
141. Fox, P.M., et al., *Characterization of natural organic matter in low-carbon sediments: extraction and analytical approaches*. Organic Geochemistry, 2017. **114**: p. 12-22.
142. Lopez-Sangil, L. and P. Rovira, *Sequential chemical extractions of the mineral-associated soil organic matter: An integrated approach for the fractionation of organo-mineral complexes*. Soil Biology and Biochemistry, 2013. **62**: p. 57-67.
143. McKeague, J., *An evaluation of 0.1 M pyrophosphate and pyrophosphate-dithionite in comparison with oxalate as extractants of the accumulation products in podzols and some other soils*. Canadian Journal of Soil Science, 1967. **47**(2): p. 95-99.
144. Quevauviller, P., G. Rauret, and B. Griepink, *Single and sequential extraction in sediments and soils*. International Journal of Environmental Analytical Chemistry, 1993. **51**(1-4): p. 231-235.
145. Martinez-Aguirre, A. and R. Perianez, *Sedimentary speciation of U and Th isotopes in a marsh area at the southwest of Spain*. Journal of Radioanalytical and Nuclear Chemistry, 2001. **247**(1): p. 45-52.
146. Sohrabi, M., *The state-of-the-art on worldwide studies in some environments with elevated naturally occurring radioactive materials (NORM)*. Applied Radiation and Isotopes, 1998. **49**(3): p. 169-188.
147. Fujinami, N., T. Koga, and H. Morishima. *External exposure rates from terrestrial radiation at Guarapari and Meaipe in Brazil*. in *International Congress of the International Radiation Protection Association*. 2000. Hiroshima, Japan.
148. de Moura, J.C., C.M. Wallfuss, and P. Bossew, *Health hazards of radioactive sands along the coast of Espirito Santo/Brazil*. Neues Jahrbuch fur Geologie und Palaontologie-Abhandlungen, 2002. **225**: p. 127-136.
149. Cullen, T. *Review of Brazilian investigations in areas of high natural radioactivity. Part I: Radiometric and dosimetric studies*. in *International Symposium on Areas of High Natural Radioactivity*. 1977. Rio de Janeiro, Brazil: Academia Brasileria De Ciencias.

150. Sohrabi, M. *World high level natural radiation and/or radon-prone areas with special regards to dwellings*. in *International Conference on High levels of Natural Radiation*. 1997. Beijing, China: Elsevier.
151. Wei, L., et al. *Epidemiological investigation in high background radiation areas of Yangjiang, China*. in *International Conference on High Levels of Natural Radiation*. 1993. International Atomic Energy Agency (IAEA): IAEA.
152. Omori, Y., et al., *A pilot study for dose evaluation in high-level natural radiation areas of Yangjiang, China*. *Journal of Radioanalytical and Nuclear Chemistry*, 2015. **306**(1): p. 317-323.
153. Derin, M.T., et al., *Radionuclides and radiation indices of high background radiation area in Chavara-Neendakara placer deposits (Kerala, India)*. *PloS one*, 2012. **7**(11).
154. Kannan, V., et al., *Distribution of natural and anthropogenic radionuclides in soil and beach sand samples of Kalpakkam (India) using hyper pure germanium (HPGe) gamma ray spectrometry*. *Applied Radiation and isotopes*, 2002. **57**(1): p. 109-119.
155. Selvasekarapandian, S., et al., *Gamma radiation dose from radionuclides in soil samples of Udagamandalam (Ooty) in India*. *Radiation protection dosimetry*, 1999. **82**(3): p. 225-228.
156. Selvasekarapandian, S., et al., *Natural radionuclide distribution in soils of Gudalore, India*. *Applied radiation and isotopes*, 2000. **52**(2): p. 299-306.
157. Mohanty, A., et al., *Natural radioactivity in the newly discovered high background radiation area on the eastern coast of Orissa, India*. *Radiation measurements*, 2004. **38**(2): p. 153-165.
158. Badawy, W.M., et al., *Environmental radioactivity of soils and sediments: Egyptian sector of the Nile valley*. *Isotopes in environmental and health studies*, 2018. **54**(5): p. 535-547.
159. Ebaid, Y., et al., *Environmental radioactivity measurements of Egyptian soils*. *Journal of Radioanalytical and Nuclear Chemistry*, 2000. **243**(2): p. 543-550.
160. El-Gamal, A., S. Nasr, and A. El-Taher, *Study of the spatial distribution of natural radioactivity in the upper Egypt Nile River sediments*. *Radiation Measurements*, 2007. **42**(3): p. 457-465.
161. Gad, A., A. Saleh, and M. Khalifa, *Assessment of natural radionuclides and related occupational risk in agricultural soil, southeastern Nile Delta, Egypt*. *Arabian Journal of Geosciences*, 2019. **12**(6): p. 188.
162. Ramasamy, V., et al., *Role of light and heavy minerals on natural radioactivity level of high background radiation area, Kerala, India*. *Applied Radiation and Isotopes*, 2014. **85**: p. 1-10.
163. Yousef, M., A.A. El-Ela, and H. Yousef, *Natural radioactivity levels in surface soil of Kitchener Drain in the Nile Delta of Egypt*. *Journal of nuclear and radiation physics*, 2007. **2**(1): p. 61-68.

164. Warnakulasuriya, T., et al., *Background radiation levels near a mineral sand mining factory in Sri Lanka: Correlation of radiation measurements with micronuclei frequency*. Radiation Protection Dosimetry, 2020. **189**(1): p. 114-126.
165. Withanage, A. and P. Mahawatte, *Radioactivity of beach sand in the south western coast of Sri Lanka*. Radiation protection dosimetry, 2013. **153**(3): p. 384-389.
166. Mahawatte, P. and K. Fernando, *Radioactivity levels in beach sand from the West Coast of Sri Lanka*. Journal of the National Science Foundation of Sri Lanka, 2013. **41**(4).
167. Bandara, W. and P. Mahawatte. *Radioactivity levels in beach sand from Hambantota to Dondra, Sri Lanka*. in *International Research Conference*. 2015. Sri Lanka: General Sir John Kotelawala Defense University.
168. Nalaka, D.S., et al., *Measuring radon and thoron levels in Sri Lanka*. Advanced Materials Research, 2013. **718-720**: p. 721-724.
169. Herath, M., *Beach Mineral Sands in Sri Lanka. Occurrence, Global Trends and Current Issues*, in 2008, Geological Survey & Mines Bureau: Colombo.
170. Tropper, P., C.E. Manning, and D.E. Harlov, *Solubility of CePO₄ monazite and YPO₄ xenotime in H₂O and H₂O–NaCl at 800 C and 1 GPa: Implications for REE and Y transport during high-grade metamorphism*. Chemical Geology, 2011. **282**(1-2): p. 58-66.
171. Stepanov, A.S., et al., *Experimental study of monazite/melt partitioning with implications for the REE, Th and U geochemistry of crustal rocks*. Chemical Geology, 2012. **300**: p. 200-220.
172. Achary, S., S. Bevara, and A. Tyagi, *Recent progress on synthesis and structural aspects of rare-earth phosphates*. Coordination Chemistry Reviews, 2017. **340**: p. 266-297.
173. Clavier, N., R. Podor, and N. Dacheux, *Crystal chemistry of the monazite structure*. Journal of the European Ceramic Society, 2011. **31**(6): p. 941-976.
174. SLAEB, *Baseline Radioactivity Data*, in *Sri Lanka Atomic Energy Board*. 2018.
175. Silva, E. and L. Manuweera, *Surface and rainwater chemistry in Sri Lanka—A risk of acidification*. Asian Journal of Water, Environment and Pollution, 2004. **1**(1, 2): p. 79-86.
176. Ranasinghe, R., D. Werellagama, and R. Weerasooriya, *Arsenite removal from drinking water using naturally available laterite in Sri Lanka*. Engineer: Journal of the Institution of Engineers, Sri Lanka, 2014. **47**(2).
177. FAO. *Acid Soils*. FAO Soils Portal 2019 [cited 2019 22.07.2019]; Available from: <http://www.fao.org/soils-portal/soil-management/management-of-some-problem-soils/acid-soils/en/>.
178. IAEA, *Measurement of Radionuclides in Food and the Environment*. 1989, Vienna: International Atomic Energy Agency.

179. Almayahi, B., A. Tajuddin, and M. Jaafar, *Radiation hazard indices of soil and water samples in Northern Malaysian Peninsula*. Applied radiation and isotopes, 2012. **70**(11): p. 2652-2660.
180. Ibraheem, A.A., A. El-Taher, and M.H. Alruwaili, *Assessment of natural radioactivity levels and radiation hazard indices for soil samples from Abha, Saudi Arabia*. Results in Physics, 2018. **11**: p. 325-330.
181. Agbalagba, E., G. Avwiri, and Y. Chad-Umoreh, *γ -Spectroscopy measurement of natural radioactivity and assessment of radiation hazard indices in soil samples from oil fields environment of Delta State, Nigeria*. Journal of environmental radioactivity, 2012. **109**: p. 64-70.
182. Aladeniyi, K., C. Olowookere, and B.B. Oladele, *Measurement of natural radioactivity and radiological hazard evaluation in the soil samples collected from Owo, Ondo State, Nigeria*. Journal of Radiation Research and Applied Sciences, 2019. **12**(1): p. 200-209.
183. Alzubaidi, G., F. Hamid, and I. Abdul Rahman, *Assessment of natural radioactivity levels and radiation hazards in agricultural and virgin soil in the state of Kedah, North of Malaysia*. The Scientific World Journal, 2016. **2016**.
184. Beck, H.L., C. Gogolak, and J. DeCampo, *In situ Ge (Li) and NaI (TI) gamma-ray spectrometry*. 1972, Environmental Measurements Laboratory, HASL-195: New York: US DOE.
185. Beretka, J. and P. Mathew, *Natural radioactivity of Australian building materials, industrial wastes and by-products*. Health physics, 1985. **48**(1): p. 87-95.
186. Lee, S.K., et al., *Radiological monitoring: terrestrial natural radionuclides in Kinta District, Perak, Malaysia*. Journal of environmental radioactivity, 2009. **100**(5): p. 368-374.
187. OECD, *Exposure to radiation from natural radioactivity in building materials*. 1979, Nuclear Energy Agency: Paris.
188. Singh, S., A. Rani, and R.K. Mahajan, *^{226}Ra , ^{232}Th and ^{40}K analysis in soil samples from some areas of Punjab and Himachal Pradesh, India using gamma ray spectrometry*. Radiation measurements, 2005. **39**(4): p. 431-439.
189. Alam, M., et al., *The ^{226}Ra , ^{232}Th and ^{40}K activities in beach sand minerals and beach soils of Cox's Bazar, Bangladesh*. Journal of Environmental Radioactivity, 1999. **46**(2): p. 243-250.
190. ICRP, *The 2007 Recommendations of the International Commission on Radiological Protection*, in *ICRP Publication 103*. 2007, ICRP. p. 1-332.
191. UNSCEAR, *UNSCEAR. 1993. Sources, effects and risks of ionising radiations*. New York, 1993.
192. Popic, J.M., et al., *Outdoor ^{220}Rn , ^{222}Rn and terrestrial gamma radiation levels: investigation study in the thorium rich Fen Complex, Norway*. Journal of Environmental Monitoring, 2012. **14**(1): p. 193-201.

193. Hosoda, M., et al., *Characteristic of thoron (^{220}Rn) in environment*. Applied Radiation and Isotopes, 2017. **120**: p. 7-10.
194. Little, I., *The relationship between soil pH measurements in calcium chloride and water suspensions*. Soil Research, 1992. **30**(5): p. 587-592.
195. Minasny, B., et al., *Models relating soil pH measurements in water and calcium chloride that incorporate electrolyte concentration*. European Journal of Soil Science, 2011. **62**(5): p. 728-732.
196. Ahern, C.R., D.E. Baker, and R.L. Aitken, *Models for relating pH measurements in water and calcium chloride for a wide range of pH, soil types and depths*. Plant and Soil, 1995. **171**(1): p. 47-52.
197. Gregorich, E.G. and M.R. Carter, *Soil sampling and methods of analysis*. 2007, Boca Raton, FL: CRC Press.
198. Walkley, A., *A critical examination of a rapid method for determining organic carbon in soils—effect of variations in digestion conditions and of inorganic soil constituents*. Soil science, 1947. **63**(4): p. 251-264.
199. Estefan, G., R. Sommer, and J. Ryan, *Methods of soil, plant, and water analysis: A manual for the West Asia and North Africa region*. 3 ed. 2013, Beirut, Lebanon: ICARDA.
200. Rothe, J., et al., *The INE-Beamline for actinide science at ANKA*. Review of scientific instruments, 2012. **83**(4): p. 043105.
201. Ravel, B. and M. Newville, *ATHENA, ARTEMIS, HEPHAESTUS: data analysis for X-ray absorption spectroscopy using IFEFFIT*. Journal of synchrotron radiation, 2005. **12**(4): p. 537-541.
202. Solé, V., et al., *A multiplatform code for the analysis of energy-dispersive X-ray fluorescence spectra*. Spectrochimica Acta Part B: Atomic Spectroscopy, 2007. **62**(1): p. 63-68.
203. Team, R.D.C. *R: A language and environment for statistical computing*. 2008 [cited 2020 25.05.2020]; Available from: <http://www.R-project.org>.
204. Gustafsson, J.P., *Visual MINTEQ 3.0 User Guide*. 2011, KTH, Department of Land and Water Resources: Stockholm, Sweden.
205. Benedetti, M.F., et al., *Metal ion binding to humic substances: application of the non-ideal competitive adsorption model*. Environmental Science & Technology, 1995. **29**(2): p. 446-457.
206. Rao, N.S., et al., *Natural radioactivity measurements in beach sand along southern coast of Orissa, eastern India*. Environmental Earth Sciences, 2009. **59**(3): p. 593-601.
207. EC, *Radiological protection principles concerning the natural radioactivity of building materials*, in *Radiation Protection*. 2000, European Commission: Luxembourg.

208. Deqing, C. and W. Luxin, *Chromosome aberration, cancer mortality and hermetic phenomena among inhabitants in areas of high background radiation in China*. Journal of Radiation Research, 1991. **32**(Suppl_2): p. 46-53.
209. Nair, R.R.K., et al., *Background radiation and cancer incidence in Kerala, India—Karanagappally cohort study*. Health physics, 2009. **96**(1): p. 55-66.
210. Veiga, L.H. and S. Koifman. *Pattern of cancer mortality in some Brazilian HBRA's*. in *International Conference on High Levels of Natural Radiation and Radon Areas*. 2005. Osaka, Japan: Elsevier.
211. Monica, S., et al., *Estimation of indoor and outdoor effective doses and lifetime cancer risk from gamma dose rates along the coastal regions of Kollam district, Kerala*. Radiation Protection and Environment, 2016. **39**(1): p. 38.
212. Chakraborty, S.R., et al., *Radioactivity concentrations in soil and transfer factors of radionuclides from soil to grass and plants in the Chittagong city of Bangladesh*. Journal of Physical Science, 2013. **24**(1): p. 95.
213. Thabayneh, K., *Transfer of natural radionuclides from soil to plants and grass in the Western North of West Bank Environment, Palestine*. International Journal of Environmental Monitoring and Analysis, 2014. **2**(5): p. 252-258.
214. Roivainen, P., et al., *Transfer of elements relevant to radioactive waste from soil to five boreal plant species*. Chemosphere, 2011. **83**(3): p. 385-390.
215. Shahandeh, H. and L. Hossner, *Role of soil properties in phytoaccumulation of uranium*. Water, Air, and Soil Pollution, 2002. **141**(1-4): p. 165-180.
216. Koranda, J.J. and W.L. Robison, *Accumulation of radionuclides by plants as a monitor system*. Environmental health perspectives, 1978. **27**: p. 165-179.
217. Yamada, Y., et al., *Radon–thoron discriminative measurements in Gansu Province, China, and their implication for dose estimates*. Journal of Toxicology and Environmental Health, Part A, 2006. **69**(7-8): p. 723-734.
218. Chambers, D., *Thoron and decay products, beyond UNSCEAR 2006 Annex E*. Radiation protection dosimetry, 2010. **141**(4): p. 351-356.
219. Chittapore, P., N. Harley, and R. Medora, *Measurement of outdoor radon and thoron at Fernald, OH, New York City and New Jersey*. Health Phys, 2001. **80**: p. S171.
220. Stewart, H. and D.J. Steck. *Radon, thoron and their progeny in Lancaster PA homes*. in *American association of radon scientists and technologists 2008 international symposium*. 2008. Las Vegas.
221. Kant, K., et al., *Seasonal variation of radon, thoron and their progeny levels in dwellings of Haryana and Western Uttar Pradesh*. Iranian Journal of Radiation Research, 2009. **7**(2): p. 79-84.
222. Harley, N., et al., *Measurement of the indoor and outdoor ^{220}Rn (thoron) equilibrium factor: application to lung dose*. Radiation protection dosimetry, 2010. **141**(4): p. 357-362.

223. Prajith, R., et al., *Measurements of radon (^{222}Rn) and thoron (^{220}Rn) exhalations and their decay product concentrations at Indian Stations in Antarctica*. Environmental earth sciences, 2019. **78**(1): p. 35.
224. Van Schmus, W., *Natural radioactivity of the crust and mantle*, in *Global earth physics: A handbook of physical constants*. 1995, American Geophysical Union: Washington, DC. p. 283-291.
225. Vasconcelos, D.C., et al., *Modelling natural radioactivity in sand beaches of Guarapari, Espírito Santo State, Brazil*. World J. of Nucl. Sci. and Technol. , 2013. **3**: p. 65-71.
226. Tufail, M., et al., *Measurement of natural radioactivity in soil from Peshawar basin of Pakistan*. Journal of Radioanalytical and Nuclear Chemistry, 2013. **298**(2): p. 1085-1096.
227. Tzortzis, M. and H. Tsertos, *Determination of thorium, uranium and potassium elemental concentrations in surface soils in Cyprus*. Journal of Environmental radioactivity, 2004. **77**(3): p. 325-338.
228. NRCS. *Examination and Description of Soil Profiles*. National Soil Survey Handbook 2019 [cited 2020 03/06/2020]; Available from: http://www.nrcs.usda.gov/wps/portal/nrcs/detail/soils/ref/?cid=nrcs142p2_054242.
229. Breemen, N.v., C.T. Driscoll, and J. Mulder, *Acidic deposition and internal proton sources in acidification of soils and waters*. Nature, 1984. **307**(5952): p. 599-604.
230. Sparks, D.L., *Environmental soil chemistry*. 2003, London, UK: Academic Press.
231. Schumacher, B.A., *Methods for the determination of total organic carbon (TOC) in soils and sediments*. 2002, U.S. Environmental Protection Agency, National Exposure Research Laboratory: Washington, DC
232. Boudeulle, M. and J.-P. Muller, *Structural characteristics of hematite and goethite and their relationships with kaolinite in a laterite from Cameroon. A TEM study*. Bulletin de minéralogie, 1988. **111**(2): p. 149-166.
233. Johnston, J. and D. Lewis, *A detailed study of the transformation of ferrihydrite to hematite in an aqueous medium at 92 C*. Geochimica et Cosmochimica Acta, 1983. **47**(11): p. 1823-1831.
234. Niu, J., et al., *Concentration Distribution and Bioaccessibility of Trace Elements in Nano and Fine Urban Airborne Particulate Matter: Influence of Particle Size*. Water, Air, & Soil Pollution, 2010. **213**(1): p. 211-225.
235. Parra, S., et al., *Distribution of trace elements in particle size fractions for contaminated soils by a copper smelting from different zones of the Puchuncaví Valley (Chile)*. Chemosphere, 2014. **111**: p. 513-521.
236. Acosta, J.A., et al., *Accumulations of major and trace elements in particle size fractions of soils on eight different parent materials*. Geoderma, 2011. **161**(1): p. 30-42.

237. Megumi, K. and T. Mamuro, *Concentration of uranium series nuclides in soil particles in relation to their size*. Journal of geophysical research, 1977. **82**(2): p. 353-356.
238. Schulthess, C. and C. Huang, *Adsorption of heavy metals by silicon and aluminum oxide surfaces on clay minerals*. Soil Science Society of America Journal, 1990. **54**(3): p. 679-688.
239. Usman, A., Y. Kuzyakov, and K. Stahr, *Effect of clay minerals on extractability of heavy metals and sewage sludge mineralization in soil*. Chemistry and Ecology, 2004. **20**(2): p. 123-135.
240. Qin, F., et al., *Evaluation of trace elements and identification of pollution sources in particle size fractions of soil from iron ore areas along the Chao River*. Journal of Geochemical Exploration, 2014. **138**: p. 33-49.
241. Rudnick, R.L. and S. Gao, *Composition of the Continental Crust*, in *Treatise on Geochemistry*. 2003, Elsevier: Amsterdam. p. 1-64.
242. Dahanayake, K., *Laterites of Sri Lanka—a reconnaissance study*. Mineralium Deposita, 1982. **17**(2): p. 245-256.
243. Chandrajith, R., C. Dissanayake, and H. Tobschall, *Application of multi-element relationships in stream sediments to mineral exploration: a case study of Walawe Ganga Basin, Sri Lanka*. Applied Geochemistry, 2001. **16**(3): p. 339-350.
244. Pitawala, A., et al., *Geochemical and petrological characteristics of Eppawala phosphate deposits, Sri Lanka*. Mineralium deposita, 2003. **38**(4): p. 505-515.
245. Rupasinghe, M. and C. Dissanayake, *The rare-earth element abundance in the sedimentary gem deposits of Sri Lanka*. Lithos, 1984. **17**: p. 329-342.
246. Kayzar, T.M., et al., *Investigating uranium distribution in surface sediments and waters: a case study of contamination from the Juniper Uranium Mine, Stanislaus National Forest, CA*. Journal of environmental radioactivity, 2014. **136**: p. 85-97.
247. Wang, X. and W.S. Broecker, *Long-term reworking of volcanic ash deposited in the abyssal ocean based on uranium and thorium isotope measurements*. Journal of volcanology and geothermal research, 2013. **264**: p. 66-71.
248. Maity, S., S. Sahu, and G. Pandit, *Distribution of uranium and thorium in fractionated sediment samples obtained from different locations across Thane Creek area (Mumbai, India)*. Journal of Radioanalytical and Nuclear Chemistry, 2014. **302**(3): p. 1363-1370.
249. Wickremeratne, W.S., *Preliminary studies on the offshore occurrences of monazite-bearing heavy-mineral placers, southwestern Sri Lanka*. Marine geology, 1986. **72**(1-2): p. 1-9.
250. Shannon, R.D., *Revised effective ionic radii and systematic studies of interatomic distances in halides and chalcogenides*. Acta crystallographica section A: crystal physics, diffraction, theoretical and general crystallography, 1976. **32**(5): p. 751-767.

251. Gambrell, R., et al., *The effects of pH, redox, and salinity on metal release from a contaminated sediment*. *Water, Air, and Soil Pollution*, 1991. **57**(1): p. 359-367.
252. Závodská, L., et al., *Environmental chemistry of uranium*, in *HV ISSN 1418-7108*. 2008.
253. Tennakone, K., *Thorium minerals in Sri Lanka, history of radioactivity and thorium as a future energy source: a compendium to commemorate the International Year of Chemistry 2011*. *Journal of the National Science Foundation of Sri Lanka*, 2011. **39**(2).
254. René, M., *Nature, sources, resources, and production of thorium*. *Descriptive Inorganic Chemistry Researches of Metal Compounds Vol. 9*. 2017, London: IntechOpen. 201-212.
255. Ebyan, O., et al., *Low-temperature alteration of uranium–thorium bearing minerals and its significance in neof ormation of radioactive minerals in stream sediments of Wadi El-Reddah, North Eastern Desert, Egypt*. *Acta Geochimica*, 2019. **39**(1): p. 96-115.
256. Martínez-Frías, J., R. Lunar, and R. Benito García, *Th- and U-bearing minerals in the SE Mediterranean margin of Spain*. *Episode*, 2004. **27**: p. 33-38.
257. Hector, A.L. and W. Levason, *Periodates of tetravalent titanium, zirconium, hafnium and thorium: Synthesis, characterisation and EXAFS study*. *European Journal of Inorganic Chemistry*, 2005(16): p. 3365-3370.
258. Denecke, M.A., et al., *EXAFS investigation of the interaction of hafnium and thorium with humic acid and Bio-Rex70*. *Journal of Synchrotron Radiation*, 1999. **6**: p. 394-396.
259. Hennig, C., et al. *Identification of hexanuclear Actinide (IV) carboxylates with Thorium, Uranium and Neptunium by EXAFS spectroscopy*. in *Journal of Physics: Conference Series*. 2013. IOP Publishing.
260. Luo, Y., et al., *Crystal chemistry of Th in fluorapatite*. *American Mineralogist*, 2011. **96**(1): p. 23-33.
261. Osthols, E., et al., *Adsorption of thorium on amorphous silica: An EXAFS study*. *Journal of Colloid and Interface Science*, 1997. **194**(1): p. 10-21.
262. Hu, B.W., et al., *New insights into Th(IV) speciation on sepiolite: Evidence for EXAFS and modeling investigation*. *Chemical Engineering Journal*, 2017. **322**: p. 66-72.
263. Dähn, R., et al., *Local structure of Th complexes on montmorillonite clay mineral determined by extended X-ray absorption fine structure (EXAFS) spectroscopy*, in *Biannual Report 1999/2000*. 2001, Project-Group ESRF-Beamline (ROBI-eRG): FZR-322. p. 33.
264. Galanzew, J., *Electronic Structure Studies of Th Systems by high Energy X-Ray Spectroscopy and Computational Methods*, in *Institute for Nuclear Waste Disposal*. 2018, Karlsruher Institut für Technologie.

265. Munoz, M., P. Argoul, and F. Farges, *Continuous Cauchy wavelet transform analyses of EXAFS spectra: A qualitative approach*. *American mineralogist*, 2003. **88**(4): p. 694-700.
266. Benard, P., et al., *Th₄ (PO₄)₄P₂O₇, a new thorium phosphate: synthesis, characterization, and structure determination*. *Chemistry of materials*, 1996. **8**(1): p. 181-188.
267. Komatani, S., et al., *Comparison of SEM-EDS, Micro-XRF and Confocal Micro-XRF for Electric Device Analysis*. *e-Journal of Surface Science and Nanotechnology*, 2013. **11**: p. 133-137.
268. Shannon, R.T. and C.T. Prewitt, *Effective ionic radii in oxides and fluorides*. *Acta Crystallographica Section B: Structural Crystallography and Crystal Chemistry*, 1969. **25**(5): p. 925-946.
269. Seydoux-Guillaume, A.-M., et al., *Low-temperature alteration of monazite: Fluid mediated coupled dissolution–precipitation, irradiation damage, and disturbance of the U–Pb and Th–Pb chronometers*. *Chemical Geology*, 2012. **330**: p. 140-158.
270. Chabaux, F., B. Bourdon, and J. Riotte, *U-series geochemistry in weathering profiles, river waters and lakes*. *Radioactivity in the Environment*, 2008. **13**: p. 49-104.
271. Porcelli, D., *Investigating groundwater processes using U-and Th-series nuclides*. *Radioactivity in the Environment*, 2008. **13**: p. 105-153.
272. Lee, B.-D., et al., *Statistical Analysis and Thermodynamic Equilibrium Modelling for Chemical Composition of Groundwater and Spring Water at Jeju Island, South Korea*. *Water*, 2020. **12**(3): p. 777.
273. Rubasinghe, R., S. Gunatilake, and R. Chandrajith, *Geochemical characteristics of groundwater in different climatic zones of Sri Lanka*. *Environmental earth sciences*, 2015. **74**(4): p. 3067-3076.
274. Babu, M.S., et al., *Concentration of uranium levels in groundwater*. *International Journal of Environmental Science & Technology*, 2008. **5**(2): p. 263-266.
275. Johannesson, K.H., et al., *Geochemistry of the rare-earth elements in hypersaline and dilute acidic natural terrestrial waters: complexation behavior and middle rare-earth element enrichments*. *Chemical Geology*, 1996. **133**(1-4): p. 125-144.
276. Johannesson, K.H., K.J. Stetzenbach, and V.F. Hodge, *Rare earth elements as geochemical tracers of regional groundwater mixing*. *Geochimica et Cosmochimica Acta*, 1997. **61**(17): p. 3605-3618.
277. Smedley, P.L., *The geochemistry of rare earth elements in groundwater from the Carnmenellis area, southwest England*. *Geochimica et Cosmochimica Acta*, 1991. **55**(10): p. 2767-2779.
278. Johannesson, K.H., et al., *Delineation of ground-water flow systems in the Southern Great Basin using aqueous rare earth element distributions*. *Groundwater*, 1997. **35**(5): p. 807-819.

279. Semhi, K., et al., *Mobility of rare earth elements in the system soils–plants–groundwaters: a case study of an arid area (Oman)*. Arabian Journal of Geosciences, 2009. **2**(2): p. 143-150.
280. Felmy, A.R., V.L. Legore, and S.A. Hartley, *Solubility and Leaching of Radionuclides in Site Decommissioning Management Plan (SDMP) Soil and Pondered Wastes*. 2003: US Nuclear Regulatory Commission.
281. Organization, W.H., *Guidelines for drinking-water quality*. 1996, Geneva: World Health Organization.
282. EPA, U., *Drinking water standards and health advisories table*. 2009.
283. Standards, S.L., *Specification for potable water*, in *SLS 614: 2013*. 2013, Sri Lanka Standards Institution: Colombo.
284. De Boer, J., et al., *Levels of rare earth elements in Dutch drinking water and its sources. Determination by inductively coupled plasma mass spectrometry and toxicological implications. A pilot study*. Water Research, 1996. **30**(1): p. 190-198.
285. Fanghänel, T. and V. Neck, *Aquatic chemistry and solubility phenomena of actinide oxides/hydroxides*. Pure and Applied Chemistry, 2002. **74**(10): p. 1895-1907.
286. Stumm, W. and B. Sulzberger, *The cycling of iron in natural environments: considerations based on laboratory studies of heterogeneous redox processes*. Geochimica et Cosmochimica Acta, 1992. **56**(8): p. 3233-3257.
287. OECD, *Chemical Thermodynamics of Thorium*. 2008: Nuclear Energy Agency.
288. Rai, D., et al., *Thermodynamic Approach for Predicting Actinide and Rare Earth Concentrations in Leachates from Radioactive Waste Glasses*. Journal of Solution Chemistry, 2011. **40**(8): p. 1473.
289. Salminen, R., W. De Vos, and T. Tarvainen, *Geochemical atlas of Europe*. 2006: Geological survey of Finland.
290. Pérez-Moreno, S., et al., *Validation of the BCR sequential extraction procedure for natural radionuclides*. Chemosphere, 2018. **198**: p. 397-408.
291. Wang, X., S. Ni, and Z. Shi, *Uranium distribution in the sediment of the Mianyuan River near a phosphate mining region in China and the related uranium speciation in water*. Geochemistry, 2014. **74**(4): p. 661-669.
292. Altmaier, M., et al., *Solubility of U (VI) in chloride solutions. I. The stable oxides/hydroxides in NaCl systems, solubility products, hydrolysis constants and SIT coefficients*. The Journal of Chemical Thermodynamics, 2017. **114**: p. 2-13.
293. Xinde, C., W. Xiaorong, and Z. Guiwen, *Assessment of the bioavailability of rare earth elements in soils by chemical fractionation and multiple regression analysis*. Chemosphere, 2000. **40**(1): p. 23-28.

294. Usmanova, N., et al., *Comparative Analysis of Sequential Leaching Procedures for Dissociation of Rare Earth Elements in Gold-Bearing Material*. Journal of Mining Science, 2017. **53**(6): p. 1124-1132.
295. Aubert, D., A. Probst, and P. Stille, *Distribution and origin of major and trace elements (particularly REE, U and Th) into labile and residual phases in an acid soil profile (Vosges Mountains, France)*. Applied Geochemistry, 2004. **19**(6): p. 899-916.
296. Land, M., et al., *Solid speciation and fractionation of rare earth elements in a spodosol profile from northern Sweden as revealed by sequential extraction*. Chemical Geology, 1999. **160**(1-2): p. 121-138.
297. Moniruzzaman, M., T. Kobayashi, and T. Sasaki, *Solubility and solid phase of trivalent lanthanide hydroxides and oxides*. Journal of Nuclear and Radiochemical Sciences, 2020. **20**: p. 32-42.
298. Kawase, M., T. Suzuki, and K. Miura, *Growth mechanism of lanthanum phosphate particles by continuous precipitation*. Chemical engineering science, 2007. **62**(18-20): p. 4875-4879.
299. Kosmulski, M., *Compilation of PZC and IEP of sparingly soluble metal oxides and hydroxides from literature*. Advances in colloid and interface science, 2009. **152**(1-2): p. 14-25.
300. Chen, Y., et al., *Phosphate solubilizing bacteria from subtropical soil and their tricalcium phosphate solubilizing abilities*. Applied soil ecology, 2006. **34**(1): p. 33-41.
301. Zänker, H. and C. Hennig, *Colloid-borne forms of tetravalent actinides: a brief review*. Journal of contaminant hydrology, 2014. **157**: p. 87-105.
302. Geckeis, H., T. Rabung, and T. Schäfer, *Actinide-nanoparticle interaction: Generation, stability and mobility*, in *Actinide Nanoparticle Research*. 2011, Springer: Berlin. p. 1-30.
303. Miekeley, N., et al., *Rare-earth elements in groundwaters from the Osamu Utsumi mine and Morro do Ferro analogue study sites, Poços de Caldas, Brazil*. Journal of Geochemical Exploration, 1992. **45**(1-3): p. 365-387.
304. Short, S., *Chemical transport of uranium and thorium in the Alligator Rivers Uranium Province, Northern Territory, Australia*. 1988, University of Wollongong: New South Wales, Australia.
305. Guo, Z., H. Su, and W. Wu, *Sorption and desorption of uranium (VI) on silica: experimental and modeling studies*. Radiochimica Acta, 2009. **97**(3): p. 133-140.
306. Marmier, N., A. Delisée, and F. Fromage, *Surface complexation modeling of Yb (III) and Cs (I) sorption on silica*. Journal of colloid and interface science, 1999. **212**(2): p. 228-233.
307. Kosmulski, M., *Adsorption of trivalent cations on silica*. Journal of colloid and interface science, 1997. **195**(2): p. 395-403.

APPENDICES

Appendix 2.1: Experimental section

Table A2.1: List of chemicals used in this study

Name	Chemical formula	Molar weight (g mol ⁻¹)	Provider
Acetic acid	CH ₃ COOH	60.05	Merck (EMSURE®)
Ammonium ferrous sulfate	(NH ₄) ₂ Fe(SO ₄) ₂ ·6H ₂ O	392.13	VWR Chemicals (≥99.0%)
Ammonium oxalate	(NH ₄) ₂ C ₂ O ₄ ·H ₂ O	142.11	Merck (EMSURE®)
Calcium chloride -dihydrate	CaCl ₂ ·2H ₂ O	147.02	Merck (p.a.)
Citric acid	C ₆ H ₈ O ₇	192.13	VWR Chemicals
Diphenylamine indicator	(C ₆ H ₅) ₂ NH	169.23	Merck
Humic acid (crystalline powder)	-	-	Alfa Aeser
Humic acid (sodium salt)			Sigma Aldrich
Hydrochloric acid	HCl	36.46	Merck Titrisol®
Iso-propanol	CH ₃ CH(OH)CH ₃	60.10	Merck (EMSURE®)
Magnesium chloride hexahydrate	MgCl ₂ ·6H ₂ O	203.30	Merck (EMSURE®)
Nitric acid (69%)	HNO ₃	63.01	Carl Roth (ROTIPURAN®Ultra)
ortho-Phosphoric acid	H ₃ PO ₄	98.00	Merck (EMSURE®)
Oxalic acid	C ₂ H ₂ O ₄ ·2H ₂ O	126.07	VWR Chemicals (100.4%)
Perchloric acid	HClO ₄	100.46	Merck (EMSURE®)
Potassium chloride	KCl	74.55	Merck (EMSURE®)
Potassium dichromate	K ₂ Cr ₂ O ₇	294.19	ACROS Organics™
Potassium nitrate	KNO ₃	101.10	Merck (EMSURE®)
Sodium acetate	C ₂ H ₃ NaO ₂	82.03	Honeywell (≥99.0%)
Sulfuric acid	H ₂ SO ₄	98.07	Merck EMSURE® (95-97%)
Sodium chloride	NaCl	58.44	Merck (p.a.)
Sodium citrate	C ₆ H ₅ Na ₃ O ₇ ·2H ₂ O	294.10	VWR Chemicals (99.8%)
Sodium dihydrogenphosphate	NaH ₂ PO ₄ ·2H ₂ O	156.02	Merck (EMSURE®)
Sodium dithionite	Na ₂ S ₂ O ₄	174.11	Merck (≥85%)
Sodium hydroxide	NaOH	40.00	Honeywell Fluka
Silica nanoparticles	SiO ₂	60.08	Evonik (AEROSIL®200)
Sodium nitrate	NaNO ₃	84.99	Merck (EMSURE®)
Sodium perchlorate monohydrate	NaClO ₄ ·H ₂ O	140.46	Merck (EMSURE®)
Sodium pyrophosphate	Na ₄ P ₂ O ₇ ·10H ₂ O	446.06	Alfa Aeser (99.0-103.0%)
Sodium sulfate	Na ₂ SO ₄	142.04	Merck (EMSURE®)

Table A2.2: Radionuclides with the energy of gamma ray

Parent radionuclide	Daughters	Energy (keV)	Abundance P_{γ}^* (%)
Th-232	Pb-212	238.63	43.20
	Ac-228	338.32	11.27
		911.23	25.80
		968.97	15.80
	Tl-208	583.19	30.37
Ra-226	Ra-226	186.10	3.50
	Pb-214	295.22	19.30
		351.93	37.60
	Bi-214	609.31	46.10
		1120.29	15.10
1764.49		15.10	
K-40	K-40	1460.81	10.67

* P_{γ} is the absolute transition probability

Table A2.3: Results from analytical quality of the ED-XRF measurements for all the analyzed elements, checked with certified reference materials of rock samples (units are in mg kg⁻¹)

	La	Ce	Th	Nd
Sy-3-M	1340±11	2267±21	1019±8	649±3
Sy-3-S	1317±20	2251±20	904±10	796±10
Accuracy (%)	100±1	102±1	102±1	97±0
Sy-2-M	70±1	174±6	402±7	76±4
Sy-2-S	77±5	161±10	386±10	77±5
Accuracy (%)	94±2	99±3	106±2	104±6
BE-N-M	92±1	180±4	17±1	74±6
BE-N-S	82±5	153±10	11±5	66±5
Accuracy (%)	113±2	118±3	163±7	111±9

*M – measured value, S – standard value

Table A2.4: Averaged results from analytical quality of the ICP-MS measurements for the analyzed trace elements, checked with certified reference materials of SPS-SW1 and detection limits (units are in ng L⁻¹)

	La	Ce	Th	Nd
SPS-SW1-M	503±6	496±18	519±19	504±16
SPS-SW1-S	500±10	500±10	500±10	500±10
Accuracy (%)	101±1	99±4	104±4	101±3
Detection limit	0.04 – 0.14	0.06 – 0.14	0.04 – 0.10	0.07 – 0.13

*M – measured value, S – standard value

Appendix 2.2: Calculations for solid phase total organic carbon (TOC)

$$M = \frac{10}{V_{blank}} \quad (\text{Eq. A. 1})$$

$$\text{Oxidizable Organic Carbon (\%)} = \frac{[V_{blank} - V_{sample}] \times 0.3 \times M}{W_t} \quad (\text{Eq. A. 2})$$

$$\text{TOC (\%)} = 1.334 \times \text{oxidizable Organic Carbon (\%)} \quad (\text{Eq. A. 3})$$

Where: M – Molarity of $(\text{NH}_4)_2\text{SO}_4 \cdot \text{FeSO}_4 \cdot 6\text{H}_2\text{O}$ solution (about 0.5 M)

V_{blank} – volume of $(\text{NH}_4)_2\text{SO}_4 \cdot \text{FeSO}_4 \cdot 6\text{H}_2\text{O}$ solution required to titrate the blank (mL)

V_{sample} – volume of $(\text{NH}_4)_2\text{SO}_4 \cdot \text{FeSO}_4 \cdot 6\text{H}_2\text{O}$ solution required to titrate the sample (mL)

W_t – weight of air-dry soil (g)

0.3 – $3 \times 10^{-3} \times 100$, where 3 is the equivalent weight of carbon.

The estimated OC in the soil using this Walkley-Black method gives about 89% recovery of carbon as compared to the dry combustion method. Therefore, the conversion factor 0.336 was obtained by dividing 0.003 (the milli-equivalent weight of carbon) by 89% and multiplied by 100 to convert it into percentage. The interference from chloride (Cl^-) can be eliminated by adding silver sulfate (Ag_2SO_4) to the oxidizing reagent whereas the presence of nitrates (NO_3^-) and carbonates (CO_3^{2-}) up to 5% and 50% respectively, does not interfere.

Appendix 2.3: Specific Surface Area (SSA)

There are several methods to measure the specific surface area of a material. The routine method for fine-grained materials is the gas adsorption method using non-polar gas like N_2 , Ar, Kr, or CO_2 . Among these, N_2 -gas adsorption (BET: Brunauer–Emmett–Teller) method is by far the most common and was used in this study. A Quantachrome Autosorb Automated Gas Sorption System with $\text{N}_2(\text{g})$ adsorbate instrument was used to obtain the SSA for ~1 g of each soil sample.

Appendix 2.4: Attenuated Total Reflection-Fourier Transform Infrared (ATR-FTIR) spectroscopy

The main IR-active groups in the soil matrices were identified by recording ATR-FTIR spectra using a Bruker IFS 55 spectrometer. The soil samples were mildly ground to

obtain a homogenous distribution without destroying the mineral phases. Those samples were mounted on the ATR sample stage and spectra were collected at 4 cm^{-1} resolution in the $400\text{-}4000\text{ cm}^{-1}$ spectral range. OPUS 7.5 software was used for data treatment.

Appendix 2.5: X-ray Photoelectron Spectroscopy (XPS)

Further investigations of the main soil components were performed using XPS. Measurements were performed using a PHI 5000 VersaProbeII (ULVAC-PHI Inc.) system, where the photoelectrons were generated by a scanning microprobe X-ray source (monochromatic Al-K α (1486.7 eV) X-rays) as the excitation source, collected at 45° with respect to the surface normal, and detected with a hemispherical analyzer. Data analysis was performed using the ULVAC-PHI MultiPak program, version 9.8.

Appendix 2.6: NPOC and anions measurements in batch experiment with SRW-A1

Another batch experiment was done for $\sim 2.5\text{ g}$ of L 04 and L 05 soil samples using 50 mL of SRW A1 per each sample, to measure the NPOC. After 7 days of rotation, the samples were centrifuged at 3500 rpm for 10 minutes and 500 μL pipetted out from the decanted samples and diluted to 5 mL using 2% HNO_3 for ICP-MS analysis. In addition, 10 mL of samples were prepared for NPOC measurements and 1.5 mL samples were prepared for IC analysis.

Appendix 2.7: pH dependent extractions

Since the extraction steps involve a range of pH values, it is not clear whether pH plays a role for the obtained results. Therefore, only L-04 soil sample was used for this additional batch extraction experiment to check the influence of pH on the extracted amounts of Th, U, and REEs. A solution of 1 mmol L^{-1} NaClO_4 was prepared and the pH values were adjusted in 50 mL aliquot solutions separately using HClO_4 acid (pH 2 – 5.5) and NaOH (pH 6 – 10) to obtain the desired pH values. The selected pH values were pH 2, 2.5, 3, 3.5, 4, 4.5, 5, 5.5, 6, 7, 8, 9, and 10. A mass of approximately 2 g of the L-04 soil was added to a volume of 20 mL of each pH solution. Aliquots of 100 μL were taken out after 2 hrs, 5 hrs, 7 hrs and 7 days and analyzed by ICP-MS after dilution to 5 mL with 2% HNO_3 . The final pH values after each time period of the extractions were also measured.

Appendix 2.8: Column experiment run with an empty column

Additionally, an empty column (XK 26, GE Healthcare, Sweden) was used to check potential dissolution of silica from the inner surface of the borosilicate glass columns. A solution of 1 mmol L⁻¹ NaCl was passed through the column from bottom to top with the same flowrate of 0.05 mL min⁻¹ and 5 mL fractions were collected in the fraction collector. All the samples were acidified with 50 µL of 69% HNO₃ and analyzed in ICP-MS and ICP-OES.

Appendix 2.9: Tube injection of silica suspension and use of NaCl as infiltration leachant

The same L-04 soil column, which had been previously used with the SRW A1, was utilized for this experiment as well to gain some experience with this kind of experiments before carrying out the experiments with L-05 soil. About 20 mL of silica suspension of 0.1 g L⁻¹ AEROSIL 200 silica in 0.1 mmol L⁻¹ NaCl at pH 5 and 2 L of 1 mmol L⁻¹ NaCl solution at pH 5 were prepared as the infiltration leachants. A separate rubber tube with a volume of ~20 mL was fixed to the ÄKTA pure system. Initially, 75 mL of 1 mmol L⁻¹ NaCl solution was passed through the column at a flowrate of 0.05 mL min⁻¹. A volume of about 20 mL of the silica suspension in a separate syringe fixed to the instrument was injected into the rubber tube. A volume of 15 mL was then automatically passed into the system. After this injection, 1 mmol L⁻¹ NaCl solution was continuously passed through the column for a few days at the same flowrate. Each 15th tube in the fraction collector was kept without adding acid to allow for separate pH measurements. The rest of the collected 5 mL samples that already contained 50 µL of 69% HNO₃ in the fraction collector were analyzed in both ICP-MS and ICP-OES.

Appendix 2.10: Tube injection of HA with NaCl solution

The L-04 soil column, which had already been leached out with SRW A1 and subsequently with silica suspension and 1 mmol L⁻¹ NaCl solution, was used for this preliminary experiment. About 20 mL of 100 mg L⁻¹ HA solution in 0.1 mmol L⁻¹ NaCl at pH 5 and 2 L of 0.5 mmol L⁻¹ NaCl solution at pH 5 were prepared as leachant solutions. A separate rubber tube, similar to the tube used with silica suspension, with a volume of ~20 mL was fixed to the system. Initially, a volume 15 mL of 0.5 mmol L⁻¹ NaCl solution was passed through the column at a flowrate of 0.05 mL min⁻¹. In the meantime, a volume of 15 mL of the prepared HA solution in a separate syringe was

fixed to the instrument and injected into the rubber tube. The loading solution was then automatically passed into the system. After that 15 mL injection, 0.5 mmol L⁻¹ NaCl solution was continuously passed through the column for a few days at the same flowrate. The fraction volume per each tube was fixed to 15 mL and no HNO₃ was added to avoid precipitation of HA. The 15 mL samples were split into 5 mL fractions and then analyzed by ICP-MS after digestion with HF and ICP-OES and into 7 mL for NPOC.

Two different salt concentrations were used in Appendices 4 and 5 to check if differences in the conductivity could be used to identify any breakthrough points along with the change of conductivity. After this experiment, the whole set up was washed by flushing the system with Milli-Q, HCl, and NaOH before running the next column experiments.

Appendix 3.1: Activity concentration of Th-232 from Gamma spectrometry in Germany

Table A3.1: Activity concentration of Th-232 from gamma spectrometry carried out for the soil samples in Germany

Sample	Th-232
	DE - Gamma (Bq kg ⁻¹)
L-03	3207.2 ± 28.1
L-04	6091.4 ± 75.9
L-05	7278.4 ± 94.5
L-06	5899.8 ± 176.7

Appendix 3.2: Elemental concentrations of major and trace elements in soil samples by ICP-OES

Table A3.2: Amounts of main components and trace elements present in the samples measured by ICP-OES

	Si g kg ⁻¹	Al g kg ⁻¹	Fe g kg ⁻¹	Ce g kg ⁻¹	La g kg ⁻¹	Nd g kg ⁻¹	Th g kg ⁻¹	Ti g kg ⁻¹
L-03	191.0 ± 2.5	122.0 ± 0.6	94.5 ± 1.4	0.92 ± 0.01	0.93 ± 0.00	0.55±0.00	0.59±0.01	3.0 ± 0.0
L-04	179.1 ± 3.0	150.5 ± 1.1	113.6 ± 3.3	1.30 ± 0.10	0.91 ± 0.09	0.53±0.05	1.03±0.02	4.3 ± 0.0
L-05	210.1 ± 7.7	127.2 ± 3.0	63.6 ± 0.6	1.51 ± 0.13	0.93 ± 0.02	0.50±0.01	1.99±0.03	4.1 ± 0.1
L-06	182.8 ± 18.2	125.1 ± 7.3	51.9 ± 4.7	1.34 ± 0.09	0.88 ± 0.04	0.49±0.02	2.41±0.21	3.7 ± 0.2

Appendix 3.3: Specific Surface Area (SSA)

Table A3.3: Specific surface area of the soil samples

Sample	BET Surface area (m ² g ⁻¹)
L-03	28.1 ± 1.3
L-04	30.5 ± 1.5
L-05	22.7 ± 0.3
L-06	21.6 ± 0.3

Appendix 3.4: Attenuated Total Reflection-Fourier Transform Infrared (ATR-FTIR) spectroscopy

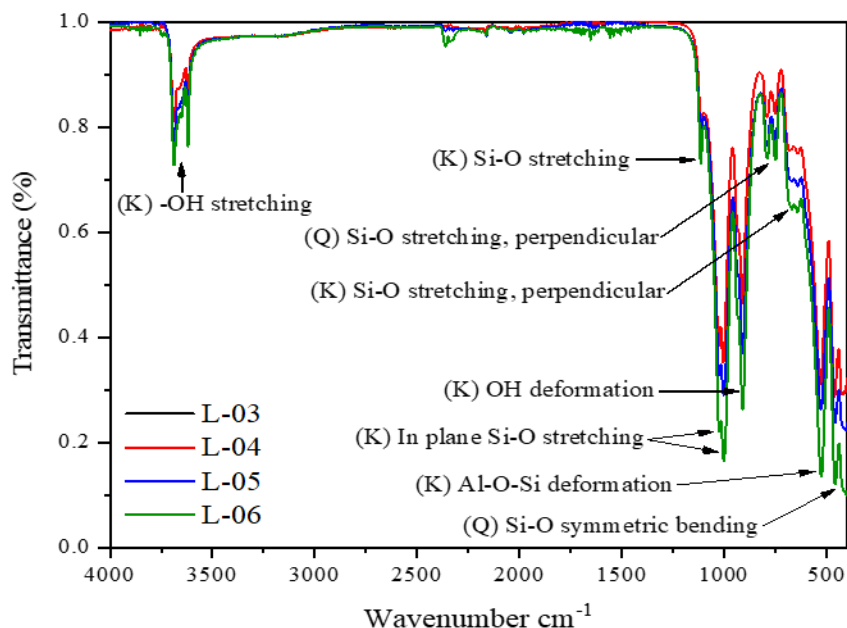


Figure A3.1: ATR-FTIR spectra of the four soil samples studied, major components kaolinite (K) and quartz (Q) are indicated by arrows

Appendix 3.5: X-ray Photoelectron Spectroscopy (XPS)

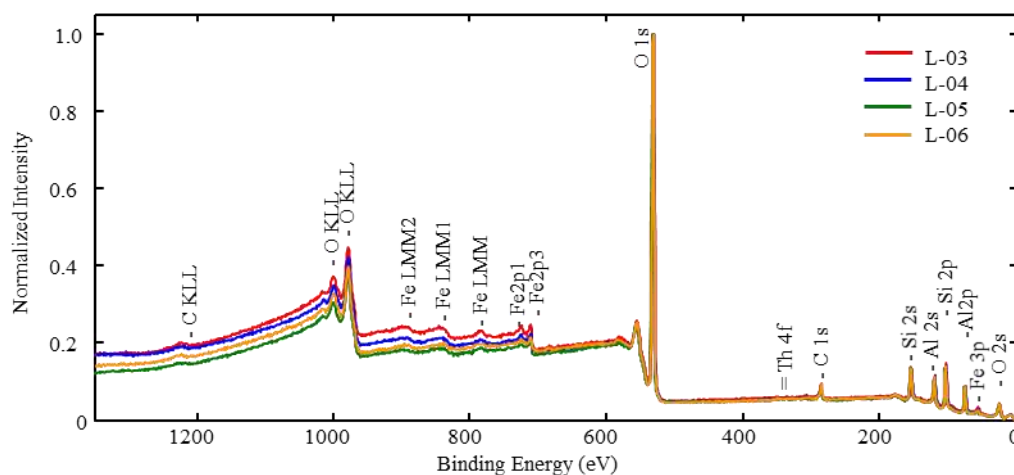


Figure A3.2: XPS spectrum of the soil samples. The positions of the Th 4f main lines are also indicated

Table A3.4: Element content as atomic weight (wt%) as determined by XPS, relative error \pm (10-20) %

Sample	C	O	Al	Si	Fe
L-03	7.2	67.0	10.0	13.1	2.7
L-04	6.4	67.5	10.7	13.4	2.0
L-05	6.4	67.6	10.4	14.1	1.5
L-06	7.1	67.2	10.3	14.0	1.4

Appendix 3.6: Elemental distribution in size fractions

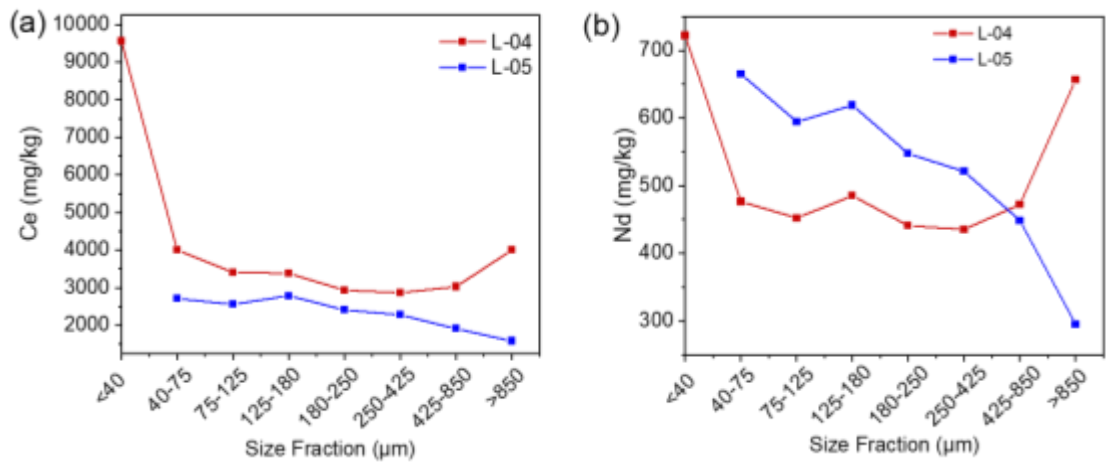


Figure A3.3: Concentration of (a) Ce and (b) Nd in each size fraction of L-04 and L-05 soil samples measured by XRF

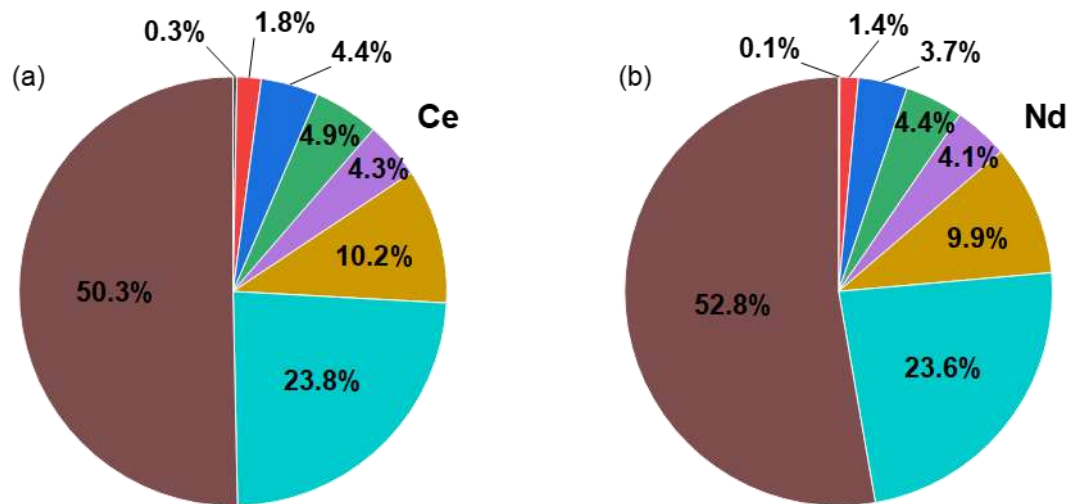


Figure A3.4: Elemental distribution of (a) Ce and (b) Nd in each size fraction of L-04 by XRF

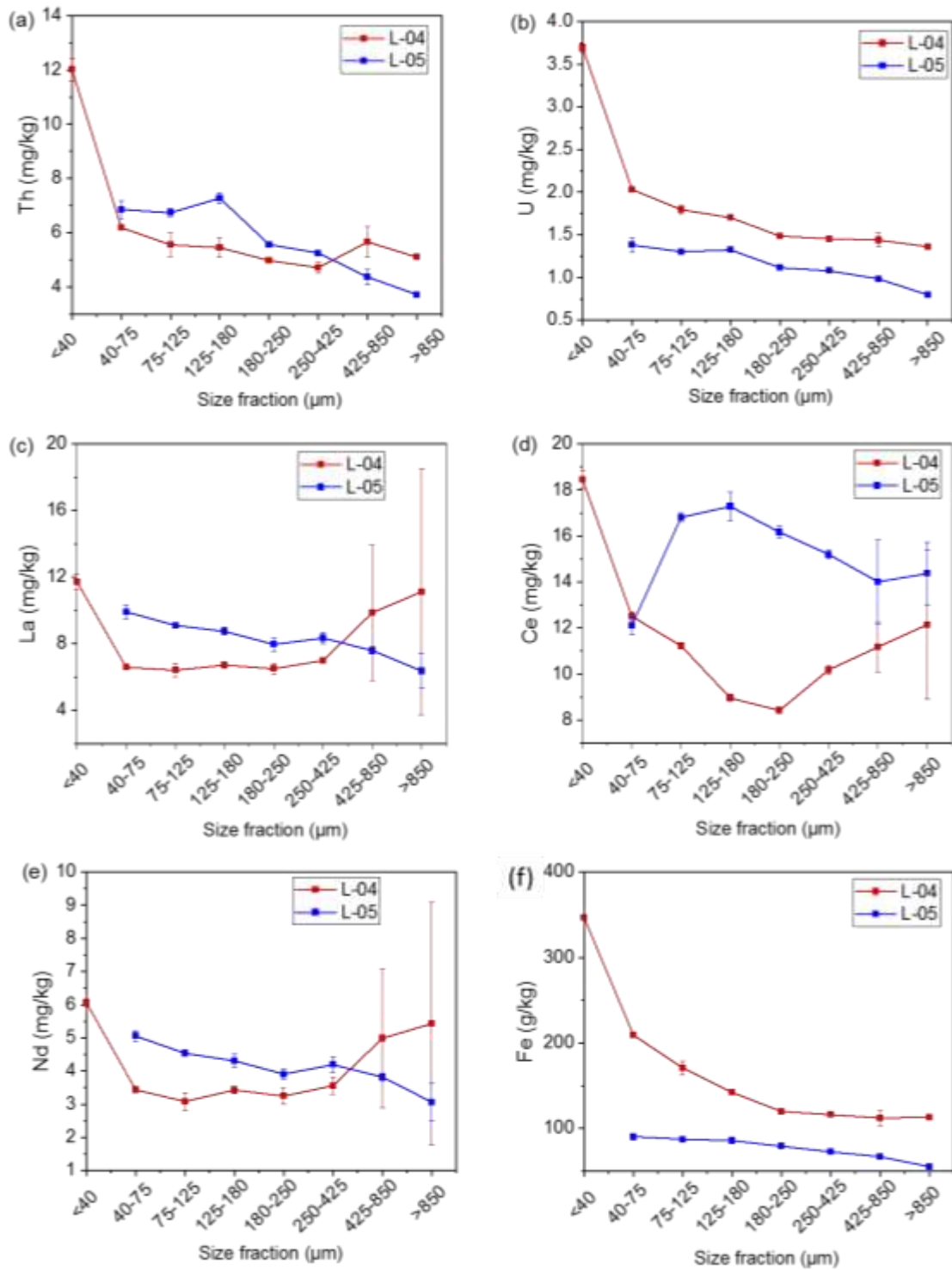


Figure A3.5: Concentration of (a) Th, (b) U, (c) La, (d) Ce, (e) Nd and (f) Fe in each size fraction of L-04 and L-05 soil samples measured by ICP-OES

Appendix 3.7: Correlation diagrams for μ -XRF maps

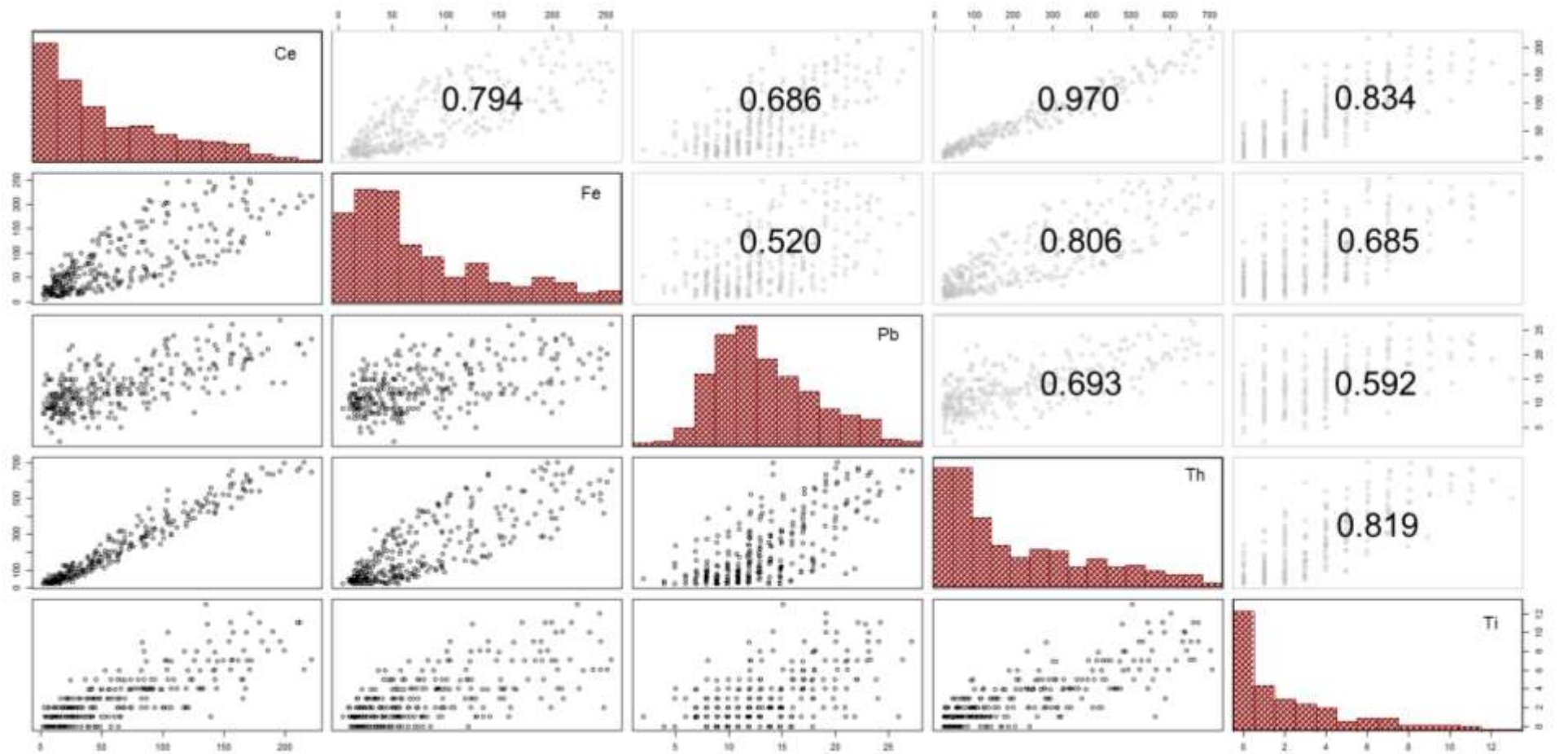


Figure A3.6: X-ray fluorescence scatter plots, histograms and Spearman correlation coefficients between fluorescence counts of Ce, Fe, Pb, Th, and Ti for the Th-oxide particle

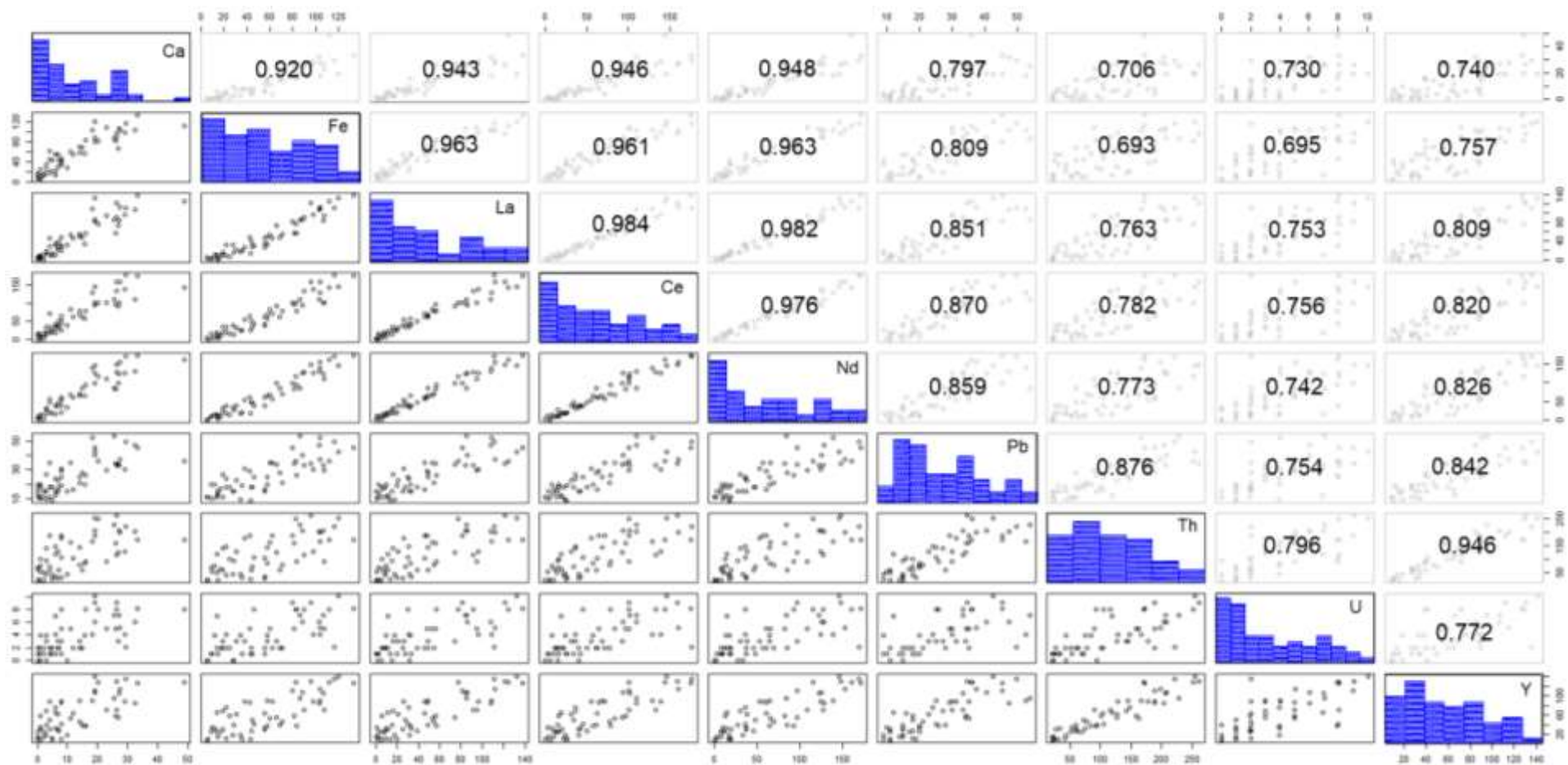


Figure A3.7: X-ray fluorescence scatter plots, histograms and Spearman correlation coefficients between fluorescence counts of Ca, Fe, La, Nd, Pb, Th, U, and Y for the Th-phosphate particle

Appendix 3.8: Groundwater data for some selected major elements and trace elements

Table A3.5: Concentrations of major elements and trace elements, Ce and Nd, in groundwater samples with the drinking water limit standards of WHO (W), EPA (E) and SLS (S)

Sampling campaign – S1							W	E	S
	WL-01	WL-02	WL-03	WL-04	WL-05	WL-06			
Fe ($\mu\text{g L}^{-1}$)							--		300
0.45 μm	4.4 \pm 2.0	9.5 \pm 0.3	7.6 \pm 0.1	2.4 \pm 0.2	4.0 \pm 0.0	7.5 \pm 0.0			
0.20 μm	4.1 \pm 0.4	10.4 \pm 2.2	6.9 \pm 0.2	2.1 \pm 0.1	3.9 \pm 0.5	2.9 \pm 0.3			
Na (mg L⁻¹)							--	--	200
0.45 μm	8.5 \pm 0.3	6.8 \pm 0.1	7.3 \pm 0.0	9.2 \pm 0.0	10.6 \pm 0.1	8.4 \pm 0.0			
0.20 μm	8.1 \pm 0.0	7.1 \pm 0.0	7.3 \pm 0.1	9.2 \pm 0.0	10.6 \pm 0.1	8.5 \pm 0.1			
Mg (mg L⁻¹)							--	--	30
0.45 μm	8.6 \pm 0.3	27.0 \pm 0.4	25.7 \pm 0.0	8.4 \pm 0.0	20.3 \pm 0.1	3.9 \pm 0.1			
0.20 μm	8.2 \pm 0.0	28.1 \pm 0.4	25.6 \pm 0.1	8.4 \pm 0.0	20.4 \pm 0.2	3.9 \pm 0.0			
Al ($\mu\text{g L}^{-1}$)							--		200
0.45 μm	0.9 \pm 0.5	0.4 \pm 0.2	0.1 \pm 0.0	0.7 \pm 0.4	1.4 \pm 0.2	2.2 \pm 0.5			
0.20 μm	0.8 \pm 0.1	0.7 \pm 0.2	0.2 \pm 0.0	0.6 \pm 0.3	1.6 \pm 0.1	1.3 \pm 0.2			
K (mg L⁻¹)							--	--	--
0.45 μm	2.1 \pm 0.1	2.5 \pm 0.0	2.3 \pm 0.0	2.2 \pm 0.0	3.4 \pm 0.0	1.4 \pm 0.0			
0.20 μm	2.0 \pm 0.0	2.6 \pm 0.0	2.3 \pm 0.0	2.2 \pm 0.0	3.5 \pm 0.0	1.4 \pm 0.0			
Ca (mg L⁻¹)							--	--	100
0.45 μm	22.4 \pm 0.6	66.6 \pm 2.0	61.0 \pm 0.3	21.1 \pm 0.1	52.4 \pm 0.3	9.3 \pm 0.3			
0.20 μm	21.6 \pm 0.3	68.9 \pm 0.8	60.7 \pm 0.1	21.1 \pm 0.1	52.0 \pm 0.4	9.4 \pm 0.1			

Mn ($\mu\text{g L}^{-1}$)							400	50	100
0.45 μm	12.9 \pm 0.5	0.1 \pm 0.0	6.6 \pm 0.2	3.8 \pm 0.1	0.3 \pm 0.0	3.8 \pm 0.1			
0.20 μm	12.4 \pm 0.0	0.2 \pm 0.0	7.0 \pm 0.0	3.8 \pm 0.0	0.2 \pm 0.0	3.9 \pm 0.0			
Ce ($\mu\text{g L}^{-1}$)							--	-	--
0.45 μm	0.2 \pm 0.0	--	--	0.3 \pm 0.0	--	0.2 \pm 0.0			
0.20 μm	0.2 \pm 0.0	--	--	0.2 \pm 0.0	--	--			
Nd ($\mu\text{g L}^{-1}$)							--	-	--
0.45 μm	1.2 \pm 0.2	0.4 \pm 0.0	0.5 \pm 0.0	1.1 \pm 0.2	2.1 \pm 0.0	1.9 \pm 0.1			
0.20 μm	1.2 \pm 0.1	0.5 \pm 0.0	0.5 \pm 0.0	0.9 \pm 0.1	2.1 \pm 0.0	0.4 \pm 0.0			
Sampling campaign – S2									
	WL-01	WL-02	WL-03	WL-04	WL-05	WL-06			
Targeted elements									
Fe ($\mu\text{g L}^{-1}$)							--	--	--
0.45 μm	14.3 \pm 0.3	15.1 \pm 0.2	5.1 \pm 0.2	18.6 \pm 0.1	16.1 \pm 0.6	21.7 \pm 0.3			
0.20 μm	19.6 \pm 0.5	24.2 \pm 0.7	21.7 \pm 0.6	16.3 \pm 0.4	17.9 \pm 0.1	20.7 \pm 0.1			
Na (mg L⁻¹)							--	--	--
0.45 μm	11.4 \pm 0.2	9.1 \pm 0.1	8.1 \pm 0.1	11.7 \pm 0.2	14.1 \pm 0.2	11.6 \pm 0.2			
0.20 μm	12.4 \pm 0.8	10.1 \pm 0.6	8.6 \pm 0.2	12.3 \pm 0.4	14.3 \pm 0.4	12.1 \pm 0.4			
Mg (mg L⁻¹)							--	--	--
0.45 μm	10.7 \pm 0.2	34.5 \pm 0.4	25.1 \pm 0.2	10.2 \pm 0.2	24.2 \pm 0.3	6.0 \pm 0.1			
0.20 μm	11.5 \pm 0.7	35.8 \pm 0.4	26.7 \pm 0.8	10.6 \pm 0.3	25.0 \pm 0.6	6.3 \pm 0.2			
Al ($\mu\text{g L}^{-1}$)							--	--	--

0.45 μm	10.5 \pm 0.2	7.5 \pm 0.2	6.0 \pm 0.2	12.6 \pm 0.1	11.9 \pm 0.6	11.0 \pm 0.1			
0.20 μm	14.8 \pm 0.9	24.9 \pm 0.2	17.8 \pm 0.5	13.3 \pm 0.6	12.6 \pm 0.4	9.9 \pm 0.3			
K (mg L⁻¹)							--	--	--
0.45 μm	3.0 \pm 0.0	3.5 \pm 0.0	0.9 \pm 0.0	2.9 \pm 0.0	4.4 \pm 0.0	2.2 \pm 0.0			
0.20 μm	3.1 \pm 0.1	3.9 \pm 0.1	1.2 \pm 0.0	3.0 \pm 0.0	4.3 \pm 0.0	2.2 \pm 0.0			
Ca (mg L⁻¹)							--	--	--
0.45 μm	23.4 \pm 0.2	73.9 \pm 0.2	47.9 \pm 0.1	21.5 \pm 0.7	53.4 \pm 0.3	10.8 \pm 0.1			
0.20 μm	24.3 \pm 0.5	76.6 \pm 2.1	50.2 \pm 0.4	22.2 \pm 0.4	54.2 \pm 0.5	11.0 \pm 0.2			
Mn ($\mu\text{g L}^{-1}$)							--	--	--
0.45 μm	24.7 \pm 0.1	1.0 \pm 0.0	9.0 \pm 0.0	7.2 \pm 0.1	1.5 \pm 0.0	3.7 \pm 0.0			
0.20 μm	25.5 \pm 0.4	10.9 \pm 0.1	8.6 \pm 0.2	7.0 \pm 0.1	1.5 \pm 0.0	3.4 \pm 0.0			
Ce ($\mu\text{g L}^{-1}$)							--	--	--
0.45 μm	0.15 \pm 0.00	0.05 \pm 0.00	0.07 \pm 0.00	0.12 \pm 0.00	0.08 \pm 0.00	0.07 \pm 0.00			
0.20 μm	0.26 \pm 0.00	0.17 \pm 0.00	0.16 \pm 0.00	0.12 \pm 0.00	0.09 \pm 0.00	0.06 \pm 0.00			
Nd ($\mu\text{g L}^{-1}$)							--	--	--
0.45 μm	0.20 \pm 0.00	0.02 \pm 0.00	0.30 \pm 0.00	0.10 \pm 0.00	0.12 \pm 0.00	0.13 \pm 0.00			
0.20 μm	0.27 \pm 0.01	0.08 \pm 0.00	0.34 \pm 0.00	0.11 \pm 0.00	0.12 \pm 0.00	0.14 \pm 0.01			

Appendix 4.1: Chemical batch extractions

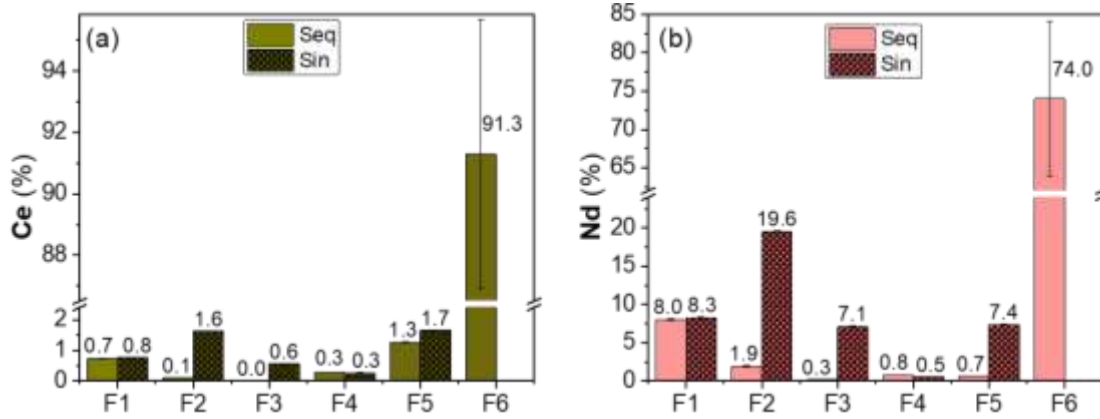


Figure A4.1: Percentage distribution of (a) Ce and (b) Nd in each chemically extracted fractions of soil sample L-05 in sequential (Seq) and single (Sin) extractions

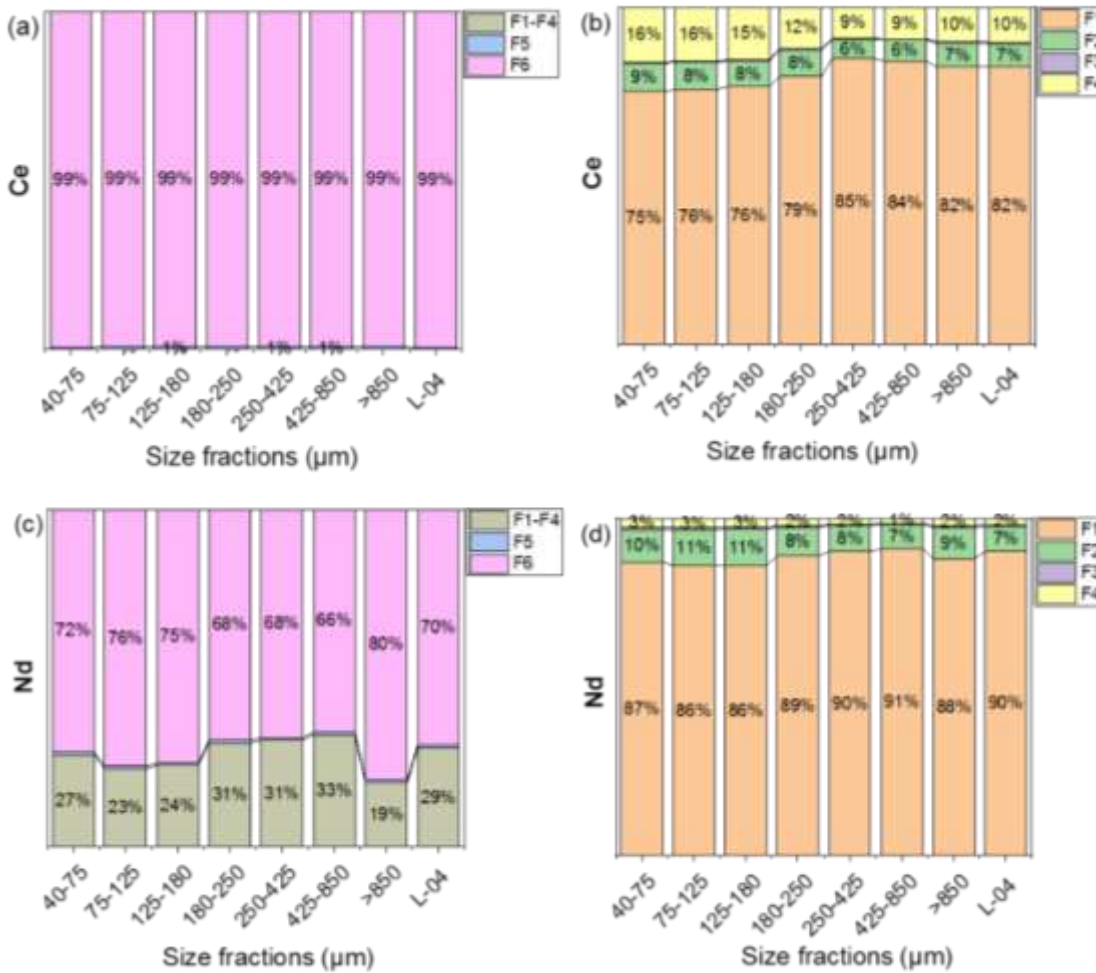


Figure A4.2: Relative percentage values of Ce (a,b) and Nd (c,d) extracted sequentially from each size fraction of sieved L-04, showing both overall F1-F6 (a,c) and expanded F1-F4 (b,d). A comparison with unsieved L-04 soil sample is included

Table A4.1: Extracted percentages of Th, U and La in both sequential (Seq) and single (Sin) approaches for all the soil sample

%	Th		U		La		Ce		Nd	
	Seq	Sin	Seq	Sin	Seq	Sin	Seq	Sin	Seq	Sin
Overall	82-114		65-146		82-105		72-98		81-100	
recovery										
Easily	0.5-	0.6-	6-15	7-18	8-	24-40	0.3-1.3	0.6-2.6	10-24	27-48
mobile	1.2	2.2			20					
(F1+F2)										
Maximum	4-6	3-8	12-29	12-	9-	0.7-	0.6-1.7	0.1-0.3	11-25	0.5-0.7
chemically				33	21	1.0				
mobilized										
(F1+F2+F3										
+F4)										

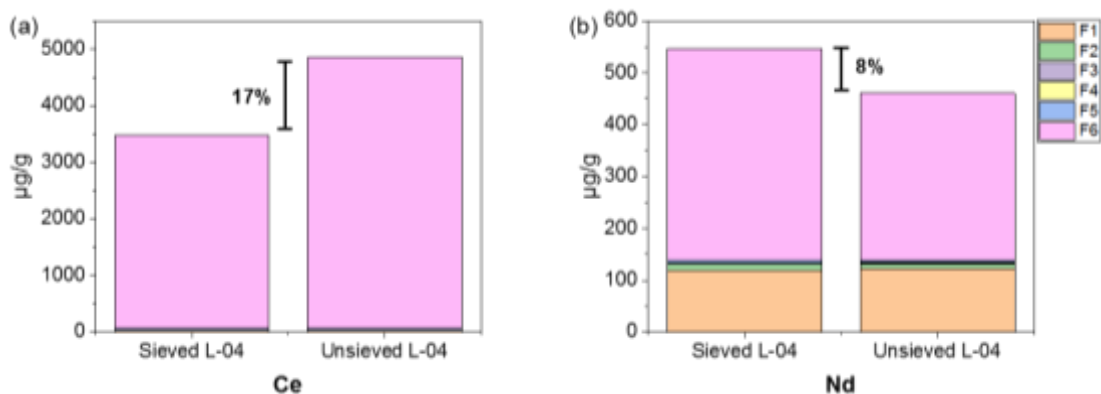


Figure A4.3: Mass balance for (a) Ce and (b) Nd obtained in extractions per sieved soil fraction to the total of unsieved L-04 considering F1-F6

Table A4.2: Amount of Th extracted in sequential (Seq) and single (Sin) extractions (concentration in elutes)

	F1 ($\mu\text{g L}^{-1}$)		F2 ($\mu\text{g L}^{-1}$)		F3 ($\mu\text{g L}^{-1}$)		F4 (mg L^{-1})		F5 (mg L^{-1})	
	Seq	Sin	Seq	Sin	Seq	Sin	Seq	Sin	Seq	Sin
L-03	4.45 \pm 1.91	4.46 \pm 0.33	330 \pm 5	433 \pm 6	402 \pm 12	438 \pm 1	2.58 \pm 0.03	3.88 \pm 0.07	9.63 \pm 0.23	7.13 \pm 0.45
L-04	6.11 \pm 1.40	5.80 \pm 1.25	445 \pm 8	542 \pm 29	372 \pm 20	350 \pm 6	4.28 \pm 0.07	5.67 \pm 0.02	19.8 \pm 0.4	19.4 \pm 0.0
L-05	3.51 \pm 0.59	3.93 \pm 0	977 \pm 21	2236 \pm 17	960 \pm 31	1160 \pm 33	6.38 \pm 0.01	11.5 \pm 0.1	17.1 \pm 0.5	25.8 \pm 0.1
L-06	4.40 \pm 1.36	4.65 \pm 1.65	988 \pm 1	1115 \pm 9	897 \pm 4	1060 \pm 8	5.78 \pm 0.01	8.54 \pm 0.08	18.6 \pm 0.3	24.7 \pm 0.1

Table A4.3: Amount of Th extracted in sequential (Seq) and single (Sin) extractions; mass of Th released from the soil (mass eluted per mass of soil)

	F1 (ng g^{-1})		F2 ($\mu\text{g g}^{-1}$)		F3 ($\mu\text{g g}^{-1}$)		F4 ($\mu\text{g g}^{-1}$)		F5 ($\mu\text{g g}^{-1}$)		F6 (mg kg^{-1})	Total
	Seq	Sin	Seq	Sin	Seq	Sin	Seq	Sin	Seq	Sin	Seq	(mg kg^{-1})
L-03	44.6 \pm 19.1	44.6 \pm 3.3	4.94 \pm 0.08	6.49 \pm 0.09	4.02 \pm 0.12	4.38 \pm 0.01	25.8 \pm 0.3	38.8 \pm 0.7	47.1 \pm 0.3	71.3 \pm 4.5	656 \pm 5	794 \pm 162
L-04	61.1 \pm 14.0	58.0 \pm 12.5	6.68 \pm 0.11	8.13 \pm 0.44	3.72 \pm 0.20	3.50 \pm 0.06	42.8 \pm 0.7	56.7 \pm 0.2	145 \pm 0	193 \pm 1	1020 \pm 149	1480 \pm 5
L-05	35.1 \pm 5.9	39.3 \pm 0.0	14.7 \pm 0.3	33.5 \pm 0.26	9.60 \pm 0.31	11.6 \pm 0.3	63.8 \pm 0.1	115 \pm 1	176 \pm 1	258 \pm 1	1150 \pm 99	1560 \pm 98
L-06	44.0 \pm 13.6	46.5 \pm 16.5	14.8 \pm 0.0	16.7 \pm 0.1	8.97 \pm 0.04	10.6 \pm 0.1	57.8 \pm 0.1	85.4 \pm 0.8	177 \pm 1	247 \pm 1	1200 \pm 132	1280 \pm 76

Table A4.4: Amount of U extracted in sequential (Seq) and single (Sin) extractions (concentration in elutes)

	F1 ($\mu\text{g L}^{-1}$)		F2 ($\mu\text{g L}^{-1}$)		F3 ($\mu\text{g L}^{-1}$)		F4 ($\mu\text{g L}^{-1}$)		F5 ($\mu\text{g L}^{-1}$)	
	Seq	Sin	Seq	Sin	Seq	Sin	Seq	Sin	Seq	Sin
L-03	4.36±0.00	4.36±0.00	133±1	154±2	47.7±2.2	169±0	132±2	425±9	270±13	625±12
L-04	2.22±0.76	3.10±0.49	136±2	154±2	49.1±2.3	140±2	156±2	457±6	349±10	676±11
L-05	2.56±1.18	2.71±1.22	91.2±2.4	208±2	39.8±1.2	136±5	108±0	310±8	325±8	541±23
L-06	3.57±1.24	3.66±1.19	92.7±0.2	112±1	39.1±0.4	124±0	114±1	314±3	346±3	539±32

Table A4.5: Amount of U extracted in sequential (Seq) and single (Sin) extractions; mass of U released from the soil (mass eluted per mass of soil)

	F1 (ng g^{-1})		F2 ($\mu\text{g g}^{-1}$)		F3 ($\mu\text{g g}^{-1}$)		F4 ($\mu\text{g g}^{-1}$)		F5 ($\mu\text{g g}^{-1}$)		F6 (mg kg^{-1})	Total
	Seq	Sin	Seq	Sin	Seq	Sin	Seq	Sin	Seq	Sin	Seq	(mg kg^{-1})
L-03	43.6±0.0	43.6±0.0	2.00±0.02	2.30±0.03	0.48±0.02	1.69±0.00	4.25±0.09	38.8±0.7	2.70±0.13	6.25±0.12	13±1	13±0
L-04	22.2±7.6	31.0±4.9	2.05±0.03	2.31±0.02	0.49±0.02	1.40±0.02	4.57±0.06	56.7±0.2	3.49±0.10	6.76±0.11	17±1	36±1
L-05	25.6±11.8	27.1±12.2	1.37±0.04	3.13±0.03	0.40±0.01	1.36±0.05	3.10±0.08	115±1	3.25±0.08	5.41±0.23	15±1	20±0
L-06	35.7±12.4	36.6±11.9	1.39±0.00	1.67±0.02	0.39±0.00	1.24±0.00	3.14±0.03	85.4±0.8	3.46±0.03	5.39±0.32	8±0	22±1

Table A4.6: Amount of La extracted in sequential (Seq) and single (Sin) extractions (concentration in elutes)

	F1 (mg L ⁻¹)		F2 (µg L ⁻¹)		F3 (µg L ⁻¹)		F4 (µg L ⁻¹)		F5 (µg L ⁻¹)	
	Seq	Sin	Seq	Sin	Seq	Sin	Seq	Sin	Seq	Sin
L-03	15.5±0.8	15.6±0.3	1.88±0.02	12.1±0.2	0.28±0.00	13.8±0.2	0.60±0.01	1.02±0.02	0.28±0.02	7.64±0.02
L-04	18.4±0.5	18.6±0.4	0.66±0.00	13.2±0.0	0.06±0.00	13.7±0.3	0.22±0.00	0.89±0.02	0.31±0.01	9.67±0.09
L-05	8.9±0.1	9.2±0.3	0.66±0.01	12.9±0.1	0.14±0.00	6.9±0.1	0.67±0.00	0.87±0.01	0.49±0.01	6.57±0.01
L-06	10.1±0.0	10.5±0.1	0.55±0.00	7.6±0.0	0.10±0.00	8.3±0.1	0.69±0.00	0.91±0.03	0.71±0.01	7.89±0.34

Table A4.7: Amount of La extracted in sequential (Seq) and single (Sin) extractions; mass of La released from the soil (mass eluted per mass of soil)

	F1 (µg g ⁻¹)		F2 (µg g ⁻¹)		F3 (µg g ⁻¹)		F4 (µg g ⁻¹)		F5 (µg g ⁻¹)		F6 (mg kg ⁻¹)	Total
	Seq	Sin	Seq	Sin	Seq	Sin	Seq	Sin	Seq	Sin	Seq	(mg kg ⁻¹)
L-03	155±8	156±3	28.2±0.4	182±3	2.79±0.05	138±2	6.00±0.05	10.2±0.2	2.85±0.16	76.4±0.2	882±166	1312±304
L-04	184±5	186±4	9.8±0.1	198±0	0.57±0.02	137±3	2.24±0.03	8.9±0.2	3.09±0.05	96.7±0.9	621±90	948±231
L-05	89±1	92±3	9.9±0.1	193±2	1.39±0.03	69±1	6.69±0.01	8.7±0.1	4.94±0.08	65.7±0.1	934±110	1201±189
L-06	101±0	105±1	8.3±0.1	115±1	0.97±0.01	83±1	6.91±0.00	9.1±0.3	7.05±0.14	78.9±3.4	813±29	896±59

Table A4.8: Amount of Ce extracted in sequential (Seq) and single (Sin) extractions (concentration in elutes)

	F1 ($\mu\text{g L}^{-1}$)		F2 ($\mu\text{g L}^{-1}$)		F3 ($\mu\text{g L}^{-1}$)		F4 ($\mu\text{g L}^{-1}$)		F5 ($\mu\text{g L}^{-1}$)	
	Seq	Sin	Seq	Sin	Seq	Sin	Seq	Sin	Seq	Sin
L-03	0.38±0.00	0.38±0.00	0.04±0.00	0.38±0.01	0.03±0.00	0.28±0.00	0.53±0.01	0.21±0.01	1.83±0.03	1.55±0.02
L-04	2.85±0.05	2.97±0.04	0.11±0.01	2.14±0.09	0.02±0.00	1.67±0.03	0.37±0.00	0.42±0.01	2.57±0.06	3.55±0.04
L-05	2.28±0.07	2.37±0.07	0.23±0.01	3.38±0.01	0.08±0.00	1.75±0.04	0.92±0.00	0.84±0.02	3.95±0.03	5.16±0.05
L-06	2.69±0.06	2.88±0.00	0.18±0.01	2.08±0.01	0.06±0.00	2.18±0.01	0.82±0.00	0.73±0.03	4.47±0.05	5.49±0.19

Table A4.9: Amount of Ce extracted in sequential (Seq) and single (Sin) extractions; mass of Ce released from the soil (mass eluted per mass of soil)

	F1 ($\mu\text{g g}^{-1}$)		F2 ($\mu\text{g g}^{-1}$)		F3 ($\mu\text{g g}^{-1}$)		F4 ($\mu\text{g g}^{-1}$)		F5 ($\mu\text{g g}^{-1}$)		F6 (mg kg^{-1})	Total
	Seq	Sin	Seq	Sin	Seq	Sin	Seq	Sin	Seq	Sin	Seq	(mg kg^{-1})
L-03	3.8±0.0	3.8±0.0	0.62±0.05	5.7±0.2	0.30±0.02	2.8±0.0	5.33±0.14	2.14±0.07	18.3±0.3	15.5±0.2	1474±78	1612±98
L-04	28.5±0.5	29.7±0.4	1.62±0.10	32.2±1.3	0.19±0.01	16.7±0.3	3.75±0.01	4.23±0.08	25.7±0.6	35.5±0.4	3454±950	4857±992
L-05	22.8±0.7	23.7±0.7	3.51±0.02	50.7±0.2	0.84±0.01	17.5±0.4	9.25±0.00	8.42±0.21	39.5±0.3	51.6±0.5	2836±138	3107±191
L-06	26.9±0.6	28.8±0.0	2.63±0.12	31.1±0.2	0.60±0.01	21.8±0.1	8.25±0.05	7.28±0.28	44.7±0.5	54.9±1.9	2141±33	2270±92

Table A4.10: Amount of Nd extracted in sequential (Seq) and single (Sin) extractions (concentration in elutes)

	F1 ($\mu\text{g L}^{-1}$)		F2 ($\mu\text{g L}^{-1}$)		F3 ($\mu\text{g L}^{-1}$)		F4 ($\mu\text{g L}^{-1}$)		F5 ($\mu\text{g L}^{-1}$)	
	Seq	Sin	Seq	Sin	Seq	Sin	Seq	Sin	Seq	Sin
L-03	6.32±0.05	6.38±0.10	2.33±0.04	6.77±0.19	0.35±0.01	7.72±0.01	0.64±0.02	0.35±0.01	0.41±0.01	5.50±0.03
L-04	10.2±0.01	10.4±0.03	0.67±0.01	7.90±0.19	0.07±0.00	8.58±0.14	0.21±0.00	0.29±0.01	0.31±0.01	6.81±0.06
L-05	4.79±0.06	4.92±0.09	0.77±0.03	7.77±0.04	0.15±0.00	4.22±0.11	0.51±0.00	0.32±0.01	0.41±0.01	4.40±0.05
L-06	5.37±0.11	5.71±0.10	0.56±0.01	4.44±0.02	0.10±0.00	4.83±0.01	0.47±0.00	0.32±0.02	0.56±0.01	4.94±0.16

Table A4.11: Amount of Nd extracted in sequential (Seq) and single (Sin) extractions; mass of Nd released from the soil (mass eluted per mass of soil)

	F1 ($\mu\text{g g}^{-1}$)		F2 ($\mu\text{g g}^{-1}$)		F3 ($\mu\text{g g}^{-1}$)		F4 ($\mu\text{g g}^{-1}$)		F5 ($\mu\text{g g}^{-1}$)		F6 (mg kg^{-1})	Total
	Seq	Sin	Seq	Sin	Seq	Sin	Seq	Sin	Seq	Sin	Seq	(mg kg^{-1})
L-03	63.2±0.5	63.8±1.0	35.0±0.6	102±3	3.49±0.13	77.2±0.1	6.39±0.16	3.45±0.10	4.12±0.09	55.0±0.3	377±83	607±63
L-04	102±1	104±0	10.0±0.2	118±3	0.69±0.04	85.8±1.4	2.13±0.01	2.86±0.07	3.08±0.08	68.1±0.6	270±51	461±35
L-05	47.9±0.6	49.2±0.9	11.5±0.5	117±1	1.49±0.05	42.2±1.1	5.06±0.02	3.23±0.07	4.10±0.11	44.0±0.5	441±60	596±10
L-06	53.7±1.1	57.1±1.0	8.3±0.1	67±0	1.00±0.03	48.3±0.1	4.66±0.02	3.25±0.18	5.61±0.09	49.4±1.6	372±1	446±53

Table A4.12: Released amounts of Th, U, La, Ce, and Nd per gram of soil in the washing steps between each sequential extraction

	F1 ($\mu\text{g g}^{-1}$)	F2 ($\mu\text{g g}^{-1}$)	F3 ($\mu\text{g g}^{-1}$)	F4 ($\mu\text{g g}^{-1}$)	F5 ($\mu\text{g g}^{-1}$)
Th					
L-05	<	0.1±0.0	11.8±0.0	1.8±0.0	0.1±0.0
L-04	<	0.1±0.0	11.1±0.0	2.3±0.0	20.7±0.0
U					
L-05	<	<	0.1±0.0	0.1±0.0	0.1±0.0
L-04	<	0.1±0.0	0.2±0.0	0.1±0.0	0.5±0.0
La					
L-05	54±0.8	0.1±0.0	2.7±0.0	0.1±0.0	10.0±0.9
L-04	11.5±1.6	0.3±0.0	4.2±0.1	0.1±0.0	0.4±0.0
Ce					
L-05	2.0±0.2	0.1±0.0	14.4±0.1	0.3±0.0	1.8±0.2
L-04	2.5±0.2	0.1±0.0	17.0±0.1	0.2±0.0	2.9±0.0
Nd					
L-05	3.1±0.5	0.1±0.0	1.8±0.0	0.1±0.0	6.2±0.6
L-04	8.4±1.0	0.3±0.0	2.6±0.0	0.1±0.0	0.4±0.0

* "<" - below the detection limit

Table A4.13: Amount of Th extracted in the elute of each size fraction in sequential extractions ($\mu\text{g L}^{-1}$) and mass of Th released per gram of soil ($\mu\text{g g}^{-1}$)

Th	F1		F2		F3		F4		F5	
	$\mu\text{g L}^{-1}$	$\mu\text{g g}^{-1}$	$\mu\text{g L}^{-1}$	$\mu\text{g g}^{-1}$	$\mu\text{g L}^{-1}$	$\mu\text{g g}^{-1}$	$\mu\text{g L}^{-1}$	$\mu\text{g g}^{-1}$	$\mu\text{g L}^{-1}$	$\mu\text{g g}^{-1}$
40-75	0.03±0.00	0.28±0.00	0.46±0.01	6.87±0.10	0.38±0.01	3.78±0.05	6.35±0.06	63.5±0.6	29.0±0.3	290±3
75-125	0.05±0.01	0.54±0.05	0.46±0.02	6.89±0.27	0.42±0.00	4.16±0.02	5.47±0.07	54.7±0.7	27.9±0.1	279±1
125-180	0.01±0.00	0.13±0.01	0.48±0.00	7.21±0.04	0.42±0.00	4.22±0.01	5.45±0.09	54.5±0.9	23.4±0.2	234±2
180-250	0.02±0.00	0.17±0.01	0.45±0.00	6.73±0.04	0.40±0.01	3.96±0.08	5.09±0.02	50.9±0.2	22.9±0.1	229±1
250-425	0.02±0.00	0.23±0.03	0.44±0.01	6.65±0.12	0.39±0.01	3.93±0.13	4.40±0.05	44.0±0.5	25.4±0.7	254±7
425-850	0.02±0.00	0.18±0.03	0.44±0.02	6.65±0.25	0.42±0.01	4.18±0.10	4.12±0.02	41.2±0.2	25.8±0.2	258±2
>850	0.00±0.00	0.00±0.00	0.39±0.01	5.86±0.21	0.43±0.00	4.25±0.01	3.75±0.07	37.5±0.7	27.5±0.1	275±1

Table A4.14: Amount of U extracted in the elute of each size fraction in sequential extractions ($\mu\text{g L}^{-1}$) and mass of U released per gram of soil ($\mu\text{g g}^{-1}$)

U	F1		F2		F3		F4		F5	
	$\mu\text{g L}^{-1}$	$\mu\text{g g}^{-1}$	$\mu\text{g L}^{-1}$	$\mu\text{g g}^{-1}$	$\mu\text{g L}^{-1}$	$\mu\text{g g}^{-1}$	$\mu\text{g L}^{-1}$	$\mu\text{g g}^{-1}$	$\mu\text{g L}^{-1}$	$\mu\text{g g}^{-1}$
40-75	<	<	0.14±0.00	2.07±0.06	0.04±0.01	0.44±0.03	0.17±0.00	1.71±0.02	0.55±0.01	5.49±0.10
75-125	<	<	0.14±0.01	2.13±0.10	0.05±0.00	0.48±0.02	0.16±0.00	1.64±0.02	0.55±0.00	5.51±0.02
125-180	<	<	0.15±0.00	2.18±0.05	0.05±0.00	0.55±0.03	0.17±0.00	1.67±0.01	0.52±0.00	5.24±0.01
180-250	<	<	0.15±0.00	2.26±0.04	0.05±0.00	0.49±0.01	0.16±0.01	1.63±0.06	0.51±0.00	5.05±0.03
250-425	<	<	0.14±0.00	2.17±0.03	0.05±0.00	0.50±0.01	0.14±0.00	1.41±0.01	0.54±0.00	5.44±0.01
425-850	<	<	0.13±0.00	2.01±0.02	0.06±0.00	0.55±0.02	0.14±0.00	1.35±0.04	0.55±0.00	5.54±0.04
>850	<	<	0.14±0.00	2.03±0.05	0.06±0.00	0.56±0.04	0.12±0.00	1.23±0.01	0.67±0.04	6.70±0.43

* “<” - below the detection limit

Table A4.15: Amount of La extracted in the elute of each size fraction in sequential extractions ($\mu\text{g L}^{-1}$) and mass of La released per gram of soil ($\mu\text{g g}^{-1}$)

La	F1		F2		F3		F4		F5	
	$\mu\text{g L}^{-1}$	$\mu\text{g g}^{-1}$	$\mu\text{g L}^{-1}$	$\mu\text{g g}^{-1}$	$\mu\text{g L}^{-1}$	$\mu\text{g g}^{-1}$	$\mu\text{g L}^{-1}$	$\mu\text{g g}^{-1}$	$\mu\text{g L}^{-1}$	$\mu\text{g g}^{-1}$
40-75	19.2±1.9	192±19	0.61±0.03	9.16±0.41	0.05±0.00	0.47±0.03	0.32±0.00	3.16±0.04	0.38±0.01	3.86±0.02
75-125	15.1±0.0	151±0	0.55±0.02	8.24±0.31	0.04±0.00	0.44±0.01	0.29±0.00	2.90±0.00	0.37±0.01	3.78±0.03
125-180	17.1±0.3	171±3	0.67±0.00	10.0±0.01	0.05±0.00	0.47±0.02	0.31±0.01	3.06±0.07	0.36±0.03	3.57±0.32
180-250	19.7±1.0	197±10	0.65±0.02	9.98±0.28	0.05±0.00	0.49±0.02	0.27±0.00	2.67±0.00	0.32±0.00	3.21±0.03
250-425	19.9±0.3	199±3	0.58±0.00	8.75±0.07	0.05±0.00	0.46±0.01	0.25±0.00	2.54±0.02	0.37±0.00	3.71±0.00
425-850	21.4±0.5	214±5	0.66±0.03	9.91±0.44	0.06±0.00	0.59±0.04	0.22±0.00	2.17±0.05	0.37±0.00	3.69±0.00
>850	17.9±0.6	179±6	0.71±0.03	10.7±0.49	0.07±0.00	0.69±0.01	0.26±0.00	2.56±0.02	0.56±0.04	5.61±0.38

Table A4.16: Amount of Ce extracted in the elute of each size fraction in sequential extractions ($\mu\text{g L}^{-1}$) and mass of Ce released per gram of soil ($\mu\text{g g}^{-1}$)

Ce	F1		F2		F3		F4		F5	
	$\mu\text{g L}^{-1}$	$\mu\text{g g}^{-1}$	$\mu\text{g L}^{-1}$	$\mu\text{g g}^{-1}$	$\mu\text{g L}^{-1}$	$\mu\text{g g}^{-1}$	$\mu\text{g L}^{-1}$	$\mu\text{g g}^{-1}$	$\mu\text{g L}^{-1}$	$\mu\text{g g}^{-1}$
40-75	2.99±0.33	29.9±3.3	0.23±0.01	3.42±0.18	0.01±0.00	0.14±0.01	0.65±0.00	6.48±0.01	3.17±0.02	31.7±0.2
75-125	2.48±0.19	24.8±1.9	0.17±0.01	2.57±0.09	0.01±0.00	0.14±0.00	0.53±0.01	5.35±0.06	3.13±0.02	31.3±0.2
125-180	2.72±0.25	27.2±2.5	0.18±0.00	2.71±0.04	0.02±0.00	0.19±0.03	0.55±0.00	5.53±0.04	3.52±0.23	35.2±2.3
180-250	3.18±0.32	31.8±3.2	0.21±0.01	3.11±0.11	0.02±0.00	0.17±0.01	0.49±0.02	4.91±0.16	2.84±0.01	28.4±0.1
250-425	3.46±0.49	34.6±4.9	0.16±0.00	2.33±0.07	0.01±0.00	0.13±0.02	0.38±0.00	3.83±0.04	3.06±0.13	30.6±1.3
425-850	3.37±0.21	33.7±2.1	0.16±0.01	2.46±0.20	0.01±0.00	0.14±0.02	0.38±0.01	3.77±0.06	3.16±0.01	31.6±0.1
>850	2.70±0.04	27.0±0.4	0.15±0.00	2.27±0.07	0.02±0.00	0.17±0.03	0.33±0.01	3.33±0.07	3.94±0.20	39.4±2.0

Table A4.17: Amount of Nd extracted in the elute of each size fraction in sequential extractions ($\mu\text{g L}^{-1}$) and mass of Nd released per gram of soil ($\mu\text{g g}^{-1}$)

Nd	F1		F2		F3		F4		F5	
	$\mu\text{g L}^{-1}$	$\mu\text{g g}^{-1}$	$\mu\text{g L}^{-1}$	$\mu\text{g g}^{-1}$	$\mu\text{g L}^{-1}$	$\mu\text{g g}^{-1}$	$\mu\text{g L}^{-1}$	$\mu\text{g g}^{-1}$	$\mu\text{g L}^{-1}$	$\mu\text{g g}^{-1}$
40-75	11.4±0.1	114±10	0.84±0.01	12.6±0.2	0.08±0.01	0.77±0.04	0.36±0.01	3.63±0.08	0.39±0.00	3.85±0.02
75-125	9.0±0.2	90±2	0.73±0.02	11.0±0.2	0.06±0.00	0.65±0.03	0.30±0.01	3.00±0.08	0.37±0.00	3.74±0.01
125-180	10.1±0.2	101±2	0.86±0.01	12.9±0.1	0.07±0.00	0.73±0.03	0.30±0.01	3.01±0.08	0.37±0.01	3.71±0.15
180-250	12.1±0.6	121±6	0.79±0.03	11.4±0.4	0.07±0.00	0.75±0.02	0.30±0.01	3.03±0.06	0.35±0.00	3.49±0.00
250-425	12.4±0.0	124±0	0.70±0.01	10.6±0.2	0.05±0.01	0.54±0.05	0.25±0.01	2.51±0.12	0.38±0.01	3.77±0.08
425-850	14.2±0.3	142±3	0.75±0.02	11.2±0.3	0.07±0.00	0.67±0.03	0.23±0.00	2.29±0.04	0.37±0.00	3.74±0.01
>850	10.9±0.5	109±5	0.76±0.01	11.4±0.1	0.08±0.01	0.76±0.09	0.26±0.01	2.59±0.06	0.55±0.03	5.53±0.29

Appendix 4.2: Batch extractions with simulated rainwaters

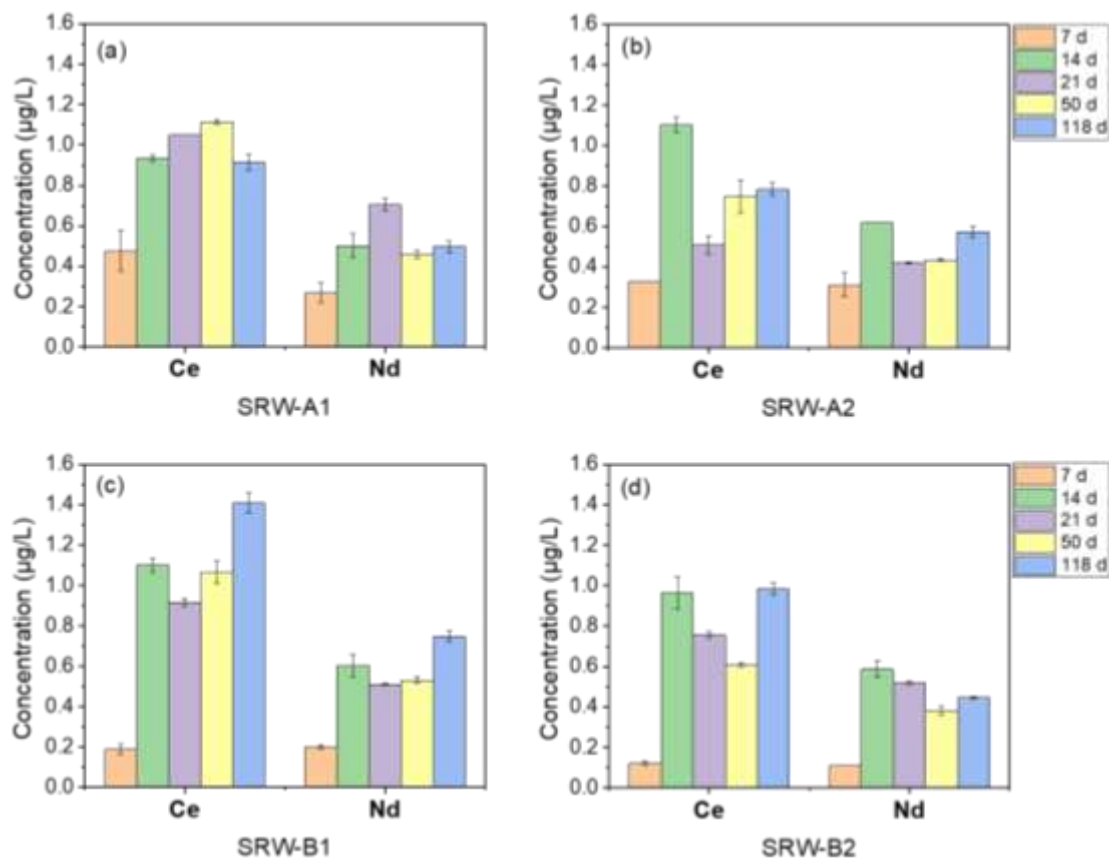


Figure A4.4: Concentrations of Ce and Nd in the supernatant after rotating with different SRW compositions (a) SRW-A1, (b) SRW-A2, (c) SRW-B1, and (d) SRW-B2 from samples for several time periods (7, 14, 21, 50, and 118 days) for L-05

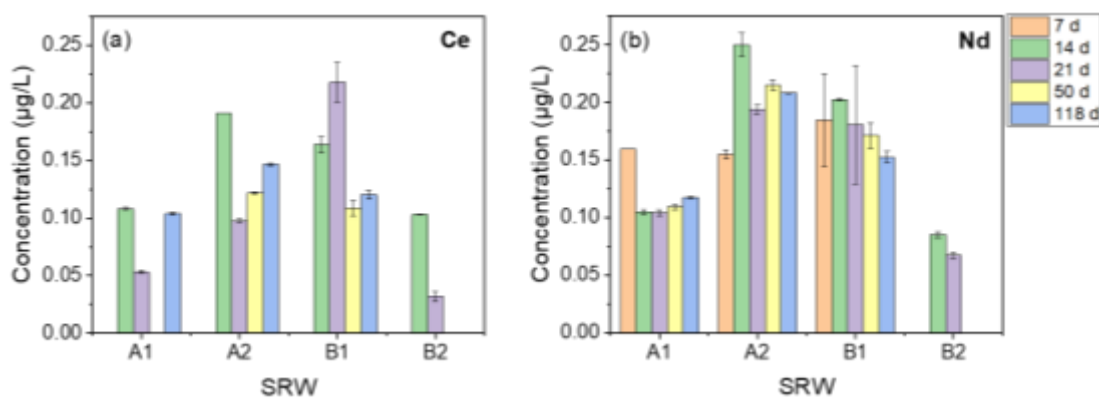


Figure A4.5: Concentrations of (a) Ce and (b) Nd in the supernatant with different SRW compositions SRW-A1, A2, B1, and B2 from samples standing still (not rotated) for several time periods (7, 14, 21, 50, and 118 days) for L-05.

Table A4.18: Released amounts of Th, U, La, Ce and Nd with SRW-A1 in rotated and stand-still samples of L-03

SRW-A1	7 days	14 days	21 days	50 days	118 days
L-03					
Rotated	µg g⁻¹	µg g⁻¹	µg g⁻¹	µg g⁻¹	µg g⁻¹
Th	0.04±0.01	0.11±0.01	0.03±0.00	0.04±0.00	0.05±0.00
U	0.01±0.00	0.01±0.00	0.01±0.00	0.01±0.00	0.01±0.00
La	0.26±0.09	0.38±0.01	0.17±0.00	0.14±0.00	0.21±0.02
Ce	0.07±0.00	0.23±0.02	0.08±0.00	0.10±0.00	0.11±0.00
Nd	0.17±0.03	0.24±0.00	0.11±0.00	0.09±0.01	0.14±0.01
Stand-still					
Th	<	<	<	<	<
U	<	0.01±0.00	0.01±0.00	0.01±0.00	0.01±0.00
La	0.09±0.00	0.05±0.00	0.05±0.00	0.05±0.00	0.04±0.00
Ce	<	0.02±0.00	0.004±0.000	<	0.04±0.00
Nd	0.04±0.01	0.03±0.00	0.03±0.00	0.02±0.00	0.02±0.00

* "<" - below the detection limit

Table A4.19: Released amounts of Th, U, La, Ce and Nd with SRW-A2 in rotated and stand-still samples of L-03

SRW-A2	7 days	14 days	21 days	50 days	118 days
L-03					
Rotated	µg g⁻¹	µg g⁻¹	µg g⁻¹	µg g⁻¹	µg g⁻¹
Th	0.02±0.01	0.07±0.00	0.04±0.01	0.04±0.00	0.03±0.00
U	0.01±0.00	0.01±0.00	0.01±0.00	0.01±0.00	0.01±0.00
La	0.33±0.02	0.32±0.03	0.30±0.01	0.21±0.00	0.22±0.02
Ce	0.09±0.01	0.16±0.02	0.07±0.00	0.11±0.00	0.07±0.00
Nd	0.21±0.02	0.19±0.01	0.18±0.01	0.14±0.01	0.14±0.00
Stand-still					
Th	<	<	<	<	<
U	<	0.01±0.00	0.01±0.00	0.01±0.00	0.01±0.00
La	0.12±0.02	0.10±0.00	0.08±0.00	0.08±0.00	0.08±0.01
Ce	<	0.02±0.00	0.004±0.000	<	<
Nd	0.06±0.00	0.06±0.00	0.05±0.00	0.04±0.00	0.04±0.01

* "<" - below the detection limit

Table A4.20: Released amounts of Th, U, La, Ce and Nd with SRW-B1 in rotated and stand-still samples of L-03

SRW-B1	7 days	14 days	21 days	50 days	118 days
L-03					
Rotated	µg g⁻¹	µg g⁻¹	µg g⁻¹	µg g⁻¹	µg g⁻¹
Th	0.01±0.00	0.05±0.00	0.04±0.00	0.03±0.00	0.05±0.01
U	0.01±0.00	0.01±0.00	0.01±0.00	0.01±0.00	0.01±0.00
La	0.14±0.02	0.22±0.01	0.20±0.02	0.18±0.02	0.22±0.01
Ce	0.04±0.01	0.11±0.01	0.08±0.02	0.08±0.01	0.08±0.01
Nd	0.09±0.00	0.13±0.01	0.13±0.01	0.10±0.00	0.13±0.01
Stand-still	±	±	±	±	±
Th	<	<	<	<	<
U	<	0.01±0.00	0.01±0.00	0.01±0.00	0.01±0.00
La	0.12±0.03	0.07±0.00	0.06±0.00	0.06±0.00	0.05±0.00
Ce	<	0.02±0.00	0.004±0.000	<	<
Nd	0.08±0.01	0.04±0.00	0.03±0.00	0.03±0.00	0.03±0.00

* "<" - below the detection limit

Table A4.21: Released amounts of Th, U, La, Ce and Nd with SRW-B2 in rotated and stand-still samples of L-03

SRW-B2 L-03	7 days	14 days	21 days	50 days	118 days
Rotated	µg g⁻¹	µg g⁻¹	µg g⁻¹	µg g⁻¹	µg g⁻¹
Th	0.01±0.00	0.05±0.00	0.04±0.00	0.04±0.00	0.07±0.00
U	0.01±0.00	0.01±0.00	0.01±0.00	0.01±0.00	0.01±0.00
La	0.08±0.00	0.19±0.01	0.17±0.03	0.14±0.00	0.19±0.01
Ce	<	0.11±0.02	0.08±0.00	0.13±0.02	0.14±0.01
Nd	0.04±0.00	0.12±0.01	0.11±0.02	0.09±0.00	0.12±0.00
Stand-still					
Th	<	<	<	<	<
U	<	0.01±0.00	0.01±0.00	0.01±0.00	0.01±0.00
La	0.04±0.00	0.03±0.00	0.02±0.00	0.02±0.00	0.02±0.00
Ce	<	0.02±0.00	<	<	<
Nd	<	0.02±0.00	0.01±0.00	<	0.02±0.00

* "<" - below the detection limit

Table A4.22: Released amounts of Th, U, La, Ce and Nd with SRW-A1 in rotated and stand-still samples of L-04

SRW-A1 L-04	7 days	14 days	21 days	50 days	118 days
Rotated	µg g⁻¹	µg g⁻¹	µg g⁻¹	µg g⁻¹	µg g⁻¹
Th	0.05±0.03	0.10±0.00	0.18±0.01	0.06±0.00	0.06±0.00
U	0.02±0.00	0.02±0.00	0.04±0.00	0.02±0.00	0.02±0.00
La	0.25±0.01	0.46±0.03	0.95±0.03	0.33±0.00	0.39±0.00
Ce	0.06±0.01	0.26±0.00	0.47±0.04	0.28±0.01	0.19±0.01
Nd	0.13±0.01	0.27±0.00	0.58±0.03	0.21±0.01	0.26±0.00
Stand-still					
Th	<	<	<	<	<
U	<	0.02±0.00	0.02±0.00	0.01±0.00	0.01±0.00
La	0.14±0.00	0.15±0.00	0.14±0.00	0.15±0.00	0.15±0.00
Ce	<	0.05±0.00	0.03±0.00	0.03±0.00	0.04±0.00
Nd	0.08±0.01	0.09±0.00	0.09±0.00	0.09±0.00	0.09±0.00

* "<" - below the detection limit

Table A4.23: Released amounts of Th, U, La, Ce and Nd with SRW-A2 in rotated and stand-still samples of L-04

SRW-A2 L-04	7 days	14 days	21 days	50 days	118 days
Rotated	µg g⁻¹	µg g⁻¹	µg g⁻¹	µg g⁻¹	µg g⁻¹
Th	0.04±0.01	0.13±0.03	0.09±0.01	0.09±0.02	0.01±0.01
U	0.02±0.00	0.03±0.00	0.02±0.00	0.02±0.00	0.02±0.00
La	0.48±0.04	0.65±0.03	0.57±0.01	0.44±0.02	0.52±0.02
Ce	0.11±0.01	0.29±0.08	0.21±0.02	0.26±0.02	0.18±0.02
Nd	0.30±0.00	0.39±0.01	0.39±0.03	0.27±0.01	0.33±0.00
Stand-still					
Th	<	<	<	<	<
U	<	0.02±0.00	0.01±0.00	0.01±0.00	0.02±0.00
La	0.35±0.00	0.37±0.01	0.30±0.00	0.30±0.00	0.29±0.01
Ce	0.06±0.01	0.08±0.00	0.05±0.00	0.07±0.01	0.06±0.01
Nd	0.15±0.01	0.23±0.01	0.19±0.01	0.19±0.00	0.19±0.00

* "<" - below the detection limit

Table A4.24: Released amounts of Th, U, La, Ce and Nd with SRW-B1 in rotated and stand-still samples of L-04

SRW-B1 L-04	7 days	14 days	21 days	50 days	118 days
Rotated	µg g⁻¹	µg g⁻¹	µg g⁻¹	µg g⁻¹	µg g⁻¹
Th	0.02±0.00	0.07±0.01	0.07±0.01	0.04±0.00	0.05±0.01
U	0.02±0.00	0.02±0.00	0.02±0.00	0.02±0.00	0.02±0.00
La	0.41±0.03	0.46±0.00	0.44±0.02	0.33±0.04	0.43±0.01
Ce	0.11±0.02	0.25±0.01	0.19±0.01	0.17±0.02	0.17±0.00
Nd	0.21±0.03	0.28±0.00	0.27±0.01	0.21±0.02	0.27±0.00
Stand-still	±	±	±	±	±
Th	<	<	<	<	<
U	<	0.02±0.00	0.02±0.00	0.02±0.00	0.02±0.00
La	0.24±0.00	0.29±0.01	0.24±0.00	0.24±0.01	0.23±0.00
Ce	0.05±0.00	0.06±0.00	0.04±0.00	0.05±0.00	0.05±0.00
Nd	0.17±0.00	0.19±0.01	0.15±0.00	0.14±0.00	0.15±0.01

* "<" - below the detection limit

Table A4.25: Released amounts of Th, U, La, Ce and Nd with SRW-B2 in rotated and stand-still samples of L-04

SRW-B2 L-04	7 days	14 days	21 days	50 days	118 days
Rotated	µg g⁻¹	µg g⁻¹	µg g⁻¹	µg g⁻¹	µg g⁻¹
Th	0.03±0.01	0.06±0.01	0.05±0.00	0.04±0.00	0.08±0.01
U	0.01±0.00	0.01±0.00	0.01±0.00	0.01±0.00	0.01±0.00
La	0.15±0.01	0.23±0.01	0.15±0.03	0.13±0.01	0.23±0.01
Ce	0.07±0.02	0.17±0.00	0.12±0.00	0.11±0.02	0.17±0.00
Nd	0.08±0.00	0.13±0.01	0.09±0.01	0.08±0.00	0.14±0.00
Stand-still					
Th	<	<	<	<	<
U	<	0.01±0.00	0.01±0.00	0.01±0.00	0.01±0.00
La	0.07±0.00	0.07±0.00	0.05±0.00	0.04±0.00	0.04±0.00
Ce	<	0.03±0.00	0.01±0.00	<	<
Nd	<	0.04±0.00	0.03±0.00	0.03±0.00	<

* "<" - below the detection limit

Table A4.26: Released amounts of Th, U, La, Ce and Nd with SRW-A1 in rotated and stand-still samples of L-05

SRW-A1 L-05	7 days	14 days	21 days	50 days	118 days
Rotated	µg g⁻¹	µg g⁻¹	µg g⁻¹	µg g⁻¹	µg g⁻¹
Th	0.09±0.03	0.11±0.00	0.12±0.00	0.12±0.00	0.13±0.02
U	0.01±0.00	0.01±0.00	0.01±0.00	0.01±0.00	0.01±0.00
La	0.14±0.00	0.19±0.01	0.28±0.04	0.17±0.01	0.19±0.01
Ce	0.11±0.02	0.22±0.00	0.25±0.02	0.24±0.00	0.19±0.01
Nd	0.06±0.01	0.10±0.01	0.15±0.01	0.10±0.00	0.10±0.01
Stand-still					
Th	<	<	<	<	<
U	<	0.01±0.00	0.01±0.00	0.01±0.00	0.01±0.00
La	0.05±0.01	0.05±0.00	0.04±0.00	0.04±0.00	0.04±0.00
Ce	<	0.03±0.00	0.01±0.00	<	0.02±0.00
Nd	0.04±0.00	0.02±0.00	0.02±0.00	0.02±0.00	0.02±0.00

* "<" - below the detection limit

Table A4.27: Released amounts of Th, U, La, Ce and Nd with SRW-A2 in rotated and stand-still samples of L-05

SRW-A2 L-05	7 days	14 days	21 days	50 days	118 days
Rotated	µg g⁻¹	µg g⁻¹	µg g⁻¹	µg g⁻¹	µg g⁻¹
Th	0.04±0.00	0.14±0.02	0.07±0.00	0.12±0.04	0.08±0.01
U	0.01±0.00	0.01±0.00	0.01±0.00	0.01±0.00	0.01±0.00
La	0.18±0.00	0.25±0.01	0.16±0.00	0.16±0.00	0.20±0.01
Ce	0.08±0.00	0.24±0.03	0.12±0.01	0.18±0.03	0.16±0.01
Nd	0.08±0.01	0.14±0.00	0.09±0.00	0.10±0.01	0.12±0.01
Stand-still					
Th	<	<	<	<	<
U	<	0.01±0.00	0.01±0.00	0.01±0.00	0.01±0.00
La	0.07±0.00	0.11±0.01	0.08±0.00	0.08±0.00	0.07±0.00
Ce	<	0.04±0.00	0.02±0.00	0.03±0.00	0.03±0.00
Nd	0.04±0.00	0.06±0.00	0.04±0.00	0.05±0.00	0.04±0.00

* "<" - below the detection limit

Table A4.28: Released amounts of Th, U, La, Ce and Nd with SRW-B1 in rotated and stand-still samples of L-05

SRW-B1 L-05	7 days	14 days	21 days	50 days	118 days
Rotated	µg g⁻¹	µg g⁻¹	µg g⁻¹	µg g⁻¹	µg g⁻¹
Th	0.01±0.00	0.11±0.01	0.09±0.01	0.08±0.01	0.10±0.01
U	0.01±0.00	0.01±0.00	0.01±0.00	0.01±0.00	0.01±0.00
La	0.09±0.02	0.23±0.02	0.23±0.03	0.22±0.03	0.27±0.02
Ce	0.05±0.01	0.26±0.01	0.21±0.00	0.26±0.04	0.29±0.02
Nd	0.05±0.00	0.14±0.01	0.11±0.00	0.12±0.00	0.19±0.01
Stand-still	±	±	±	±	±
Th	<	<	<	<	<
U	<	0.01±0.00	0.01±0.00	0.01±0.00	0.01±0.00
La	0.09±0.00	0.08±0.00	0.18±0.01	0.07±0.00	0.05±0.00
Ce	<	0.04±0.00	0.05±0.00	0.02±0.00	0.03±0.00
Nd	0.04±0.01	0.05±0.00	0.04±0.01	0.04±0.00	0.03±0.00

* "<" - below the detection limit

Table A4.29: Released amounts of Th, U, La, Ce and Nd with SRW-B2 in rotated and stand-still samples of L-05

SRW-B2 L-05	7 days	14 days	21 days	50 days	118 days
Rotated	µg g⁻¹	µg g⁻¹	µg g⁻¹	µg g⁻¹	µg g⁻¹
Th	0.01±0.00	0.12±0.00	0.09±0.00	0.07±0.00	0.08±0.01
U	<	0.01±0.00	0.01±0.00	0.01±0.00	0.01±0.00
La	0.06±0.01	0.26±0.02	0.20±0.00	0.15±0.01	0.16±0.00
Ce	0.03±0.00	0.24±0.03	0.16±0.01	0.14±0.01	0.21±0.01
Nd	0.03±0.00	0.14±0.01	0.12±0.00	0.08±0.01	0.09±0.00
Stand-still					
Th	<	<	<	<	<
U	<	0.01±0.00	0.01±0.00	0.01±0.00	0.01±0.00
La	0.04±0.01	0.04±0.00	0.03±0.00	0.03±0.00	0.02±0.00
Ce	<	0.02±0.00	0.01±0.00	<	<
Nd	<	0.02±0.00	0.02±0.00	<	<

* "<" - below the detection limit

Table A4.30: Released amounts of Th, U, La, Ce and Nd with SRW-A1 in rotated and stand-still samples of L-06

SRW-A1	7 days	14 days	21 days	50 days	118 days
L-06					
Rotated	µg g⁻¹	µg g⁻¹	µg g⁻¹	µg g⁻¹	µg g⁻¹
Th	0.03±0.01	0.09±0.00	0.08±0.01	0.06±0.00	0.08±0.00
U	0.01±0.00	0.01±0.00	0.01±0.00	0.01±0.00	0.01±0.00
La	0.12±0.01	0.16±0.00	0.17±0.02	0.11±0.02	0.16±0.01
Ce	0.08±0.01	0.17±0.01	0.14±0.02	0.15±0.03	0.18±0.01
Nd	0.05±0.01	0.10±0.00	0.10±0.02	0.06±0.01	0.10±0.00
Stand-still					
Th	<	<	<	<	<
U	<	0.01±0.00	0.01±0.00	0.01±0.00	0.01±0.00
La	0.05±0.00	0.05±0.00	0.07±0.01	0.05±0.00	0.05±0.00
Ce	<	0.03±0.00	0.02±0.00	<	0.02±0.00
Nd	<	0.03±0.00	0.04±0.00	0.03±0.00	0.03±0.00

* "<" - below the detection limit

Table A4.31: Released amounts of Th, U, La, Ce and Nd with SRW-A2 in rotated and stand-still samples of L-06

SRW-A2	7 days	14 days	21 days	50 days	118 days
L-06					
Rotated	µg g⁻¹	µg g⁻¹	µg g⁻¹	µg g⁻¹	µg g⁻¹
Th	0.02±0.00	0.07±0.01	0.20±0.01	0.04±0.00	0.08±0.01
U	0.01±0.00	0.01±0.00	0.01±0.00	0.01±0.00	0.01±0.00
La	0.12±0.00	0.21±0.00	0.21±0.02	0.17±0.01	0.22±0.01
Ce	0.08±0.00	0.16±0.01	0.17±0.02	0.12±0.00	0.19±0.02
Nd	0.07±0.00	0.12±0.00	0.12±0.00	0.10±0.00	0.13±0.00
Stand-still					
Th	<	<	<	<	<
U	<	0.01±0.00	0.01±0.00	0.01±0.00	0.01±0.00
La	0.09±0.00	0.11±0.00	0.09±0.00	0.09±0.00	0.08±0.00
Ce	<	0.04±0.00	0.02±0.00	0.03±0.00	0.03±0.00
Nd	0.05±0.02	0.06±0.00	0.05±0.00	0.05±0.00	0.05±0.00

* "<" - below the detection limit

Table A4.32: Released amounts of Th, U, La, Ce and Nd with SRW-B1 in rotated and stand-still samples of L-06

SRW-B1	7 days	14 days	21 days	50 days	118 days
L-06					
Rotated	µg g⁻¹	µg g⁻¹	µg g⁻¹	µg g⁻¹	µg g⁻¹
Th	0.02±0.00	0.08±0.02	0.09±0.00	0.10±0.03	0.09±0.00
U	0.01±0.00	0.01±0.00	0.01±0.00	0.01±0.00	0.01±0.00
La	0.13±0.01	0.19±0.04	0.18±0.00	0.26±0.05	0.18±0.02
Ce	0.07±0.01	0.17±0.00	0.17±0.00	0.38±0.03	0.18±0.01
Nd	0.06±0.01	0.11±0.03	0.11±0.00	0.12±0.02	0.11±0.00
Stand-still					
	±	±	±	±	±
Th	<	<	<	<	<
U	<	0.01±0.00	0.01±0.00	0.01±0.00	0.01±0.00
La	0.07±0.00	0.08±0.00	0.07±0.00	0.06±0.00	0.06±0.00
Ce	<	0.04±0.00	0.02±0.00	0.03±0.00	0.03±0.00
Nd	0.03±0.00	0.05±0.00	0.04±0.00	0.03±0.00	0.04±0.00

* "<" - below the detection limit

Table A4.33: Released amounts of Th, U, La, Ce and Nd with SRW-B2 in rotated and stand-still samples of L-06

SRW-B2 L-06	7 days	14 days	21 days	50 days	118 days
Rotated	µg g⁻¹	µg g⁻¹	µg g⁻¹	µg g⁻¹	µg g⁻¹
Th	0.02±0.00	0.18±0.02	0.05±0.00	0.03±0.00	0.06±0.00
U	<	0.01±0.00	0.01±0.00	0.01±0.00	0.01±0.00
La	0.09±0.00	0.32±0.08	0.11±0.01	0.08±0.02	0.11±0.00
Ce	0.07±0.01	0.33±0.05	0.10±0.00	0.06±0.01	0.11±0.01
Nd	0.05±0.00	0.22±0.02	0.07±0.01	0.04±0.01	0.06±0.00
Stand-still					
Th	<	<	<	<	<
U	<	0.01±0.00	0.01±0.00	0.01±0.00	0.01±0.00
La	0.03±0.00	0.03±0.00	0.02±0.00	0.02±0.00	0.02±0.01
Ce	<	0.02±0.00	0.01±0.00	<	<
Nd	<	0.02±0.00	0.01±0.00	<	<

* "<" - below the detection limit

Appendix 4.3: Batch extractions with silica nanoparticles

Table A4.34: Released amounts of Th, U, La, Ce and Nd per gram of soil and concentration of Si in the supernatant in L-05 for Si NPs batch extractions

Si NP L-05	Th µg g ⁻¹	U ng g ⁻¹	La µg g ⁻¹	Ce µg g ⁻¹	Nd µg g ⁻¹	Si mg L ⁻¹
0.5	1.19±0.40	29.3±1.8	0.47±0.06	1.05±0.06	0.31±0.00	13.3±0.1
1	2.62±0.70	66.0±2.1	1.09±0.19	2.89±1.24	0.62±0.09	82.3±0.1
2	3.95±1.50	109±2	1.25±0.03	3.25±0.46	0.77±0.03	203±1
4	7.50±1.02	186±3	2.35±0.12	7.29±0.53	1.41±0.21	553±1
8	14.05±5.57	688±32	5.00±3.29	14.8±6.19	2.84±1.82	748±3

Table A4.35: Released amounts of Th, U, La, Ce and Nd per gram of soil and concentration of Si in the supernatant in L-04 for Si NPs batch extractions

Si NP L-04	Th µg g ⁻¹	U µg g ⁻¹	La µg g ⁻¹	Ce µg g ⁻¹	Nd µg g ⁻¹	Si mg L ⁻¹
0.5	0.59±0.18	0.07±0.00	0.48±0.03	1.02±0.50	0.21±0.00	39.8±0.1
1	1.24±0.03	0.11±0.01	1.19±0.47	2.24±0.11	0.63±0.32	92.7±4.7
2	1.20±0.43	0.15±0.01	0.91±0.62	1.70±0.63	0.48±0.40	198±4
4	0.81±0.31	0.21±0.01	0.53±0.35	1.33±0.56	0.30±0.23	466±59
8	2.47±2.19	0.34±0.02	0.70±0.33	4.31±4.18	0.38±0.24	1733±38

Appendix 4.4: Batch extractions with humic acid

Table 36: Released amounts of Th, U, La, Ce and Nd per gram of soil in all soil samples for humic acid batch extractions

	Th µg g ⁻¹	U ng g ⁻¹	La µg g ⁻¹	Ce µg g ⁻¹	Nd µg g ⁻¹
HA1					
L-03	0.16±0.01	6.91±0.45	0.42±0.02	0.30±0.03	0.35±0.04
L-04	0.18±0.02	5.16±0.13	0.29±0.02	0.26±0.03	0.29±0.03
L-05	0.41±0.04	7.51±0.38	0.47±0.02	0.70±0.05	0.43±0.02
L-06	0.35±0.05	6.17±0.82	0.38±0.01	0.64±0.10	0.35±0.03
HA2					
L-03	0.12±0.00	6.02±0.45	0.41±0.04	0.23±0.02	0.34±0.02
L-04	0.10±0.01	6.38±0.43	0.30±0.01	0.24±0.03	0.31±0.02
L-05	0.47±0.04	7.90±0.45	0.43±0.02	0.66±0.05	0.38±0.01
L-06	0.33±0.03	6.67±0.65	0.35±0.02	0.58±0.03	0.33±0.02

Appendix 4.5: Column experiments with simulated rainwater for L-05

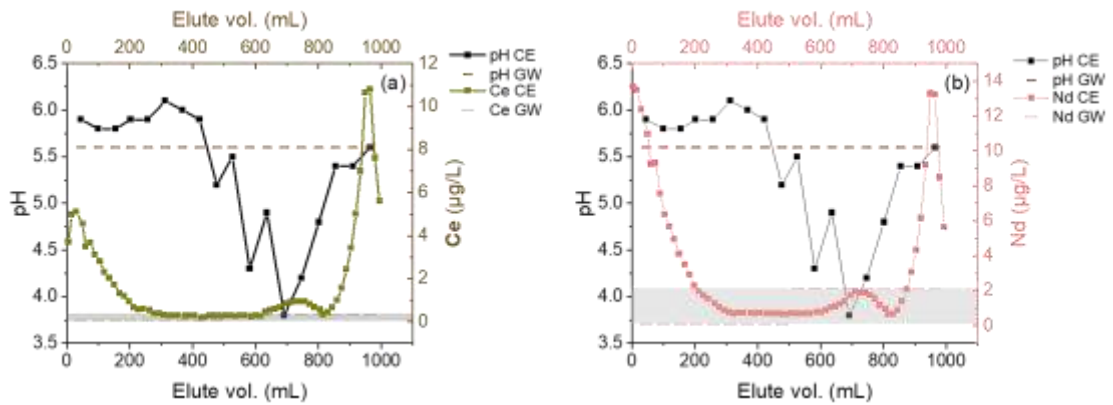


Figure A4.6: Comparison of the leached amounts of (a) Ce and (b) Nd with simulated rainwater (SRW-A1). Corresponding pH of the elutes and respective elemental concentration ranges (highlighted in grey color) including averaged pH of the groundwater are also presented. CE – column elute and GW – Groundwater

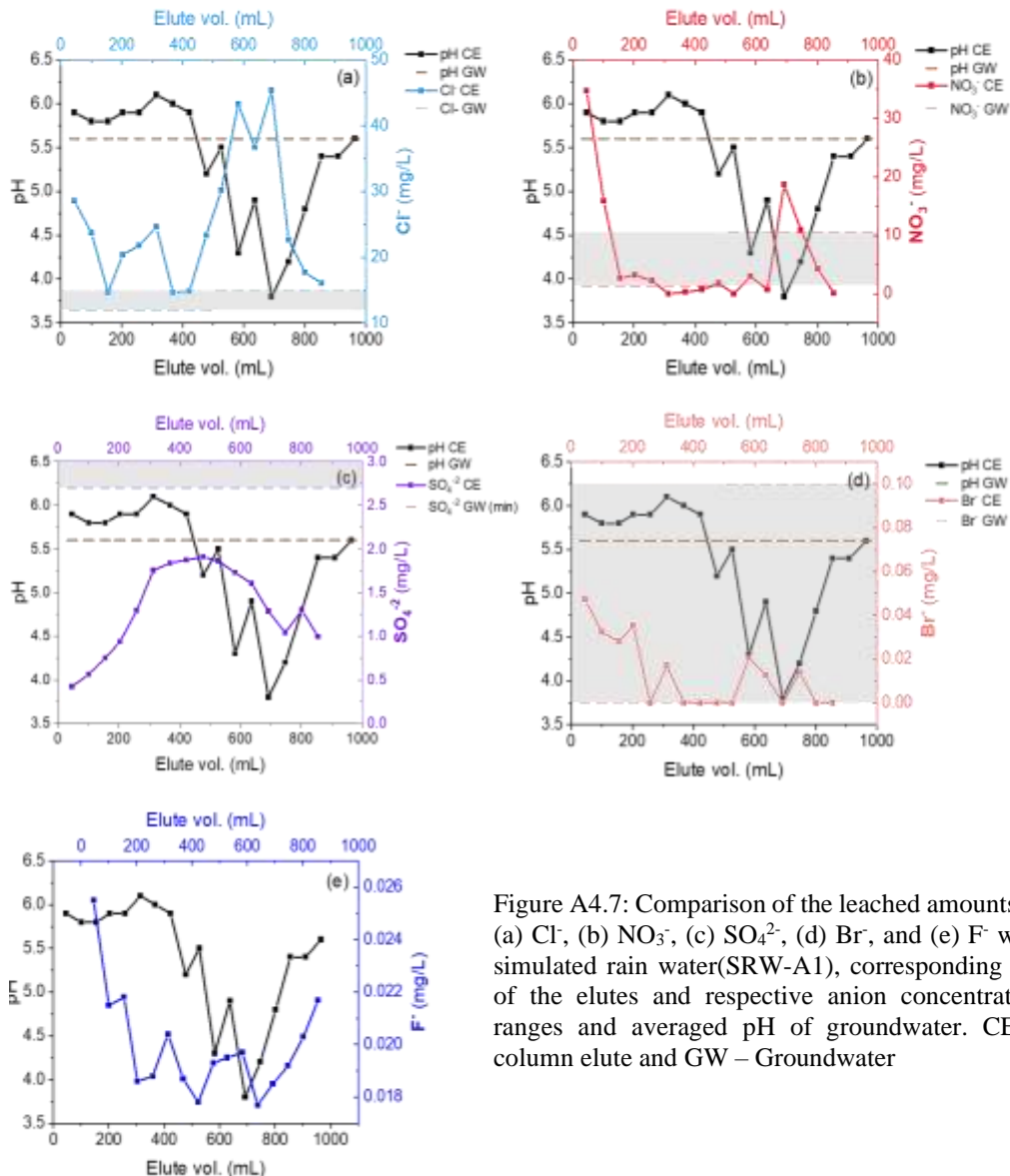


Figure A4.7: Comparison of the leached amounts of (a) Cl⁻, (b) NO₃⁻, (c) SO₄²⁻, (d) Br⁻, and (e) F⁻ with simulated rain water (SRW-A1), corresponding pH of the elutes and respective anion concentration ranges and averaged pH of groundwater. CE – column elute and GW – Groundwater

Appendix 4.6: Column experiments with silica nanoparticles for L-05

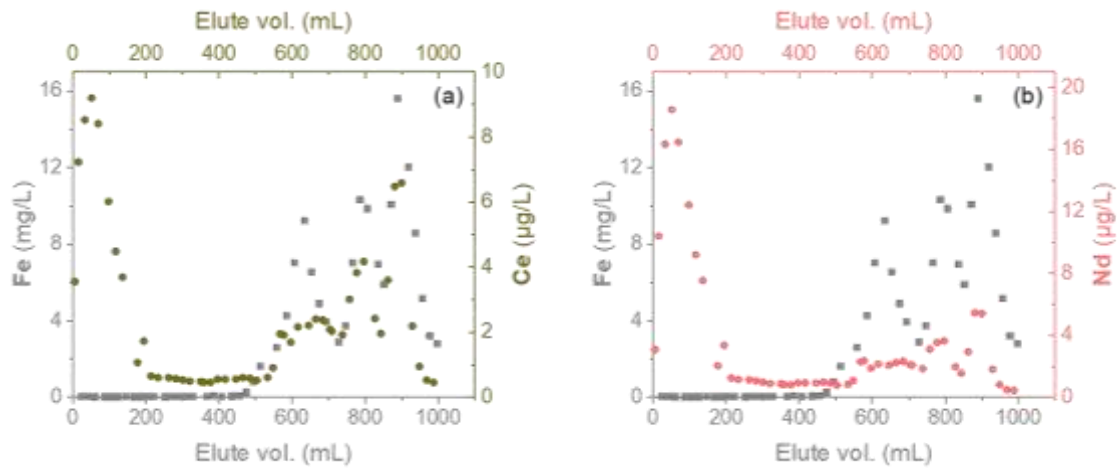


Figure A4.8: Comparison of the leached amounts of (a) Fe and Ce and (b) Fe and Nd with simulated rainwater (SRW-A1) for the soil sample mixed with silica AEROSIL 200

Appendix 4.7: Column experiments with humic acid for L-05

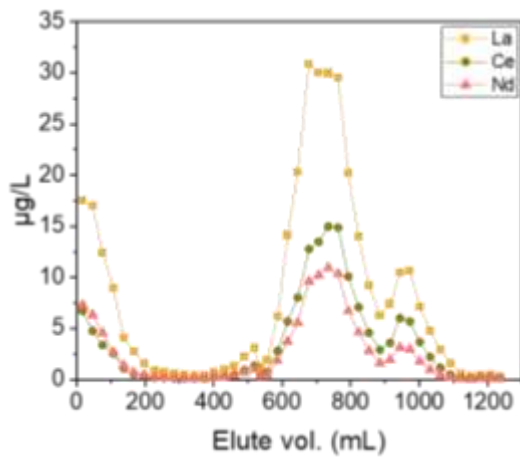


Figure A4.9: Comparison of the leached amounts of La, Ce and Nd in the column injected with 100 mg L⁻¹ Humic acid (HA1)

Appendix 4.8: Column experiments with simulated rainwater for L-04

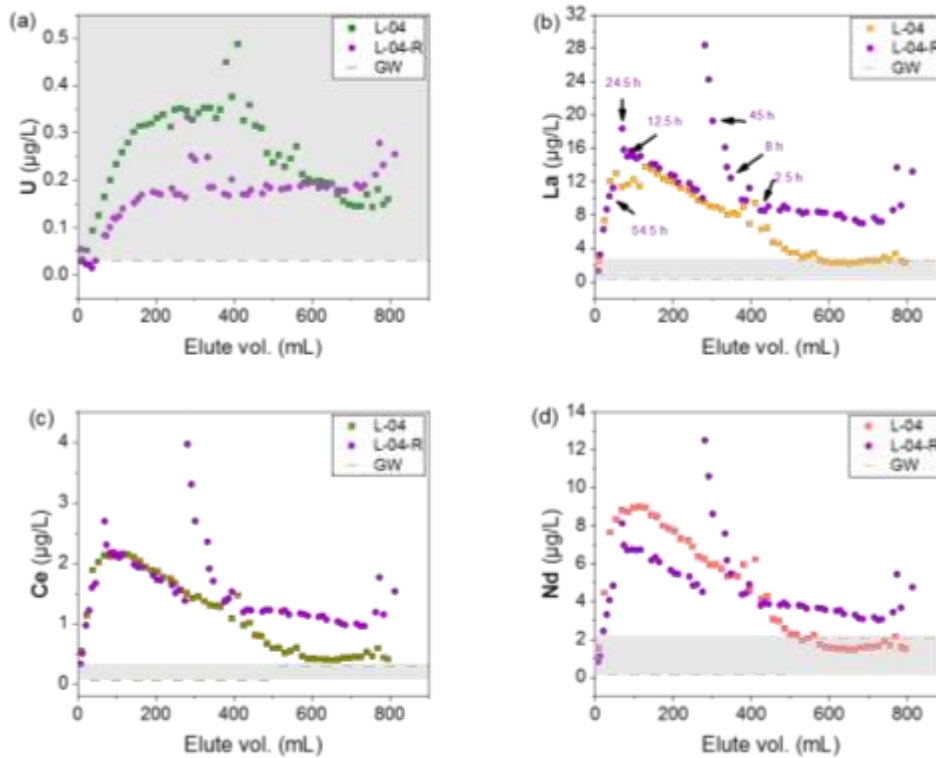


Figure A4.10: The leached amounts of (a) U, (b) La, (c) Ce, and (d) Nd with simulated rainwater using two different flowrates (violet dots always represent the 0.5 mL min^{-1} and the rest represent the 0.05 mL min^{-1} flowrate. R-Repeated column using fresh sample, in comparison to GW-groundwater level of each element

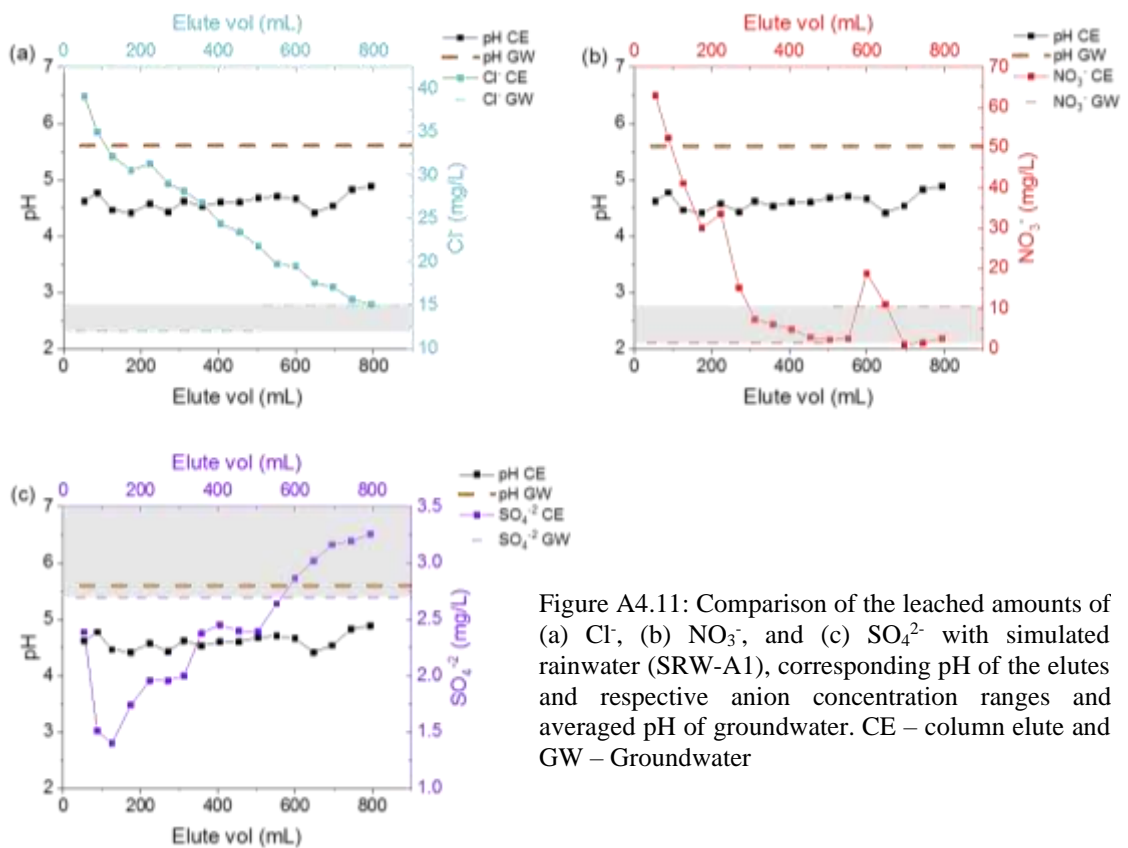


Figure A4.11: Comparison of the leached amounts of (a) Cl^- , (b) NO_3^- , and (c) SO_4^{2-} with simulated rainwater (SRW-A1), corresponding pH of the elutes and respective anion concentration ranges and averaged pH of groundwater. CE – column elute and GW – Groundwater

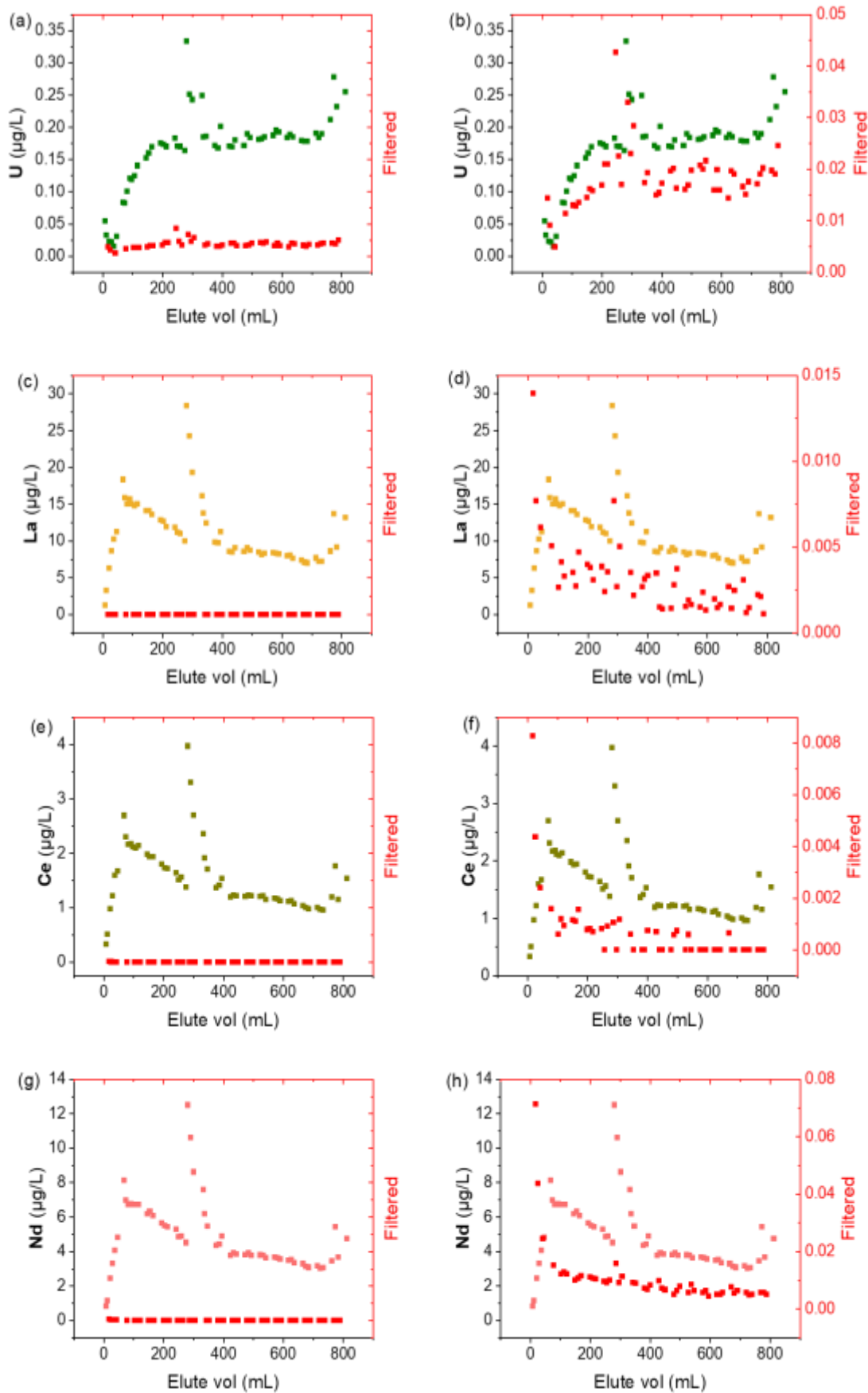


Figure A4.12: Comparison of the released amounts of U (a,b), La (c,d), Ce (e,f) and Nd (g,h) in filtered (0.2 μm pore size) and unfiltered samples with an expanded scales for the filtered samples (b,d,f,h) from the column L-04 infiltrated with SRW-A1

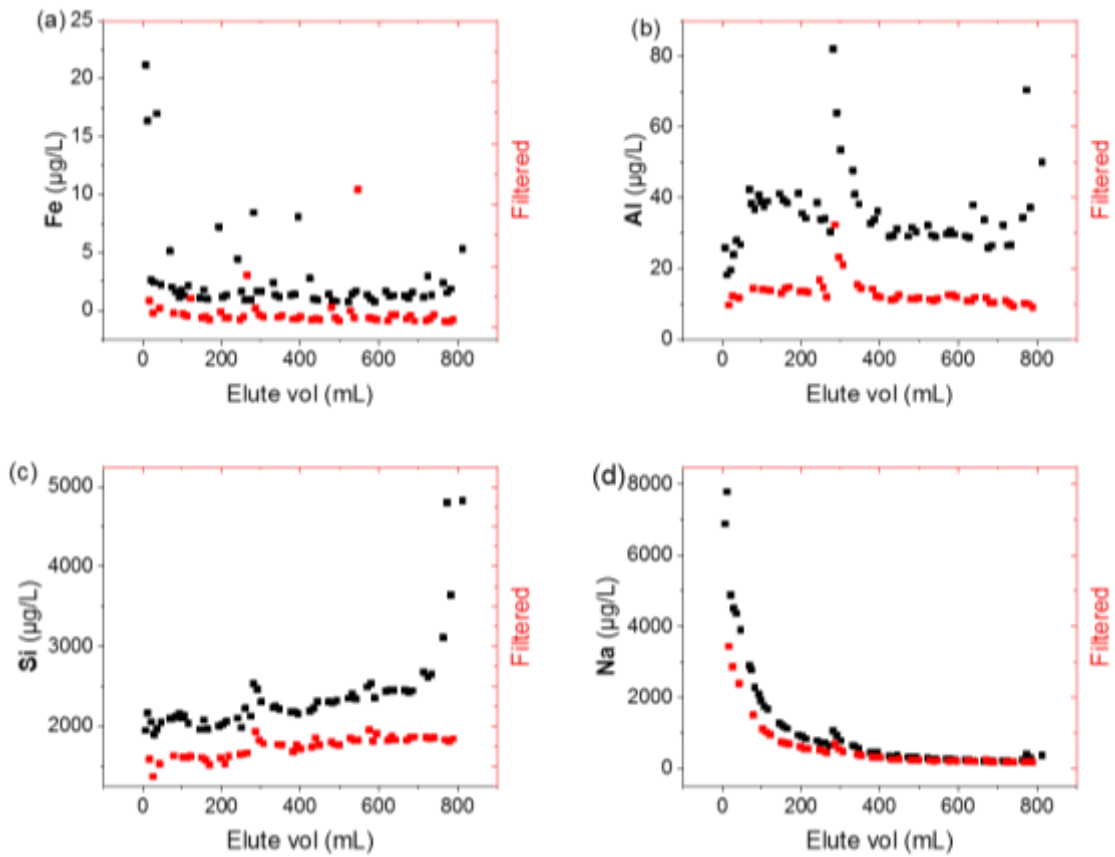


Figure A4.13: Comparison of the released amounts of (a) Fe (b) Al, (c) Si, and (d) Na in filtered (0.2 μm pore size) and unfiltered samples of the leachate from the column L-04 infiltrated with SRW-A1 (black dots represent unfiltered and red dots represent filtered values)

Appendix 4.9: Tube injection of silica suspension and use of NaCl as infiltration leachant for L-04

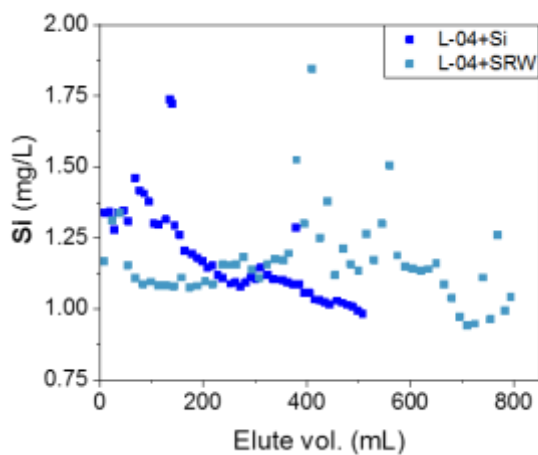


Figure A4.14: Comparison of the leached amounts of Si with the simulated rain water (SRW-A1) only with the soil sample (light blue points) and with the soil sample injected with Si NP suspension and infiltrated with 1 mM NaCl (blue points)

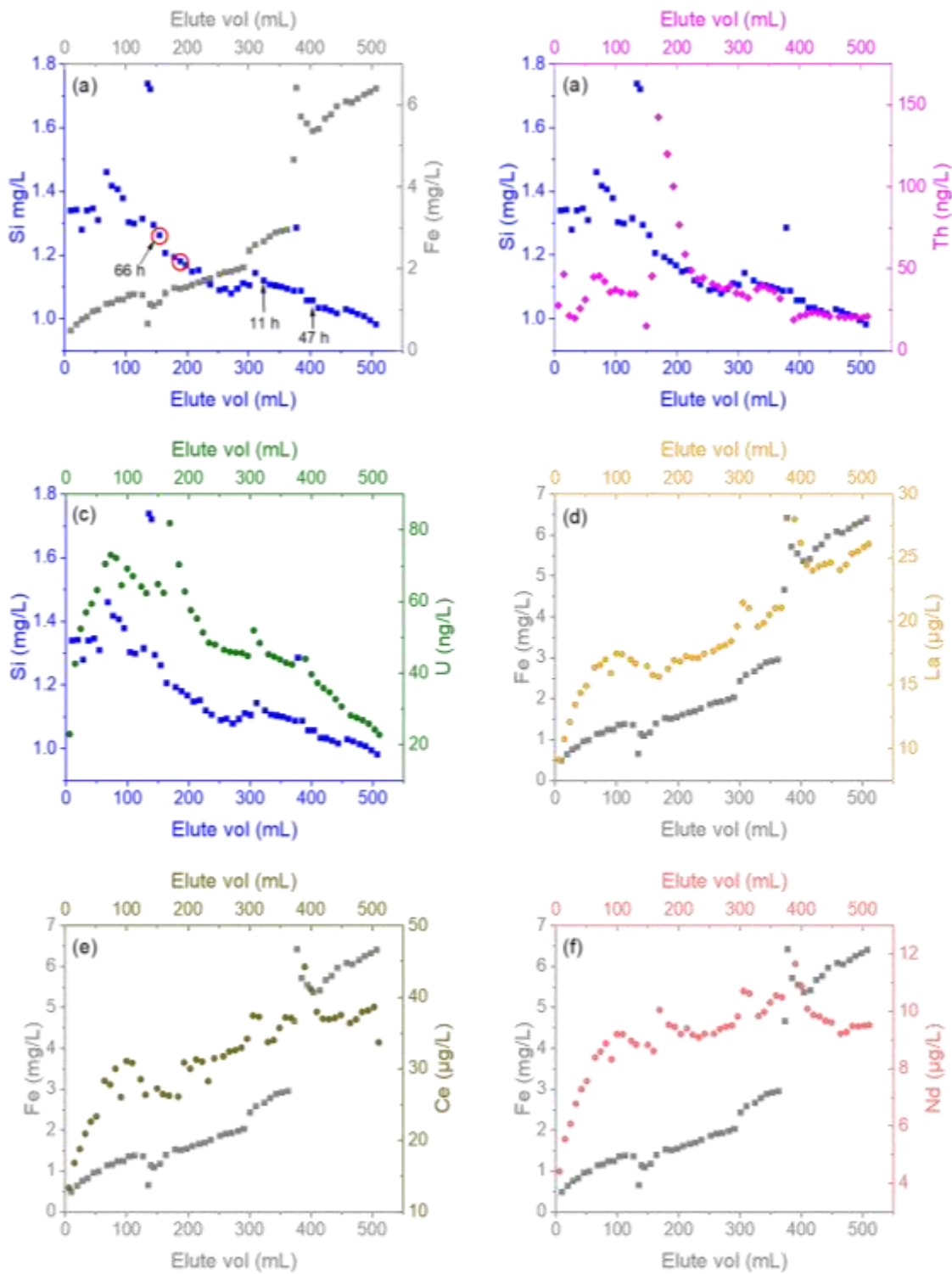


Figure A4.15: Comparison of the leached amounts of (a) Si and Fe while arrows showing the places where the column stops and the period while the red circles represent the points where injected Si suspension should come out, (b) Si and Th, (c) Si and U, (d) Fe and La (e) Fe and Ce, (f) Fe and Nd with injected with silica AEROSIL 200 and infiltrated with 1 mM NaCl for the soil sample L-04

Appendix 4.10: Tube injection of HA with NaCl solution for L-04

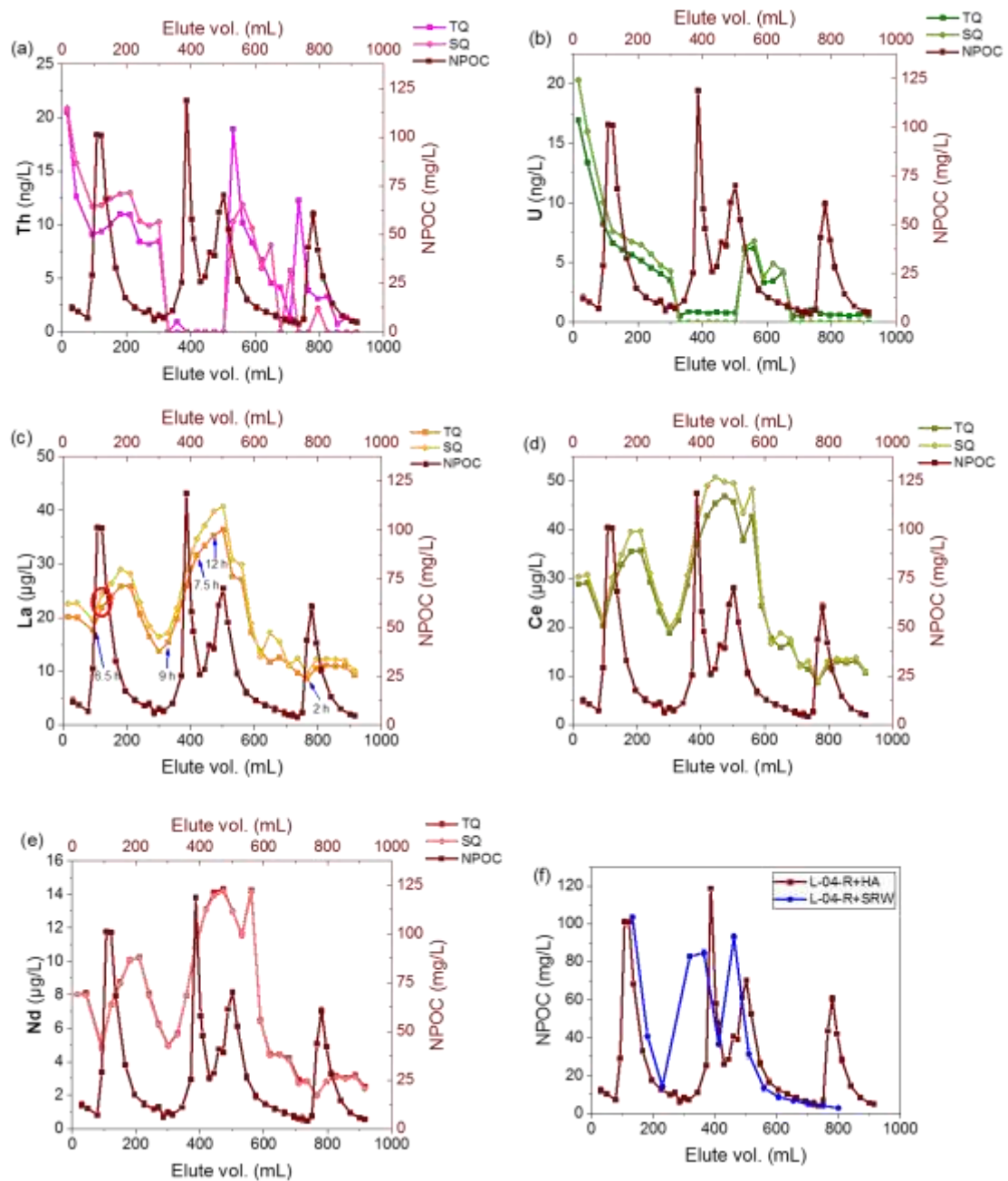


Figure A4.16: Comparison of the leached amounts of NPOC with (a) Th, (b) U, (c) La, (d) Ce, (e) Nd and (f) only leached with simulated rainwater (SRW-A1) and injected with 100 mg L⁻¹ Humic acid (HA1). The red circle in (c) is the point where the injected humics should come out. TQ-analyzed only Th, U and La and SQ-analyzed all elements including major elements

Appendix 4.11: NPOC and anions measurements in batch experiment with SRW-A1

Table A4.37: Released amounts of Th, U, La, NPOC and anions with SRW batch experiment (Solid-to liquid ratio is 0.05 g mL⁻¹) after rotation for 7 days

Sample	Elemental concentration (ng g ⁻¹)			NPOC (mg L ⁻¹)	Anion concentrations (mg L ⁻¹)		
	Th	U	La		Cl ⁻	NO ₃ ⁻	SO ₄ ²⁻
L-05	15.6±0.5	1.6±0.1	45.3±0.4	2.69±0.05	4.5±0.4	2.0±0.0	1.3±0.0
L-04	6.4±0.9	4.6±0.1	79.3±0.4	2.66±0.02	3.8±0.3	0.6±0.0	0.2±0.0

Appendix 4.12: pH dependent extractions

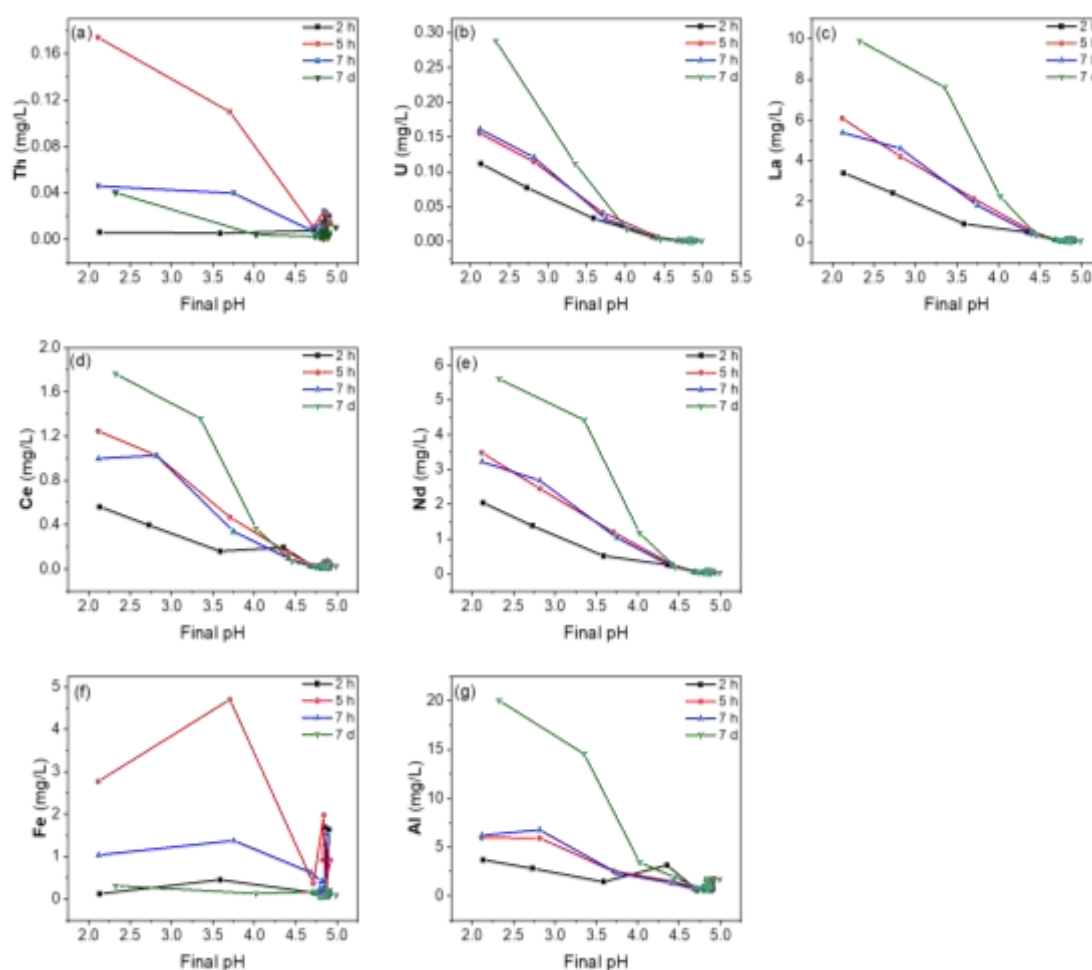


Figure A4.17: Comparison of the released amounts of (a) Th, (b) U, (c) La, (d) Ce, (e) Nd, (f) Fe, and (g) Al with the final pH after rotating at different time periods

Appendix 4.14: Column experiment run with an empty column

The ICP-OES data of Si from the empty column gave an average value of 0.033 ± 0.006 mg L⁻¹ and ICP-MS data were below the detection limit of Si.

RESUME

SANDUNI YASANKA RATNAYAKE

Personal Information

Full Name Sanduni Yasanka Ratnayake
E-mail sanduni@aeb.gov.lk
Nationality Sri Lankan

Education

Doctoral candidate, **Institute for Nuclear Waste Disposal, Karlsruhe Institute of Technology**, Karlsruhe, Germany (2017 – up to date)

M. Phil. in Chemistry, **Postgraduate Institute of Science, University of Peradeniya, Peradeniya**, Sri Lanka (Effective date: 13.09.2016). Obtained overall grade 3.88/4.00

B. Sc. Special Degree in Chemistry (Honours), **University of Peradeniya, Peradeniya**, Sri Lanka (Effective date: 15.07.2009). Obtained overall grade 3.35/4.00

Publications

Ahmed Abdelmonem, **Sanduni Ratnayake**, Jonathan D. Toner, Johannes Lutzenkirchen, Atmospheric Chemistry and Physics, **2020**, 20(2), 1075-1087.

Ratnayake S, Ratnayake A, Schild D, Maczka E, Jartych E, Luetzenkirchen J, Kosmulski M, Weerasooriya R., Nukleonika **2018**, 62 (4), 269-275.

Ratnayake S, Luetzenkirchen J, Kosmulski M, Bandara A, Weerasooriya R, Colloid Polym Sci. **2016**, 294, 1557-1569.

Scholarships

Scholarship award from German Academic Exchange Service (DAAD) under the funding program “Research Grants – Doctoral Programmes in Germany, 2017/18”

Experience

Institute for Nuclear Waste Disposal (INE), Karlsruhe Institute of Technology, Karlsruhe, Germany – Doctoral candidate (in Chemistry)

Conducted a research project to assess the fate and behaviour of naturally occurring thorium and uranium in the environment of central Sri Lanka. Radiological measurements and extensive basic and advanced characterization of environmental samples (soil, grass and groundwater), identification of potential environmental mobility of Th, U and REEs using several batch and column experiments and scoping geochemical calculations.

Obtained knowledge and experience in nonlinear second-harmonic generation spectroscopy.

Experienced as an instructor in Radioisotope course at Training Centre for Technology and Environment, KIT.

Sri Lanka Atomic Energy Board, Colombo, Sri Lanka – Scientific Officer

Skills

Microsoft office, Visual MINTEQ 3.1, Teamwork, Analytical thinking, Project management

Languages

Sinhala (mother tongue), English (fluent), German (beginner)